DELFT UNIVERSITY OF TECHNOLOGY

DESIGN SYNTHESIS EXERCISE - GROUP 2

AE3200

January 26, 2021

IKAROS - Space Based Solar Power: Final Report

Authors:

Christopher Overtveld	4429621
Evert De Vroey	4685156
Michiel van Dalsum	4647556
Thomas Nagels	4657977
Storm Holman	4645715
Maciej Jankowski	4651294
Loïc Macken	4555066
Quinten Eric Johannes van Hilten	4459172
Gabriel Alayon Blanco	4447662
Christiaan Laurens Baljé	4556305

Assistance:

Position	Name	Organisation
Tutor	Marc Naeije	SPE/AS (Astrodynamics)
Coaches	Hugo Veldhuizen	ASM/NAM (Aerospace materials)
	Sharif Khoshmanesh	AWEP/WE (Wind Energy)
External	Jeroen Koorevaar	Airbus DSN
	Henk Cruijssen	Airbus DSN

TU Delft Delft University of Technology

Preface

The need for more sustainable power is growing increasingly and thus new ways of powering our homes need to be found. In this joint venture that the peoples of the earth are undertaking, space based solar power is but a small part, but it is thought this report might inspire its readers to look for solutions outside of the initially thought possible and to approach the problem boldly.

Our great inspiration for this project is the sun, the energy source that is powering all life on earth.

Ode to the Sun

O radiant sun of light,
A soul-inspiring sight.
I Unrivalled king of kings,
Thy praise through ages rings.
Thou'rt wisest of the wise,
Exalted to the skies.
The mightiest of all might,
The brightest of the bright.
To thee, O sun, I pray,
Turn not from me away.
Reduced to slavery,
Oppressed by misery,
A captive held in thrall,
From here to thee I call
To guide me on my way,
With thy far-reaching ray.
- David Guramishvili -

This is the final report of the DSE that is given as a final 10 week course at the end of the bachelor of Aerospace Engineering at the Technical University of Delft in the Netherlands. In this report the subsystem design of the Space Based Solar Power system will be worked out into more detail. Due to the limited time span of this project, the design included in this report will still be very preliminary.

This report could not have been made alone and therefore we want to express our special thanks to all the people that helped make this report possible. Special thanks goes to Ir. Marc Naeije, Lecturer at the TU Delft, who was our main tutor and coach of this project. Next off we want to thank the coaches H.V. Veldhuizen Msc. PhD Researcher and S. Koshmanesh PhD Candidate that gave feedback on the report and coached us throughout the project.

Also our special thanks goes to Jeroen Koorevaar and Henk Cruijssen from Airbus for giving us feedback and coaching us throughout this project.

Executive Overview

This report is concerned with the final design phase of the Fall 2020-2021 Design Synthesis Exercise for group 2, titled "Project IKAROS". In the previous Midterm report, a trade-off was performed to determine the design concept that would be proceeded with in the Final design phase. The concept chosen was "Honey": a single large satellite in a geosynchronous orbit which would aggregate and focus sunlight through two opposed parabolas to a downlink station on the surface.

The functioning of the system was divided into 12 phases, which are as follows:

1. Pre-Launch -> 2. Launch -> 3. System Initialisation -> 4. System Organisation -> 5. Assembly in Space -> 6. Inject into GEO -> 7. Payload Deployment -> 8. Power Downlink Initialisation -> 9. Operation -> 10. Maintenance of System -> 9. Operation -> 11. Mission Stop -> 12. End of Life

The design process was split up into subsystems which were designed in an integrated manner using system engineering techniques.

The first subsystem is the power downlink system. In Figure 1 the system configuration is shown. The system will be composed of, as in the original "Honey" concept, two opposing parabolas. The large parabola will aggregate the power to a focal point after which it is collimated by the small parabola. They are aptly named the "Queen" and the "Worker" respectively. The collimated light then passes through an aperture in the Queen after which it is reflected on a mirror offset from the main body. This mirror is named the "Sting", which performs part of the downlink throughout the orbit duration. The Queen and Worker create a blind spot through which the Sting can not relay, thus a second reflector is added to the rim of the Queen to reflect the light around the satellite and reduce the oblique angles that need to be addressed by the sting. This second reflector is named the "Relay". The values of the parameters related to the layout of the system are presented in Figure 1 can be found in Table 1.

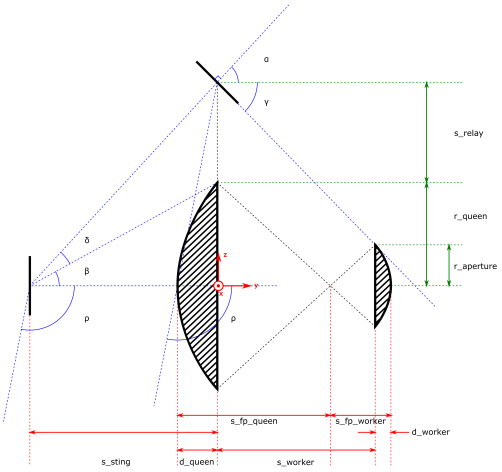

Figure 1: Layout parameters of the downlink system.

The downlink sends the collected power down to the ground station, which is composed of several reservoirs with a molten salt mixture where a HTF is heated up and used to convert the thermal energy into electricity with a turbine. The ground station radius is 350m.

Another subsystem (or rather system aspect) is the astrodynamics of the IKAROS project. This mainly concerns the approach that would be pursued to launch the system into its proper orbit. The SpaceX Starship can only deliver its payload of 100 tons to a LEO orbit with a height of 500km. A transfer is thus required to get the system into GEO. Four approaches were identified to perform this transfer, which were traded off according to Table 2. A spiral

Module	**Queen**	**Worker**	**Sting**	**Relay**
radius [m]	482	25	37.91	226.86
radius (short)	-	-	26	26
area [m^2]	756054.63	2033.94	3040.96	18197.13
depth [m]	92.38	4.79	-	-
offset [m]	-	564.16	413.67	330.44

Table 1: Relevant values for the downlink system layout

transfer would involve constant boosting of the transfer modules, which are assembled in orbit, by ion thrusters over a longer duration. A Hohmann with custom propulsion would require two thrust impulses with custom engines. The 21 tons Starship would reduce payload weight to 21 tons to directly inject the payload into a GTO orbit with a perigee of 185km, to be boosted into a full GEO orbit by custom propulsion. Finally, the Hohmann transfer with a refuelling Starship would use additional launches to refuel and get the modules into a GTO of 500km, once again to be boosted to GEO by custom propulsion.

	P.M. Parking Orbit	P.M. GEO	Time to GEO	Sustainability	Logistics	**Scores**
Spiral Transfer	3	2	1	2	2	**1.94**
Custom Propulsion	3	1	3	1	2	**2.06**
Starship 21 Tons	1	3	2	1	1	**1.75**
Starship 100 Tons	1	3	3	2	2	**2.31**
Weight	3	4	4	2	3	

Table 2: Trade-off scores on transfer mission plans

From this trade-off, the Starship refuelling transfer was chosen, from which the following final transfer plan was established:

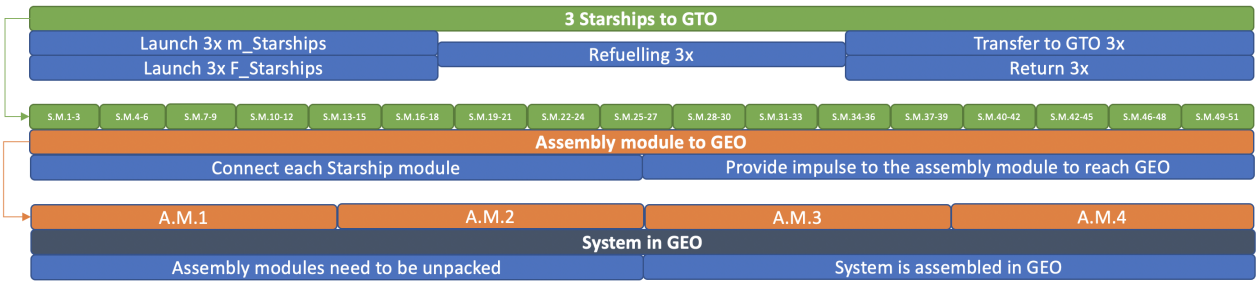

Figure 2: Transfer plan

The total time to reach GEO was thus calculated to be 1.23 years after first launch.

The next logical subsystem is of course the propulsion for the transfer modules. Once again a trade-off was performed between three propulsion configurations. These are as follows: SpaceX Raptor using liquid methane, Snecma HM-7B using liquid hydrogen and the Snecma Vinci also using liquid hydrogen. The results of this trade-off are in Table 3

	Performance [5x]	**Safety & Risk [4x]**	**Mass Performance [5x]**	**Sustainability [2x]**	**Final Grade**
Raptor	4	2	4	3	3.38
HM7B	3	4	1	4	2.75
Vinci	4	2	1	4	2.56

Table 3: Final Rocket Engine Comparison Trade-Off Results

Thus the Raptor engine was selected, in addition of the selection of fuel tanks that use multi layer insulation to store the oxidiser and liquid methane. The engine has the following performance characteristics:

Length [m]	Diameter [m]	Dry Weight [kg]	Thrust [kN]	Isp [sec]	Thrust/Weight [-]	Mixture Ratio [-]	Chamber Pressure [bar]
3.1	1.3	~1500 (goal)	2000	380	~150	3.55	300

Table 4: Specification SpaceX Raptor Engine[1][2][3][4]

The next subsystem to be tackled was the Attitude Determination & Control System. To determine the required control systems, the disturbances that the satellite would undergo were first identified in Table 5

Both the determination and control systems provided multiple avenues of approach, which were once again traded off.

The result of the attitude determination system trade-off was a configuration using Cubesatshop NFSS-411 Sun sensors, Sagitta Star strackers and a Sensonor STIM377H Inertial Measurement Units. Two of each were selected to provide redundancy in case of failure.

The attitude control method that was chosen from the trade-off was 4 pairs of 4 Heritage hydrazine 1N thrusters in the configuration presented in Figure 3.

Disturbance torque	Value	**Unit**
Solar radiation	-	Nm
Atmospheric drag	-	N
Magnetic field	2.12E-07	Nm
Gravity gradient	1.53E-01	Nm

Table 5: Disturbance Torque Results

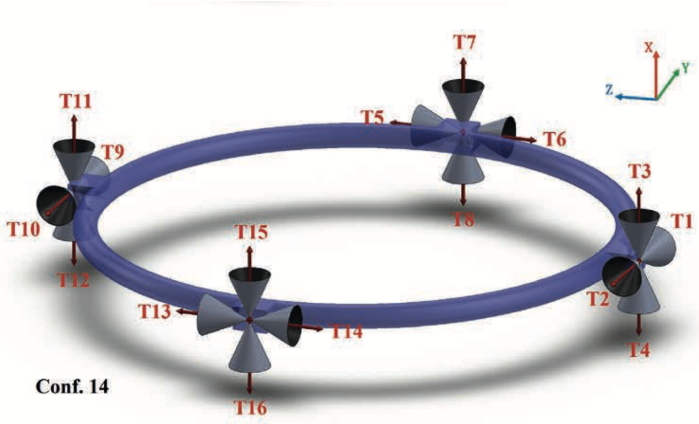

Figure 3: Thruster configuration ADCS[5]

The subsequent subsystem is Assembly, Integration and Verification. This system is mainly concerned with the method for converting the individual Starship Modules into the Assembly Modules and ensuing full system assembly in GEO. The Assembly Module configuration is shown in Figure 4.

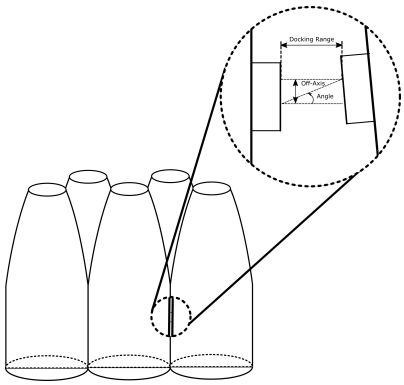

(a) Docking between Starship modules demonstrating docking errors.

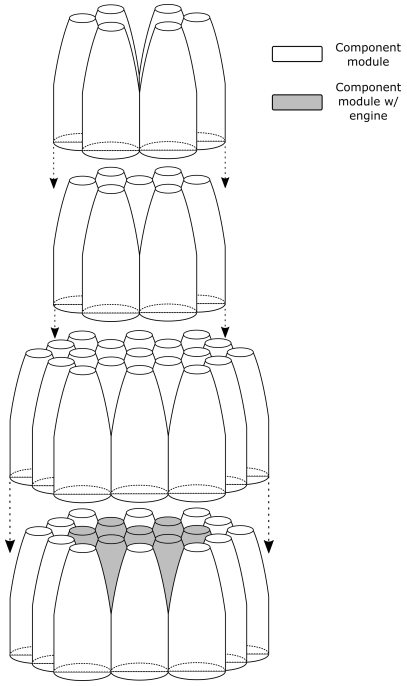

(b) Assembly module general configuration, propulsion modules shown in bottom-most section.

Figure 4: Assembly module docking and configuration.

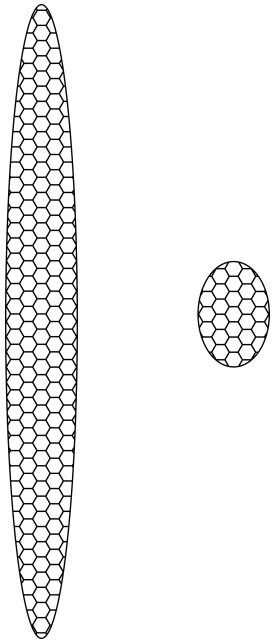

Figure 5: Relay and Sting initial segmentation and relative scale.

For the final assembly, the two reflectors, the Sting and the Relay will be made up of rigid hexagonal mirrors which are launched as segmented panels as per Figure 5.

The Queen's assembly will involve the construction of a skeleton structure, to which rolls of reflector foil will be attached. These rolls are then extended over the structure to create the reflective surface, as shown in Figure 6a. The Worker will be composed of a folded origami structure that can be deployed into a parabola, as visible in Figure 6b.

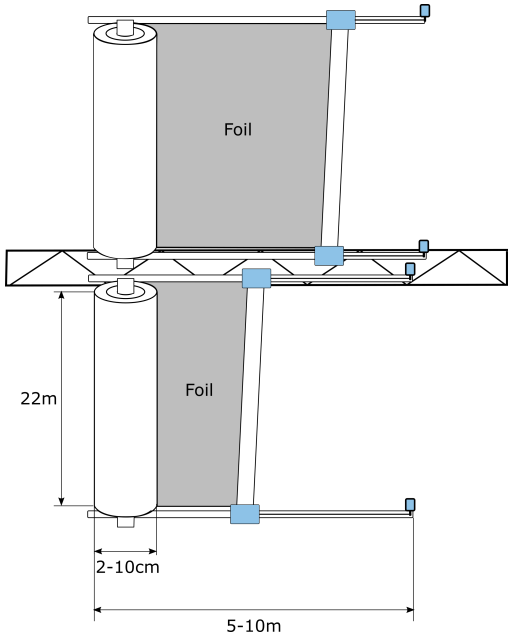

(a) Configuration of deployment mechanism.

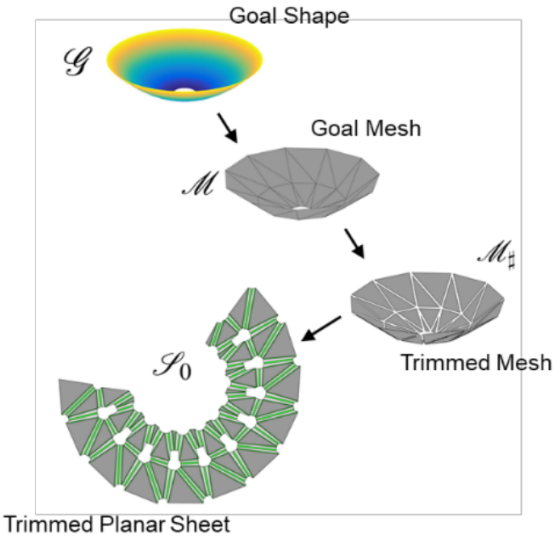

(b) Steps in the design process for origami with smooth folds [6] [7]

Figure 6: Queen Roller and Worker Origami

With the assembly approach defined, the next logical step is of course the structures subsystem. For this subsystem, a rather unorthodox approach was chosen where the design was performed backwards. The shape was obtained from the downlink design and in an integrated manner the structures and AIV was performed together. The material decided on for the primary structure was Aluminium 6061-T6. The structural characteristics that resulted are presented in Table 6.

c.g. in X $[m]$	0
c.g. in Y $[m]$	371.5
c.g. in Z $[m]$	131.9
MMOI X $[kgm^2]$	1.4E12
MMOI Y $[kgm^2]$	1.75E12
MMOI Z $[kgm^2]$	6.9E11

Table 6: Satellite characteristics

Next up is the thermal control subsystem. To resolve the large amount of heat accumulation on the small parabola, a LDR will be used to maintain temperatures at reasonable levels. The back of the Queen will also receive an aluminium coating to prevent excessive cooling and improve heat retention. The temperature with and without thermal control can be seen in Figure 7

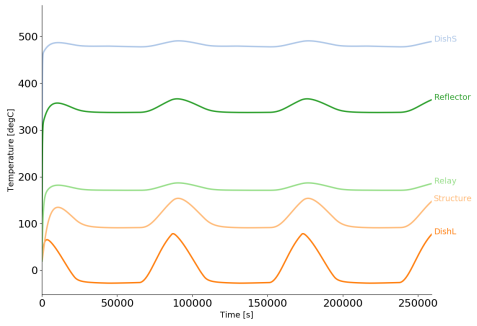

(a) Temperature over time per component using a 10 second time-step for a 72 hour simulation in orbit, without any added thermal control

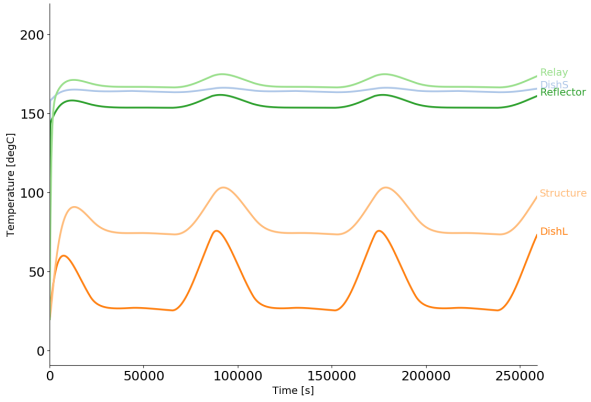

(b) Temperature over time per component using a 10 second time-step for a 72 hour simulation in orbit, with added thermal control

Figure 7: Difference in temperatures with and without thermal control

The electric power system is the next subsystem. It will use a ring of Gallium Arsenide solar cells, namely AzureSpace Quadruple Junction 4G32C-Advanced. To store the power for discharge during eclipse Li-Ion batteries are selected. Power distribution is handled by a RUAG Space PCDU. The layout of the system is shown in Figure 8 below.

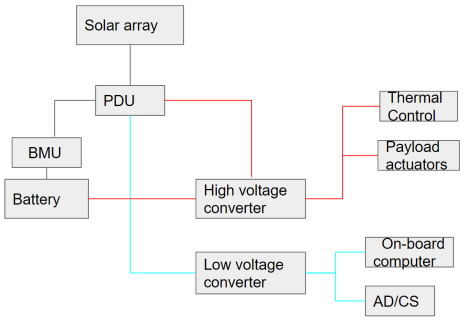

Figure 8: EPS layout

Finally, the command and data handling subsystem is arrived at. The subsystem will use two parabolic antennas transmitting 1 W worth of power each for redundancy. The selected on-board computer is the Space Inventor OBC-P3.

In the hardware diagram below, all the individual components can be retraced in addition to the interfaces they might have with other components. Figure 9

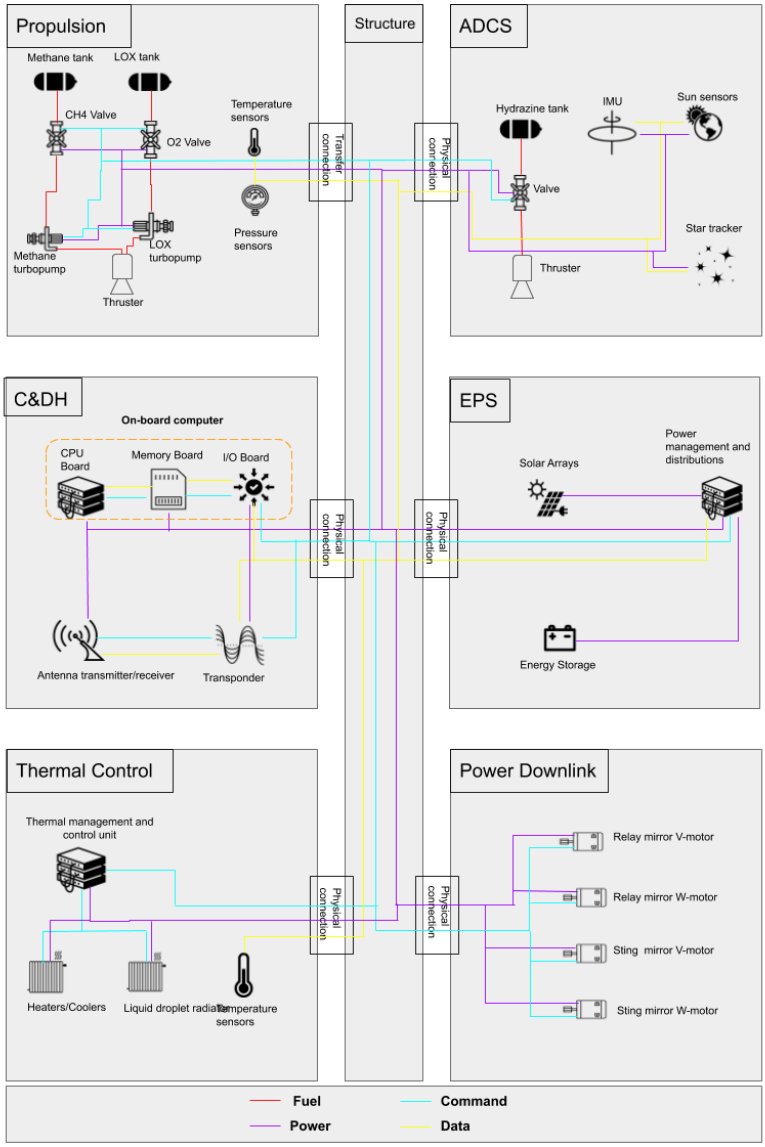

Figure 9: Hardware Diagram IKAROS system

The resource allocation & budget breakdown data can be viewed in Table 7

Subsystem	AD/CS	C&DH	EPS	Thermal Control	Propulsion	Power Downlink	Structures	Assembly & Modularity
Mass [kg]	25	3.5	10 560	47 970	5 847 953	575 896	11 452 600	15 000
Power [W]	100	250	300	120 000	50	100 000	-	-

Table 7: Breakdown of subsystem mass and power use

Of course, many risk will be encountered to this project, both during and before operations. These are shown in Table 10 below. This risk map shows that after mitigation, there will be no risk with a high impact that have a medium or high probability.

A business and market analysis is also performed, where the decisions was made to use the power generated by the IKAROS system to desalinate water and sell it to the city of Mumbai. A SWOT analysis is performed, the results of which are presented in Table 11

Impact/Probability	Very Low	Low	Medium	High
Large	CDH.1 CDH.4 PAY.1 PAY.4 THERM.3	PRJ.5 PROP.1 PROP.3 ADCS.5 CDH.3 POW.1 POW.2 POW.3 THERM.1 STRUC.1 STRUC.4	PRJ.6 STRUC.6 CDH.2 ASSEM.1	PAY.6
Moderate	ASSEM.4	PRJ.3 PRJ.4 PROP.2 PROP.4 ADCS.2 ADCS.3 ADCS.4 ASSEM.2 THERM.2 PAY.3 STRUC.2 STRUC.3	ADCS.1	STRUC.7
Mild	PAY.2 ASSEM.3	STRUC.5	PRJ.1 PRJ.2 PAY.5	PROP.5
Small	GROUND.1 GROUND.3	ASSEM.5	GROUND.2	

Table 8: Risk Map before risk mitigation

Impact/Probability	Very Low	Low	Medium	High
Large	PROP.1 PROP.3 ADCS.5 STRUC.1 STRUC.4 STRUC.6 POW.3	ASSEM.1		
Moderate	PRJ.3 PRJ.4 PRJ.5 ADCS.2 ADCS.3 ADCS.4 STRUC.2 STRUC.3 PAY.3			
Mild	PRJ.1 PRJ.6 PROP.2 CDH.1 CDH.2 POW.2 PAY.4 PAY.5 ASSEM.2 ASSEM.4 THERM.3	PROP.4 PROP.5 CDH.3 THERM.1		
Small	PRJ.2 CDH.4 STRUC.5 POW.1 PAY.1 PAY.2 ASSEM.3 GROUND.1 GROUND.2 GROUND.3	ASSEM.5	ADCS.1 THERM.2	STRUC.7 PAY.6

Table 9: Risk Map after risk mitigation

Table 10

Strengths	**Weaknesses**	**Opportunities**	**Threats**
Renewable	High seed cost	Absence of desalination plants	Space debris
24/7 operation	High maintenance cost	High growth in market	Reliance on external contractors for access
Vertically integrated ground station design producing rare commodity	Downlink may be liability	Regulatory environment conductive	Many competitors if feasibility proven
Higher solar radiation w.r.t. ground-based	Inflexible	High disparity demand/supply	

Table 11: SWOT Table

A cost and income analysis was also performed, with the costs presented in detail in Figure 12. A return on investment graph is also created in Figure 13 to illustrate the disparity between the expected costs and income from revenues.

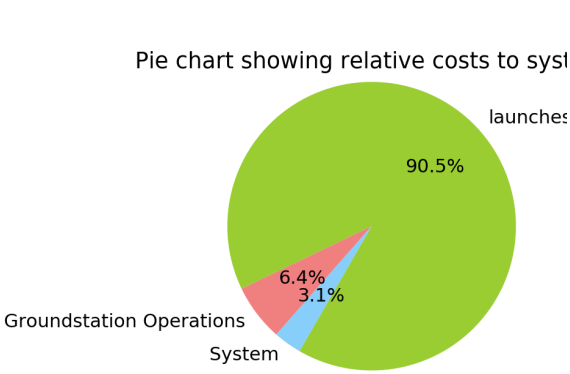

Figure 10: relative costs of the system

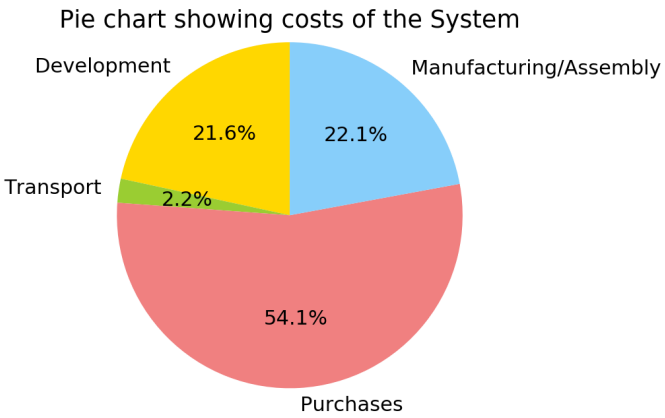

Figure 11: Relative cost of the entire project

Figure 12

As a conclusion, it was found that the main obstacle that was encountered in the design of this system was the in-space assembly. No similar project of equal size has been attempted before. The structural limitation that was limiting in the design was the size of sheets for the Queen, not the rigidity, as previously expected. The other large challenge that was predicted from earlier reports was thermal control, namely at those locations of the satellite that would receive highly intensified sunlight. This problem was resolved with the fledgling technology of Liquid Droplet Radiator, which promises high mass-specific performance although it will be the greatest power consumer in the satellite's power budget. Finally, it was determined that the current design will not be economically sustainable in its determined market case. The current costs of electricity but also the construction of renewable energy generators is significantly low enough that there is no incentive to pursue this approach. Even switching over to an alternative market target by selling desalinated water will not resolve the excessive burden imposed by launch costs.

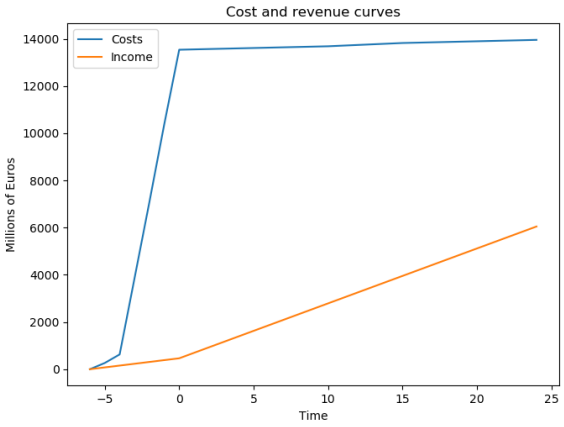

Figure 13: Graph displaying cost and income over the lifetime of the project.

This also ties into the recommendations that were determined from this report. Significant reductions in launch costs are still required before project such as IKAROS become competitive thus the main focus of future research and development should be on reducing these or finding more efficient launch alternatives. To reduce the time between launch and operation commencement, further development should be invested in developing autonomously powered swarm technologies in combination with building out both computational and practical resources which can simulate in-space assembly. Investigation into recycling spacecraft components into orbit could also be a highly effective way of reducing costs in the future, especially with respect to spacecraft at the size of the IKAROS project. Structurally, research into larger mirror sheets with shape memory could increase performance. System precision would also benefit from more advanced large lens technology. To improve ground station efficiency, research into more efficient desalination technologies could be performed. Finally, a demonstrator of a smaller scale of e.g. 1MW could be developed to obtain experience into construction of such satellites which could later be evolved into a large constellation of smaller satellites.

Contents

Acronyms

ADCS Attitude Determination & Control System. iv, 10, 13, 31, 40, 45, 46, 48, 50, 93, 94, 102, 112, 133
AIV Assembly, Integration & Verification. vi, 47, 90, 91, 112
AoP Argument of Perigee. 24
AWG American Wire Gage. 77

c.g. center of gravity. vi, 18, 64
C&DH Command & Data Handling. 14, 20, 21, 31
CNC Computer Numeric Control. 99
COEs Classical Orbital Elements. 22, 24

DARPA Defense Advanced Research Projects Agency. 47, 49, 50
DISCOM Distribution Companies. 120
DoD Department of Defense. 109

ECSI Economic Sustainability Indicator. 129
ECSS European Cooperation for Space Standardization. 109, 113
ENSI Environmental Sustainability Indicator. 129
EoL End-of-Life. 124
EPS Electrical Power System. 17, 47, 82, 90, 91, 94, 112
EV Electric vehicles. 79

FOV field of view. 13, 14, 18, 114, 133

GEO Geo-synchronous Equatorial Orbit. ii–iv, 3, 10, 20, 22, 24–26, 28–34, 36, 38, 41, 42, 44, 47, 49, 53, 66, 77, 94, 95, 101, 103, 114, 122, 123, 132–134
GTO Geosynchronous Transfer Orbit. iii, 25, 27–34, 36, 38, 47, 48, 53, 94

HTF heat transfer fluid. ii

IMF International Monetary Fund. 120
IMU Inertial Measurement Unit. 102, 126
IR Infra-red. 66
ISS International Space Station. 49, 72
ITU International Telecommunications Union. 114

LDR Liquid Droplet Radiator. vi, ix, 72–74, 97, 132
LEO Low Earth Orbit. ii, 24, 27–31, 94, 113, 133
LR Level of Redundancy. 45, 46

MED Multi Effect Distillation. 121, 134
MLI Multi-Layer Insulation. 69–71, 97
MMOI Mass Moment of Inertia. vi, 42, 64

NASA National Aeronautics and Space Administration. 109

P.M. Payload Mass. iii
PCDU Power control and distribution unit. 79, 80
PSS Propulsion Subsystem. 34
PV Photovoltaic. 10, 15–17, 21

RAAN Right Ascension of Ascending Node. 22, 24
RAMS Reliability, Availability, Maintainability, and Safety. 105
RO Reverse Osmosis. 92, 121
ROI Return on Investment. 127
RSGS Robotic Servicing of Geostationary Satellites. 49

SBSP Space Based Solar Power. 2, 38, 39, 100, 122, 123, 127, 132
SI Sustainable Indicator. 119
SNR Signal-to-Noise Ratio. 112
SOSI Social Sustainability Indicator. 129
SSO Sun-Synchronous Orbit. 3
SWOT Strength, Weakness, Opportunity and Threat. vii, viii, xi, 120–123

TRL Technology Readiness Level. 27, 36, 37, 72, 94, 100, 102, 109, 113, 124, 132

1
Introduction

The concept for space based solar power is not new as the energy problem has been around for quite some time now. Even since the early '70's these concepts have been researched, but now that the launch costs are diminishing quickly, these once wild plans might actually be realised in the near future. Space institutions have aimed to solve the problem in the past. Unfortunately without much success because of technological limitations. Recently the interest in space based solar power has returned. Newspapers, journals and online articles are looking into the possibility and if space based power could become a thing. The technological advances since the last Space Based Solar Power concept may allow for a feasible design.

The aim of this report is to describe a system that takes on the challenges of designing a SBSP system. it is in essence an enormous parabolic mirror in geostationary orbit around the Earth, that is to redirect rays of the sun back to Earth. The concept designed in this report aims to overcome the technological limitations. The report will reach detail down to subsystem design in order to create a through and robust system. The report will not limit to just the satellite but include a conceptual ground stations for the completeness of the system. The reader will understand its workings and concepts as it reads through this report.

The report will first cover the previous steps taken in the project (in Chapter 2,Chapter 3), which will describe the functional overview of the system as well as provide an overview of the performed design option trade-off. Furthermore, this project will contain information about the detail designs of the subsystems of the IKAROS system (in Chapter 4 through Chapter 12). These chapters will cover the way the system works, the subsystems it will require and the sizing of the subsystems. The report will then provide an analysis of the design as a whole (Chapter 13 through Chapter 19), these chapters will cover the non-technical aspects of the system to provide a full picture of the system from a non-engineering perspective. Finally the report ends with a conclusion (Section 20.1) and a recommendation chapter (Section 20.3) which will cover what was learned, and where the current limitations lie.

2
Concept Trade-off Summary

This chapter functions as a summary of the trade-off that was performed in the previous midterm report, so that the reader can have a better overview. This chapter contains a section of the different design concepts on which the trade-off was performed and a section of the trade-off criteria on which the trade-off was based. Finally the chapter includes a section about the results of the trade-off and tell something about the final concept design that came out of the trade-off

2.1. The different concepts

This section discusses the different concepts on which the trade-off was performed and discusses them briefly. For a more detailed description the reader is advised the look through the midterm report. The trade-off was performed on five different concepts, which all will be explained below.

- **Honey:** The Honey concept is an enormous parabolic mirror in a GEO orbit that is to direct sun rays towards a solar array farm back on Earth. The mirror consists of four main components. The Queen is the main parabolic mirror with a hole in the middle that is used to catch the sun rays and directs the rays to the Worker mirror, which is a smaller mirror that directs it through the hole of the Queen mirror again. At the back end of the Queen mirror there will be yet another mirror that is called the Stinger. This flat mirror's function is to aim down the rays back to earth. Sometimes the sun will be in such a position that the Queen mirror will block the Stinger mirror to send down the light to Earth. When this happens to Stinger points the light to a mirror on top of the Queen mirror that can than redirect to light to Earth after all.
- **Lacey:** The Lacey system consists of a large solar array satellite in GEO orbit that uses an electrically charged diode laser to send down the energy through the atmosphere at a greater efficiency than normal sunlight would. The laser would be pointed at an existing solar array farm on Earth where the laser light would be transformed into electricity.
- **Macey:** The Macey system is a similar concept to the Lacey system, with its main difference being that the energy is not transferred back to Earth by means of a diode laser, but by means of microwaves. The microwaves can unfortunately not be absorbed by solar panels and thus a different ground infrastructure must be made to transform the microwaves into electricity. Microwaves have a high efficiency to go through the atmosphere.
- **Rodney:** The Rodney system is a similar concept to the Lacey concept, with the only difference is that the lasers are directly powered by the sunlight. This is due to a relatively new technology that uses laser rods that can be exited by sun rays to emit a laser back to earth. The system would comprise of many of these lasers all pointed towards a common solar farm back on the surface of the Earth.
- **Manny:** The many concept uses multiple mirrors in a SSO orbit with a slight inclination to match the dusk-dawn line. The mirrors would point at existing solar array farms on the ground and would extend the amount of daylight the solar array farms would receive by 1.5 hours per day.

2.2. Trade-off criteria

This section outlines the different trade-off criteria that were being used to perform the trade-off. It only briefly explains the different criteria and does not go into detail on how these criteria were assessed. For this information the reader is advised to read through the midterm report.

- **Financial Considerations:** This criteria will look into the financial feasibility of a concept. The main things that will be considered in this criteria are the cost of the system to full operation and the market adaptability of the system, such that it can be sold better to the costumers.
- **Technology Readiness Level & Reliability:** This criteria will look into the availability of the technology that the system aims to use and the reliability of the intended use of the technology.
- **Safety & Risk:** This criteria looks into any safety concern a concept may have, such as being used as a weapon, environmental hazards etc. and also considers the risks that is involved in a mission that uses the system.
- **Maintainability & Complexity:** This criteria will be evaluated upon the amount of downtime that is needed to maintain the system. This closely ties into the complexity of the system and is thus evaluated in a single trade-off criteria.
- **Throughput Time:** This criteria evaluates the systems based upon the amount of time it will take to get the systems operational.
- **Sustainability:** This criteria is split into three sub-criteria, which are environmental, social and economic sustainability.

2.3. Trade-off Results

This section goes over the scores of the trade-off and will show, which concept was considered to be the winner. The results are not be discussed in detail here, for a more detailed overview the reader is advised to read through the midterm report. The results can be seen in Table 2.1, as can be seen in the table the final winner of the trade-off is the honey concept. Even when a sensitivity analysis is performed the winner remains to be the Honey concept (for more information about the sensitivity analysis please refer to the midterm report).

Concept/ Criteria	Financial Considerations	TRL & Reliability	Safety & Risk	Maintainability & Complexity	Throughput Time	Sustainability	Average Score
Honey	4	3	3	4	4	4	**3.7**
Lacey	3	2	2	2	3	2	**2.3**
Macey	4	2	3	3	4	3	**3.1**
Rodney	3	3	4	3	3	2	**3.0**
Manny	1	4	5	3	2	4	**3.2**
weight	**10**	**12**	**8**	**6**	**6**	**6**	

Table 2.1: Trade-Off Summary Table

The Honey concept has a combination of high scores on several trade-off criteria, which made it a clear winner in the end. Most notably we can see that the final considerations and the TRL & Reliability has a high score, which was deemed to be the two most important trade-off criteria. Even when the launch costs will be cheaper in the future the Honey concept would still win due to it being the cheapest to launch into space.

3
Functional analysis

This chapter aims to provide a description of the functioning of the Honey system. To that end, two diagrams will be presented: the functional flow diagram and the functional breakdown structure. The functional flow diagram provides an outline of the order in which the function is to be performed. The functional breakdown structure provides further detail into each function.

3.1. Functional flow diagram

This section presents the functional flow diagrams of the IKAROS system. The diagram is as complete as it can be at this phase of the project. The arrows in the figure depict the flow of functionality of the system. Due to the enormous size of the flow diagram it was opted to cut the diagram into multiple sections. The functional flow diagram can be seen in Figure 3.1, Figure 3.2 and Figure 3.3. In the diagrams it can be seen that the functionality is divided into a certain hierarchy of functionality, with on top being the 12 phases (indicated in the yellow circles) and below in the green boxes the tasks that need to be performed in order to complete the functionality under its phase. In the orange boxes the subs tasks are depicted that need to be completed in the indicated order to complete a task (green box). The functionality is not by all means complete as this project only aims to deliver a preliminary design, all the functionality of a finished design is not in the diagram.

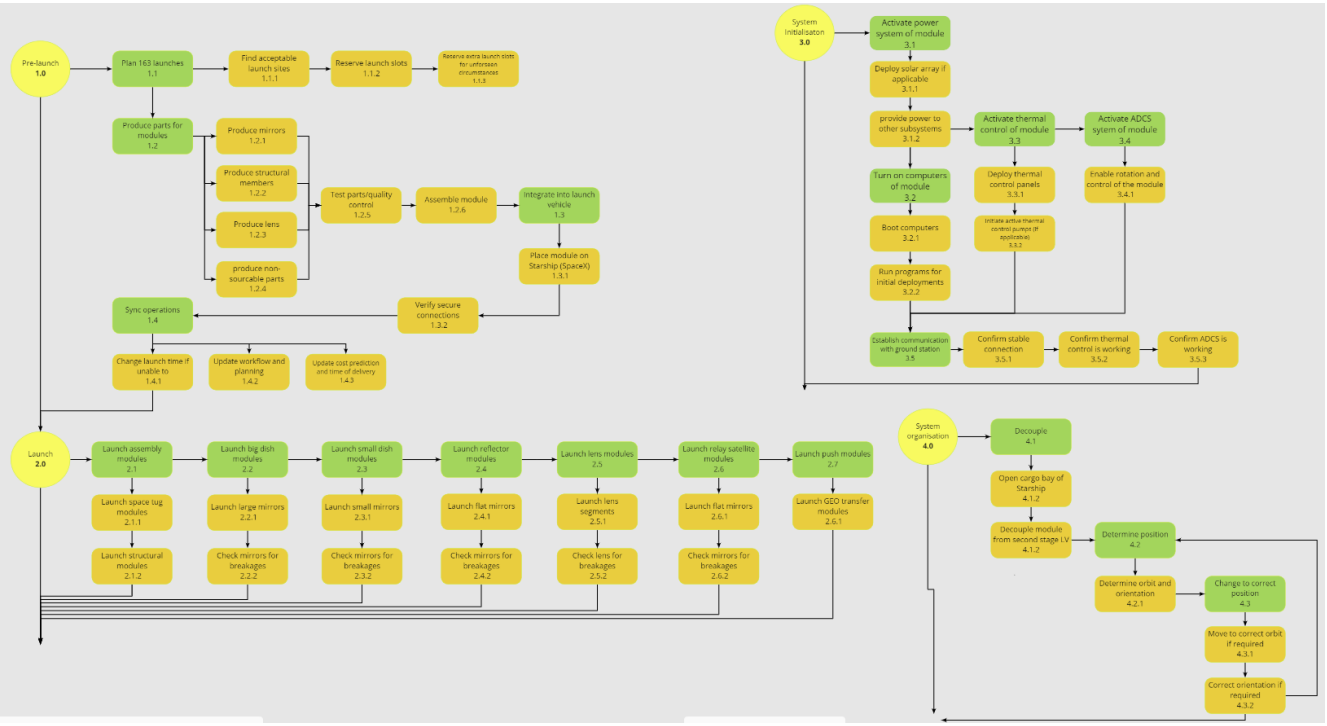

Figure 3.1: Functional Diagram of the IKAROS system 1/3

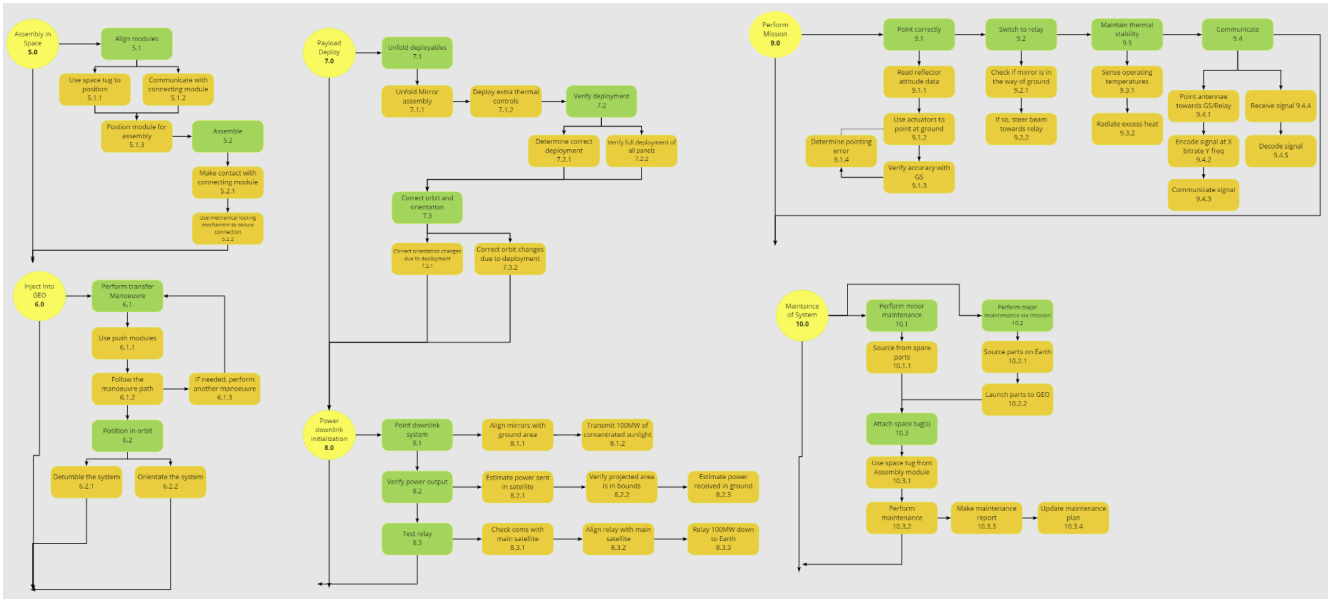

Figure 3.2: Functional Diagram of the IKAROS system 2/3

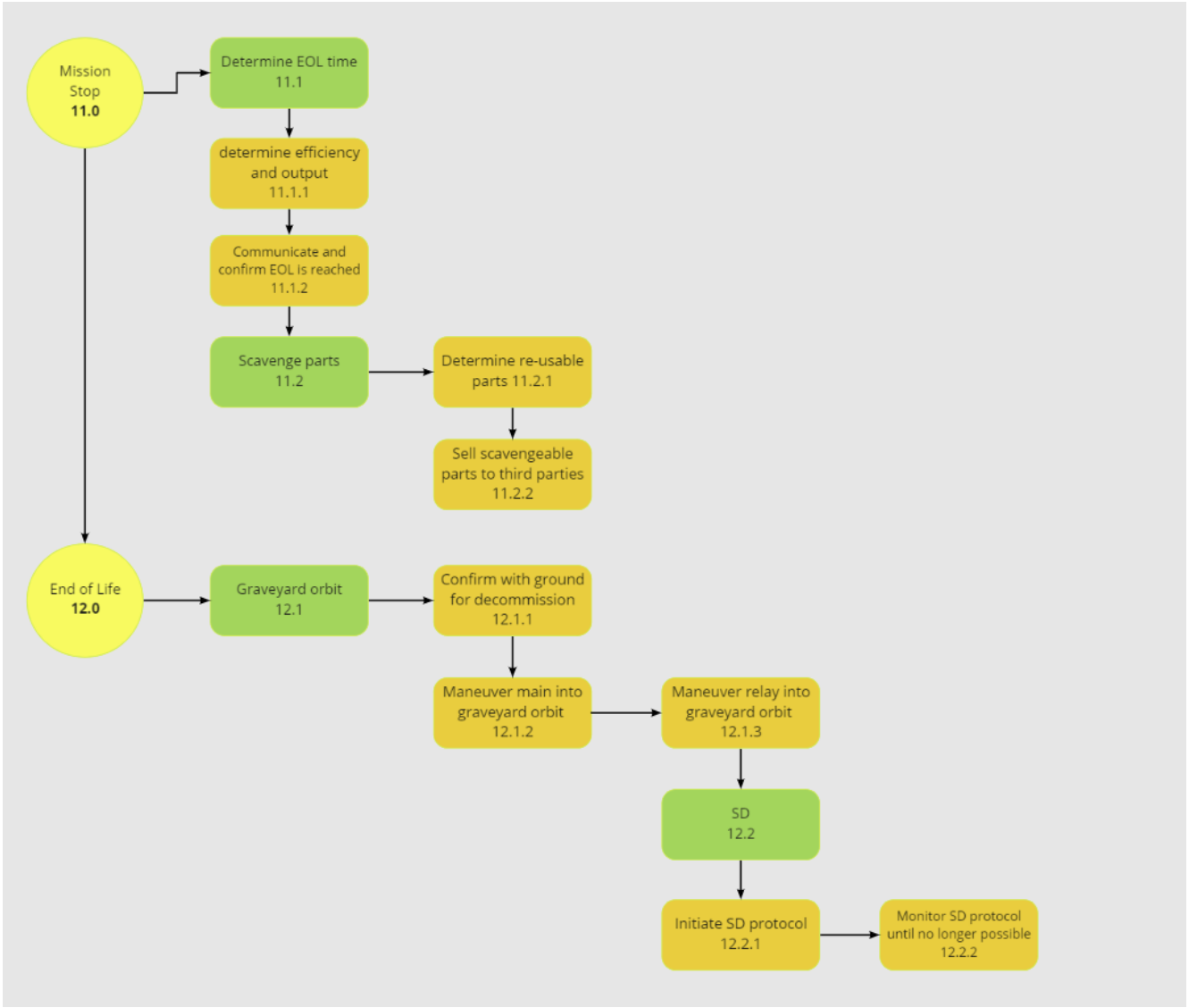

Figure 3.3: Functional Diagram of the IKAROS system 3/3

3.2. Functional Breakdown Structure

This section features the functional breakdown structure of the IKAROS system. Although similar to the functional flow diagram it does not depict the flow of the functionality of the system. The main purpose of this diagram is to show the breakdown of the functionality and thus it is also more detailed than the functional flow diagram. It also has a hierarchy structure to it where the yellow circles again depict the different functional phases and the green boxes the different tasks that belong to each phase. The orange boxes are again the sub tasks that need to be completed before its above task is completed. There is however in this diagram a new grey box that work out in more detail the functionality of each sub task and is thus another layer in the hierarchy structure.

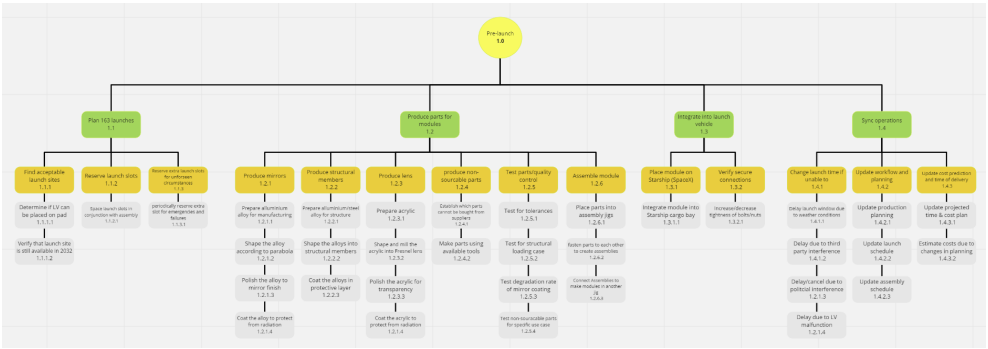

Figure 3.4: Functional Breakdown of the IKAROS system 1/9

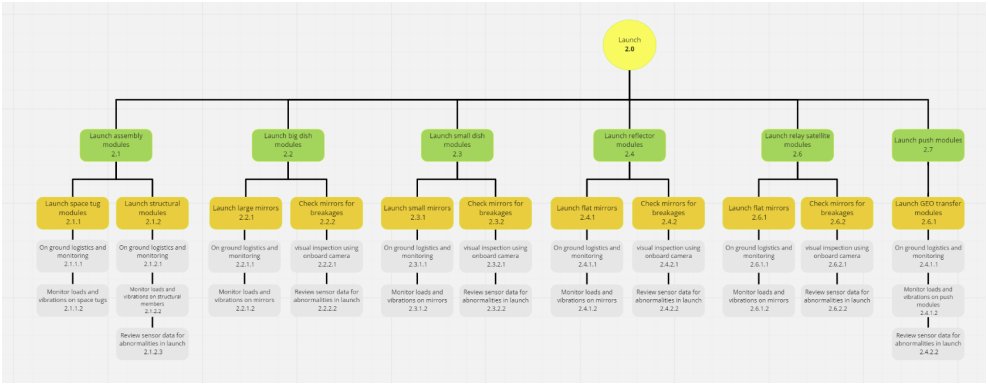

Figure 3.5: Functional Breakdown of the IKAROS system 2/9

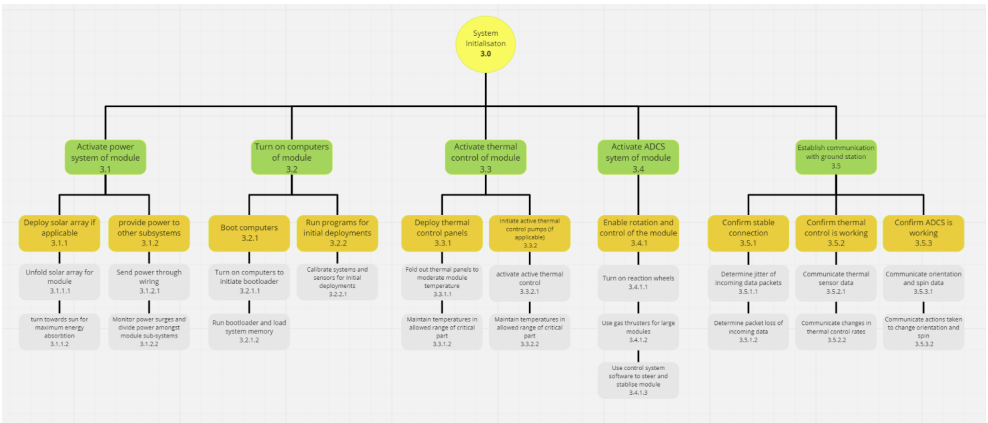

Figure 3.6: Functional Breakdown of the IKAROS system 3/9

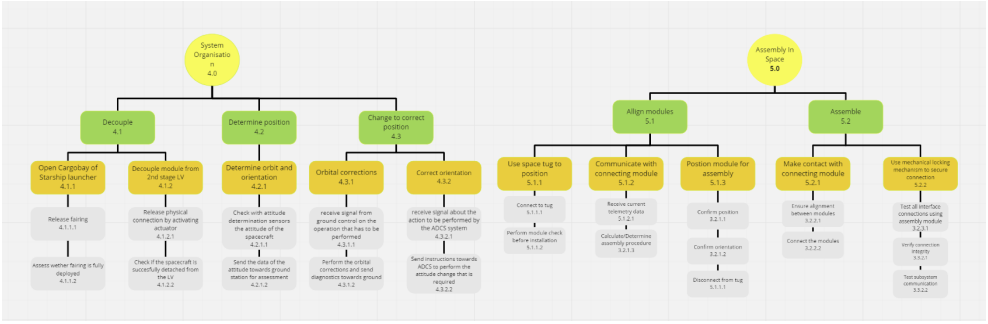

Figure 3.7: Functional Breakdown of the IKAROS system 4/9

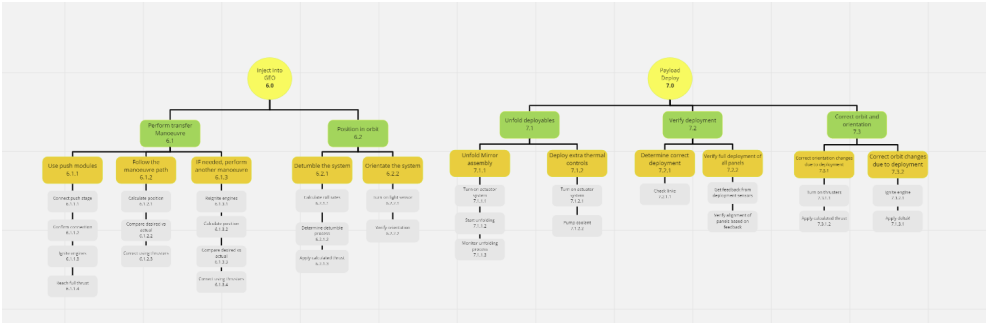

Figure 3.8: Functional Breakdown of the IKAROS system 5/9

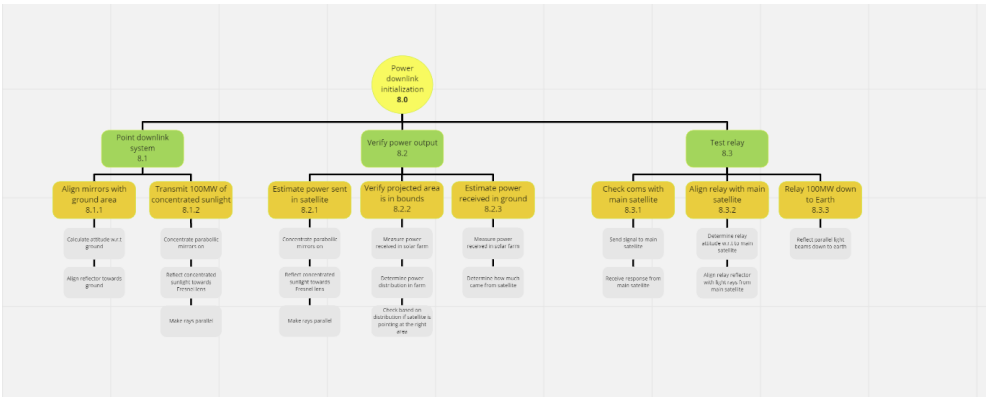

Figure 3.9: Functional Breakdown of the IKAROS system 6/9

Figure 3.10: Functional Breakdown of the IKAROS system 7/9

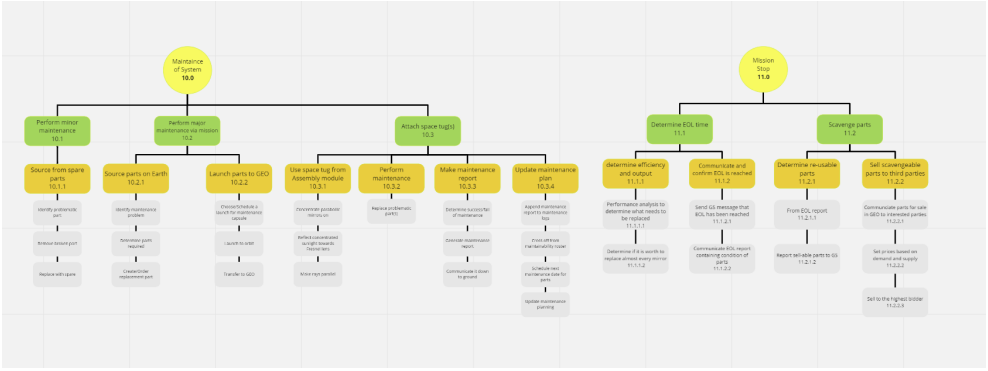

Figure 3.11: Functional Breakdown of the IKAROS system 8/9

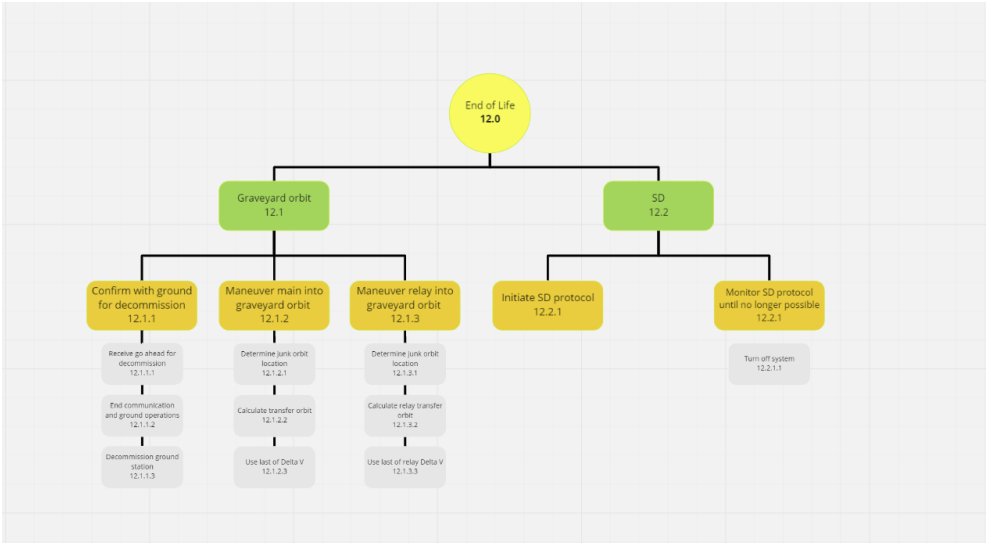

Figure 3.12: Functional Breakdown of the IKAROS system 9/9

4
Power Downlink

This chapter will provide the reader with the steps taken during the design of the downlink subsystem. Section 4.1 will provide the necessary information on the basic functioning and nomenclature of the system to allow the reader to develop a general understanding of the functionality. Section 4.2 will discuss various design problems that have to be overcome along with the requirements that could be drawn up from these problems. Section 4.3 discusses the solutions to the design problems and the methods that were used in order to solve them.

4.1. General Nomenclature and Axis-system

The design of the power downlink system is interconnected with many of the other subsystems: for example, the general layout of the modules related to the downlink will influence structural aspects of the system as well as ADCS, thermal control might constrain the sizing of some of the modules etc.
The downlink subsystem is thus of very high importance, and a basic understanding of its functionality is critical before continuing with the description and explanation of the various subsystems. A brief overview:

The satellite orbits in GEO, and is always situated above the same location on the surface of the Earth. A large reflective parabolic dish (paraboloid) is oriented towards the Sun and receives its parallel[i] rays, focusing them - as paraboloids do - on a focal point located some distance along the dish's "polar" axis. This focal point is shared by a smaller parabolic dish, facing the opposite direction, which receives the now diverging rays from the focal point and - again, as paraboloids do - collimates them and reflects them back towards the large dish. Luckily, due to the amazing foresight of the engineers involved in this project, a small circular hole was made at the center of the large dish, allowing the collimated beam to pass through and beyond the large dish. On a sidenote: around this hole, a strip or ring of Photovoltaic cells is placed to produce enough power for the S/C bus itself.
Back to the beam of light: some distance beyond the large dish the beam is received by a flat reflector, which can rotate appropriately to direct the beam towards the desired location on Earth. Since at certain moments during the orbit, the large dish will be blocking the desired location from view for the reflector, a second flat reflector is added to the system, situated at some offset distance on the plane described by the circular rim of the large dish. Now, whenever necessary, the first reflector can direct the beam to the second reflector, which can in turn direct it to the earth.

Likely, the many mentions of large and small parabolic dishes, first and second reflectors seem somewhat confusing, to remedy this some of the main modules were given names, allowing for easy reference and to avoid further confusion. From now on the large parabolic dish will be referred to as the Queen, the small dish as the Worker, the cleverly placed hole in the center as the Aperture, the first reflector as the Sting, and the second relay reflector as the Relay. The Queen and Worker can be grouped under *parabolic dishes* and the Sting and Relay can be grouped under *reflectors*. An overview of the general layout and nomenclature is provided in Figure 4.1.
Furthermore, a general coordinate system was drawn up to make sure that all subsystems are on the same page, this one can be found in Figure 4.2 although it should be noted that the figure does not aim to provide a location for the origin.

[i] Or are they? More on this topic will be briefly discussed in subsection 4.2.3

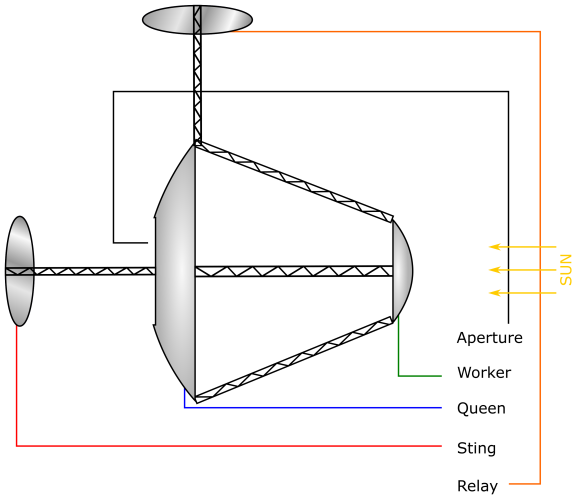

Figure 4.1: Nomenclature for the main modules of the system

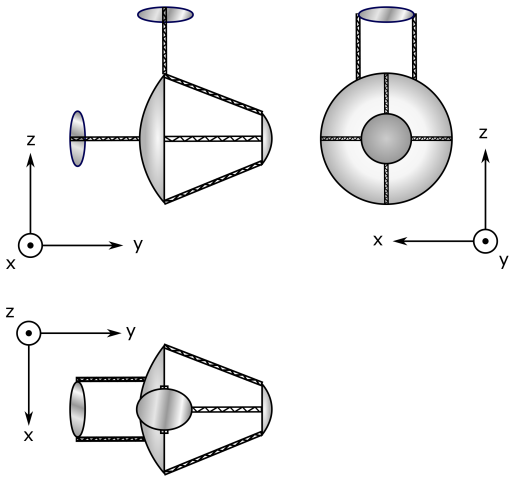

Figure 4.2: Body reference axes for the system

4.2. Problem Description and Requirements

4.2.1. Blind spot Mitigation

As mentioned in Section 4.1 the layout of the downlink subsystem will have to cope with blind spots, but how and why exactly?

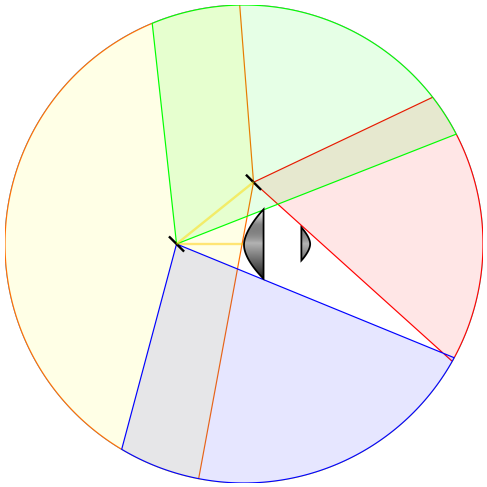

(a) General overview of blind spot mitigation [ii]

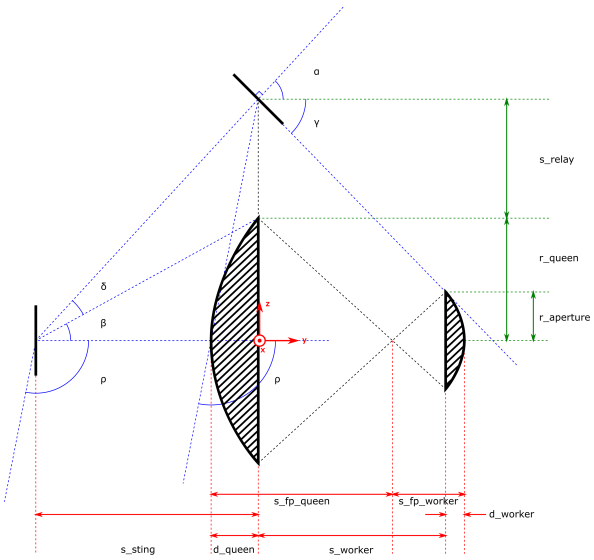

(b) Relevant parameters related to blind spot mitigation

Figure 4.3: Blind spot mitigation diagrams.

Figure 4.3a shows the basic problem and its solution: in the center, the parabolic dishes can be seen, with the reflectors drawn as simple lines. The plane in which these modules are situated is the system's y, z-plane, for now assume that this plane is coinciding with the equatorial plane[iii]. Let's start by having a beam needing to be directed towards 6 o'clock (in the blue zone: 4 - 7 o'clock): the Sting is perfectly capable of doing this. However, a few arcminutes later the Sting would have to be impractically large in order to redirect the entire beam, since the radius of a reflector is inversely related to the cosine of the

[ii] The colours aim to clarify different zones/periods for the type of reflector that is being used. In reality, the system will not provide Disco lighting.

[iii] *i.e.* the plane in which the satellite orbits Earth, subsection 4.2.2 will explain why this is not the case, but also why this assumption has no (significant) influence on the blind spot mitigation.

angle it has to turn to. The Sting instead opts to direct the beam towards the Relay, which is capable of redirecting it over the range of the yellow zone (7 - 11 o'clock). As soon as the Sting is able to *do the job* on its own again, it stops directing the beam to the Relay and instead directs it over the range of the green zone (11 - 2 o'clock), which is a mirrored image of the blue zone. At some point now, the beam will encounter the Queen, thus the Sting sends the beam to the Relay, which can redirect it to various locations, spanning the red zone (2 - 4 o'clock) until it encounters the Worker, at which point the Sting takes over again and the process has come full circle.

Having this general idea of how and why the system will encounter these blind spots, it is now important to understand the relations between the blind spots and the values related to the layout of the system. Figure 4.3b provides an overview, using the coordinate system from Figure 4.2, where for now the origin is placed at the center of the circle described by the rim of the Queen.

There are the following parameters of importance:
Queen radius (r_{Queen}) is the intake radius of the Queen, it is related only to the amount of power required for the system and the overall efficiency of the system. Aperture radius ($r_{Aperture}$) equals the radius of the Worker and is constrained by the thermal control subsystem (refer to Chapter 10). Queen depth (d_{Queen}) and Worker depth (d_{Worker}) are the maximum depths of the Queen and Worker respectively. For now, they are arbitrary with the exception that the ratios between radius and depth of the parabolic dishes have to be equal, as in Equation 4.1. The shape of the parabola is then given by Equation 4.2, where 'sign' denotes the direction towards which the parabola faces (a positive sign conveying a parabola facing towards the left, or negative y):

$$\frac{d_{Queen}}{r_{Queen}} = \frac{d_{Worker}}{r_{Aperture}} \tag{4.1}$$

$$d(z) = sign \cdot d_{max}(1 - \frac{z^2}{r^2}) \tag{4.2}$$

The *rim-to-rim* distance between the Queen and Worker (s_{Worker}) is related to their focal lengths as in $s_{Worker} = s_{fp,Queen} - d_{Queen} + s_{fp,Worker} - d_{Worker}$ where the focal length of a parabola (or paraboloid for that matter) can be found by Equation 4.3, yielding the focal length of the Queen ($s_{fp,Queen}$) and Worker ($s_{fp,Worker}$).

$$s_{fp,parabola} = \frac{r^2_{parabola}}{4 \cdot d_{parabola}} \tag{4.3}$$

The offset of the Sting (s_{Sting}) and Relay (s_{Relay}) are arbitrary for now and not influenced by anything yet, however they influence the various angles related to the blind spots.

β and δ are the angular sizes of the Queen radius and the Relay offset respectively, as seen from the Sting. α is the sum of these angles, or alternatively, for some more convenient formula's, δ is the difference between α and β. The angles are given by Equation 4.4 to 4.6.

$$\alpha = \arctan\left(\frac{r_{Queen} + s_{Relay}}{s_{Sting}}\right) \tag{4.4}$$

$$\beta = \arctan\left(\frac{r_{Queen}}{s_{Sting}}\right) \tag{4.5}$$

$$\delta = \alpha - \beta = \arctan\left(\frac{r_{Queen} + s_{Relay}}{s_{Sting}}\right) - \arctan\left(\frac{r_{Queen}}{s_{Sting}}\right) \tag{4.6}$$

ρ (the driving angle for the sizing of the Sting) is related to the Relay offset, Queen radius and Queen depth, as stated in Equation 4.7, since the Sting has at least to be able to transmit the beam to an angle that lies outside of a blind spot for the Relay.
γ defines the start of a blind spot for the Relay and is related to the Worker offset, Aperture size, Queen radius and Relay offset. It is given by Equation 4.8

$$\rho = \frac{\pi}{2} + \arctan\left(\frac{d_{Queen}}{r_{Queen} + s_{Relay}}\right) \quad (4.7) \qquad \gamma = \arctan\left(\frac{r_{Queen} + s_{Relay} - r_{Aperture}}{s_{Worker}}\right) \quad (4.8)$$

Having specified these parameters, some requirements can be drawn up concerning blind spot mitigation.

- **SSR.DOWN.BLIND.1**: The downlink layout will allow for a 360° range in which the power can be transmitted.
- **SSR.DOWN.BLIND.2**: The angle γ shall be $\geq \beta$ related to blind spot mitigation.
- **SSR.DOWN.BLIND.3**: The Sting reflector shall be sized to allow for redirecting the power under an angle of ρ.
- **SSR.DOWN.BLIND.4**: The Relay reflector shall be sized to allow for redirecting the power under an angle of $\frac{\pi-\delta}{2}$ and $\frac{\pi-\rho+\alpha}{2}$.

4.2.2. Equatorial Alignment

In subsection 4.2.1 it was hinted at that the equatorial plane does not coincide with the system's y,z-plane, the reason for this is of course the axial tilt of the earth's axis relative to the ecliptic plane[iv]. This tilt results in an angle of 23.44° between the equatorial plane and the ecliptic plane, a visualisation is given in Figure 4.4.

The Sting and Relay thus have to perform their blind spot mitigation in the equatorial plane and not the systems y,z-plane.
But why not have ADCS rotate the entire system around its y-axis and resolve this problem? Granted, in the situation illustrated in Figure 4.4, this would work, however imagine the situation during the summer solstice: no rotation around the system's y-axis can solve the problem now. A single rotation around the z-axis or a series of rotations around body axes x and then y can align the 2 planes, however the system's y-axis has to point towards the Sun at all times in order to properly focus an collimate the incoming rays. In fact, the orientation relative to the y,z-plane will precess over 360° during the course of a year. Thus, the required rotations will have to be provided by the individual reflectors themselves. An impression of the range in which they will have to be able to transmit the beam of energy is provided in Figure 4.5, one can imagine this as the equatorial plane being rotated 360° around the ecliptic's normal.

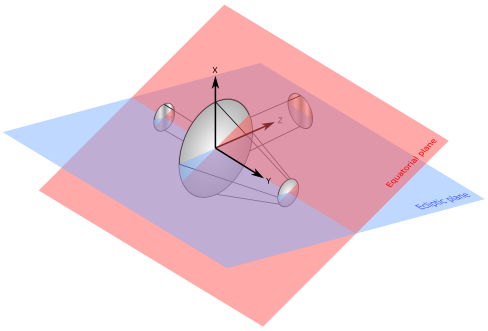

Figure 4.4: Example of equatorial and ecliptic plane alignment. Showing the orientation during the autumn equinox.

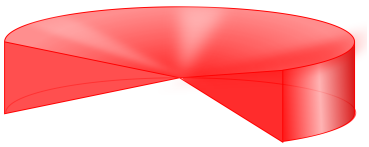

Figure 4.5: Section of the required field of view (FOV) for a reflector

How does this influence the blind spot mitigation discussed in subsection 4.2.1? One could think this makes the issue much more complicated, after all, the intersection of the equatorial plane and the system is now continuously changing. This is true, however the largest intersection would be the one displayed

[iv] The plane in which Earth orbits the Sun.

in Figure 4.3b, and having mitigated the blind spots for this situation, it can be assured that all other situations are covered as well.

The following requirement can now be drawn up:

- **SSR.DOWN.FOV.1**: The reflectors shall be able to direct the beam over the equatorial plane, during any time of the year.
- **SSR.DOWN.FOV.2**: No more than 0.15 days/year downtime shall be used for aligning the FOV of the reflectors
- **SSR.DOWN.FOV.3**: The reflectors shall have a pointing accuracy equal to at least 2 arcseconds.
- **SSR.DOWN.FOV.4**: The reflector actuators shall not induce a torque larger than 23.7 kNm.

4.2.3. Ground Station

The ground station is responsible for converting the concentrated sunlight on the ground to a useful medium that can be sold to a customer. To fulfil this task, certain problems have to be overcome.

A problem that arises is the limit in pointing accuracy imposed on the satellite by the C&DH, as presented in Chapter 12. In short, the C&DH can measure the system's relative position to the ground station with an accuracy of 2 arcseconds. This will inevitably lead to the beam over or undershooting the target area, possibly by around 350m. The design of the ground station thus must incorporate a measure to ensure the full energy of the beam is collected. Another problem in the chain that is encountered is the increase in spot size at the surface of the earth. This increase in spot size is due to the diverging nature of the beam that exits the Aperture of the Queen, as it does not consist of perfectly parallel rays. To quantify this divergence of the beam the possible sources of divergence must be identified and evaluated. Upon inspection, there are three main sources of error in the beam collimation:

- Parabola discretisation: the Queen will not be a continuous paraboloid, therefore rays will not be perfectly concentrated and collimated.
- Diffraction: the phenomenon where waves start diverging after passing through a hole.
- Natural divergence: if the sun is modelled as a point source, the rays reaching the earth will be slightly diverging.

The first one is the discretisation of the parabola. As will be discussed in Chapter 9, the Queen's surface will not be continuous, rather being composed of individual "strips" that are put on increasing angles from the inside out to approach the reflective properties of a perfect parabola whilst avoiding the structural complexity of a continuous sloped interface of such size. Being an approximation, the reflections will thus never be perfect, and an aberration will form around the focal point. As a resultant of this aberration the rays of light will be slightly off on the second parabola, making their reflection slightly diverging, depending on the width of these strips.

The second kind of divergence happens due to a phenomena called diffraction. This phenomena occurs when a wave of light is forced through an opening such as the Aperture of the Queen. The light bends around the corners of the Aperture, causing a slight diffraction, the minimum diffraction angle is given by Equation 4.9.

$$\theta_{min} = \frac{1.22\lambda}{2r_{aperture}} \tag{4.9}$$

Where λ is the wavelength. This phenomenon only significantly influences apertures in the order of magnitude of the wavelength of the wave. Thus the Aperture should be larger than that, but quick inspection of the spectral composition reveals that the highest wavelength lies in the order of thousands of nanometers, several orders of magnitude of the expected Aperture size in the order of tens of meters.

The third kind of divergence is due to the inherent divergence of sunlight which occurs as the rays get smeared out over a larger and larger area as they travel farther away from the sun. Due to the appalling

lack of literature on this subject, the divergence was calculated indirectly from the solar flux distribution throughout the solar system. The difference in solar flux between to two planets located furthest from the sun results in a decent approximation for the natural divergence. Imagine the power going through a circular area of $1m^2$ at Uranus, how much larger would the radius of a circular area near Neptune have to be to accommodate the same amount of power? The difference between the two radii over the distance between the two planets yields an approximation of the natural divergence.

From these three problems the following ground station requirement come forth:

- **SSR.DOWN.GROUND.1**: The ground station shall have no operational downtime.
- **SSR.DOWN.GROUND.2**: The ground station shall accommodate a pointing accuracy of 2 arcseconds.
- **SSR.DOWN.GROUND.3**: The ground station shall accommodate a spot size with a radius equal to the Aperture radius

4.3. Design Analysis

4.3.1. Meteorological Effects

Going into the design analysis of the downlink subsystem, a first question that might spontaneously arise is: *"The system sends down sunlight, so what if it is cloudy?"*
It turns out that the weather conditions will not influence the performance of the system much, but rather the system will influence the weather conditions. Simply put, the energy transmitted from the satellite can (although not instantaneously) evaporate clouds, afterwards the air would be heated up, creating a high pressure zone around which clouds would be repelled. However, regions around the ground station will experience an increase in rainy days.

4.3.2. System Layout

The layout of the design is naturally heavily influenced by the Queen's exact size, which in turn influenced the layout of the Worker and reflectors (subsection 4.2.1). The Queen's radius is dependent on the amount of power required, following the relation from Equation 4.10.

$$A_{in,Queen} = \pi r_{Queen}^2 = \frac{P_{required}}{1362} \tag{4.10}$$

Where 1362 is the value of the solar flux ($[W/m^2]$) near Earth.

Two things need to be remembered now: some of the intake area is lost to the Aperture, as in the Worker is blocking some of the incoming radiation. In addition to that, recall that a ring of Photovoltaic cells was placed around the Aperture to provide the spacecraft with electricity. The Queen radius will thus have to accommodate both the power required for the system as well as the power that needs to be delivered on Earth. Figure 4.6 gives an overview of the relevant parameters.

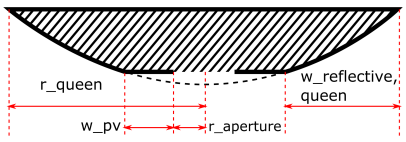

Figure 4.6: Sketch of the various parameters involved in the Queen radius.

w_{pv} is the width of (one half) of the *Saturn ring* of PV cells and $w_{reflective,Queen}$ is the required width for the intake area needed for reflecting rays to the Worker. The PV-width can be written as an quadratic function, given in Equation 4.11.

$$\begin{aligned} A_{pv} &= \pi(w_{pv} + r_{Aperture})^2 - \pi \cdot r_{Aperture} \\ \Leftrightarrow 0 &= \pi \cdot w_{pv}^2 + 2\pi r_{Aperture} \cdot w_{pv} - A_{pv} \end{aligned} \tag{4.11}$$

To find $w_{reflective,Queen}$, the same procedure can be followed, introducing $A_{reflective,Queen}$ corresponding to the area of the *Saturn ring* with width $w_{reflective,Queen}$[v]. The Queen radius is then simply the sum of $r_{Aperture}$, w_{pv} and $w_{reflective,Queen}$.
The required power for the downlink and PV-module are easily calculated using $P_{required} = \frac{P_{out}}{\eta_{total}}$, where η_{total} for the solar cells simply equals the solar cell efficiency, whilst for the downlink it equals $\eta_{total} = \eta_{reflective,Queen} \cdot \eta_{reflective,Worker} \cdot \eta_{reflective,reflectors} \cdot \eta_{atmosphere} \cdot \eta_{Groundstation}$. Actual values will be discussed later.

Having a set Queen radius, the process of configuring the system's layout continues. From subsection 4.2.1 the angles involved in blind spot mitigation were all dependent on values for several distances (e.g. s_{Sting}, s_{Relay}, d_{Queen}). Most of these are thus 'free' to choose, however random values would result in a completely arbitrary layout. To give the process a sense of direction, it was chosen to make it strive to minimise the mass. This was done by assigning some weights[vi] to a few basic parameters from the system layout. Referring to Figure 4.1, the chosen parameters were:

- 4 times the truss length from Queen to Worker, multiplied by $m_{truss,QW}$ [kg/m].
- 2 times the truss length from Queen to Sting, multiplied by $m_{truss,QS}$ [kg/m].
- 2 times the truss length from Queen to Relay, multiplied by $m_{truss,QR}$ [kg/m].
- The area of the Queen paraboloid multiplied by m_{foil} [kg/m^2].
- The area of the Queen paraboloid multiplied by $m_{structure}$ [kg/m^2].
- The area of the Worker paraboloid multiplied by m_{mirror} [kg/m^2].
- The area of the Sting multiplied by m_{mirror} [kg/m^2].
- The area of the Relay multiplied by m_{mirror} [kg/m^2].

Now that the weights and goal are defined, the process can start. Using as constants r_{Queen} and r_{Worker}, and variables d_{Queen}, s_{Relay} and s_{Sting}.

Beginning with varying the depth of the Queen to obtain a Worker offset. A maximum Queen depth can be chosen corresponding to a situation where the focal point would lie in the plane described by the Queen's rim: $s_{fp,Queen} = d_{Queen}$. Equation 4.3 can be rewritten to obtain a maximum depth of $\frac{r_{Queen}}{2}$. Having this range between 0 and the maximum depth, the Relay offset will now be varied (setting a realistic upper bound through several iterations), this provides enough information to obtain the angles γ and ρ. Varying the Sting offset is the next step, an upper limit can be obtained by differentiating δ from Equation 4.6, as can be seen in Equation 4.12.

$$\delta'(y) = \frac{r_{Queen}}{y^2\left(\frac{r_{Queen}^2}{y^2} + 1\right)} - \frac{r_{Queen} + s_{Relay}}{y^2\left(\frac{r_{Queen} + s_{Relay}^2}{y^2} + 1\right)} \tag{4.12}$$

The y-value (*i.e.* Sting offset) where $\delta'(y)$ is zero corresponds to a maximum δ, which is advantageous for the sizing of the Relay, further increasing the offset will only decrease δ and increase structural mass of the trusses. The Sting offset is thus varied up to that y-value, yielding enough information to obtain angles α, β and δ according to Equation 4.4 to 4.6. The angles obtained from mitigating the blind spots can now be used to size the reflectors, which will be elliptically shaped in an effort to reduce their mass, the radii of a reflector, as well as the area corresponding to those radii, are given by Equation 4.13 to 4.15.

[v] $A_{reflective,Queen}$ is thus not the reflective area of the Queen paraboloid! It is the intake area used for the concentration of the sunlight etc.
[vi] As in *weights* for a *weighted score*, but in this case it could also be taken literally.

$$r_{long,reflector} = \frac{r_{Aperture}}{\cos(\Delta\theta_{max,reflector})} \quad (4.13) \qquad r_{short,reflector} = \frac{r_{Aperture}}{\cos(\theta_{tilt})} \quad (4.14)$$

$$A_{reflector} = \pi \cdot r_{long,reflector} \cdot r_{short,reflector} \quad (4.15)$$

Where θ_{tilt} relates to the earth's axial tilt. $\Delta\theta_{max,Relay}$ and $\Delta\theta_{max,Sting}$ (both drawn to be 0 in Figure 4.3b) convey the maximum angle the Relay and Sting will have to turn to. The angles are given in Equation 4.16 and 4.17.

$$\Delta\theta_{max,Relay} = \max\left(\left|\frac{\pi-\delta}{2}\right|;\left|\frac{\pi-\rho+\alpha}{2}\right|\right) \quad (4.16) \qquad \Delta\theta_{max,Sting} = \left|\frac{\rho}{2}\right| \quad (4.17)$$

So now there are three variables, d_{Queen}, s_{Relay} and s_{Sting}, given as ranges in which each of these three can vary, and yielding all values needed to obtain a weighted score for the system layout.
Of course, manually calculating each single combination of these three ranges would be infeasible, so instead a computer program does this by *brute force*. Some conditionals were also added, namely: The radius of a reflector cannot be larger than its offset, to allow for 360° rotations.

Some assumptions have to be listed:

1. When the Sting is directly beaming the rays to the desired location, the Relay will not cast a shadow (this is relevant for the green zone in Figure 4.3a).
2. For the configuration of the various angles toward which the beam will have to be sent, the width of the beam will be assumed to be zero, *i.e.* the beam is a ray going from the center of a reflector (to the center of another reflector). In order to somewhat mitigate this assumption a safety margin angle of 5° was introduced, e.g.: $\rho = \rho + 5°$.
   Of course, for the sizing of the radii of the reflectors, this assumption will be lifted.
3. The Queen will be considered as a full paraboloid, no Aperture present.

In a first iteration the weight values for trusses were all set equal to be 1500 ([kg/m]), whilst the masses of a rigid mirror and reflective foil were set to 15 and 0.3 ([kg/m^2]) respectively[vii]. The supporting structure for the Queen was first estimated at 100 ([kg/m^2]). After some *back and forth* iterations between the downlink layout and structural subsystem, the final weights were set to be: $m_{truss,QW} = 3$, $m_{truss,QS} = 1500$, $m_{truss,QR} = 3000$, $m_{mirror} = 15$, $m_{foil} = 0.3$ and $m_{structure} = 20$.

Using a PV-area of 544m^2 and an Aperture radius of 25m (obtained from EPS and thermal control subsystems), a resulting Queen radius of 482m was obtained using efficiencies $\eta_{reflective,Queen} = 0.91$, $\eta_{reflective,Worker} = \eta_{reflective,reflectors} = 0.94$, $\eta_{atmosphere} = 0.55$ and $\eta_{Groundstation} = 0.24$[viii].

This can be translated into the final layout of the system, given in Figure 4.7 and Table 4.1.

[vii] Estimates based on the ISS main truss, space-telescope mirrors and metalised polyimide films (like mylar or Kapton®).
[viii] Spoiler alert for subsection 4.3.4 where this efficiency will be explained.

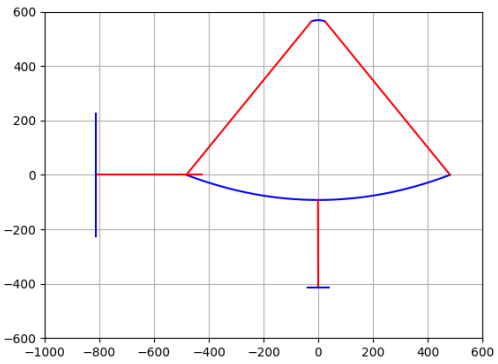

Figure 4.7: Final layout of the downlink system.

Module	**Queen**	**Worker**	**Sting**	**Relay**
radius [m]	482	25	37.91	226.86
radius (short)	-	-	26	26
area [m^2]	756054.63	2033.94	3040.96	18197.13
depth [m]	92.38	4.79	-	-
offset [m]	-	564.16	413.67	330.44
angles	α	β	γ	ρ
magnitude [°]	63.02	49.36	54.38	97.49
trusses	**Q-W**	**Q-S**	**Q-R**	
length [m]	726.04	321.29	387.17	

Table 4.1: Relevant values for the downlink system layout

4.3.3. Reflector Actuators

In order to size the reflectors' actuators, the space in which the reflectors have to redirect the beam of energy was defined in subsection 4.2.2, it corresponds to the equatorial plane tilted 23.44° w.r.t. the ecliptic plane and rotated a full 360° around the ecliptic's normal (refer to Figure 4.5). This space can easily be spanned by just two rotations around a reflector's body axes. The body reference system that will be used for a reflector is given in Figure 4.8, where $\boldsymbol{u}$ points outwards perpendicular to the reflective surface, $\boldsymbol{v}$ is perpendicular to $\boldsymbol{u}$ and aligned with the reflector's short radius (subsection 4.3.2), $\boldsymbol{w}$ is perpendicular to both $\boldsymbol{u}$ and $\boldsymbol{v}$ and points towards the positive direction for a rotation for $\boldsymbol{u}$ to $\boldsymbol{v}$. Finally, a distinction between the local and global system is made, where the local system rotates along with the body itself.

Two assumptions that have to be mentioned:

1. In reality the equatorial plane will intersect the system's y,z-plane (Figure 4.4) through the system's center of gravity, which would create an offset between the center of the reflectors' FOV and the equatorial plane. This is not taken into account, however mitigating this would consist of simply lightly increasing or decreasing the rotation.
2. The reflectors have an infinitesimally small pointing accuracy.

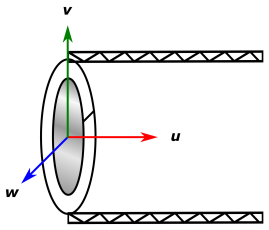

Figure 4.8: Body reference system for reflectors

The method of pointing the reflectors is relatively straightforward. The desired direction of the beam can be modelled as a vector $\boldsymbol{u'}$, rotated globally around $\boldsymbol{w}$ and then $\boldsymbol{v}$, rotating the vector from the ecliptic to the equatorial plane, followed by a local rotation around $\boldsymbol{v}$ to point it in the right direction within the equatorial : $R_v R_w \boldsymbol{u'} R_v$. With R_v and R_w being rotation matrices for rotations around $\boldsymbol{v}$ and $\boldsymbol{w}$ respectively, and pre-multiplication is used for global transformations, whilst post-multiplication is used for local transformations. To align our body axis $\boldsymbol{u}$ with this vector in two rotations, the angles between $\boldsymbol{u'}$ w.r.t. the $\boldsymbol{u,v}$- and $\boldsymbol{u,w}$-planes have to be found[ix]. This can be done using the dot product between those planes' normals (obtained through the cross product of their unit vectors) and $\boldsymbol{u'}$, following Equation 4.18.

$$\boldsymbol{u'} \cdot \boldsymbol{n} = |\boldsymbol{u'}| \cdot |\boldsymbol{n}| \cdot \cos(\theta) \Longleftrightarrow \theta = \arccos\left(\frac{\boldsymbol{u'} \cdot \boldsymbol{n}}{|\boldsymbol{u'}| \cdot |\boldsymbol{n}|}\right) \tag{4.18}$$

There is now a combination of rotations around local axis that aligns $\boldsymbol{u}$ with $\boldsymbol{u'}$, given by: $\boldsymbol{u'} = \boldsymbol{u} R_{v,\theta_v} R_{w,\theta_w}$.

To find the power and torque required for the rotary actuators that will perform these rotations, Equation 4.19 and 4.20 can be used.

[ix] For the explanation given here, the body axis will be aligned with $\boldsymbol{u'}$ because of the slightly more convenient documentation for that process. Bear in mind that in reality the beam would have to be redirected, in practise this simply means that the angles for required rotations would have to be halved.

$$T = \ddot{\theta} I \quad (4.19) \qquad P = T\omega \quad (4.20)$$

With $\ddot{\theta}$ the angular acceleration, I the moment of inertia around the axis of rotation and ω the angular velocity. So which are the critical rotations that have to be performed? Have a look at the Sting in Figure 4.3a: the first critical rotation happens when the Sting has to direct the beam from $-\rho$ to α, switching between direct transfer and transfer using the Relay. The rotation thus has the magnitude $\theta_1 = \frac{\alpha}{2} + \frac{\rho}{2}$.
The same is done for all instances where the beam switches from direct transfer to Relay transfer and vice versa. The following angles are found: $\theta_1 = \frac{\alpha}{2} + \frac{\rho}{2}$, $\theta_2 = \frac{\rho}{2} - \frac{\alpha}{2}$, $\theta_3 = \frac{\delta}{2}$ and $\theta_4 = \frac{-\beta}{2} + \frac{-\alpha}{2}$.
Following requirement **SSR.DOWN.FOV.2** of 0.15 days/year of downtime for allowing for these rotations we have a time frame of 35.5 seconds each day. It would be nice if we could divide this timeframe among the various rotations in such a way that all rotations require the same amount of power. Knowing the relations between an angle, time, angular velocity and acceleration, and noting the presence of the last two in Equation 4.20, an estimate for dividing the time proportionally was made using Equation 4.21.

$$t_{\theta_n} = c \cdot 35.5 \cdot \left(\frac{\theta_n}{\Sigma\theta}\right)^{\frac{2}{3}} \quad (4.21) \qquad \ddot{\theta}_n = \theta_n \cdot \left(\frac{2}{t_{\theta_n}}\right)^2 \quad (4.22) \qquad \omega_n = \ddot{\theta}_n \cdot \left(\frac{t_{\theta_n}}{2}\right) \quad (4.23)$$

Where $\Sigma\theta$ denotes the sum of all critical angles. With some trial and error, a value for c of $\frac{2}{3}$ was found to have a very close match, *i.e.* assigning timeframes to the angles with Equation 4.21 using $c = \frac{2}{3}$ and then summing up those timeframes results in a downtime of 35.0 seconds. The respective times are: $t_{\theta_1} = 14.9$s, $t_{\theta_2} = 5.4$s, $t_{\theta_3} = 2.9$s and $t_{\theta_4} = 11.8$s.

Some more assumptions should now be listed:

1. Only rotations around body $\boldsymbol{v}$-axis will be considered, they will be critical.
2. A rotation starts and ends with zero velocity.
3. Rotations with constant velocity require no power or torque.

Finding the mass moment of inertia for the Sting is done using $I_v = \frac{1}{4} \cdot m_{mirror} \cdot \pi \cdot r_{large}^3 \cdot r_{small}$, with m_{mirror} being the estimate of 15 kg/m^2. The accelerations and velocities are found using Equation 4.22 and 4.23. Thus the power required for the rotations (which is the same for each one, due to our time division) is 79 kW with a maximum occurring torque of 955.96 kNm.

The same process is followed for the Relay, finding one critical rotation for which a power of 0.14 W and a torque of 291.9 Nm will be required.

In order to have somewhat realistic and achievable values, a gearbox could be introduced: gear reductions can decrease the amount of torque required by increasing the rotational speed of the motor's shaft, the power required would still remain the same[x]. For example, for the Sting a gear reduction of 1/650000 would result in a required torque of only 1.54 Nm, and a shaft rotation of 360° would equal a Sting rotation of 2 arcseconds. There is another advantage however, the ability to possibly connect and disconnect from the gearbox can be helpful as well: once a reflector is brought up to speed (around 360° per day) the gearbox could disconnect, leaving the angular momentum of the reflector to do all the work, and only connecting again for minor corrections until a critical rotation has to be performed.

4.3.4. Ground Station

The ground station used to convert the radiation to electricity will be of the type of a concentrated solar power plant, such a plant uses mirrors to concentrate sunlight onto a medium containing a molten salt mixture that efficiently converts it to heat that is consequently used to power a turbine. Since the satellite already provides a concentration factor, the concentration using mirrors on the ground will be omitted to avoid another reflective efficiency.

[x] As gearboxes are - unfortunately - not magical devices.

To size the ground station, the accuracy of the C&DH and the spotsize of the beam are the most influential factors, as discussed in subsection 4.2.3. The spotsize is a result of divergence, being a result itself of the discretisation, diffraction and natural divergence. Taking a look at diffraction and using Equation 4.9 with λ = 1000nm and $r_{Aperture}$ = 25, we have a value of 24E^{-9} radians, practically zero. The same goes for the value of natural divergence of sunlight, estimating it to be 1.13E^{-11} degrees. Whatever increase in size this will produce in the radius of the beam as in travels from GEO to Earth's surface will be in the order of single meters. Intuitively, it will be negligible compared to the increase in spotsize induced by the discretisation of the Queen paraboloid. However, without any advanced ray-tracing simulation of the concentration process using the exact structure from the satellite, there is no way of knowing how large this value will actually be.
Maybe the most important assumption of the entire project should be stated now:

1. The beam exiting the satellite is considered perfectly parallel, no divergence present. The spotsize on Earth equalling the size of the Aperture.
2. The beam will always have an angle of incidence equal to 0 with the earth's surface.

As one might remember from the Midterm Report, originally a (Fresnel) lens was involved in the power downlink to avoid an impractical divergence of the beam, due to the reasons stated above, this idea was omitted from the design, since there is no starting in designing a lens without knowing how much divergence needs to be mitigated[xi].

We thus have a ground station consisting of an area of reservoirs, directly heated by the concentrated beam from space. To accommodate the C&DH accuracy of 2 arcseconds, the area of the ground station is simply enlarged to make sure that the beam is always received by a (or multiple) reservoir(s). Over the distance of 36000 km a circular area with radius 350m would suffice.

This area would be filled with reservoirs shaped as rectangular beams and square top and bottom surfaces, sized in such a way that they could provide the required power to a turbine. The numerous reservoirs can now also be used in a control loop for checking the pointing accuracy of the reflector actuators: Knowing the location of each reservoir, temperature (or even luminosity) sensors could be used to check which ones are receiving power from the downlink system. In case too few reservoirs are receiving power, the location of the receiving reservoirs gives an indication as to the amount and direction for the beam transmission correction. Sending this information up to the satellite, which then corrects its transmission, closes the control loop.

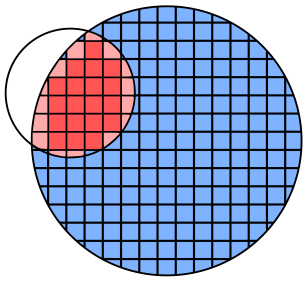

Figure 4.9: Inaccurate pointing (not to scale).

The efficiency of the energy conversion consists of $\eta_{reservoir}$, η_{Carnot}, $\eta_{generator}$. Where $\eta_{reservoir}$ is the efficiency from radiation to heat. Typical values of electrical generator efficiencies vary around 85%. The efficiency preceding that, namely $\eta_{reservoir} \cdot \eta_{Carnot}$, is given by Equation 4.24.

$$\eta = \left(\alpha - \frac{\epsilon\sigma T_{opt}^4}{IC}\right) \cdot \left(1 - \frac{T_0}{T_{opt}^4}\right) \tag{4.24}$$

Where α is the absorptivity, ϵ is the emissivity, σ is the Stefan-Boltzmann constant, T_{opt} is the optimal operating temperature for a reservoir, I is the solar irradiation, C is the concentration factor and (finally) T_0 is the heat sink temperature.
Due to constraints for the length of this report, this equation will not be dived into in detail. Suffices to say that it flows from modelling the reservoirs as black body radiators that absorb and radiate away heat. Another assumption has to be mentioned:

[xi] In reality this would be a recommendation to look into

The reservoirs will be modelled as black body radiators, with the absorption and emissivity of typical molten salt mixtures.

Beginning with starting values of $\eta = 0.3$ and $T_0 = 323$K, an iterative process can now calculate C[xii] and consequently find the new η corresponding to the optimal value from a range of several T_{opt} values. Using $\alpha = 0.85$ and $\epsilon = 0.7$, 10 iterations result in a concentration factor of 210 suns, an efficiency (including the generator) of 24.2% and an optimal operating temperature of 578K.

Now for the sizing of individual reservoirs, as stated, they will be modelled as rectangular black body radiators with square top and bottom surfaces (see Figure 4.10. The volume of the reservoirs will partly determine how fast a reservoir can be heated up from ambient temperature to the optimal operating temperature. However for now, only the ratio between the width and the height of a reservoir will be looked into, since this will influence the maintenance of the operating temperature.

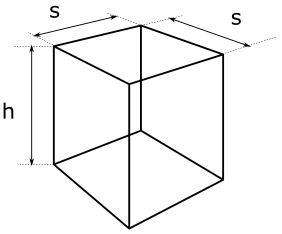

Figure 4.10: A single ground station reservoir

The surface area of a reservoir is given by $S_{reservoir} = 2A_{reservoir} + 4hs = 2s^2 + 4hs$. We have that P_{in} should equal P_{out} or simply $P_{net} = 0$. P_{in} is mostly the radiation from the beam in addition to some intake from the direct environment, as can be found in Equation 4.25 with T_{amb} being the ambient temperature (taken as 293K). The power radiated away is given by Equation 4.26, so this results in Equation 4.27.

$$P_{in} = C \cdot I \cdot A_{reservoir} + S_{reservoir} \cdot \sigma\epsilon \cdot T_{amb}^4 \quad (4.25)$$

$$P_{out} = S_{reservoir} \cdot \sigma\epsilon \cdot T_{opt}^4 \quad (4.26)$$

$$\begin{aligned} P_{net} = S_{reservoir} \cdot \sigma \cdot \epsilon \cdot T_{opt}^4 - S_{reservoir} \cdot \sigma \cdot \epsilon \cdot T_{amb}^4 - C \cdot I \cdot A_{reservoir} = 0 \\ \Leftrightarrow s^2[2 \cdot (1 + 2\frac{h}{s}) \cdot \sigma\epsilon(T_{opt}^4 - T_{amb}^4) - CI] = 0 \end{aligned} \quad (4.27)$$

To find the ratio $\frac{h}{s}$, the equation is reworked, resulting in:

$$\frac{h}{s} = 0.5 \cdot \left(\frac{CI}{2\sigma\epsilon(T_{opt}^4 - T_{amb}^4)} - 1 \right)$$

This yields a value of 12.2, so the height of a reservoir should be 12.2 times its width. Of course, given the layout of the ground station, many reservoirs will not be in use during most of the time, so the actual volume of a reservoir should aim to minimise the downtime related to the time necessary to heat the reservoir up.

In the foregoing section, a non-conventional type of solar thermal plant was looked into, however, the nature of the Downlink subsystem allows for a lot of flexibility in the choice for the ground station: If the spot size turns out to be larger than expected, the concentration factor might be low enough to allow for a conventional PV station. Another option for a high concentration station, apart from the one previously discussed, could be a more conventional solar thermal plant. A ground station like that could have a single reservoir in the center, using the circular area for the placement of many reflectors, that concentrate the incoming beam onto that reservoir. This adds another optical (in)efficiency, but also increases the concentration factor. To make an educated choice between ground stations, more literature research and an extensive trade-off would have to be performed, which is beyond the scope of this report. Finally, a more accurate C&DH system could result in a Ground station that would only have to be a fraction of the current size, since most of the area is now a result of mitigating inaccurate position determination.

[xii] Using a power output of 100MW divided by the efficiency, and the spot area with radius 25m

5
Astrodynamics

In this chapter the problem description concerning the astrodynamics will be laid out. With this, requirements were formed and transfer mission plans could be established. From these plans one was selected after a trade-off. The chosen transfer mission plan was analysed into further detail and a Δv-budget, decay rate and the propellant mass was calculated.

Requirements
After analysing literature of reference missions, the following set of requirements were established, regarding orbital mechanics and transfer logistics:

- **SSR.LAU.ORB.1**: The peerage of the parking orbit shall have an orbit altitude from Earth's surface of 500 km.
- **SSR.LAU.ORB.2**: The transfer time of the whole system shall not exceed two years.
- **SSR.LAU.ORB.3**: The total propellant mass of the transfer mission shall not exceed 6M[i] kg.
- **SSR.LAU.ORB.4**: The Starship Modules should be connected in Assembly Modules before arriving in GEO.

5.1. Astrodynamics Modelling
This section will outline the process, calculations, and assumptions made in the modelling of orbits and transfers for the given mission. subsection 5.1.1 will detail the steps taken in building the model and how the propagation of orbits is achieved through step-wise calculations. subsection 5.1.2 will then outline the verification procedure for which these calculations and assumptions can be made to a sufficient degree of confidence.

5.1.1. Modelling
To design a viable trajectory for this mission, it is important to have an accurate model to describe the various orbital parameters and perturbations. The outcome of this model is to describe the mission plan in terms of orbit and transfer times as well as to give a predicted propellant mass needed for both transfer and orbit keeping. It is important to note that for nomenclature, any bold symbol represent vector arrays while non-bold symbols represent a scalar.

A number of coordinate systems exist to describe a given orbit, one of which that will be used for orbit determination and propagation in this case will be an Earth-Centred Inertial Ecliptic frame, whereby the vectors **r** and **v** describe the body's Cartesian position and velocity relative to the Earth's centre on the equatorial plane. The second uses Classical Orbital Elements (COEs) to describe the position of the satellite body, that is the semi-major axis, eccentricity, inclination, true anomaly, argument of perigee, and Right Ascension of Ascending Node (RAAN). The conversion from the [**r**, **v**] state to the COEs will using Equation 5.1 to Equation 5.8[8].

[i] 25% of total mass + a safety factor of 1.5

$$\mathbf{h} = \mathbf{r} \times \mathbf{v} \tag{5.1}$$

$$i = \arccos h_y / h \tag{5.2}$$

$$e = \frac{\mathbf{v} \times \mathbf{h}}{\mu} - \frac{\mathbf{r}}{r} \tag{5.3}$$

$$\mathbf{N} = [0, 0, 1] \times h \tag{5.4}$$

$$raan = \arccos \frac{N_x}{N} \tag{5.5}$$

$$aop = \arccos \frac{\mathbf{N} \cdot \mathbf{e}}{N \cdot e} \tag{5.6}$$

$$ta = \arccos \frac{\mathbf{e} \cdot \mathbf{r}}{e \cdot r} \tag{5.7}$$

$$a = r \cdot \frac{1 + e \cdot \cos ta}{1 - e^2} \tag{5.8}$$

where:

- $r = [x, y, z]$ position vector
- $v = [x, y, z]$ velocity vector
- $h = [x, y, z]$ orbital momentum vector
- i = inclination angle
- e = eccentricity
- N = node line
- $raan$ = Right Ascension of Ascending Node
- aop = Argument of Perigee
- ta = True Anomaly
- a = Semi-Major Axis
- μ = Standard gravitational parameter for central body on Earth

For the orbit propagation – not including perturbations – a numerical, step-wise approach is used to determine the new Cartesian velocity and acceleration at each time step. For a given **r**, the acceleration is computed using Equation 5.9 while the velocity can be determined through differentiating the position vector as a function of time.

$$a = -\mathbf{r} \cdot \frac{\mu}{r^3} \tag{5.9}$$

To account for perturbations during propagation, additional calculations are included and these are divided per perturbation. For instance, a spiral transfer requires acceleration changes due to thrust to be accounted for at each step using Equation 5.10 and added to the previously calculated acceleration in Equation 5.9. The normalised velocity vector provides the direction of the thrust magnitude being used, thus not allowing for thrust vectoring. The mass differential can then be easily calculated using Equation 5.11 for low-thrust electric engines.

$$a_{thrust} = \frac{\mathbf{v}}{v} \cdot \frac{T}{m} \tag{5.10}$$

$$\frac{dm}{dt} = \frac{|T|}{I_{sp} \cdot g_0} \tag{5.11}$$

where:

- T = thrust
- m = mass at time t
- I_{sp} = Specific impulse (s)
- M = Mass of central body
- G = Gravitational constant
- $g_0 = G \cdot M$ = Sea level gravitational acceleration

5.1.2. Verification

With many aspects of the design relying on the calculations and output of the astrodynamics model, it is important to verify each of these calculations. This is done primarily through unit tests which verify output of smaller functions used in the program, although for larger problems an integration test was also performed to ensure that the functions are working together as expected.

The verification of each function used in the orbit propagator model is detailed in Table 5.1.

Function	Description	Input(s)	Output(s)	Unit Tests
init_perts()	Initiates dictionary describing orbit perturbations	**J2**: bool,**aero**: bool, **third_bodies**: set, **thrust**: float, **isp**: float	**perts**: dict	Value True, Value False, Value equal
ecc_anomaly()	Through trial and error or Newton's method estimates eccentric anomaly	**initial estimate**: list, **method**: string, **tolerance**: float	**eccentric anomaly**: float	Value equal, Domain verification
eci2perif()	Converts Earth-Centred Inertial vector to perifocal vector	**RAAN**: float, **AoP**: float, **inclination**: float	**transformation matrix**: ndarray	Value data type, Value shape, Value equal
coes2rv()	Converts COEs to position, velocity	**COEs state**: list, **deg**: bool, **central_body**: dict	**r**: list, **v**: list	Value data type, Value shape, Value equal
rv2coes()	Converts position, velocity to COEs	**r**: list, **v**: list, **central_body**: dict	**COEs state**: list	Value data type, Value shape, Value equal
a_thrust()	Calculates acceleration due to low-thrust engine	**v**: list, **thrust**: float, **mass**: float	a_thrust: float	Value equal
dmdt()	Calculates mass differential due to low-thrust engine	**thrust**: float, **isp**: float, $\mathbf{g}_0$: float	**dmdt**: float	Value equal, Value less than 0
hohmann_calc()	Calculates the elliptical orbit(s) of a Hohmann transfer	$\mathbf{r}_0$: float, $\mathbf{r}_f$: float, **central_body**: dict, **n_transfers**	**delta_vs**: list, **time**: float, **COEs** state: list	Value(s) equal, Value(s) greater than 0

Table 5.1: Verification of model functions

5.2. Transfer mission Plan

To get the whole system, weighing several millions of kilos, into GEO is a challenge. A robust mission plan has to be designed that performs in an efficient, sustainable and low-cost manner. To achieve this, four concept mission plans were made and are discussed below.

The launch vehicle used for this mission will be the Starship with Super Heavy configuration, the design parameters of this vehicles are laid out in Table 5.2.

Now, the concept transfer mission plans will be laid out.

Spiral transfer

With this mission plan, the Starship Modules of a 100 tons will be placed in a LEO with a height of 500 km. This is the maximum orbit Starship can deliver a cargo of 100 tons according to its users guide [9]. From this point Assembly Modules will be prepared in the parking orbit to perform a spiral transfer to GEO. This spiral transfer will be performed by ion-thrusters having a low but constant thrust. The transfer is likely to take a long time since ion-thrusters are in an early stage and only have reached 5.4 N, which is

Parameter/**Stage**	**Starship (2^{nd} Stage)**	**Super Heavy (1^{st} Stage)**
Height [m]	50	70
Diameter [m]	9	9
Propellant capacity [t]	1200	3400
Thrust [MN]	12	72
Payload Capacity [t]	100	-

Table 5.2: Starship with Super Heavy booster

the NASA's X3 ionic thruster [10]. This low thrust combined with the high mass will create a dense spiral. An example transfer is plotted in Figure 5.1.

What should be considered is that for the transfer in the figure above 5 thrusters of each 5 N were used to transfer one Starship Module. With this configuration the transfer would take 212 days. If you increase the amount of modules to create an Assembly Module the spiral will be more dense and have longer span. If you increase the thrust or amount of thrusters the spiral will be less dense and have a shorter time span.

Hohmann transfer with custom propulsion

The Starship Modules of a 100 tons shall be brought into a parking orbit of a 500 km height [9] and will be assembled into Assembly Modules. With a custom designed propulsion system, the Assembly Modules shall be placed into GEO using a Hohmann transfer. Using a Hohmann transfer is an efficient and fast way to travel between two orbits. Such a transfer require two thrust impulses - one at the perigee of the desired elliptical Geosynchronous Transfer Orbit (GTO) and a second arriving at the GEO. The trajectory of this mission is shown in Figure 5.2.

Hohmann transfer using Starship without refueling

According to the Starship Users Guide [9], Starship can bring a cargo of 21 tons into a GTO with a perigee of 185 km. This could be a convenient way to bring all the Starship Modules to GTO, since their is no need for a custom propulsion system delivering a ΔV to get into that elliptical orbit. Also, no refuelling of Starship needs to be done. The 21 tons Starship Modules will be placed in the GTO and every time a module passes the perigee of a 185 km [9], one is added to it. When reached the right amount of modules, a custom propulsion system will deliver the final ΔV to bring this Assembly Module into GEO. The trajectory is shown in Figure 5.3. A big drawback of this transfer plan is that the Starship Modules can just be 21 tons. Considering that Starship is designed to transport a 100 tons of cargo, this is extremely inefficient since the amount of launches increases drastically. This brings us to the next mission plan.

Hohmann transfer using Starship with refueling

This approach is similar to the previous one, obviously. However, the Starship Modules can now be a 100 tons and will first circle in a parking orbit of 500 km. At this point the Starship will be refuelled and can prepare to transfer the 100 tons cargo into a GTO with an perigee of 500 km. Cargo can be dropped in this orbit and the Starship can return to Earth. Every time the module passes the perigee a Starship Module of a 100 tons can be added, similar to the previous mission plan. The formed Assembly Modules will now also be placed into GEO by a thrust impulse provided by a custom propulsion system. A plot of the trajectory is show in Figure 5.4.

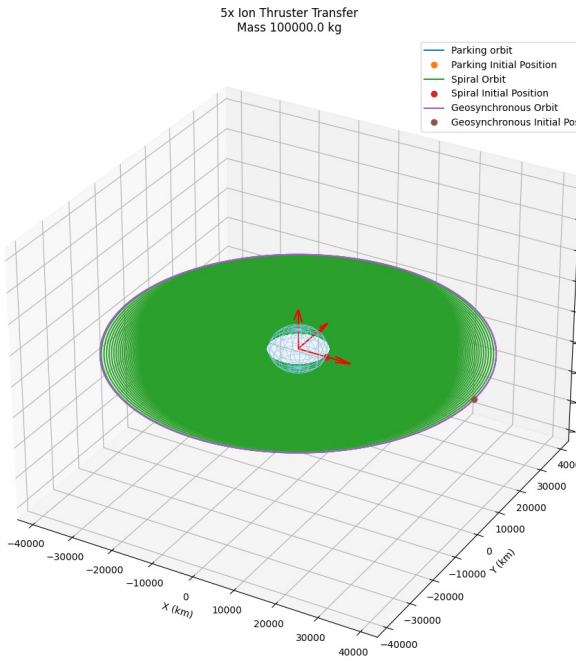

Figure 5.1: Low thrust spiral transfer

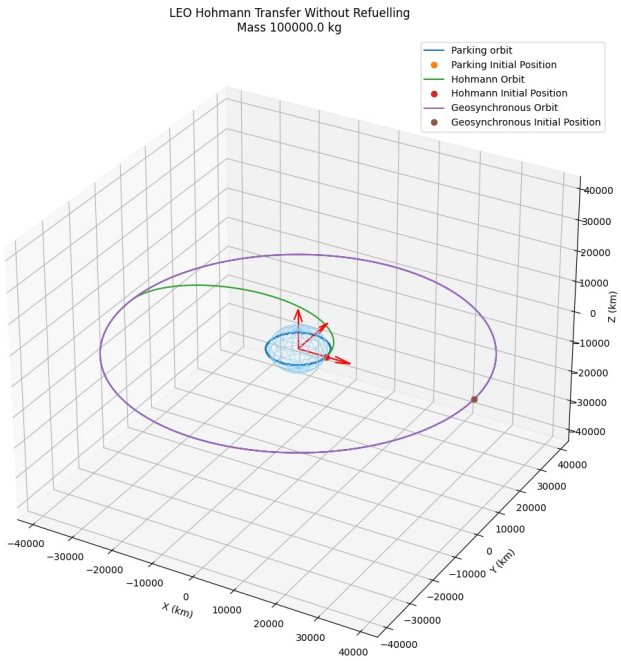

Figure 5.2: Hohmann transfer custom propulsion

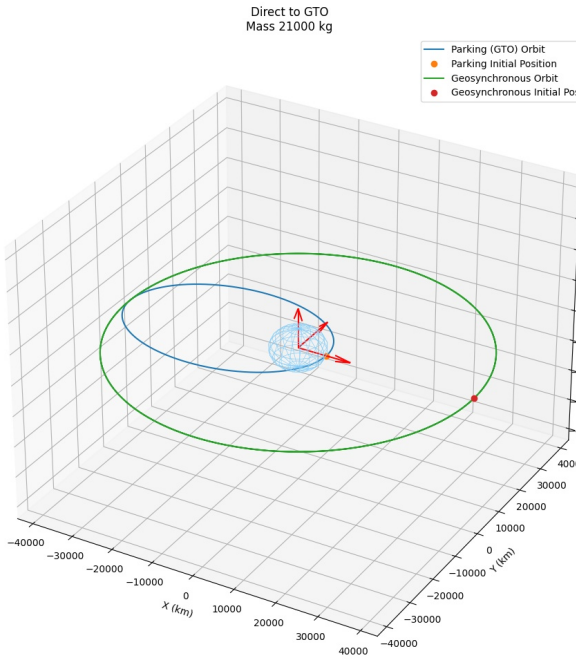

Figure 5.3: Hohmann transfer using Starship without refuelling

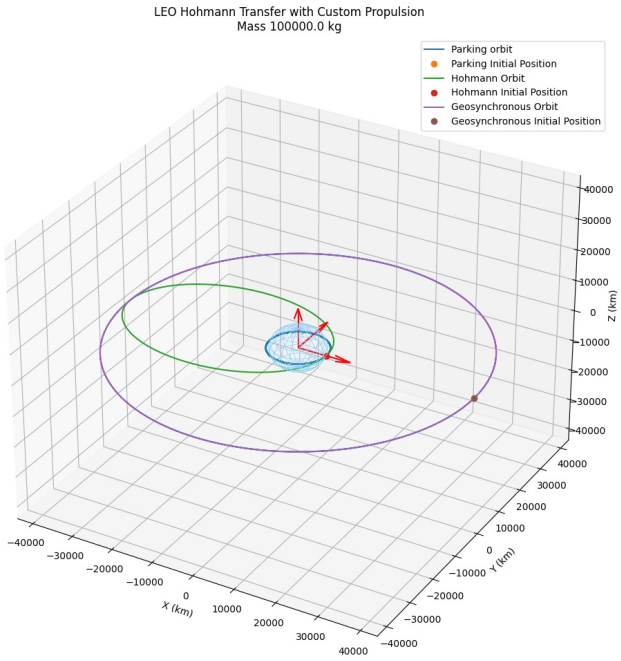

Figure 5.4: Hohmann transfer using Starship with refuelling

5.3. Transfer Trade-Off

To decide on the transfer plan, a trade-off must be performed to weigh all the benefits and flaws of each plan. Using the requirements and thinking of what would give the optimum transfer, a set of criteria was made. At first, inspired by **SSR.LAU.ORB.3**, the required propellant masses will be considered both for getting to the parking orbit and getting to GEO. To take **SSR.LAU.ORB.2** into account, the transfer time will also be looked at. Lastly Sustainability and logistics will be considered as two criteria to select a proper transfer mission. During the trade-off a set of assumptions had to be made, these are listed below.

- The Starship Super Heavy configuration will be used for all launches.
- The propellant mass required for total transfer to Geostationary Orbit will not be used to iterate the total mass required for this transfer. This is valid for the transfer trade-off as the required propellant mass will have a direct outcome on the scoring for each option, and will be weighted accordingly.
- For the trade-off, a configuration of four Assembly Modules to be transferred to GEO will be used. This results in 51 Starship Modules per four Assembly Modules.
- A turn around time of a given Starship launch vehicle of 24 hours is assumed.
- 6 Starship launch vehicles are being used for the mission, each are reusable.
- 6 Starship launch vehicles will be launched from different launch pads within a given orbital period.
- For low-thrust transfers, Xenon ion thrusters will be used.
- For continuous thrust transfers, only electric propulsion may be used.
- Each Assembly Module (for a given transfer plan) will require an equal number of chemical engines for the necessary Δv.

5.3.1. Scoring Trade-off

To properly score on the criteria earlier mentioned, a self established rubric was used. It can be found in Table 5.3, where PM refers to propellant mass and t to time.

Score/criterion	PM Parking Orbit	PM GEO	Time to GEO	Sustainability	Logistics
3	0 < PM < 10M	0 < PM < 10M	0 < t < 500	High	Low
2	10M < PM < 20M	10 < PM < 20M	500 < t < 100 days	Medium	Medium
1	PM > 20M	PM > 20M	t > 100 days	Low	High

Table 5.3: Scoring rubric for TRL & Reliability

Now, the criteria will be analysed per transfer mission plan.

Propellant mass parking orbit

The propellant mass required to reach the desired parking orbit (either Low Earth Orbit at 500km or Geosynchronous Transfer Orbit with a perigee of 500km) is calculated based on the capabilities of the Starship Super Heavy launcher, detailed in Table 5.2. For each launch of 100 tonnes to 500km, a total propellant mass of 4600 tonnes will be needed, and the same will be needed for 21 tonnes to GTO. In order to achieve the transfer of 100 tonnes to GTO, a refuelling mission will be needed and therefore will require additional launch propellant, and refuelling propellant. These calculations will now be made for each of the possible transfer options used for the trade-off.

For the spiral transfer, custom propulsion transfer, and 21 tonne transfer options, the propellant mass required to reach parking orbit will be the same at 4600 tonnes. The major difference being in the number of launches required which will be significantly higher when only 21 tonnes can be launched. Similarly for the 100 tonne refuelled launch to GTO, a greater number of launches will be needed for this refuelling, adding to the total propellant mass needed to get to this parking orbit. The calculation procedure will follow Equation 5.12 to Equation 5.15.

$$m_{ass} = \frac{m_f}{n_{ass}} \tag{5.12}$$

$$n_{mod} = \frac{m_{ass}}{m_{pay}} \tag{5.13}$$

$$m_{prop_{refuel}} = \begin{cases} 0 & n_{refuel} = 0 \\ \frac{m_{prop_{trans}} \cdot m_{prop_1}}{m_{pay}} & n_{refuel} > 0 \end{cases} \tag{5.14}$$

$$m_{prop_{tot}} = (n_{mod} \cdot m_{prop_1}) + m_{prop_{refuel}} \tag{5.15}$$

where:

- m_f = final system mass
- n_{ass} = number of Assembly Modules
- m_{ass} = mass of Assembly Module
- m_{pay} = payload capacity of one Starship
- n_{mod} = number of Starship Modules
- n_{refuel} = number of refuelling missions needed
- $m_{prop_{trans}}$ = mass of propellant required for initial Δv
- m_{prop_1} = mass of propellant for one Starship launch to 500km
- $m_{prop_{refuel}}$ = mass of refuelling propellant required
- $m_{prop_{tot}}$ = total propellant mass to parking orbit

The results are provided below in Table 5.4.

Option	Parking Orbit	Mass [tonnes]
Spiral transfer	LEO	746.45
Custom Propulsion	LEO	746.45
Starship 21 tonnes	GTO	3555
Starship 100 tonnes	GTO	28351

Table 5.4: Total propellant masses required to reach parking orbit of given transfer option.

Propellant mass to GEO

Once the Starship Modules have been unpacked in their respective parking orbit, they must be combined into Assembly Modules and finally transferred to the target GEO orbit at 35768 km above Earth's surface. The calculations for the propellant mass required in this transfer will rely on the Δv needed in the case of an impulse transfer calculated using Equation 5.16 to Equation 5.18, and the mass flow during the continuous thrust spiral transfer analysed in the step-wise approach using Equation 5.11, in subsection 5.1.1.

$$a_{transfer} = \frac{r_0 + r_1}{2.0} \tag{5.16}$$

$$v_{transfer} = \sqrt{\mu \cdot (\frac{2}{r} - \frac{1}{a_{transfer}})} \tag{5.17}$$

$$\Delta v = v_{transfer} - v_{init} \tag{5.18}$$

The results for each transfer option can therefore be shown in Table 5.5.

Option	Parking Orbit	Δv [km/s]	Mass [tonnes]
Spiral transfer	LEO	-	10385
Custom Propulsion	LEO	3.83	27603
Starship 21 tonnes	GTO	1.45	7773
Starship 100 tonnes	GTO	1.45	7773

Table 5.5: Total propellant masses required to transfer to final GEO altitude.

Time to GEO

This criterion is defined to be the total time it will take from launch to transfer the total number of Assembly Modules to the target orbit. This value must be estimated with the assumption that five Starship Modules may be transferred to a given parking orbit within that orbit's period and that these five Starships

may then be reused and refuelled within a 24 hour period. While this is a bold assumption, it is necessary to achieve the time-to-operation requirement of **CONS.DEV.SCH.6** for a number of these transfer options.

For the low-thrust spiral trajectory, the transfer time is calculated overt the number of time-steps in the modelling procedure to reach the target orbit. It is dependent on the mass of the Assembly Module being transferred, and on the performance of the electric propulsion system and therefore – as mentioned in the list of assumptions – five Xenon ion thrusters with 5N thrust capability and a specific impulse of 5000s each will be used in this calculation. For the Hohmann transfer, due to impulse manoeuvres, the time to reach GEO will be dependent on the transfer orbit itself (see Equation 5.19 with reference to Figure 5.4) and the assembly time in the parking orbit. If Assembly Modules are to be connected in GTO, this time will be dominant and an additional half-period transfer time will not be added – this assumes that Assembly Modules will be connected in time for the impulse transfer at the orbit apogee. The results are approximated using the aforementioned methods and shown in Table 5.6.

$$t_{transfer} = \pi * \sqrt{\frac{a_{transfer}^3}{\mu}} \tag{5.19}$$

Option	Parking Orbit	Time [hrs]
Spiral transfer	LEO	≈ 830000
Custom Propulsion	LEO	≈ 250
Starship 21 tonnes	GTO	≈ 41000
Starship 100 tonnes	GTO	≈ 490

Table 5.6: Total time required to connect and transfer to final GEO altitude.

The assembly model connection procedure and consequent transfer will be described in more detail in Chapter 8.

Sustainability
To determine whether a transfer mission is sustainable, the main thing that is looked at is if the resources can be recycled, so if there is a minimum amount of waste. Also, the emissions in the atmosphere will be looked at, which is related to the amount of launches. The spiral mission performs good at emissions as not much propellant has to be taken up to space to fuel the ion thrusters. These extra launches cause emissions which is bad for earth's atmosphere. A drawback, however, is that a lot of engines have to be produced to get the system travelling to GEO. These engines are unsustainable to produce as lots of highly chemical processes go along with manufacturing these electrical systems. The spiral transfer scores a 2.

The transfer mission using custom propulsion is definitely not sustainable. As the mission requires a lot of fuel, and the engines of the custom propulsion system will not be reused the mission leaves a big footprint behind. The mission scores a 1.

The mission where Starship brings the system directly into GTO in modules of 21 tons is also not scoring well. As a lot of launches have to be done to get the total system mass up, the mission performs badly on emissions. The created Assembly Modules are still have to get their final Δv to escape from the GTO. This is delivered by a propulsion system which will not be recycled. The mission receives a score of 1.

The transfer mission with a refuelled Starship scores somewhat better. This is because less launches have to be done, as the Starship Modules are now a 100 tonnes. This lowers the emission, giving this mission a score of 2 for sustainability.

Logistics
The main things that are used to score the missions on logistics are the rendezvous for refuelling and the number of Starship Modules needed to bring up the system. The spiral mission is orbiting at an altitude

of 500 km and each time it has a rendezvous a module will be added. To make sure the time requirement is met, Assembly Modules have to be transferred instead of transferring the whole system in one go. The Starship Modules will carry a 100 tons which is good for logistics. The mission scores a 2.

The transfer mission with custom propulsion requires a similar rendezvous procedure as the first one, only more rendezvous should be there as the propellant has to be delivered as well to bring it to GEO. Another difference regarding logistics will be the time of the transfer which will be shorter in this mission. The mission scores a 2 as well.

The direct transfer into GTO with a 21 tons does not perform well in logistics. This is because the Starships has to rendezvous a lot to get all 775 Starship Modules up there. The concept plan scores a 1.

The mission with refuelling is similar to the one with custom propulsion as the extra rendezvous for the propellant have to be done here as well, only these are called here refuelling mission. For that it scores a 2 as well.

The scoring of all criteria on the 4 transfer mission plans is summarised in Table 5.7.

5.3.2. Results and Verification

The results of the trade-off for the various transfer mission plans are shown in Table 5.7. The outcome shows that a Starship Module of 11 tonnes which is refuelled in LEO at 500 km and subsequently transferred to GTO for assembly, before a final transfer to GEO is the best option for the selected criteria.

	PM Parking Orbit	PM GEO	Time to GEO	Sustainability	Logistics	Scores
Spiral Transfer	3	2	1	2	2	**1.94**
Custom Propulsion	3	1	3	1	2	**2.06**
Starship 21 Tons	1	3	2	1	1	**1.75**
Starship 100 Tons	1	3	3	2	2	**2.31**
Weight	3	4	4	2	3	

Table 5.7: Trade-off scores on transfer mission plans

Sensitivity Analysis for Verification

To verify these trade-off results, a sensitivity analyses was conducted on the weights of the criteria resulting in the sub-figures seen in Figure 5.5. What can be seen is that the refuelling mission wins most of the time. To conclude, this transfer mission plan will be the plan with which will be continued.

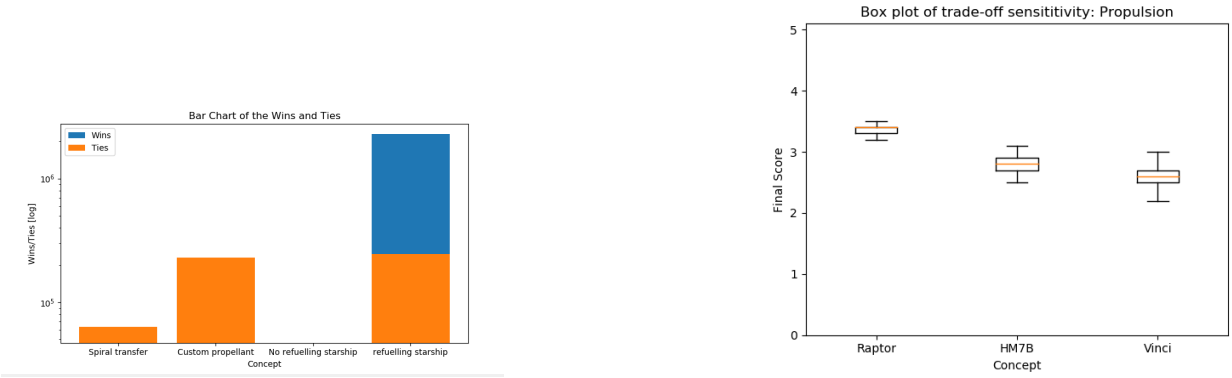

(a) Sensitivity analysis (histogram)

(b) Sensitivity analysis (Box-plot)

Figure 5.5: Sensitivity analysis conducted on the trade-off criteria and their weightings.

5.4. Final Transfer Plan Design

This section will focus on detailing the characteristics of the final transfer plan, which includes the orbital elements of the Low Earth Orbit, apogee and perigee of the Geosynchronous Transfer Orbit and the orbital elements of Geo-synchronous Equatorial Orbit, providing the Δv and propellant mass requirements to achieve these orbits. With this information, a clear definition of the number of Starship Modules can be made.

The mass of an Assembly Module is dependent on the number of Assembly Modules chosen for transfer to GEO. This design decision is based on the inertia of the Assembly Modules – determined by the configuration of Starship Modules as described in Chapter 8 – as well as the amount of C&DH and ADCS planning that would be required (proportional to the number of Starship Modules). With this in mind, an initial number of four Assembly Modules will be transferred to GEO for final assembly.

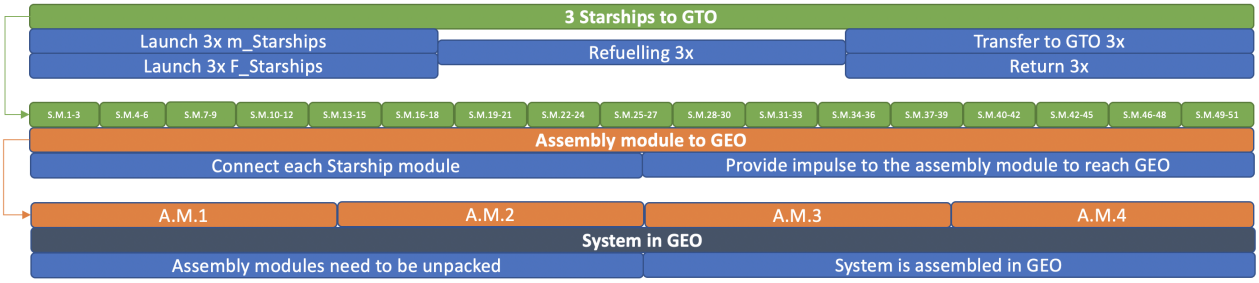

Figure 5.6: Transfer plan

Figure 5.6 describes the launch-to-operation trajectory plan for the IKAROS satellite. This procedure came to fruition through a once-over iteration of propellant mass requirements for the final system mass determined for each sub-system for which an overview can be found in Chapter 14. The step-by-step method for this trajectory design is as follows:

1. Determine initial estimate of system dry mass.
2. Divide this by the number of Assembly Modules planned for transfer from GTO to GEO to calculate Assembly Module dry mass.
3. The total mass before burn can now be calculated using Equation 5.20 where m_{pay} is the Assembly Module dry mass.
4. The number of raptor engines needed for transfer from GTO to GEO can then be determined by the amount of mass one raptor is able to accelerate to achieve the desired Δv, as defined by Equation 5.21.

5. With the Assembly Modules defined, the number of Starship Modules can now be calculated by dividing the total Assembly Module mass by the Starship payload mass, 100 tonnes.

6. Finally the propellant mass required to transfer 100 tonnes from 500km to GTO – where the apogee and perigee are 35,786 km and 500 km, respectively – is calculated using Equation 5.16 to Equation 5.18 followed by Equation 5.20.

$$m_0 = \frac{m_{pay}}{\exp -\frac{\Delta v}{I_{sp} \cdot g_0}} \tag{5.20}$$

$$m_{capability} = \frac{T \cdot t_{burn}}{\Delta v} \tag{5.21}$$

A summary of Δv requirements for the various stages of the mission and the required propellant for those stages can be found in Table 5.8.

Stage	Δv **[km/s]**	**Propellant Mass [kg]**
Δv_1	2.3698	17,824,425.77 (Starship)
Δv_2	1.4463	5,806,060 (Fuel tanks)
$\Delta v_{graveyard}$	0.007773	41,953 (Fuel tanks)

Table 5.8: Summary of trajectory parameters and propellant requirements.

With the sum of the subsystem masses (not including mass of module fairing) and the propellant mass required for fuel tanks, a final safety margin of 25% is added to account for the assumptions made in the astrodynamics modelling and design as well as the module fairing structural mass. This leads to a final mass estimate **23 227 442 kg**.

5.4.1. Time span of the transfer mission

The time of the transfer mission is heavily dependent on the cargo mass that has to be brought up. This mass can be transported in the 100 tonnes Starship Modules. Every Starship of cargo needs an extra Starship for refuelling in the parking orbit. The empty Starship can now deorbit, make its return to earth and be prepared for its next launch. Simultaneously, the refuelled cargo carrying Starship has enough propellant to deliver the cargo into GTO. After one period in GTO the cargo is decoupled and the Starship can make its return to earth by deorbiting at the perigee of the GTO. Also this Starship can now be prepared for its next launch. This is the limiting turn around time, as the Starship carrying the fuel was at earth first and is easier to be turned around. The exact time spans for the procedures can be viewed in Table 5.9.

This process requires 2 Starships, however, a duplicate of this number will be available for the mission. As there are 6 starships available for the project, the procedure above can be done with 3 Starship Modules 'a time'. It will be done until the amount of Starship Modules fitting into an Assembly Module is reached, which will be 18 times. This phase of getting an Assembly Module to GEO takes 112 days. After having one Assembly Module up, a second one can be assembled. This is done until all four Assembly Modules, which are needed to assemble the system, are in GEO. Thus, the total time to get the system into GEO takes the number of Assembly Modules multiplied by the time needed to bring up an Assembly Module resulting in a time span of 1.23 year, or 450 days. The numbers are summarised in Table 5.9.

Parameter	Value	Unit
Time to parking orbit	1	hour
Time to refuel	24	hours
GTO period	11	hours
Time to turn around cargo starships	120	hours
Total time to GTO	158	hours
Amount of Starships available	6	-
Amount of Cargo Starships available	3	-
Number of Assembly Modules	4	-
Amount of Starship Modules in Assembly Module	52	-
Total time of Assembly Module to GEO	112	days
Total time to GEO	1.23	years

Table 5.9: Parameters for transfer mission time span

For a Starship to get to the parking orbit of 500 km, one hour travelling time is taken. This phase is not considered to be a limiting one. one hour is chosen as the Soyuz spacecraft needs 45 minutes to get to the International Space Station, which has a height of 408 km. To get to 500 km should take a fraction longer as the atmosphere is the toughest part to get through. Now for the time to refuel in the parking orbit, 24 hours were taken as the docking of the Starships is a critical procedure and has to be done carefully, thus slowly. The turnaround time to get the three Starships coming from GTO ready for the new launch, together with the meanwhile refuelled other three Starships, is considered to be 5 days, or 120 hours. The deorbiting time from GTO's perigee of around 4 hours are taken[11] within this turn around time. As this is the most important bottleneck, it is crucial for the mission to have this time minimised. Following the trend of other launchers, this should be achievable at the time the mission starts.

5.4.2. Orbital Decay

Accounting only for J2 perturbations of the Earth, the orbital decay over 2 days is shown by Figure 5.7.

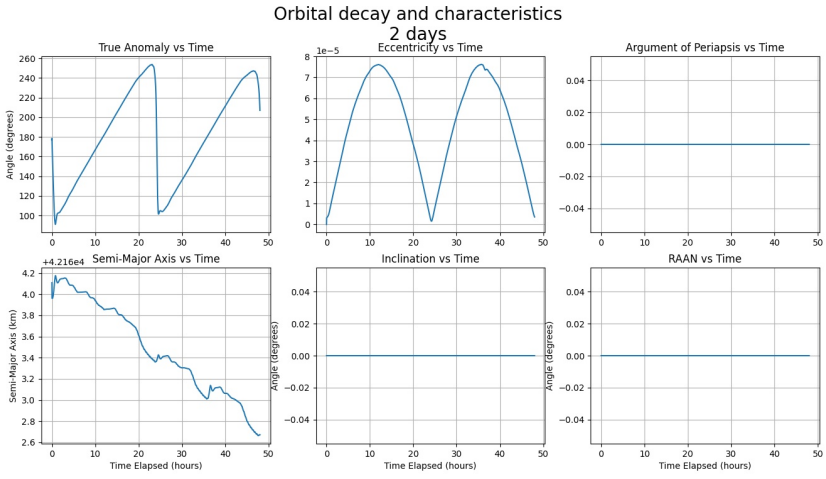

Figure 5.7: Classical orbital elements plotted over a time period of 2 days, with J2 perturbation.

More detailed perturbations on the satellite are described and accounted for in Chapter 7.

6
Propulsion Subsystem Design

In this chapter the design of the propulsion subsystem (PSS) is discussed. The chapter is divided into two phases. The first phase goes over the problem definition of the propulsion subsystem and includes Section 6.1 and Section 6.2. The second phase aims to design a solution for the defined problem and is outlined as follows: first a small literature study will be performed, then a small trade-off between design configurations, followed by a preliminary propulsion subsystem design and finally a verification and validation process is performed. The reader can find the process of the second phase in Section 6.3, Section 6.4, Section 6.5 and Section 6.6 respectively. After reading this chapter the reader will have a basic understanding of the propulsion system that is going to be used to transfer the transfer modules to a GEO orbit around earth from GTO orbit (that will be provided by the launch vehicle Starship from SpaceX. Due to time constraints the team was not able to design a propulsion unit from the ground up and instead opted to compare already existing and under development rocket propulsion engines and to select one of these engines as the main propulsion unit of the transfer modules.

Phase 1: Problem Definition

6.1. Requirement Analysis

This section goes over the requirements that are specific for the PSS. The THRUST requirements are related to the thrust of the PSS, FUEL to the fuel unsurprisingly, BUD to the engineering budgets of the system and AIV is related to assembly, integration and validation. Furthermore, the EOL requirements are related to the End Of Life phase of the system, THERM is related to thermal control requirements and VIB stands for vibration and is concerned with the vibrations that arise during burn and ignition of the PSS. In addition, ENV are requirements related to the environment, ACC is related to accuracy and finally SRR are requirements that are related to safety, risk and reliability. These requirements are obtained from either team discussions between departments or from looking up reference propulsion units to see what is currently possible or what is possible in the near future.

6.2. Functional Analysis

This section features a small functional flow diagram of the PSS shown in Figure 6.1, which shows the reader an outline of the functionality of the system. The functional diagram aids in the upcoming designing process, because every function that the system shall perform has to be considered.

Phase 2: Design Solution

6.3. Literature Study

The type of fuel the system uses largely determines its performance characteristics and the design of the entire propulsion system, thus the literature study began on what type of fuel was to be used for the propulsion system.

First, electric propulsion was looked into, but very quickly from some basic calculations it was determined that electric propulsion simply does not have the amount of thrust that would result in a reasonable burn time (see Section 5.2). Even when considering using spiral transfer orbits the transfer time would simply be way to long, because of the enormous mass that has to be transferred to GEO.

The next logical step is looking into the implementation of a cryogenic propulsion system. The main advantage of cryogenic fuel is its high specific impulse that is possible (theoretically up to 460 sec [12]).

Table 6.1: Requirements of the Propulsion System

Identifier	Explanation
SSR.PROP.THRUST.1	The system shall be able to provide a Δv of 1450 m/s.
SSR.PROP.THRUST.	The system shall have a minimum burn time of 500 sec.
SSR.PROP.THRUST.	The system shall have a maximum acceleration of 4.0 m/sˆ2.
SSR.PROP.FUEL.1	The fuel shall have a flammability range of 2-80%.
SSR.PROP.FUEL.2	The minimum fuel flow of the system shall be 500 kg/s.
SSR.PROP.BUD.1	The engine shall have a maximum mass of 2000 kg.
SSR.PROP.BUD.2	The system shall have a maximum volume of tbd mˆ3.
SSR.PROP.BUD.3	The system shall provide a minimum delta-v of 1450 m/s.
SSR.PROP.AIV.1	The system shall be integrated into to the transfer module.
SSR.PROP.AIV.2	The system shall be validated.
SSR.PROP.EOL.1	The system shall perform the transfer to the graveyard obit after the end of its operational life, which requires a Δv of 7.5 m/s.
SSR.PROP.EOL.2	The system shall safely deactivate the PSS at EOL.
SSR.PROP.THERM.1	The system shall keep the fuel at a temperature below 100 K.
SSR.PROP.ENV.1	The fuel of the PSS shall be produced in a way that is not toxic for its environment according the local laws and environmental laws.
SSR.PROP.ENV.2	The production of the system shall not expose the workers to any safety hazards.

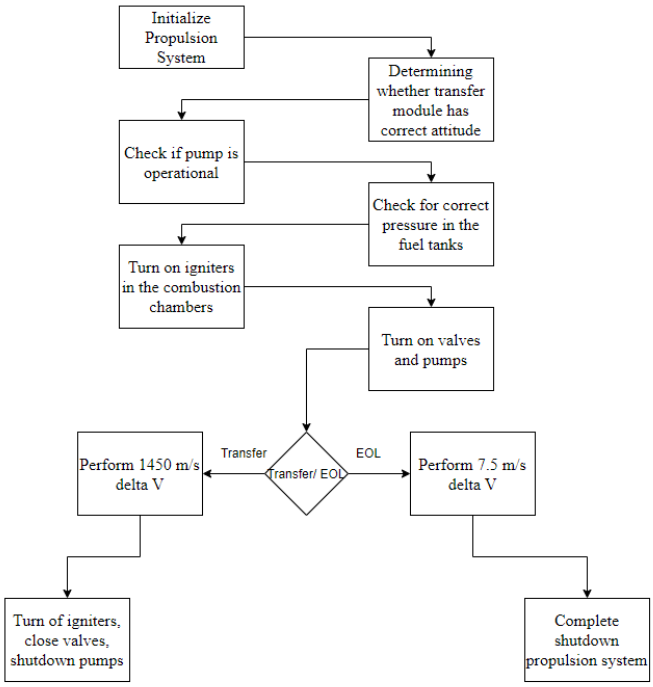

Figure 6.1: Functional Flow Diagram Propulsion

However, there are also a few downsides of using cryogenic fuel, most notably the boil-off that occurs during operation making the fuel considerably less effective as fuel will be wasted. This is not a new problem though, with plenty of literature on how to manage the boil-off in an effective manner and there has also been a lot of advancement in technology to keep the propellants below 100 K[13].

The TRL is sufficiently high, as it is already being implemented according to various accounts as an upper-stage fuel for several launch vehicles. Furthermore, a lot of research has been performed into selecting which cryogenic fuel would be most suitable for the propulsion system, but this will be discussed in more detail in the trade-off section.

6.4. Configurations Trade Off

In this section several existing engine configurations are discussed and evaluated in a trade off. The engine is to perform a transfer to a GEO from a GTO orbit that is already provided to the modules by the Starship Launch Module of SpaceX. This section will fist discuss the trade-off criteria that the small trade-off will be based upon and afterwards it will compare the different configurations and come up with a winning propulsion system.

Trade-off criteria

The trade-off will be based upon the following criteria.

- **Performance**: This criteria will evaluate the performance of the fuel that is used by the rocket engines. The assessment will be based upon propellant cost and the specific impulse of the engine.
- **Safety and Risk**: The engine and the fuel has to be safe to operate and not endanger the mission with unacceptable risks. The higher the score the less Risk and Safety concerns are present with the configuration. The assessment is done by making an estimation about the complexity of the system, the TRL and by comparing the safety of the different fuels.
- **Mass Performance**: This criteria assesses the mass of the rocket engine in relation to its maximum thrust.
- **Sustainability**: A measure of what the propulsion configuration has on the environment. A high grade means that it has a low impact on the environment.

Preliminary Propulsion configurations

- **SpaceX Raptor Engine - LOX and CH4**: This under development engine designed by SpaceX is a cryogenic engine that uses liquid oxygen and liquid methane for propellant. It is a full flow staged combustion engine that uses two turbo pumps to pump the propellant around. It has a high specific impulse of 380 [sec] in vacuum (the only thing that is relevant in this case as the transform will be performed at the apogee of the GTO orbit). The maximum thrust a single engine could deliver is around 2000 [kN]. This engine is designed to be used in missions to mars where there is methane available for refuelling. The information of this engine was obtained from [1][2][4][3].
- **HM-7B by Snecma - LOX and LH2**: This European engine is designed by the French company Snecma. It is used as an upper-stage engine for the Ariane 2 to 5. It has a specific impulse of 444.6 [sec], but at a much lower maximum thrust of 62.2 [kN]. This cryogenic engine uses liquid oxygen and hydrogen as propellant. It has been used operationally already and is thus ready to be used at any time. The information about this engine was obtained from [14].
- **Vinci by Snecma - LOX and LH2**: This is the under development successor of the HM-7B and will be used in Ariane 6 as an upper-stage thruster engine. It has a specific impulse of 465 [sec] in vacuum, which is comparable to the HM-7B, but it has a much higher thrust of 180 [kN]. The propellant of this engine will be liquid oxygen and liquid hydrogen. The information of this engine was obtained from [15].

Assessment of the trade-off criteria

	Propellant Cost	Specific Impulse	Grade
Raptor	LCH4 - 1.35 USD/kg	~380 [sec]	4
HM7B	LH2- 2.2 USD/kg	444.6 [sec]	3
Vinci	LH2 - 2.2 USD/kg	~465 [sec]	3

Table 6.2: Performance Comparison

	Propellant Cost Grade [x4]	Specific Impulse Grade [x5]	Combined Grade
Raptor	4	3	4
HM7B	2	4	3
Vinci	2	4	3

Table 6.3: Performance Comparison Grading

Performance Assessment
To assess the fuel and engine performance of each rocket engine the propellant cost are assessed as well as the specific impulse of the rocket engine. To compare the propellant cost, the prices of the fuels are compared with each other as the oxidiser is the same for all the rocket engines that are considered (LOX). The mixture ratios of the different engines are similar (all considered engines have a mixture ratio of around 5.0). As can be seen in Table 6.2 the cost of liquid methane is much lower than that of liquid hydrogen[16][17]. The specific impulse of the different rocket engines was acquired from literature[2][14][15]. The grading process is presented in Table 6.3, where the grades are obtained linearly from the values of both the cost and the impulse. The two grades are then combined with weights of x4 for the propellant cost and x5 for the specific impulse. This weights are selected based upon what was thought to be the most important aspect of the performance assessment.

Safety and Risk Assessment
To assess the Safety and Risk of the rocket engines, the rocket engines are tested upon the TRL, the safety of the fuel and the complexity of the system. In Table 6.4 the grading for these sub-criteria can be seen. Also the weight that are included in the final grade of this trade-off criteria are shown next to the sub-criteria. The grades regarding the fuel safety are based upon articles about the safety of hydrogen compared to methane and propane [18][19]. For the assessment of the system complexity the following reasoning was adopted. The Raptor engine was thought to be the most complex due to its size and all the new technologies that are involved. Second to that the Vinci engine is thought to be the most complex, as it is also a under development engine that incorporates newer technology and is thus believed to be more complex than the older HM7B engine. Below the results of the entire assessment can be seen in Table 6.4. The weights of this trade-off criteria were found by careful consideration of the importance of the several aspects towards the final propulsion system design.

Mass Performance Assessment
To assess the mass performance criteria of the rocket engines, the most important aspect is the thrust to weight ratio, because the burn time will already be determined and thus the amount of thrust that is needed is also determined. The thrust to weight ratio thus specifies he weight the rocket engines combined would weigh to provide the necessary thrust. The grading is linearly dependent on the thrust to mass ratio. The highest trust to weight ratio will receive a grade of 4. In Table 6.5 the results of the assessment can be seen. All the values obtained for this tables are obtained from literature[1][2][4][3][14][15].

	TRL [x3]	System Complexity [x3]	Fuel Safety [x1]	Final Grade
Raptor	2	2	3	2
HM7B	4	4	2	4
Vinci	2	3	2	2

Table 6.4: Safety and Risk Comparison

	Engine mass [kg]	Thrust/Mass	Grade
Raptor	1500 (goal)	~150 (170 goal)	4
HM7B	165	38.43	1
Vinci	~550	~40	1

Table 6.5: Mass Performance Comparison Engines

	Exhaust gasses [5x]	Toxicity [3x]	Manufacturing [2x]	Final Grade
Raptor	3	3	4	3
HM7B	5	2	3	4
Vinci	5	2	3	4

Table 6.6: Sustainability Comparison

Sustainability Assessment
The sustainability of an engine is assessed by considering the exhaust gasses of the rocket propellant, the toxicity of the propellant to the environment in case of an accident and the effect on the environment due to the manufacturing of the propellant. The results of the assessment can be seen in Table 6.6. To determine the toxicity of the different fuel literature was consulted[20][19]. The weights of the sustainability assessment was assessed by careful consideration. The toxicity of the propellant is more easily overcome by making sure that the propellant is treated in safe environment that will take its danger into account. The negative effects of exhaust gasses are much more difficult to control and therefore this was given a higher weight in this trade-off criteria.

Final Grading
Below the combined final results of the trade-off can be seen (Table 6.7). The weights of each trade-off criteria can be found next to the criteria name. The winner of the trade-off is the Raptor engine from SpaceX. The weights were determined in a group discussion with different people of different departments to assess what is the most important criteria that a propulsion system must adhere to. The outcome of the group discussion was that the performance criteria were to most important in the propulsion system design. After this the Safety and Risk was deemed most important, where the propulsion system is to work safely, without unacceptable risks that would endanger the mission. Sustainability was deemed to be the least important of the trade-off criteria as the transfer is so difficult and demanding of the financial and mass budgets that the trade-off criteria more directly associated with these problems had to be addressed with more weight.

6.5. Design Characteristics of the Propulsion Subsystem

Now that the trade-off is finished, this section goes over the characteristics of the main propulsion system that will be used to transport the modules of the SBSP system to GEO from GTO. The system will make use of the Raptor Engine from SpaceX to bring the transfer modules into GEO. As the engine is still under development, its detailed characteristics are unknown as of yet, the more general specification can be found in Table 6.8.

The engine is a staged combustion engine that uses full flow and is meant to be reusable. The propellant

	Performance [5x]	Safety & Risk [4x]	Mass Performance [5x]	Sustainability [2x]	Final Grade
Raptor	4	2	4	3	3.38
HM7B	3	4	1	4	2.75
Vinci	4	2	1	4	2.56

Table 6.7: Final Rocket Engine Comparison Trade-Off Results

that the engine uses is as stated previously in this chapter is liquid oxygen (LOX) and liquid methane (LCH4). The raptor will be used in the Starship launch vehicle of SpaceX in both of its stages[1][2][4][3].

Length [m]	Diameter [m]	Dry Weight [kg]	Thrust [kN]	I_{sp} [sec]	Thrust/Weight [-]	Mixture Ratio [-]	Chamber Pressure [bar]
3.1	1.3	~1500 (goal)	2000	380	~150	3.55	300

Table 6.8: Specification SpaceX Raptor Engine[1][2][4][3]

6.6. Verification and Validation

To verify the results of the trade-off a small sensitivity analysis is performed that will change the weights of all the trade-off criteria such that it can be determined how sensitive the outcome is to the chosen weights. A very general validation strategy is also discussed.

Sensitivity Analysis

This section goes over the sensitivity analysis of the trade off performed in this chapter as a part of verifying the results of this chapter. As can be seen in Figure 6.2a the raptor engine wins most of the time and rarely ties with the HM7B engine. In Figure 6.2b it can be seen that the variance of the final score of the raptor engine is also very small, only in the most ideal circumstances for the HM7B, it could tie with Raptor, but this sensitivity analysis confirms that the Raptor engine is clearly better in the most cases, thus verifying the trade-off results.

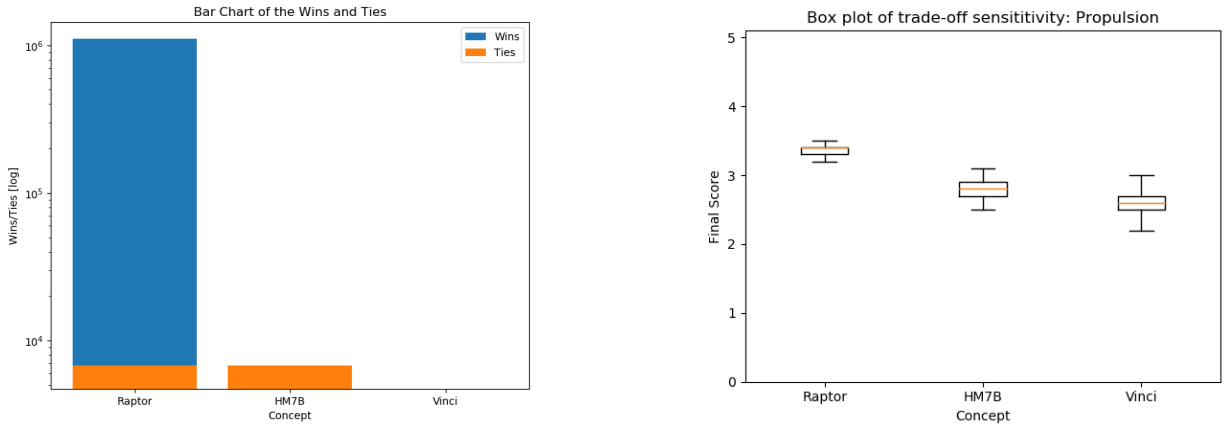

(a) Sensitivity Analysis Chart of wins and ties

(b) Box plot trade-off sensitivity

Figure 6.2: Sensitivity Analysis

Validation Strategy

As the engine is still under development the validation of the Raptor Engine is being performed currently in the form of several tests. The Raptor Engines are currently being used with the Starship launch vehicle and the launch vehicle is in its testing phase at this time (2021). Once, the Raptor engine is fully designed, the engine must of course be tested on its ability to be integrated with the transfer modules of the SBSP system. This is best done with several tests, such that it can be ensured the engine is performing to specifications when it is attached to the transfer modules. The nature of these test are difficult to describe exactly in this phase as all the subsystems are still quite preliminary.

7
Attitude Determination and Control System

Throughout the mission, the spacecraft requires some method of determining its orientation with respect to the Earth, the Sun and stars. In addition, it needs to adjust its orientation by rotation around its axes, in order to point in the direction required and to compensate for torques applied to the system. These responsibilities are taken on by the Attitude Determination and Control System, which measures the attitude of the spacecraft and corrects that attitude when required.

7.1. Subsystem Requirements

The main requirement for this mission is to rotate the spacecraft to be facing the sun, but there are several other constraints that should be taken into account for this subsystem, they are all listed below.

- **SSR.ADCS.CON.1:** The ADCS system shall provide attitude control around 3 axes.
- **SSR.ADCS.CON.1.1:** The ADCS system shall provide 0.99 degrees rotation around the y-axis per day to correct for the earth rotating around the sun.
- **SSR.ADCS.CON.1.2:** The ADCS system shall correct for the orbital perturbations
- **SSR.ADCS.CON.1.2.1:** The ADCS system shall correct for Solar radiation torque
- **SSR.ADCS.CON.1.2.2:** The ADCS system shall correct for Magnetic field torque
- **SSR.ADCS.CON.1.2.3:** The ADCS system shall correct for Gravity Gradient Torque
- **SSR.ADCS.CON.2:** The ADCS system shall have a pointing accuracy of 1.0 degrees.
- **SSR.ADCS.CON.3:** The ADCS system shall be able to slew at a rate of at least 1 degrees per 180 minutes around each axis.
- **SSR.ADCS.DET.1:** The most accurate sensor shall determine the attitude with an accuracy of at most 15 arc seconds.
- **SSR.ADCS.DET.2** The direction of the sun shall be determined with an accuracy of at least 0.5 degrees.
- **SSR.ADCS.RISK.1:** The ADCS of the satellite shall have no single point of failure.

7.2. Disturbance Torques

Throughout the mission, there are several disturbance torques acting on the spacecraft that would, if left unchecked, rotate the spacecraft continuously which would eventually lead to a significant pointing error. Therefore these torques must be computed and the system must be designed to be able to compensate for them.

7.2.1. Solar Radiation Pressure Torque

When light hits a surface, it carries a momentum with it despite its weightlessness. This momentum causes a small but non negligible torque on the spacecraft if there is a discrepancy between the centre of mass and the centre of incoming solar radiation. To compute this torque, first the momentum of a photon must be calculated, which can be determined using Einstein's relation, presented below.

$$p = \frac{E}{c} = \frac{h}{\lambda} \tag{7.1}$$

Where p stands for the momentum in kgm/s, E for the energy of the photon in J and c stands for the speed of light in vacuum in m/s. This momentum is also equal to Planck's constant h in m^2kg/s over the photon's wavelength λ in m. This is true for a single photon as well as for photon flux. Combining this relation with the solar radiation over a surface, the reflectivity of the surface of the spacecraft, the discrepancy of the centre of solar pressure and the centre of mass and with the angle of incidence, leads to Equation 7.2. This formula presents the torque induced by solar radiation on the spacecraft.

$$T_{SRP} = \frac{\phi}{c} A_s(1+q)(c_{p_s} - c_m)cos(\theta) \tag{7.2}$$

Where T_{SRP} stands for the solar radiation pressure torque in Nm, c stands for the speed of light in m/s and ϕ represents the solar constant at one astronomical unit of distance from the sun. Note that for this particular mission, the average distance to the sun will be equal to one astronomical unit, since the orbit is around Earth and Earth is, by definition, orbiting at this average distance from the sun. As for the spacecraft specific terms, A_s here stands for the sunlight surface area in m^2, q is the unitless reflectance factor, $c_{p_s} - c_m$ is the distance between the centre of solar pressure and the centre of mass in m and θ is the angle of incidence of the sunlight in rad.

7.2.2. Magnetic Field Torque

Another disturbance to the spacecraft is the influence of the magnetic field of Earth. Torque induced by a magnetic field can be determined using the formula below, where each of the components represent a 3-dimensional matrix, which accounts for all three axes of rotation.

$$\underline{T} = \underline{M} \times \underline{B} \tag{7.3}$$

In this formula, $\underline{T}$ represents the magnetic torque induced by Earth's magnetic field in Nm, while $\underline{M}$ stands for the residual dipole of the spacecraft in Am^2 and $\underline{B}$ is used to denote the strength of the magnetic field of Earth in T. Specific for the magnetic field of Earth, the following formulas can be used to describe its strength.

$$B_r = -2B_0(\frac{R_E}{r})^3 \cos\theta \tag{7.4}$$

$$B_\theta = -B_0(\frac{R_E}{r})^3 \sin\theta \tag{7.5}$$

$$|B| = B_0(\frac{R_E}{r})^3 \sqrt{1+3\cos^2\theta} \tag{7.6}$$

The formulas above describe the radial and azimuthal components of Earth's magnetic field and its magnitude. B_0 here refers to the mean value of the magnetic field of Earth at the equator, while B_r, B_θ and $|B|$ represent respectively the radial component, azimuthal component and the magnitude of this magnetic field. R_E is used to denote the radius of the Earth, while r represents the radial distance of the spacecraft to the centre of the Earth. Finally θ stands for the azimuth angle with respect to the magnetic poles of Earth.

7.2.3. Atmospheric Drag Torque

Although space missions take place far away from Earth, in lower orbits there is still some amount of air present which causes a drag on the spacecraft. Since this mission takes place in Geo-synchronous Equatorial Orbit, the air density is negligible and can be assumed to be zero. Therefore there will be no atmospheric drag torque acting on the spacecraft, thus it does not need to be calculated.

7.2.4. Gravity Gradient Torque

Since the gravitational field of the Earth is not perfectly uniform, it induces a torque on the spacecraft. Using the orbit altitude and the gravitational characteristics of the Earth, the mean motion of the orbit can be computed, which is a useful intermediate step in calculating the gravity gradient induced torque. The formula for this is presented below.

$$n = \sqrt{\frac{\mu}{r^3}} \tag{7.7}$$

Where n represents the mean motion in s^{-1}, μ the gravitational parameter of Earth in $m^3 s^{-2}$ and r the radius of the orbit in m. Now the gravity gradient torque can be computed as follows. It can be separated into three formulas, one for each of the axes of rotation.

$$T_x = \frac{3}{2} n^2 (I_y - I_z) sin(2\phi) \quad (7.8) \qquad T_y = \frac{3}{2} n^2 (I_x - I_z) sin(2\theta) \quad (7.9) \qquad T_z = 0 \quad (7.10)$$

T_x, T_y and T_z here represents the gravity gradient torque in the x, y and z axes respectively, in Nm. n is used to denote the mean motion calculated above, in s^{-1}. I_x, I_y, I_z are the mass moments of inertia (MMOI) of the spacecraft in the x, y and z axes respectively, in kgm^2. ϕ and θ represent the angles on those axes with respect to the Earth, in rad.

7.2.5. Results

The maximum value of each of the disturbance torques is presented in Table 7.1.

Table 7.1: Disturbance Torque Results

Disturbance torque	Value	Unit
Solar radiation	2.34E+00	Nm
Atmospheric drag	-	Nm
Magnetic field	1.04E-07	Nm
Gravity gradient	1.53E-01	Nm

The most significant disturbance torque is the solar radiation pressure torque, which does not come as a surprise, considering the large sunlit surface area of the spacecraft. The torque induced by the gravity gradient is also quite significant, while the magnetic field torque is negligible, due to the weakness of Earth's magnetic field at such a distance from the surface.

7.3. Attitude Determination

The objective of attitude determination is to pinpoint the orientation of the spacecraft with respect to celestial bodies such as the sun and other stars and with respect to the ground station on Earth. In addition, the spacecraft should be able to observe in some way or another when it is experiencing angular acceleration and when it is rotating at a certain rate. Both of these goals should be achieved with the highest accuracy possible, in order to minimise power downlink losses caused by pointing inaccuracies.

7.3.1. Determination Methods

There are various possible options for measuring the attitude and inertia of a spacecraft, but not all are applicable in this particular situation. Firstly, we can disregard magnetometers - devices used to measure the Earth's magnetic field and thus determine the attitude of the spacecraft - due to the Earth's magnetic field being too weak at the altitude of Geo-synchronous Equatorial Orbit (GEO). Additionally, Earth sensors and horizon sensors can be disregarded, since the use of these would make the subsystem much more complicated, considering that the attitude of the spacecraft is constantly changing with respect to the Earth.

Another method of attitude determination is a sun sensor and this is particularly useful for this specific mission, as the spacecraft will have to be pointed towards the sun at all times, so this has been chosen for use in the final design. In addition, a star tracker is used, because these can provide a very high accuracy and using this in addition to the aforementioned sun sensor adds an additional level of redundancy. Finally for the inertia of the spacecraft, an Inertial Measurement Unit is used, since these can accurately determine spacecraft rotation and angular acceleration, which is useful both for determining disturbances and as feedback to the attitude control system.

Of each of the aforementioned components, two units are used, in order to provide a redundancy that prevents a single point of failure in the attitude determination system.

7.3.2. Sun Sensors Trade-Off

For the sun sensor, several options have been considered in the trade-off, presented in Table 7.2. All of these components are being produced in the Netherlands, which is positive for sustainability. The Cubesatshop NFSS-411[i] has the best characteristics in the trade-off and has therefore been chosen for use in this mission.

Sun sensor	Accuracy (deg)	Field of view (deg)	Mass (g)	Power (mW)	Country of origin
NewSpace NFSS-411	0.1	140	35	130	Netherlands
Bradford space course sun sensor	3	180	215	0	Netherlands
Bradford space fine sun sensor	0.3	128	375	250	Netherlands
BiSon64-ET	0.5	124	33	0	Netherlands

Table 7.2: Sun Sensor Trade-Off Results

7.3.3. Star Tracker Trade-Off

As for star trackers, various options are available from different countries, shown in Table 7.3. The most viable option has turned out to be the Sagitta Star Tracker[ii], because of a very high accuracy and the best performance in all other categories. In addition, it is produced in Belgium, which is beneficial to sustainability.

Star tracker	Accuracy (arc-sec)	Field of view (deg)	Mass (g)	Power (mW)	Country of origin
Sagitta Star Tracker	2	40	250	1000	Belgium
Terma T1	9	20	760	3250	International
Terma T3	12	20	350	1000	International
Sodern Hydra	11	26	3200	9500	France

Table 7.3: Star Tracker Trade-Off Results

7.3.4. Inertial Measurement Unit Trade-Off

For Inertial Measurement Units, several options have been considered, which are listed in Table 7.4. Out of these options, the Sensonor STIM377H[iii] emerges as the victor, due to high stability and manufacturing in a sustainable country, Norway.

7.4. Attitude Control

Once the attitude of the spacecraft has been determined, it needs to adjust this attitude to compensate for disturbance torques and to provide rotations specified by the subsystem requirements. The subsystem must provide this attitude control over all three axes of rotation, therefore the options should be scaled to cover these. There are several ways to control the attitude of a spacecraft, these are listed below.

[i] https://www.cubesatshop.com/product/digital-fine-sun-sensor
[ii] https://www.cubesatshop.com/product/kul-star-tracker/
[iii] https://www.sensonor.com/applications/space/

IMU	acceleration range (g)	gyro bias instability (deg/h)	accelerometer bias instability (mg)	Country of origin
Sensonor STIM377H	10	0.3	0.05	Norway
Analog ADIS16480	18	6.25	0.1	United States
KVH P-1775	10	0.1	0.05	United States

Table 7.4: Inertial Measurement Unit Trade-Off Results

7.4.1. Control methods

- **Gravity gradient stabilisation:** This is a passive form of attitude control, it works by shaping the satellite in such a way that the gravity gradient induced torque causes it to rotate towards a stable equilibrium.
- **Spin stabilisation:** With this method the spacecraft launches with a spin applied, which stabilises the spacecraft passively due to the conservation of angular momentum.
- **Magnetic torquers:** These are electromagnets that, when activated, rotate the spacecraft due to the presence of the magnetic field of Earth/
- **Reaction wheels:** Using this method, stationary wheels are placed in the spacecraft that rotate in reaction to a disturbance torque or when a command is received. In reaction to this rotation, the rest of the spacecraft rotates in the opposite direction.
- **Momentum wheels:** Similar to a reaction wheel, momentum wheels rotate to control the attitude of the spacecraft, but these are never stationary, instead also functioning as a flywheel to store angular momentum. Thus these cannot be used in isolation, because they need a method to dump the gathered momentum of the wheels.
- **Control momentum gyros:** This device is similar to a momentum wheel, but uses a single wheel attached to a gimbal, instead of several non-adjusting wheels.
- **Thrusters:** In this method a set of thrusters are attached to the spacecraft, as far as possible away from the centre of mass. These thrusters usually work in pairs to provide pure torque and thus cause rotation without translation. In order to cover all three axes of rotation, a minimum of 12 stationary thrusters are required.

Using gravity gradient stabilisation as a method for attitude control can already be discarded, as this would require a complete redesign of the spacecraft structure and would further complicate pointing towards the sun, which is essential for the feasibility of this system. Furthermore, spin stabilisation is considered unfeasible, as this would greatly complicate the matter of power downlink from the spacecraft. As for magnetic torquers, the magnetic field of Earth is significantly weakened at the altitude of Geo-synchronous Equatorial Orbit (GEO), therefore this would not be a very efficient solution.

When considering reaction wheels, momentum wheels and a momentum gyro, it can easily be observed that relying on these methods to rotate a spacecraft with very large moments of inertia will be quite inefficient, due to the torque that will have to be produced by these wheels.

Lastly, thrusters are considered. Due to the significant diameter of the main disc of the spacecraft, attaching thrusters on the far edges will provide them with a long moment arm, thus greatly increasing the torque that they apply to the spacecraft. Furthermore, thrusters are a relatively inexpensive and light option and they work independently of orbit altitude. There are still some downsides, however, such as requiring at least 12 thrusters for full three axis control, which complicates structural design and increases loads on the structure when applying torque.

7.4.2. Thruster Trade-Off

Several thruster models are compared in a trade-off in Table 7.5. This table lists some important characteristics of each model, including MIB, which stands for Minimum Impulse Bit, this value refers to the minimum impulse a thruster can provide. This is an important variable to analyse, because this determines how slowly the spacecraft can be rotated.

After analysing the results of this table, the Heritage hydrazine 20N[iv] stands out as the most feasible option. Although the minimal impulse bit is not the lowest, its mass is higher than the alternatives and hydrazine is more toxic than gaseous nitrogen, the thrust is quite high, which is important for this mission since the moments of inertia of the spacecraft are very large. Furthermore, this thruster is produced in Germany which receives a higher score for sustainability than the United States.

Thruster	Thrust (N)	Mass (g)	MIB (Ns)	Specific Impulse (s)	Gas	Country of origin
Moog 058-118	3.6	23		57	GN2	United States
Heritage hydrazine 20N	24.6	650	0.685	230	N2H4	Germany
Heritage hydrazine 1N	1	290	0.043	223	N2H4	Germany

Table 7.5: Thruster Trade-Off Results

7.4.3. Attitude control torque

The moment acted on the system by a pair of thrusters on each of the three axes is a function of the force of one thruster and the distance to the centre of mass of the spacecraft. It can be computed using Equation 7.11.

$$M_T = 2F_T L_T \tag{7.11}$$

$$\alpha = \frac{\sum M}{I} \tag{7.12}$$

Where M_T is the moment produced by the pair of thrusters around the axis on which they act, in Nm. F_T is the force of each thruster in N and L_T is the distance from the thruster to the centre of mass of the spacecraft in m. In order to calculate the angular acceleration, Equation 7.12 can be used. Where α is the angular acceleration of the spacecraft around a specific axis in rad/s^2, $\sum M$ is the resultant moment acting on the spacecraft around that axis in Nm and I is the moment of inertia of that axis in kgm^2. This angular acceleration can then be used to compute the rotation using the formulas below, under the assumption that the thrust is constant.

$$\omega = \alpha t + \omega_0 \tag{7.13}$$

$$\Delta\theta = \omega t = \frac{1}{2}\alpha t^2 + \omega_0 t \tag{7.14}$$

Where ω is the angular velocity in rad/s, α the angular acceleration in rad/s^2, t the time in s and ω_0 the initial angular velocity of the spacecraft in rad/s. Then we insert this into the second formula to obtain the change in attitude $\Delta\theta$ about an axis of the spacecraft in rad.

7.4.4. Thruster Configuration

To decide on the configuration of the thrusters, some things have to be considered. The configuration should provide a control of the system that meets the requirements. An important requirement is **SSR.ADCS.RISK.**, where the system shall be fail safe. In other words, there should be a decent Level of Redundancy (LR). The greater this LR, the more thrusters can fall out without having a fatal consequence for the whole ADCS system. The next thing that can be looked at is the amount of thrusters the configuration has. This number obviously influences the weight of the ADCS and thus the system weight. Another factor that influences the weight of the ADCS is the fuel consumption. To meet **SSR.ADCS.CON.2** system accuracy will be considered as well. The weights of the thrusters and the fuel are considered to be less

[iv] https://www.space-propulsion.com/spacecraft-propulsion/hydrazine-thrusters/20n-hydrazine-thruster.html

important than the LR and accuracy of the configuration. This is because the masses are considered to be relatively small to the whole system.
A Study of Spacecraft Reaction Thruster Configurations for Attitude Control System [5] shows how different configurations lead to different control characteristics. 14 configurations were considered, where most of them were used in missions of the passed decades. In general; the higher the index number of the configuration, the more thrusters it gets. Configuration-1 just has 4 thrusters, where configuration-14 uses 16. The configurations vary in places where the thrusters are mounted along a ring shaped body. Also the angles at which the thrusters are mounted vary along the different configurations.

From configuration-6 on, the configurations get a Level of Redundancy (LR). This means configurations 1-5 can not be used as **SSR.ADCS.RISK.** needs to be met. Configurations 10-12 have a LR of 2 and configurations 13-14 have a LR of 3. As this is considered to be a important criterion, a LR of 3 will be picked. The choice between configuration-13 and configuration-14 has to be made. This means the largest amount of thrusters is taken, resulting in the highest thruster weight contributing to the weight of the ADCS-system. As earlier stated, this is not considered to be important. According to the study[5], configuration-13 score with 1 kg better than configuration-14 on fuel consumption. However, configuration-14 performs better at the dynamic analysis, having a lower tracking error. For the parameters in the study, configuration-14 has a tracking error Mean of 0.046°and standard deviation of 0.082°, where configuration-13 has 0.047°and 0.091°, respectively. This all leads to the chosen configuration being configuration-14, having 16 thruster in pairs of 4 at every quadrant of the circle. The selected configuration is illustrated in Figure 7.1.

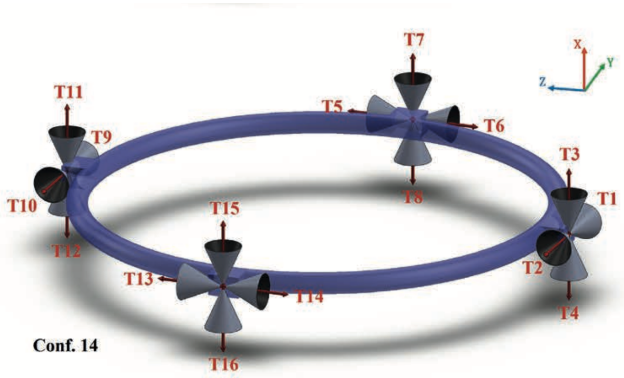

Figure 7.1: Thruster configuration ADCS[5]

7.4.5. Stability and Control

Using the aforementioned thrusters mounted at the edges of the parabola, the torques and angular rotations can be computed, these are presented in Table 7.6. Also, the attitude determination accuracy and the pointing accuracy are presented here. The attitude determination accuracy is determined by the most accurate attitude sensor, which in this case is the star tracker with an accuracy of 10 arc seconds. For the attitude pointing accuracy, the limiting factor is the minimum impulse bit of the thruster, so in this case when the thruster is activated for the shortest time possible, it results in an extremely small rotation, so the limiting factor here is the attitude determination.

As for the slew rate, for reference a maximum rotational velocity in 10 minutes is chosen (without deceleration) and an angular rotation in 20 minutes, which includes deceleration, so the same maximum rotational velocity is reached. The torques reached are more than sufficient to counteract the disturbance torques acted on the spacecraft in **SSR.ADCS.CON.1.2** and the rotations achieved are sufficient to fulfil the sun pointing requirement **SSR.ADCS.CON.1.1** and the slew requirement **SSR.ADCS.CON.3**.

Variable	X-axis	Y-axis	Z-axis	Unit
Attitude determination accuracy	5.56E-04	5.56E-04	5.56E-04	deg
Attitude pointing accuracy	7.29E-10	6.03E-10	1.54E-09	deg
Thruster pair torque	23714	23714	23714	Nm
Angular acceleration	1.64E-08	1.36E-08	3.46E-08	rad/s^2
Max angular velocity in 10 minutes	1.97E-05	1.63E-05	4.15E-05	rad/s
Angular rotation in 20 minutes	1.35	1.12	2.85	deg

Table 7.6: Stability and Control Characteristics

Taking account an approximation of the necessary corrections in a single orbit and a specified thruster mass flow of 0.238 g/s, the total fuel consumption per orbit comes out to be 1.1424 kg for all ADCS thrusters combined, leading to a total lifetime propellant mass of 10424.4 kg.

8
Assembly, Integration and Verification

8.1. Problem Description and Requirements

The Assembly, Integration & Verification (AIV) of the IKAROS satellite forms a core part of the ground-to-operation process. A system of this scale using near-future technologies must be launched in parts, and assembled in space. In order for this to be achieved, an assembly procedure must be established to ensure sufficient operation in Geo-synchronous Equatorial Orbit. With the Δv required for such a transfer, a full system manoeuvre would prove far too difficult and as a result, modules will first be assembled in parking orbit and transferred to the required altitude for operation. This requires strategic trajectory planning for optimised fuel usage and reliability.

The problem of AIV will therefore be tackled in two parts: Geosynchronous Transfer Orbit Assembly, and Geo-synchronous Equatorial Orbit Assembly. In Geosynchronous Transfer Orbit, Assembly Modules will be assembled to include Starship Modules of core subsystems such as the Electrical Power System (EPS), Sting and Relay, and core structural components. Following the joining of these Starship Modules, each will follow the second half of a Hohmann transfer to reach Geo-synchronous Equatorial Orbit for full system assembly. At this altitude, mating operations will be performed using guidance control and robotic assistance for full system assembly, and finally the payload and power systems will be deployed.

The challenges that face AIV are numerous, and research in this particular area of space dynamics is current. The main challenge for IKAROS will be in the interface and handling standardisation across the system as well as tracking and control. This creates critical dependencies on structural design and attitude determination and control to address all of these challenges.

8.1.1. Requirements

As an existing assembly satellite will be used from Defense Advanced Research Projects Agency (DARPA), the focus for this subsystem will be on robotic arm needs and assembly procedure, for which requirements have been defined below.

- **SSR.AIV.ROB.1**: The robotic assembly system shall use an off-the-shelf robotic assembly system, and associated requirements.
- **SSR.AIV.ROB.2**: The system assembly shall be automated where the tip precision necessary does not exceed <TBD> mm.
- **SSR.AIV.ROB.3**: The assembly will be telecontrolled where the tip precision necessary is less than 5 mm.
- **SSR.AIV.ROB.4**: The robotic arm(s) shall have a tip position accuracy of at least 5 mm.
- **SSR.AIV.ROB.5**: The robotic assembly system shall have 6 degrees of freedom.
- **SSR.AIV.ROB.6**: The robotic assembly system shall employ optical torque sensors for collision detection and reaction.
- **SSR.AIV.ROB.7**: The robotic assembly system shall not exceed 100 tonnes in mass.

- **SSR.AIV.ROB.8**: The robotic arm(s) shall have a maximum tip speed of 100 mm/s.
- **SSR.AIV.ROB.9**: The robotic assembly system shall cost no more than FY20 64.6 million.
- **SSR.AIV.POW.1**: The robotic assembly system shall have a maximum total idle time of 100 days.
- **SSR.AIV.INT.1**: The system shall employ a Physical (Fit) Verification through optical confirmation.
- **SSR.AIV.INT.2**: The robotic assembly system shall employ optical sensors with a resolution of at least 2mm.
- **SSR.AIV.INT.3**: The robotic assembly system shall relay and retry failed connections.
- **SSR.AIV.INT.4**: The system shall employ an in-space Multi-element Integrated Test to verify simulated system functionality (connections).
- **SSR.AIV.INT.5**: The Starship Modules needed for on-orbit assembly in GTO shall employ standard interface points for guided docking.
- **SSR.AIV.INT.6**: The system shall be assembled in a maximum of 2200 days.
- **SSR.AIV.DEP.1**: The system shall employ an in-space Multi-element Integrated Test to verify simulated system functionality (deployment).
- **SSR.AIV.DEP.2**: The power system shall be deployed within 24 hours of assembly.
- **SSR.AIV.DEP.3**: The payload and power systems shall be deployed in the target orbit.

8.2. Design Options and Selection

8.2.1. Assembly Module

As discussed in Section 5.4, the Assembly Module is built out of the Starship Modules. A set of Starship Modules will be added to the assembly system each time and will be connected mechanically. The ADCS of each Starship Module, discussed in Chapter 7, provides the needed attitude control to position the modules well to connect. A decision has to be made on how the modules will connect to each other to form the Assembly Module. The aim is to minimise the moments of inertia, and maximise the connections between modules. Also, a symmetric configuration of the Assembly Module is preferred to apply thrust efficiently.

Two ways of adding the Starships modules to the Assembly Module are considered. Rings can be added in lateral direction and layers can be stapled in longitudinal direction. Starting with the rings, there are two ways of adding the rings and remain a symmetric structure. The modules can be added around one module to get a circular or hexagonic structure, or they can be added next to each other to achieve a square structure. Both are illustrated in Figure 8.1a. Each cylinder represents a Starship Module and is simplified by not showing the cone shaped top.

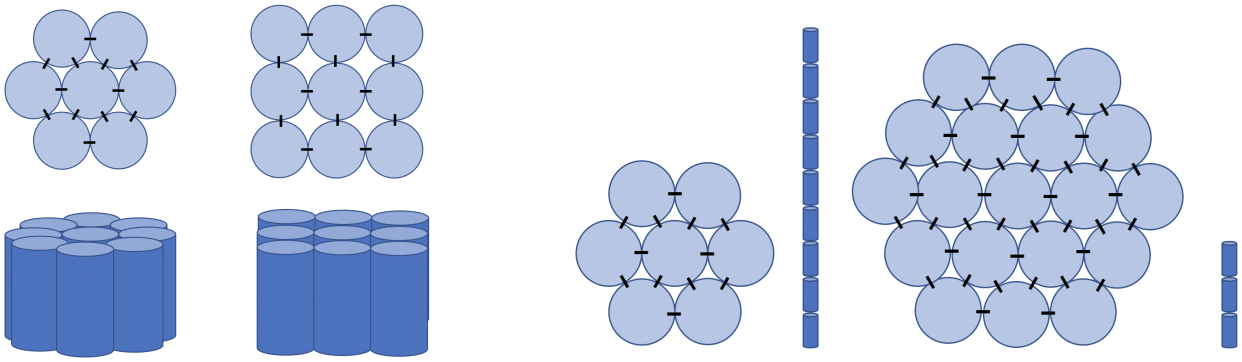

(a) Circular and square shaped configurations

(b) Lateral vs. longitudinal configuration

Figure 8.1: Assembly Module design options

The circular shaped assembly is packed more efficiently, and thus has a lower moment of inertia. Also, it has more points of interaction to connect. Every module has at least 3 connection point, which are

crucial to transfer the loads.

Now the amount of modules in longitudinal direction has to be decided on. The modules will be stapled up directly on top of each other. This means that the smaller top of the module connects to the wider bottom of another module. This is done for optimal load transfer in longitudinal direction. Now the amount of rings has to be decided on. Increasing the configuration with a ring, drastically lowers the modules in longitudinal direction. Two considerable options are given in Figure 8.1b. The left option has one ring and the right option has two rings. To the right of each option, it shows an indication of the amount of layers in longitudinal direction.

Having no rings was not considered, as there will be issues with the mounting of the raptors. Too much force acts on the module with the raptors and the longitudinal forces will be at its maximum. Having more than two rings makes the configuration too wide and the connections would undergo a lot of stresses. A choice between the two options in Figure 8.1b has to be made.

8.2.2. On-Orbit Assembly of Spacecraft

It is well known that the satellite system will need to be assembled on-orbit, due to its size being larger than any similar technology even on Earth. This makes manufacturing and assembly of the full system on Earth a mammoth task, let alone making the launch of the system impossible. This is not a new idea, with one of the greatest examples and proofs for on-orbit assembly being the International Space Station (ISS), which was the first system to be assembled in this way and sees constant upgrading and expansion even to this day. This, however, was a system weighing 'only' 419,700 kg (today) and took ten years and over 30 missions while the IKAROS system is roughly 23M kg and must be assembled in six years (including time taken to reach GEO). Needless to say, this challenge is far from trivial and requires great progress in the field of on-orbit assembly and maintenance.

As on-Earth manufacturing techniques improve, the possibility for standardisation and efficiency to develop the parts for such large systems comes closer into view, and as such on-orbit assembly research has been on the heels of this development. State-of-the-art is limited to less than a handful of technologies, the most promising of which to-date is the DARPA Phoenix program and DARPA Robotic Servicing of Geostationary Satellites (RSGS). Systems that built the ISS, however, should also be considered as these are proven to have built the largest man-made structure in space and are therefore also detailed below.

On-Board Robotic Arms

The most proven in-space assembly techniques, as previously described, are those employing on-board robotic arms. Since the early conception of the ISS, development of these arms has been at the forefront of achievement in robotics. The **Canadarm**, launched in 1981 and made 90 flights over 30 years, is the preceding technology to the **Canadarm2**. This arm was launched in 2001 and was crucial for assembling the space station and continues to move supplies, equipment, and astronauts. Seven years later, the **Dextre**, a robotic handyman, arrived to the ISS. This robot can extend the Canadarm2, reducing the need for risky spacewalks. There is then the **Remote Manipulator System**, for the Japanese Experiment Module and uses a similar grapple fixture to the Canadarm2. Most recently the **European Robotic Arm** has reached its final stages of development, tasked with installation and deployment of solar arrays, replacement of solar arrays, inspection of the station, handling of external payloads, and support of astronauts during space walks. With no need to manipulate the spacecraft (due to automatic docking of Russian and European spacecraft), the arm is half the length and less powerful than Canadarm2. The ERA weighs in at 630 kg an a total length of 11.3 metres (only 9.7m reach) and has a maximum tip speed of 100mm/s.

Since the majority of robotic systems on the ISS are designed to assist humans on board, the closest comparison for part assembly speed and methods in space are those performed, in part, by humans. A summary of these assisted assemblies can be found in Figure 8.3. Of course, the latest comparison in this table is from 1992 and since then the Dextre has been launched (2008) and most recently the European Robotic Arm which have/will provide greater capabilities in assembly and maintenance.

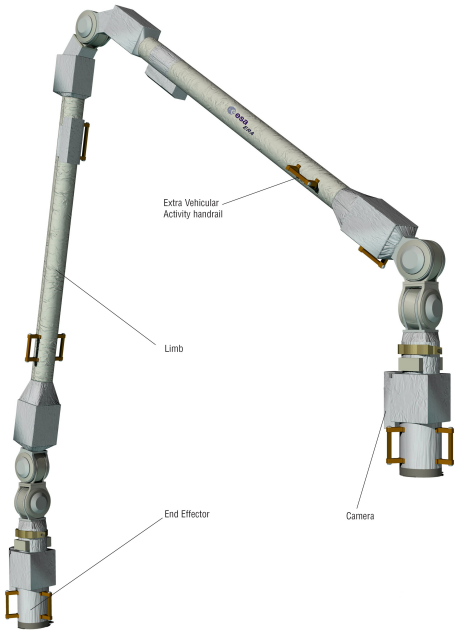

(a) Artistic impression of the ERA.

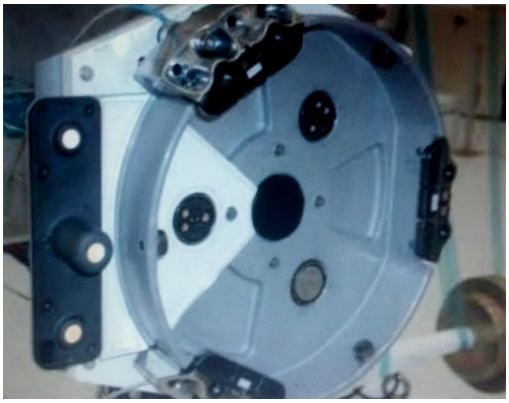

(b) Grapple base of the European Robotic Arm.

Figure 8.2: European Robotic Arm.

Free-Flying Assembly Agents

On-board robotic arms would be required to traverse the system with each step along the structure, for a system as large as IKAROS this traversal speed is outmatched by a free-flying assembly agent with independent ADCS and a standardised gripping technique. The DARPA Phoenix is one such system that could be used, although the dexterous arms should be considered in the same respect in performance and capability as the robotic arms described in subsection 8.2.2.

With a robust assembly procedure, this difference in speed is likely to be little, however with an emphasis on servicing and end-of-life the benefits of a free-flying assembly agent outweigh that of a restricted robotic arm. A free-flying agent could also be used for servicing of other geostationary satellites and even salvage parts from these systems, and for this reason the assembly procedure will assume the capabilities of the free-flying DARPA Phoenix system, already proven on the ground as shown in Figure 8.4 [21]. With this in mind, this satellite's robotic arms allow for tool changing capabilities and the structure will therefore not be as limited in design. Standard interfaces and grippers will still be required to allow the Phoenix to sufficiently stabilise on IKAROS during assembly procedures.

8.2.3. Queen Deployment

As mentioned previously, a system of this size is very difficult to manoeuvre and transfer, thus the need to divide it into smaller launchable modules and assemble those in space. Since the main parabolic dish, the Queen, is almost a kilometre in diameter, a thorough plan for modularising and deployment has to be prepared. This process should trade-off between the number of elements, the ease of deployment and efficiency of packing into launch vehicle cargo bay. The solution should also meet the structural requirements, regarding the in-orbit stresses.

The process of designing the assembly and deployment procedure started with researching possible solutions to split a "hemispherical" object into smaller pieces. Similarity to a dome structures, frequently present in renaissance architecture, lead to the first possibility of converting the parabolic shape into a mesh of equilateral triangles. The second considered solution is a very familiar "pizza slice" idea, where you split the shape into circular sectors. After looking into finite-element-method modelling software, another type of mesh was found, namely the quadrilateral meshing, which as the name suggests, splits the shape into quadrilateral sections.

Table 1 Comparison of space structure for astronaut manual assembly.

Assembly test	Manual assembly[19]	Mobile workstation[17]	Swing-arm beam erector[20]	Erectable space structure[17,21]	Mobile transporter[22]	Precision segmented reflector assembly[23]
Year	1970	1978	1984	1985	1988	1992
Truss type	Tetrahedral unit	Tetrahedral truss beam	Tetrahedral truss beam	Triangular truss beam	Hexahedral truss beam	Tetrahedral hyperboloid platform
Number of pillars	6	38	30	93	44	315 struts, 7 panels
Number of joints	4	14	12	33	16	84
Number of astronauts	2	2	1	2	2	2
Auxiliary equipment for assembly	Foot restraint and remote manipulator	Mobile positioning assistance	Mobile positioning assistance	Foot restraint and assembly tools	Mobile positioning assistance	Mobile positioning assistance
Assembly rate with gravity on the ground		24 s/strut	18 s/strut		20 s/strut	
Assembly rate with ground simulated zero gravity (neutral buoyancy)	180 s/strut	53 s/strut	29 s/strut	14 s/strut	28 s/strut	33 s/strut, 123 s/panel
Assembly rate with space zero gravity		Calculated 38 s/strut	Calculated 29 s/strut	Actual 17 s/strut	Calculated 25 s/strut	Calculated 33 s/strut 123 s/panel
Features	Large-scale structure is difficult to assemble. Astronauts are prone to fatigue.	The mobile workstation transports materials, eliminating a lot of manpower consumption.	Reduce the astronaut's assembly burden. Improve assembly efficiency	High assembly rate but need to develop expensive experimental equipment	The joint locking indicator is visible from a long distance and easy for the operator to explain.	The combination of mechanical assistance and mission planning can greatly improve efficiency.

Figure 8.3: Comparison of space structure for astronaut manual assembly.

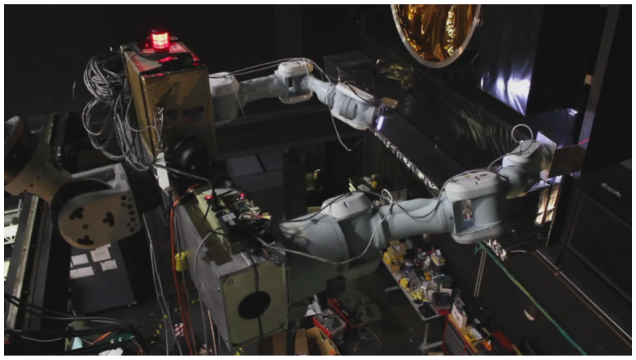

Figure 8.4: DARPA Phoenix on-ground testing.

To choose between the solutions mentioned above, all their implications on characteristics like structural rigidity, manufacturing possibility, mass optimisation, deployment possibility or packing density must be mentioned and analysed.

Starting with the triangular mesh, the dome like structure offers good structural support and has proven itself in civil engineering. The use of uniform triangles makes it easy to manufacture, but because of the density of supporting struts just to maintain the shape, it is not favourable in mass optimisation criterion. The assembly of uniform modules shouldn't be very difficult, but the amount of elements might increase the deployment time. Because of the shape, the supporting struts cannot be integrated with the reflective layer if one was to fold (roll) it for packing purpose, because that would bend them. It is also important to note, that this solution assumes flat triangular pieces which are easier to produce and transport, so the shape would be approximated with flat segments. This means that there are some losses in the reflected power, because certain rays diverge from the optimal course. To minimise the loss it is needed to refine the mesh.

The second idea, the "pizza slice" assumes significantly larger pieces, than the triangular mesh. It is only supported in two places - in the centre and the outer edge - so to maintain structural integrity possibly more ribs have to be added. Manufacturing of such big reflective surfaces is almost impossible and

certainly very expensive. Thanks to the low amount of supportive elements this solution seems to be very mass efficient. Deployment and assembly of such large segments of foil is near impossible, so this appears an unfeasible solution.

The last to consider is the quadrilateral mesh looking almost like a spider's web. To obtain the shape it needs to be supported around 4 corners, so the structural rigidity most likely doesn't need additional reinforcement. The sections in this type of mesh are not ideally symmetric, but that still should be easily manufactured. Depending on the reinforcement type and amount of segments this structure can obtain high mass efficiency. The sections could be easily unfolded between supporting ribs and is highly packable if delivered in rolls. Similar to the triangular mesh, for easiest manufacturing and assembly the shape has to be approximated with flat rectangular pieces. Similarly as before this will lead to some losses in power, higher than for triangular mesh because of lower refinement.

Analysing the aforementioned characteristics of possible solutions leads to a decision to use the quadrilateral meshing for splitting the hemispherical shape into sections. The motivation for this decision is mostly driven by the very good packing and deployment properties for sections of this shape. This solution can also be easily optimised between the segment size, structural rigidity and mass. An example of how this quadrilateral segmentation might look can be found in Figure 9.3.

8.2.4. Deployment of the Worker, Sting and Relay mirrors

This subsection will discuss ways to effectively deploy the Worker mirror system such that it is operational. The deployment will happen after the truss structure of the Worker mirror system is attached to the Queen mirror system. Below several deployment options will be discussed and eventually the deployment option will be chosen for the Sting, Worker, and Relay mirror systems.

Telescopic Boom Deployment Mechanism

This is quite a straightforward way of deploying the trusses of the mirrors outwards. The mechanism uses multiple smaller poles that are located within larger poles and uses actuators to slide the smaller beams outside of the bigger beams. The basic working of this mechanism can be seen in Figure 8.5a. The relative low complexity of this deployment mechanism makes the mechanism quite reliable in its use.

Scissor Deployment Mechanism

This is a scissor-like structure that extends once the deployment is initiated. In Figure 8.5b the basic idea of the concept can be seen. This deployment method also has a low complexity which makes it attractive for a reliable deployment mechanism. The downside of this mechanism is that the coiled up truss system will still take in quite an amount of volume, which is not ideal for storing purposes in the transfer modules.

Coilable Mast Deployment Mechanism

This mechanism folds the wires of the truss system into a big coil such that it does not take in too much space in the transfer and Assembly Module. Once the truss is to be deployed the wires are folded out and a truss is formed, which clicks into place. The basic working of the mechanism can be seen in Figure 8.5c. The downside of this mechanism is that it could get stuck if the coil is not unfolded properly, but the coil takes in not too much space in the transfer modules, which is a plus for this mechanism. Also the trusses should have some form of flexibility to be folded up, which could impair the maximum loads it could handle when it is fully folded out. To really take this into account more time should be spent on a more detailed deployment mechanism in the future.

Curtain/Rail Deployment Mechanism

This method of deployment is often seen in the deployment of large, folded solar arrays whereby attachments of the array to a rail are pulled along the length of the structure until the array is completely unfolded. This mechanism will act similarly but will work instead with a foil, where the foil will need an attachment to a more rigid body or yoke which can then be pulled radially and attached to the next rib. This mechanism is demonstrated in Figure 8.5d, and only applies to the Queen due to the 0.125 mm thickness of the foil.

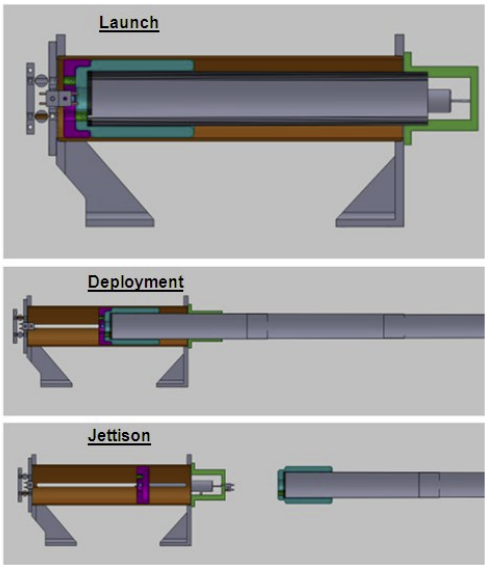

(a) Telescopic Boom Deployment Mechanism Example[22]

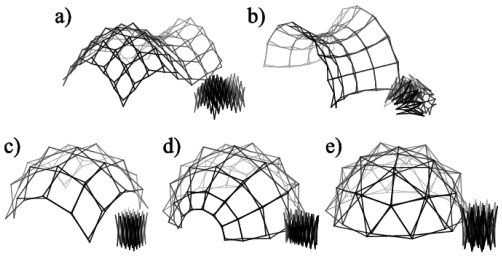

(b) Scissor Deployment Mechanism Example[23]

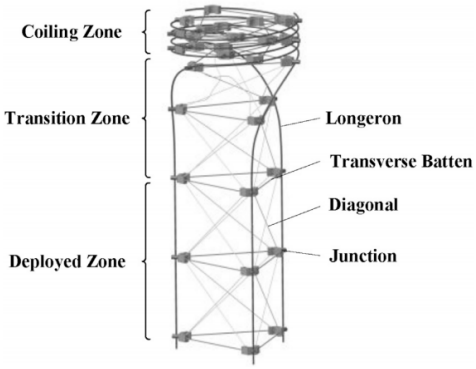

(c) Coilable mast example [24]

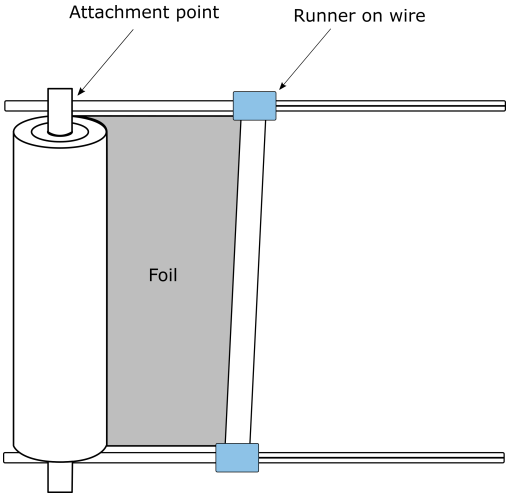

(d) Rail deployment mechanism illustration.

Figure 8.5: Various deployment mechanism concepts.

8.3. Design Analysis

8.3.1. Assembly Module

The final configuration of the Assembly Module will have 51 Starship Modules. These 51 Starships have to be placed in a structure that is symmetric along the lateral axes, and fit into the architecture given in Figure 8.1b. A convenient architecture to meet the two requirements is to have two layers of the 2-ring configuration (right on Figure 8.1b), followed by a 1-ring layer (left on Figure 8.1b), and at the top it has a 1-ring layer excluding the Starship Module in the middle. The configuration is illustrated in Figure 8.6b.

The key aspect of the Assembly Module that will be limiting for design will be the docking interfaces between the Starship Modules. Docking interfaces are an important component for many robotic procedures, but in the case of IKAROS these interfaces must also transfer extreme propulsive loads from the raptor engines carrying the module from GTO to GEO. The importance in the design of the docking interfaces is therefore reliant on two components: docking reliability, and structural design and performance. These two components will be treated separately.

8.3.1.1. Docking Reliability

To ensure docking of Starship Modules with one another, a standard interface must be designed to allow for angled docking and ensure precision errors in control are mitigated. Another aspect of the docking

interfaces is that there will be an axis-symmetric male and female interface. This design will utilise a spring-mass latch system which is engaged and disengaged through the rotation of a given interface.

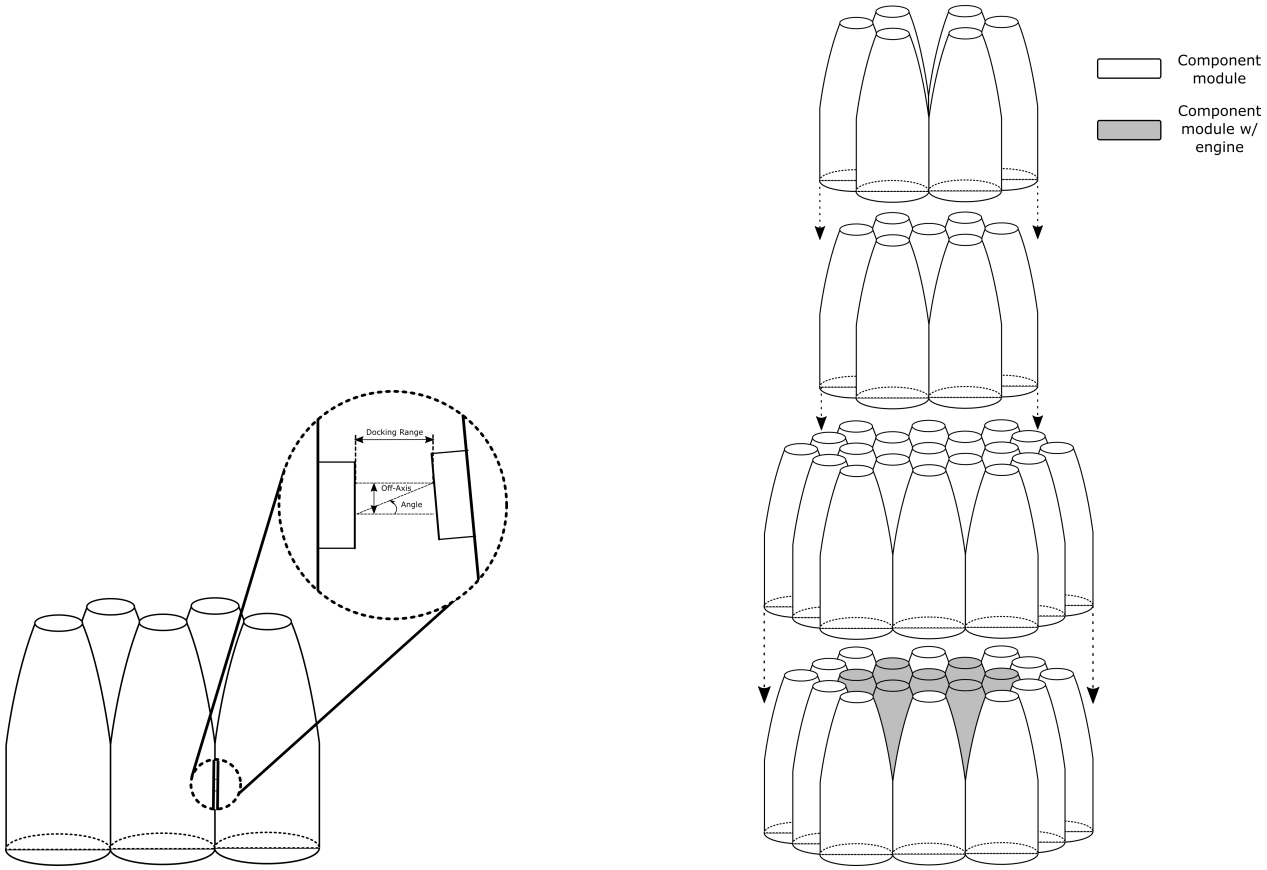

(a) Docking between Starship Modules demonstrating docking errors.

(b) Assembly Module general configuration, propulsion modules shown in bottom-most section.

Figure 8.6: Assembly Module docking and configuration.

The docking error is mitigated through the use of conical connections, where by a range of docking angles will still result in a successful locking.

8.3.1.2. Structural Design and Performance

Here the structural design of the Starship Modules and their interfaces will be analysed. This analysis is dependent on the position and thrust capabilities of the propulsion system being used, in this case the Raptor engine. To maximise the load distribution across the Assembly Module, the propulsion system/-modules will be the seven centre modules shown in Figure 8.6b. In order to analyse the forces exerted on these modules and their connections, the corner case of Starship Modules connected to only three others (Figure 8.1b) must be analysed for the interface design. This design is, however, beyond the scope of this report.

8.3.2. Assembly

Assembly of the structure will require a robust assembly procedure to incorporate as much automation as possible, this precise assembly procedure is beyond the scope of this report and therefore only a high-level procedure will be outlined per sub-system. The time-line of assembly will be detailed in Chapter 15, but estimated assembly times for the primary components will be given in the following subsections for reference, using values shown in Figure 8.3. It is important to note that these assemblies were human-assisted so assembly rates will likely be higher, and therefore a safety factor (SF) of 2.0 will be used on the assembly rates throughout these estimations, i.e. assuming it will take twice as long to complete a given task.

These assembly times are defined as the amount of working time that would be required and does not

include the time needed to travel between cargo and assembly position nor does it include any downtime that may be incurred due to failure of certain connections. Additionally the assembly rates used for these estimates will assume that three Phoenix systems will be used to add redundancy and at least mach the number of astronauts seen in Figure 8.3. This will be discussed in more detail in Chapter 15.

8.3.2.1. Queen Reflectors

The Queen reflector mirrors had to be segmented into parts in order to be stowed and transported. To simplify the design process it was decided that this segmentation would result in equal radial steps resulting in a maximum segment length of roughly 22m, which could be further divided for easier stowing but deployment would be at this maximum length. Due to the parabolic shape, segments become slightly shorter towards the centre of the dish with a minimum length of roughly 20m.

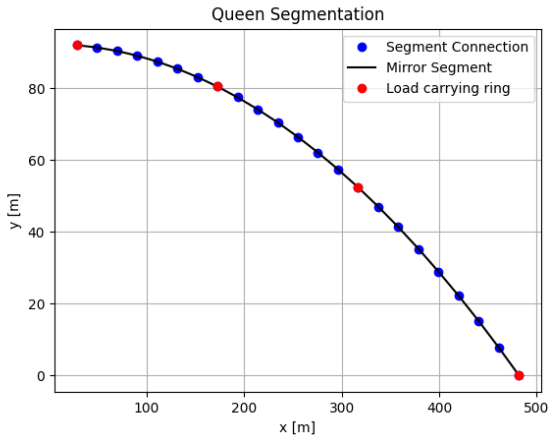

Figure 8.7: Segmentation of the Queen along the x-y plane into 22m long segments.

Chapter 9 works more in-depth on the load carrying rings shown in Figure 8.7, but aside from these elements, all segmentation points are shown in this diagram.

Relay and Sting Reflectors

The Relay and Sting reflectors both will use more rigid mirrors than the Queen, and thus require a assembly without the need for deployment. To achieve this, hexagonal segments will be used to make up each ellipse similar to the assembly of the James Webb Telescope. To standardise the design of these segments and have reasonable production deployment these individual mirrors will need to have a width that is divisible into both the Relay and Sting radius. In order to allow for stowing in the Starship, a common width of less than 4 m must be used for each hexagonal segment (where some segments are cut to fit the elliptical edge of the given reflector) although an optimal solution for manufacturing and area loss due to segmentation should be found in further iterations of design. An indication of the relative scale of these systems can be seen in Figure 8.8, where the Relay hosts ≈ 400 segments and the Sting ≈ 80.

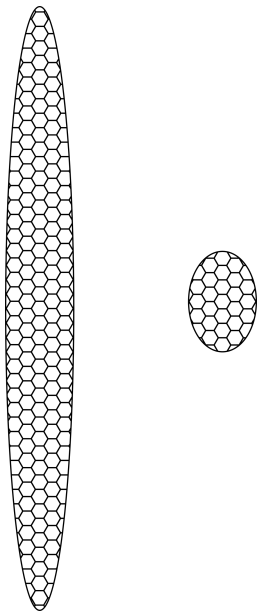

Figure 8.8: Relay and Sting initial segmentation and relative scale.

With these numbers in mind, assembly of these panels – assuming a similar time per panel as the tetrahedral panels in Figure 8.3 – would take roughly 118080 s or 32.8 hours (not including traversal time or structural assembly).

The stowing of these panels can be achieved through stacking in a rigid tower which can then be deployed from the launch vehicle. From this tower, panels can be gripped and placed in their required position on-orbit following the assembly of its supporting structure.

Skeleton Structure

The skeleton structure comprises of a total truss length of 102 578 m, as determined in Chapter 9. This may be used as an estimate for the amount of joints and ultimately the amount of time that will be required for the assembly of the total structure but does not include the attachment of smaller attachment locking mechanisms and support structures for subsystems, for example. This assumption leads to a true assembly time that is likely greater than that estimated using this total length, and therefore a 1.5 safety factor will be used on the assembly rate, as it was for the Relay and Sting assembly. Using the cargo bay dimensions of the Starship Module which allow a maximum height of 22m (although the structure will likely be folded to reduce its footprint further), the number of separate structure elements that will need to be connected can be estimated as $102,578/22 \approx 4663$.

Referring again to Figure 8.3, a worst case assembly rate of $38 \cdot SF$ s will be used, resulting in a total assembly time of ≈ 354388 s or 4.10 days.

8.3.3. Deployment

Queen Reflectors

The deployment mechanism used for the Queen reflector surfaces will be the rail mechanism. This requires some rigid appendage that can be pulled via cables by an electric motor before attaching to the necessary rib. This attachment can use existing mechanism, such as the locking mechanism for flexible appendages. Both of these mechanisms are illustrated in Figure 8.9.

As can be seen in Figure 8.9a, the radius of the reflector sheet rolls will vary depending on the amount of sheet needed for a given segment of the Queen. The calculation of this radius is performed in a step-wise fashion and analyses the circumference travelled as 0.125mm thickness is added after each roll, and is dependent on the initial inner radius which is determined by the minimum bending radius of a given sheet. With the limitation on a 0.125mm thick foil coated in silver likely having a production limit rather

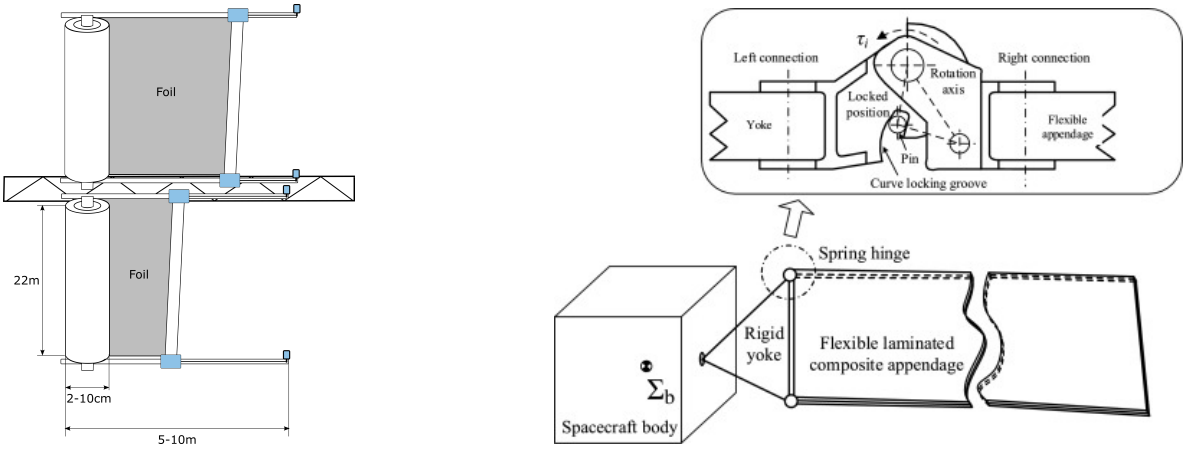

(a) Configuration of deployment mechanism.

(b) Configuration of locking mechanism [25]

Figure 8.9: Queen deployment and locking mechanisms.

than a material limit a rule of thumb of $0.5 \cdot r_{outer}$ for the inner radius will be used, resulting in an inner and outer radius of 11mm and 22.875mm, respectively.

Worker Reflector

Since the Worker will be significantly smaller in size to the other reflector surfaces, a separate deployment technique that maximises ease of assembly and thermal considerations may be used. Notably, this will be an optimised origami folding of the 50m diameter parabolic shape. This folding structure would follow a similar technique shown by Sessions et al. for parabolic antenna for radio telescopes [6], giving a goal mesh for a given curve as seen in Figure 8.10. This reflector would fold into a ring of less than half the diameter and would need to be half the depth in order to stow into the Starship Module.

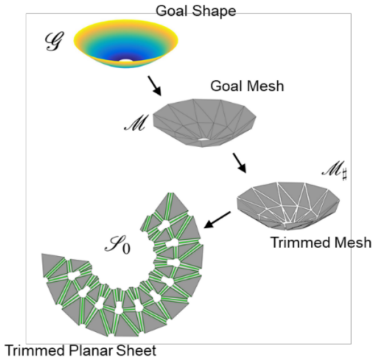

Figure 8.10: Steps in the design process for origami with smooth folds [6] [7]

An important note is that this research was conducted for active materials, which IKAROS will not be using for the Worker. Therefore, for the deployment of the reflector a telescopic boom deployment mechanism (Figure 8.5a) would need to be used for the unfolding, and then locked in place. The segmentation of this reflector is beyond the scope of this report but will, similar to the Queen, be a combination of flat segments connected by hinge joints.

9
Structures

This chapter will detail the design of the spacecraft structure. Firstly, it will define the problem that needs to be addressed in Section 9.1. This is followed by how the solution was approached together with design choices in Section 9.2. Lastly, an overview of the structural characteristics of the spacecraft will be given in Section 9.3.

9.1. Problem definition

The role of a structure is to withstand loads and allow for integration of systems and assembly. The loads that the spacecraft should be able to withstand are illustrated in the load cycle Table 9.1.

Stage	Pre-Launch	Launch	Transfer	Orbit
Loads	• Handling loads • Transportation loads • Qualification loads	Dynamic loads: • Steady state accelerations • Sinusoidal vibrations • Random vibrations • Acoustic loads • Shock loads • Pressure variations	Transfer Loads	• Deployment loads • Assembly loads • Temperature gradients • Thermal loads • 0g loads • Micro-meteorites • Debris impacts

Table 9.1: Spacecraft load cycle

Given that the spacecraft design is still at a conceptual stage, not all the loads could be taken into the upcoming analysis as their magnitude could not be determined with the current level of detail. With this in mind, the problem this chapter will solve is that of designing a structure that is able to carry certain orbit/launch loads and allow for the assembly of the whole structure. Based on this, the following requirements were formulated.

- **SSR.STRUC.LAU.1:** The launch module shall be able to withstand a steady state axial acceleration of 6g's.
- **SSR.STRUC.LAU.2:** The launch module shall be able to withstand a steady state lateral acceleration of 3.5g's.
- **SSR.STRUC.LAU.3:** The launch module shall be able to withstand a lateral vibration of 25Hz.
- **SSR.STRUC.LAU.4:** The launch module shall be able to withstand pressurisation loads.
- **SSR.STRUC.LAU.5:** The launch module shall be able to withstand acoustic loads of up to 137.7dB.
- **SSR.STRUC.LAU.6:** The launch module shall be able to withstand a shock load of <TBD>.
- **SSR.STRUC.ORB.1:** The structure shall be able to withstand transfer loads of <TBD>.
- **SSR.STRUC.ORB.2:** The structure shall be able to withstand manoeuvre loads due to a 1 degree change in attitude in 30 minutes about every axis.

- **SSR.STRUC.ORB.3:** The structure shall be able to withstand thermal loads due to temperature differences in the structure.
- **SSR.STRUC.ORB.4:** The structure shall be able to withstand impact of micro debris with a diameter of up to 1cm.
- **SSR.STRUC.ORB.5:** The structure shall be able to withstand impact of micro meteorites with a mass of up to 10^{-6} grams.
- **SSR.STRUC.ASS.1:** The structure shall allow for allow for the integration of the subsystems.
- **SSR.STRUC.MAI.1:** The structure shall allow for maintenance of the spacecraft.
- **SSR.STRUC.PAY.1:** The truss connecting the Queen with the Worker shall have a maximum deflection of 1mm.
- **SSR.STRUC.PAY.2:** The truss connecting the Queen with the Sting shall have a maximum deflection of 5mm.
- **SSR.STRUC.PAY.3:** The truss connecting the Queen with the Relay shall have a maximum deflection of 5mm.

9.2. Approach & Design Options

The approach that was used for designing the structures was to work backwards from the orbit configuration to the modules that should fit inside the Starship. This means using the configuration of the on orbit payload, the structures and assembly department worked together to come up with a structure that could be modularised and assembled. Once this was established, the structural components were designed to be able to withstand the major load cases it would experience in orbit.

The first design option that had to be chosen was the materials to be used for the structure. As the structure is extremely large, a massive amount of material will be required regardless of the material choice. Options considered were metals (steel/aluminium/titanium) and composites (carbon fibre, Kevlar). Ultimately, at this stage the choice was made to go with aluminium as it is a isotropic, lightweight, widely available, strong and proven material that is usually chosen for structures operating under 200 degrees Celsius [26] such as this spacecraft (see Chapter 10). The aluminium alloys considered can be seen in Table 9.2. It was decided that Aluminium 6061-T6 would be used for the structural components as it is the lightest of the ones listed above.

Material	ρ (kg/m^3)	σ_u (MPa)	σ_y (MPa)	E (GPa)
Al 2014-T6	2800	441	386	72
Al 2024-T36	2770	482	413	72
Al 6061-T6	2710	289	241	67
Al 7075-T6	2800	523	448	71

Table 9.2: Material properties of different aluminiums [26]

The sizing of the trusses connecting the Queen to the other mirrors was based on the schematic seen in Figure 9.1 where the blue circle represents a point mass representation of a mirror (either the Worker/Sting/Relay). Looking back at Figure 4.2 this corresponds to a rotation around x which is the most critical case for the loading of trusses. Here the problem was simplified to a beam with a load at the end, this was done by taking a co-rotating axis system when there is a positive angular acceleration about x at the snapshot of time during maximum angular acceleration (as this is sizing). Then the loads due to the angular accelerations were calculated as seen in Equation 9.1 based on circular motion theory where m is the mass at the tip of the beam, α is the angular acceleration of the manoeuvre (derived from **SSR.STRUC.ORB2**), ω is the angular velocity and r is the radius from the centre of mass (axis of rotation). Note the tangential and radial forces are opposite the direction of motion as they are inertial forces.

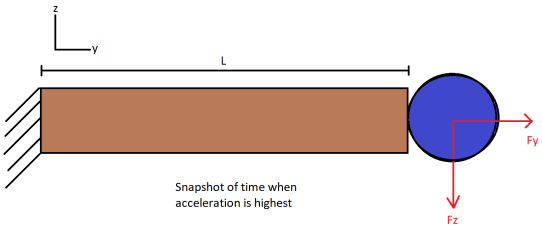

Figure 9.1: Truss sizing schematic

$$\text{Forces} = \begin{cases} F_z = m\alpha r \\ F_y = m\omega^2 r \end{cases} \tag{9.1}$$

Using the tangential force a deflection of the trusses could be found via a standard solution for a beam fixed on one end and free at the other seen in Equation 9.2 where P represents a vertical load at the end of the beam, l is the length of the beam, E is the Young's modulus of the beam material (Aluminium) and I is the area moment of inertia of the beam in Z direction. Note that only the mass of the mirror is considered in this analysis as the beams themselves are assumed to have no mass and therefore experience no forces due to the angular acceleration.

$$\delta_{max} = \frac{Pl^3}{3EI} \tag{9.2}$$

Based on Equation 9.2, the required inertia of the beam could be calculated based on the deflection requirements (**SSR.STRUC.PAY1** - **SSR.STRUC.PAY3**). The cross section was then decided upon (multiple beams of rectangular cross sectional area to represent a truss structure) as seen in Figure 9.2a, Figure 9.2b wherein the distance from the concentrated masses to the middle point was determined by the attachment with the mirror. For example, the Worker truss connected to the Worker at 4 points and the radius of the Worker was 25m therefore the squared beams were assumed to be equidistant at 25m from the middle. Then the deflection requirement was assumed to be sizing as the actual forces acting on the beam are in the order of magnitude of Newtons so no failure is expected due to shear or axial forces (specially considering trusses do well against buckling). Now that the cross sectional area was found based on the required second moment of area for each truss, and the length of the trusses were determined by the layout configuration, a mass estimate was found based on a density of aluminium of $2700 kg/m^3$. This process had to be iterated a couple of times as the mass of the trusses affected the centre of mass of the structure therefore changing the r term in Equation 9.1.

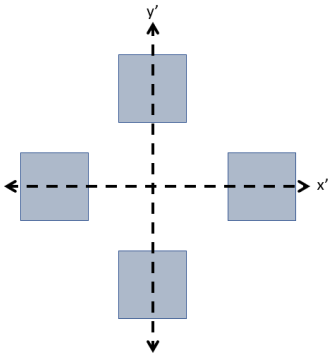

(a) Worker truss cross section simplification

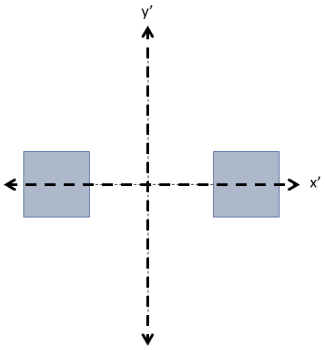

(b) Sting/relay cross section simplification

Figure 9.2: Cross section of different trusses

The next structural component that had to be designed was the supporting structure to the Queen that would allow for its shape and carry the relevant loads. The approach for this was based on the assembly of the big parabola, the structure would need to allow for the increase in amount of reflecting foils needed towards the outer radius of the parabola (as the circumference here is a lot larger than that in the inner radius). To tackle this issue, a configuration was decided with 110-296 radial spokes (more on the outer edge) and 4 concentric rings at a constant 144m intervals in the radial direction that allowed for a constant pitch of 10m at the end of each ring between each reflective foil rollout. A visualisation of this from the top view can be seen in Figure 9.3.

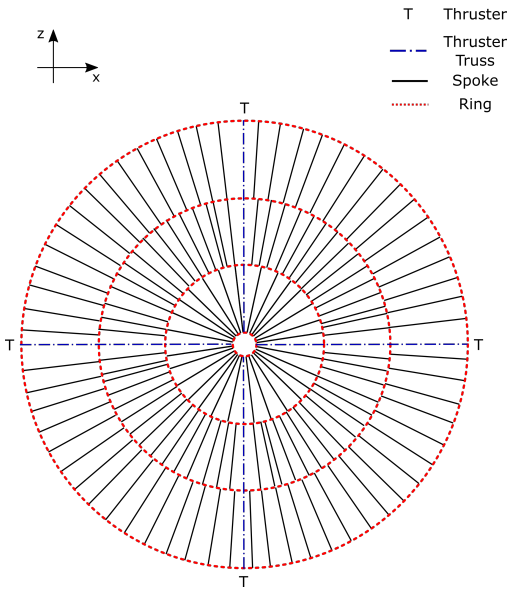

Figure 9.3: Visual representation of the Queen's skeleton structure

As seen in the [Figure 9.3, there are 4 spokes running from the inner to the outermost ring that will act as the connection point for the thrusters. These spokes were sized based on the normal forces acting through them caused by the thrusters (as the shear was assumed to be taken up by the outermost ring) with the force stress relation $\sigma_u = \frac{F_n}{A}$ assuming the same cross sectional simplification from Figure 9.2b. The sizing of the concentric rings was done taking the mass per length of the Queen to Sting connecting truss. A more accurate approach would have been to size these rings for the torque that they will be carrying as the thrusters will want to twist the structure from the outer ring inwards when rotating about the y axis (Figure 9.6 for reference).

Something that should be accounted for further down in the design is the collision of the structure with micro-meteorites and debris. This is of particular concern for the Queen as the foil would need to be able to withstand the impact of these collisions. Models for the flux of micro-meteorites/debris in terms of particles/year/m^2 can be seen in Equation 9.3 and Equation 9.4 respectively [26].

$$logF_m = -1.213logm - 14.37 \tag{9.3}$$

$$logF_d = -1.395logD - 5.46 \tag{9.4}$$

Here F_m stands for the frequency of micro-meteorites per m^2 per year, m represents a mass m or larger. Similarly F_d stands for the frequency of debris particles with a diameter of D or bigger that will impact the spacecraft per m^2 per year. Note these equations are only valid for $10^{-6} < m < 1$ gram meteorites and $1 < D < 2$ cm debris particles. As per **SSR.STRUC.ORB4** and **SSR.STRUC.ORB5** and the surface area of the Queen ($756054.63m^2$) results in a total of 1.5 micro-meteorites colliding with it along its 25 years of operation, similarly for debris it would mean a total of 65.5 particles of debris colliding with the

Queen throughout its 25 years of operation. The reason these impacts raise concern is because orbital debris orbits at 7.5km/s (+ the spacecraft's velocity if orbiting in opposite direction) around the earth with a density in the order of magnitude of $2.8 g/cm^3$ and micro-meteorites can travel at speeds exceeding 70km/s with densities in the region of $0.5 g/cm^3$ [26].

With the mass of the structures on orbit calculated, the following step was to decide on a configuration of the launching vehicle and size them supporting structure for the biggest loads the spacecraft will experience, the launch loads (**SSR.STRUC.LAU1** - **SSR.STRUC.LAU4**). The approach taken to size the supporting structure during launch was as follows:

1. Assume an idealised structure inside the cargo bay of the Starship
2. Consider the loads that are acting on the structure during launch
3. Size the structure for whichever combination of loads is critical (vibrations or due to accelerations)
4. Iterate till a suitable structure and payload mass is acceptable

Starting with the idealised structure, given the amount of launches that will be required to bring the spacecraft to space it is impossible, at the moment, to size the supporting structure in a discrete manner due the the number of launches and therefore launch modules. The approach for the structures sizing instead is to first size the supporting structure that would be needed assuming the full 100 tonnes to get an upperbound, using the dimensions seen in Figure 9.4a a simplified mass distribution of the mass inside the cargo bay was assumed as illustrated in Figure 9.4b where it is assumed to be a cylinder with a point mass acting on the top of it the mass distribution between the cylinder and the point mass is 0.9 and 0.1 respectively of the total on mass on the cargo bay due to 10% of the volume being in the section from 12 to 17.24meters.

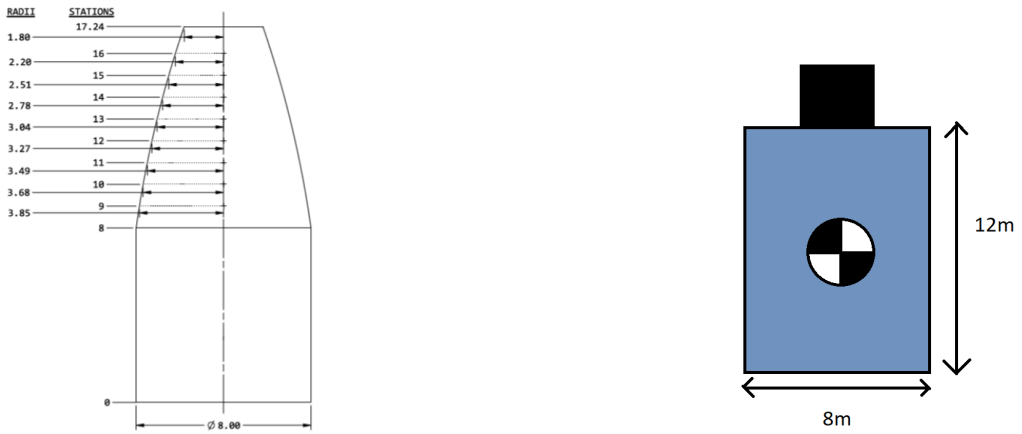

(a) Starship cargo bay dimensions [9]

(b) Simplified cargo bay launch module configuration

Figure 9.4: Starship cargo bay dimension and idealised mass fitting

Based on this configuration, a hollow cylinder (monocoque) structure was designed that would be able to carry the loads the launch module is to experience during launch. The main two load cases that were designed for were for lateral vibrations and the accelerations illustrated in Figure 9.5. The requirement for the lateral vibrations tolerance will be of $25 Hz$ this number was not given in the Starship user's manual but had to instead be assumed based on the vibrations in the Falcon Heavy and the Arianne 5 launcher which were 35Hz and 10Hz respectively. An optimistic number of 25Hz was decided upon as the Starship is still a launcher in development and hopefully will perform better than SpaceX's Falcon launchers in this regard.

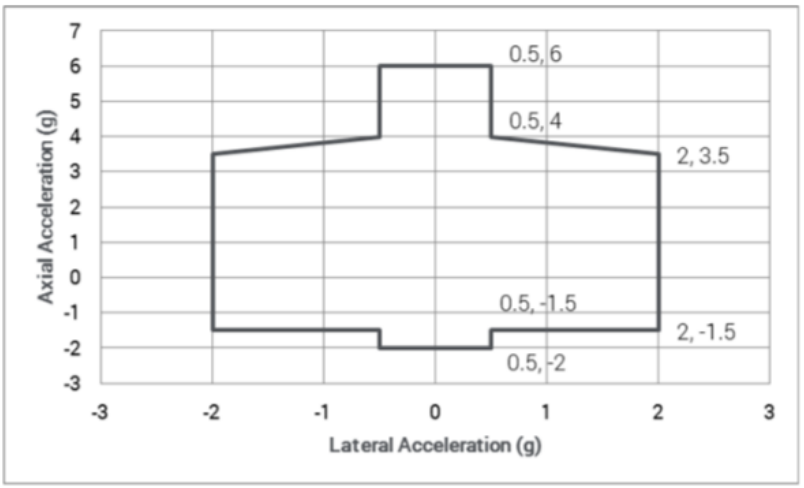

Figure 9.5: Starship accelerations enevolope [9]

The sizing for the hollow cylindrical supporting structure was done as outlined in the structures part of Space Mission Analysis and Design [27]. In short it compares these two aforementioned load cases in terms of which requires most supporting structure and then checks to verify it does not fail in buckling. For the material properties required for this sizing, the same material as the trusses was taken Aluminium 6061-T6. Starting with the frequency requirement, using a standard solution with for a cylinder fixed at its base with a point mass acting on top of it the required thickness of the cylinder can be found as seen in Equation 9.5 and Equation 9.6 by setting the required f_nat to be equal to $25Hz$.

$$f_{nat} = 0.276\sqrt{\frac{EI}{mL^3 + 0.236m_BL^3}} \quad (9.5) \qquad I = \pi R^3 t_f \quad (9.6)$$

In the above equations f_{nat} is the natural frequency, E is the Young's Modulus of the material, I is the second moment of area of the supporting cylinder, m is the point mass at the top of the idealised structure, m_B is the mass of the body of the idealised structure, L is the length of the idealised structure (12m in our case), R is the radius of the idealised structure and lastly t_f is the thickness that fulfils the frequency requirement. The other load case to be considered is that of the accelerations acting on the module, to determine how much axial stress is acting on the hollow supporting cylinder the axial and bending stresses need to be superimposed. These axial and bending stresses depend on the maximum acceleration in axial (6g) and lateral (2g) direction respectively as seen in Figure 9.5. The way this is done is seen in Equation 9.7 and Equation 9.8.

$$P_{eq} = 1.25(P_{axial} + \frac{2M}{R}) \quad (9.7) \qquad \sigma_u = P_{eq}/A \quad (9.8)$$

Here P_{eq} represents the equivalent axial stress due to the axial stress P_{axial} and the moments M coming from the lateral accelerations acting through the centres of mass at their respective height (2 since the lateral accelerations are assumed to be in the two 3D directions perpendicular to the axial reference). Note the 1.25 is a design load safety factor. Finally, the thickness required can be calculated using the fact $A = 2\pi R t_{acc}$ where t_{acc} stands for thickness required to meet acceleration requirements. Lastly, depending on which thickness is higher t_{acc} or t_f the highest one is chosen and checked for compressive buckling failure using Equation 9.9 and Equation 9.10.

$$\sigma_{cr} = 0.6\gamma\frac{Et}{R} \quad (9.9) \qquad P_{cr} = \sigma_{cr} * A \quad (9.10)$$

Where σ_{cr} is the critical buckling stress which depends on γ (which is a geometrical paramenter related to the thickness and radius) and P_{cr} is the critical buckling load. The criteria that must be fulfilled is that

$P_{cr} < P_{eq}$, if this is not fulfilled then it is iterated through increase the thickness until it is. Note for these last equations the thickness used is $max(t_f, t_{acc})$.

The mass of the supporting hollow cylinder can finally be calculated using the density of the material and the volume by $m_{cyl} = \rho \cdot A \cdot L$. For the Starship assuming a payload mass of 100 tonnes leads to a supporting structure with a mass of 16 tonnes, by varying the payload mass one can find a combination of payload + supporting structure mass that falls within the 100 ton launching capabilities of the Starship. For example, a payload mass of 85 tonnes is compatible as it requires 14 tonnes in supporting structure (with a 2.5cm thickness) for a total of 99 tonnes.

Lastly, the hoop stress on the cylinder due to the internal pressure on the cylinder can be determined using Equation 9.11 (the 1.25 is a safety factor). Where σ_h is the hoop stress, p is the internal pressure, R is the hoop radius and t is the cylinder thickness. However, since the internal pressure of the cylinder has not been decided (some components might need certain pressures) this is left parametrized until a maximum internal pressure is decided. Note this stress is not usually a sizing requirement but should be kept in mind regardless.

$$\sigma_h = 1.25 \frac{pR}{t} \tag{9.11}$$

9.3. Structural Characteristics

With the structures sized, an overview of the structural characteristics like the c.g. and MMOI of the spacecraft in orbit can be seen in Table 9.3 and Figure 9.6. These were used in Chapter 7 to deal with manoeuvres and disturbances. Table 9.3

C.G in X $[m]$	0
C.G in Y $[m]$	371.5
C.G in Z $[m]$	131.9
MMOI X $[kgm^2]$	1.4E12
MMOI Y $[kgm^2]$	1.75E12
MMOI Z $[kgm^2]$	6.9E11

Table 9.3: Spacecraft characteristics

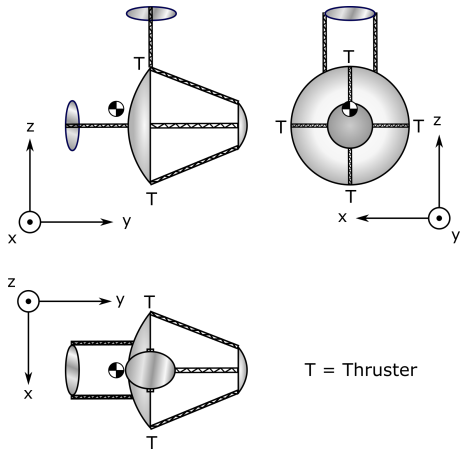

Figure 9.6: Spacecraft configuration and thruster load locations

10
Thermal Control Subsystem Design

This chapter is about the design and philosophy behind the thermal control subsystem. Starting with the problem definition, this chapter will address the requirements and a thermal flux model which is used for IKAROS. Then a suitable design solution is presented using argumentation and results of the heat flux model and the final thermal conditions are summarised.

10.1. Problem Definition

One of the critical subsystems of IKAROS is the thermal control. That is because IKAROS is concentrating a lot of energy onto small surfaces which can have catastrophic results if not taken care of. Therefore the most critical parts of IKAROS are the small dish, the reflector, and the relay. These parts will be subjected to very high concentrations of energy and will need to be cooled actively. Components such as electronics and mechanical linkages come with allowed operating temperatures, otherwise the manufacturer cannot guarantee the performance of the component. The thermal control will be required to cool parts by either emitting it locally or by moving the heat and dissipating it at a radiator or other thermal control device. From these statements, the requirements can be formulated for the thermal control subsystem.

- **SSR.THC.TOP.1**: The thermal control subsystem shall prevent overheating and under-cooling of components
- **SSR.THC.PAY.2.1**: The thermal control subsystem shall maintain large parabolic mirror temperatures between -10°C and 100°C
- **SSR.THC.PAY.2.2**: The thermal control subsystem shall maintain temperatures of the small dish, relay, and reflector mirrors between 0°C and 175°C
- **SSR.THC.PAY.3**: Active thermal control subsystems shall use loops in parallel.
- **SSR.THC.POW.1**: The thermal control subsystem shall maintain battery temperatures between 0 °C and +20 °C.
- **SSR.THC.POW.2**: The thermal control subsystem shall maintain solar array temperatures between -60 °C and +60 °C.
- **SSR.THC.AIV.1**: The thermal control of assembly robotics shall maintain temperatures between -15°C and +50°C.
- **SSR.THC.PROP.1**: The thermal control subsystem shall keep the propulsion components' temperatures between -5°C and +40°C.
- **SSR.THC.PROP.2**: The thermal control subsystem shall keep temperature of propellant <10>°C higher and lower than the freezing and melting point respectively.
- **SSR.THC.STRUC.1**: The thermal control subsystem shall maintain the temperatures of mechanisms between +5°C and +50°C during operation.
- **SSR.THC.MEAS.1**: The thermal control subsystem shall measure the temperature of other subsystems.
- **SSR.THC.TOP.2**: The thermal control subsystem shall prevent complications due to large temperature gradients.

- **SSR.THC.PROP.3**: The thermal control subsystem shall ensure a temperature difference of <5°C between propellant tanks.
- **SSR.THC.STRUC.2**: The thermal control subsystem shall ensure a spatial temperature gradient of structural elements of <3°C/m.
- **SSR.THC.TOP.3**: The thermal control subsystem shall prevent complications due to rapid temperature changes.
- **SSR.THC.ELEC.1**: The thermal control subsystem shall ensure a temperature gradient over time for electrical components of <5°C/hour.

The thermal control subsystem will have two distinct main tasks. The first task would be to keep the other subsystems in the necessary temperature range, the second task would be to keep the payload in the right temperature range. Due to the relatively large size and significance of the payload, the latter will be what this analysis is mostly focuses on. However, measures for maintaining a stable thermal environment for the other subsystems will be discussed as well.

In order to determine the level of required thermal control for the payload and the adequacy of possible solutions, a heat balance model based on the theoretical thermal fluxes is developed. The thermal model will aid in calculating the temperature balance of the main components of IKAROS as it orbits Earth by solving for the incoming radiation, outgoing radiation and the equilibrium temperature at that time. Through this method, a baseline operating temperature is found, and the necessary steps to meet the requirements can be determined. Possible steps include a higher heat retention or rejection, a higher or lower thermal conductivity to slow down temperature gradients, or slight changes to the system layout.

The first step of developing a thermal flux model in the target orbit is defining the environment. In a Geo-synchronous Equatorial Orbit, the main external influxes of thermal energy are the solar irradiation, the albedo reflection on the surface of Earth, and the IR radiation from Earth.

A number of theoretical assumptions are required to facilitate a consistent simulation of the system heat balance. Table 10.1 gives an overview of these assumptions.

One important assumption is that the specific heat as a function of temperature C_p can be modelled using Equation 10.1 of the form [29]:

$$\ln C_p = A + B \ln T + C(\ln T)^2 + D(\ln T)^3 \tag{10.1}$$

The specific heat of the system will be dominated by the aluminium used as a substrate and supporting structure for each component, as determined in Chapter 9. Through that, the values of the constants in Equation 10.1 can be determined based on experimental data. On an interval between 50.2698 K and 933.2 K, the equation is fitted to 1% accuracy using the following coefficients [30], with 50.2698 K for the temperature at the start of the interval, T_i:

$$\ln C_p = -3.3767 + 2.4552\,[\ln T - \ln T_i] - 1.1284\,[\ln T - \ln T_i]^2 + 0.18572\,[\ln T - \ln T_i]^3 \tag{10.2}$$

The properties of different components as analysed in the baseline model can be found in Table 10.2.

Descriptor		Hot Case	Cold Case
Sunlight	Assumption	constant	max. 72 minutes of downtime
	Effect	constant influx of solar energy strongly heats up the focal point	downtime means a drastically decreased solar energy influx
Mirror efficiency	Assumption	min. 90%	max. 95%
	Effect	10% of solar energy can be absorbed as heat	max. 5% of the solar energy is absorbed as heat
Earth projection	Assumption	linear interpolation between 0-90-180-270 degree projections in orbit	
	Effect	interpolating between 4 steps is not a precise step-wise calculation, but accurate enough for an orbit-wide heat balance	
Internal conductivity	Assumption	distributed equilibrium per component	
	Effect	the heat would form a distribution across each component, front to back, but due to the large area-to-thickness ratio this distribution can be neglected	
Specific heat	Assumption	dominated by aluminium, and can be modelled as an equation of the form $\ln C_p = A + B\ln T + C(\ln T)^2 + D(\ln T)^3$	
	Effect	using experimental data to fit the equation coefficients, the model reaches a 99% accuracy	
Thermal conductivity	Assumption	constant	
	Effect	experimental data suggests a temperature dependence, but on the relevant temperature range it has minimal impact [28]	

Table 10.1: An overview of the assumptions made for the thermal flux analysis

Component	Finish	Emissivity	Absorbtivity
Inside large dish	Mirror foil	0.05	0.09
Outside large dish	Black coating	0.95	0.94
Inside small dish	Rigid mirror	0.05	0.06
Outside small dish	White coating	0.95	0.35
Structure	Galvanised	0.95	0.94
Front relay	Rigid mirror	0.05	0.06
Back relay	White coating	0.95	0.35
Front reflector	Rigid mirror	0.05	0.06
Back reflector	White coating	0.95	0.35

Table 10.2: Overview of properties of components as used in the thermal flux baseline model [31]

The core of the model is the heat balance between the external heat irradiation, the internal heat level, and the radiated heat, as seen in Equation 10.3:

$$Q_{internal} + Q_{external} = Q_{radiated} = \sum^{n} \varepsilon_n \sigma A_n T_n^4 \tag{10.3}$$

Here, the radiated heat is equal to the sum of the radiation of the components. In this equation, the ε_n, A_n, and T_n are respectively the emissivity, radiating surface area, and internal temperature of each component, and σ is the Stefan-Boltzmann constant. Furthermore, in this heat balance, it is assumed that $Q_{external} = q_{solar} + q_{albedo} + q_{EarthIR} + q_{interface}$, whereas the $Q_{interface}$ is governed by heat conduction between interfaces, modelled using Fourier's law as seen in Equation 10.4 [27, 32].

$$\frac{Q}{\Delta t} = -kA\frac{\Delta T}{\Delta x} \tag{10.4}$$

Where k is the thermal conductivity, A is the interface surface and Δx is the one-dimensional distance between the ends. Finally, the internal heat $Q_{internal}$ added to the component is then found by solving Equation 10.3.

Using the internal heat, the average temperature change ΔT per component can be determined by using the specific heat c of each material, the found internal heat, and the total mass m of the component in the relation $Q_{internal} = cm\Delta T$. By running the model for three orbits without yet implementing any thermal control solutions, a baseline is obtained. The average temperature over time of the main components is plotted in Figure 10.1.

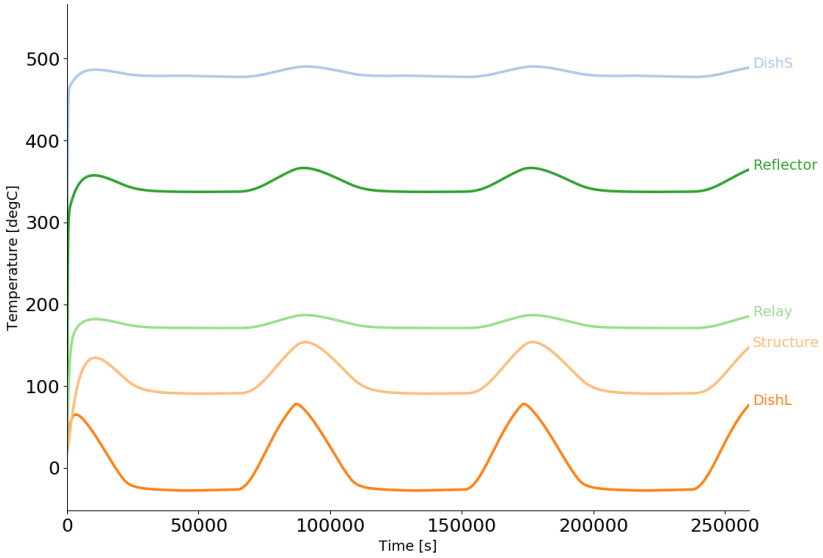

Figure 10.1: Temperature over time per component using a 10 second time-step for a 72 hour simulation in orbit, without any added thermal control

Through this preliminary analysis of the payload structure, it is seen that the reflector, small dish, and supporting struts absorb too much heat from the focused sunlight, and the large dish has a broad temperature range and gradient that indirectly affects the other components through internal diffusion. Thermal management should focus on solving these issues.

10.2. Solution Design Options

The thermal control system is divided into two categories. The first category is for components of IKAROS that do not require extensive thermal control and that can be treated using traditional thermal control methods such as coatings, protective films and small heat shields. The second category addresses the large parts which require active thermal control solutions because passive methods will not suffice.

10.2.1. Traditional Methods

The parts that can be treated using traditional methods are electronics, propellants, mechanisms and the solar arrays. Traditional methods are best applied based on the requirement and position of the part. These are proven methods that are used on many existing spacecraft and are therefore validated by other missions. Traditional methods can also be used in combination with each other which makes it easy to add or remove thermal control. When looking at the orientation of IKAROS, and considering that most of these components are not in direct sunlight, it is possible to say that the incoming energy for these components is mostly varied by the reflected heat due to the albedo of Earth. As a result, most components' thermal variation can be reduced by using insulating materials and if necessary, a high emissivity solution can be added. This way a the temperature variation can be kept low and the maximum below the specification of the manufacturer. The possible solutions explored for traditional methods are:

- **Multi-Layer Insulation (MLI)**: This is the most common form of thermal control for spacecraft as it prevents high heat losses and gains. MLI blankets are perfect solutions for systems that generate heat and have a small operating temperature range as the insulation will prevent large fluctuations. The surface area and thickness of the blanket will determine how much is radiated into space. The MLI blankets are commonly made using mylar, fibreglass, Nomex and Teflon [33].
- **Coating**: Something as simple as a coating can be very effective. Coatings are a cost effective way to lower or increase the thermal energy that is radiated into space. depending on the characteristics

of the coating, this can change the absorbtivity, emissivity and reflectivity. The main downside of a coating is that it can degrade and flake off of the part [34].

- **Foils and shields**: Foils and shields are a middle ground of MLI balankets and coatings. These are often preferred when there are flammabilty concerns with the MLI blankets and if a coating may cause damage to a part. These foils and shields do not insulate or change the properties but they have a similar effect as they prevent fluctuations by preventing the heat from entering the part in the fist place [35].
- **Heat straps and existing parts**: When there are parts that generate heat due to their inefficiency, this heat can be redirected to keep other parts at a reasonable temperature. By using thermal straps and strategic placing of parts, the temperature of parts can be increased and/or decreased. It is also possible to use the straps to move the energy into surrounding structure which may be able to radiate more energy. These straps are often made from highly conductive materials materials such as copper and silver, which have thermal conductivities up to $400 W/mK$ [36].
- **Radiators**: Radiators are a lightweight solution to dissipate extra heat. They weigh very little if integrated into existing structures and can be made dynamic through the use of louvres to contain or dissipate heat when necessary. Radiators can be used in active and passive systems, making them very flexible. Furthermore, they can radiate between 100-350 Watts per square meter, depending on their quality [37].
- **Heaters**: Heaters are a simple way of increasing the temperature of a component. This method of thermal control falls under active control because it works similarly to a thermostat. For components which have tight operating temperature ranges, a heating element, often a coil which generates heat through electrical resistance, can regulate a range of temperatures [38].

For the Electronics the MLI is the solution used by most spacecraft. However, due to the placement of the electronics on the dark side of the Queen, there is not much heat around them. Hence, this thermal system will be in combination with that of the batteries. The batteries release heat whilst charging and discharging, and this heat can be used to keep the electronics in their operating temperature. If the batteries release too much heat, a radiator with louvres for active thermal control is added. The connection between the batteries and the louvres will be through thermal straps. This way the temperature can be maintained in a tight temperature window. In order to model the released heat of the louvres, a simple equation can be set up. This equation can also be used to size the louvres once the batteries and released heat are known. The equation models the system as energy in which is the energy released by the battery pack and electronics, and the energy out which is the radiated energy of the battery pack, electronics and louvres. The input power P_{in} uses the mass of the batteries $M_{batteries}$, the mass specific power as heat of the batteries $q_{batteries}$ and the power released as heat by the electronics $Q_{electronics}$. For the power out, the louvres have a certain area $A_{louvres}$, a maximum performance of $350 W/m^2$ and a operational coefficient E which models the 'active' opening of the louvres. Therefore the maximum value of E is 1, the minimum depends on how much the panel can radiate and is likely to be around 0.2 to 0.3. The battery pack and electronics will also radiate some heat by themselves and these are modelled as $Q_{radiated}$. The values of Q_{in} will vary depending on the type of the batteries used, hence E in Q_{out} is going to increase as the louvres are opened.

$$Q_{in} = Q_{out} \tag{10.5}$$

$$Q_{in} = M_{batteries} \cdot q_{batteries} + Q_{electronics} \tag{10.6}$$

$$Q_{out} = A_{louvres} \cdot 350 \cdot E_{louvres} + Q_{radiated_{batteries}} + Q_{radiated_{electronics}} \tag{10.7}$$

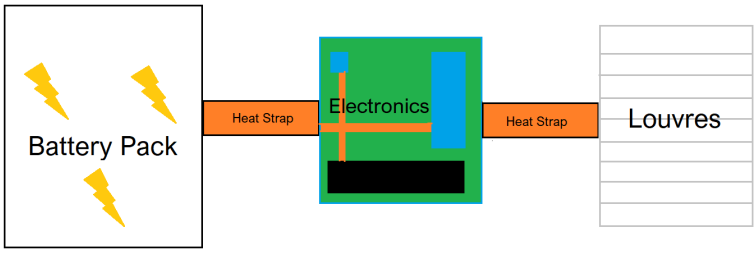

Figure 10.2: Representation of the thermal interface between battery pack and electronics

For the sensors, it is determined that covering with a foil or a shield is a sufficient method for thermal control. IKAROS's payload nor the sensors used for star tracking are highly sensitive to temperature. These sensors can simply be covered in a protective foil to keep the temperature low to improve the durability and prevent cyclical thermal loads on the sensors. Depending on the sensitivity of the sensor, a small piece if MLI can be applied before to insulate the sensor. However this MLI blanket cannot be aluminised on the bottom because then the sensor may short circuit.

Propellant tanks are filled with hydrazine which needs to be kept above 2°C and below 114°C. Depending on the placement of the tanks, the system should be able to operate with just sufficient layers of MLI blankets. As mentioned this depends on the placement. If the propellant tanks are shielded by the big dish, then a simple heating element can be added to keep the fluid from freezing [38].

Mechanisms need to be protected against freezing but have very wide operating temperature ranges. The only concern with mechanisms is lubrication which is a well known problem in space. Pressure is what causes the lubricants of mechanisms to evaporate. Using lubricants specifically designed for space will require protection from the environment and some minimal thermal control. Therefore any sensitive mechanisms are covered in an airtight sleeve, and a MLI blanket [39].

Part	Thermal Solution	Additional Thermal Solutions
Electronics	MLI	Louvres & Thermal Straps
Sensors	coating or foil	MLI
Batteries	MLI	Louvres & Thermal straps
Propellant tanks	MLI	Heating element (resistor)
Mechanisms	MLI	None

Table 10.3: Proposed solutions per subsystems

10.2.2. Developing Methods

The parts that need to be treated using high-power, newly developed methods are the small paraboloid and the reflector. The traditional methods in the previous section are deemed insufficient for managing their waste heat. These parts of the system are almost always in the concentrated sunlight, so the temperature can get very high if nothing is done to dissipate the heat. Ideally, the energy could be moved to other parts of IKAROS to balance the temperature to favourable ranges. The initial runs of the model show that the temperatures are exceeding the allowed temperatures set by the thermal requirements. Due to the geometry of the dishes and mirrors, traditional methods will not be able to provide enough cooling by themselves hence innovative solutions are needed to increase the amount of energy that can be radiated.

- **Large panels with highly conductive elements**: This method would require large copper fins on the structure to increase the area that can radiate. Although copper is a great conductor of heat, to

improve the heat transfer to the top of the panels, pyrolythic graphite rods will act like veins to guide heat to the parts of the panel that are furthest way. With proper coatings, these fins can increase the surface area that radiates very effectively without being limited by electrical components as the temperature of the panel is only limited by the melting point.

- **Liquid Droplet Radiator (LDR)**: The LDR is a conceptual heat management system traditionally used for nuclear power plants. As these have similar waste heat figures to project IKAROS, their design might be adapted for large spacecraft engine thermal control [40]. These systems can reject as much as 63 GW of waste heat and can be six to ten times lighter than conventional solutions [41]. A disadvantage of the LDR is that the TRL is low. There have been no large-scale tests to indicate that this system works in the intended environment.
- **Two-stage pumped cooling loops**: The two stage cooling system used by the ISS uses a dual loop system filled with ammonia. The ammonia can be pumped around the spacecraft whilst absorbing heat. Then there is a heat exchanger from one loop to another which loops in the radiators and radiate the heat into space. This is similar to a traditional radiator except the scale that will be required for IKAROS is going to require eight loops because of the energy that needs to be absorbed and radiated. The cooling is mainly restricted by the size of the radiators.
- **Moving belt radiator**: A moving belt radiator is a design allows for a more even temperature across the radiator. The radiator spins through a heat exchanger and by varying the speed, the temperature gradient along the belt can be altered. The concept is very simple and the design does not require much research. The main problem with the belt radiator is that the performance is only slightly better than radiators yet the complexity is higher [42].

10.2.2.1. Trade-off for high-heat concept

In order to make sure that the best possible system is chosen, the innovative methods are placed in a trade-off to determine which system is most effective to the use case. The trade-off consists of six weighted categories which are given weights to indicate importance. The importance and weighing of the factors are based on IKAROS, the weights are appointed based on a study "Review of Advanced Radiator Technologies for Spacecraft Power Systems and Space Thermal Control" [43]. The paper reviews many options for future spacecraft and rates them based on standard criteria. The paper remains objective and does not favour or recommend any system. For IKAROS, the paper provides a base for the trade-off and can be extrapolated for the 2-stage pumped cooling loop system. Based on the needs of IKAROS and the arguments in the paper, the following trade-off table is constructed. The scoring for TRL is based on the development and testing that has been done on a technology, the performance per kilogram is based on the existing prototypes and systems, required power scoring is derived from the testing and results by other scientists, the lifetime and reliability is based on the findings in [43] and finally sustainability is scored by looking at the needed materials and scoring based on rare earth metals and where these come from.

	TRL	Complexity	Performance/ Kilogram	Required Power	Lifetime	Reliability	sustainability	Total
Large radiators (Fins)	5	5	1	4	4	4	3	**3.27**
Liquid Droplet Radiator	3	2	5	2	5	3	2	**3.63**
2-stage Pumped Loop	4	2	2	3	3	3	2	**2.63**
Moving Belt Radiator	3	2	3	2	3	2	4	**2.72**
Weights	1	1	3	1	2	2	1	

Table 10.4: Trade-off table for high-heat thermal control systems

From the results of Table 10.4, the Liquid Droplet Radiators win. The radiator fins end in a close second and only loses because it requires a lot of added mass. The 2-stage pumped loop and moving belt radiator are not able to outperform either of the other two on any criterion. In order to make sure the trade-off is robust, a sensitivity analysis is performed on the weights and winner. The sensitivity analysis changes

the weights and checks the winner many times. This will indicate the robustness of the trade-off. In Figure 10.3, the results are displayed as a bar chart and clearly portray that the radiators and LDR are going head to head, with the LDR being preferable. The LDR is in particular an interesting concept, because the LDR excels in what the radiators lack. As the large radiators score a 1 in performance, which is mission critical and therefore has the highest weight, the radiators are often outperformed by the LDR. The LDR is the best all-round performer and it is chosen as the best solution for the thermal control needed.

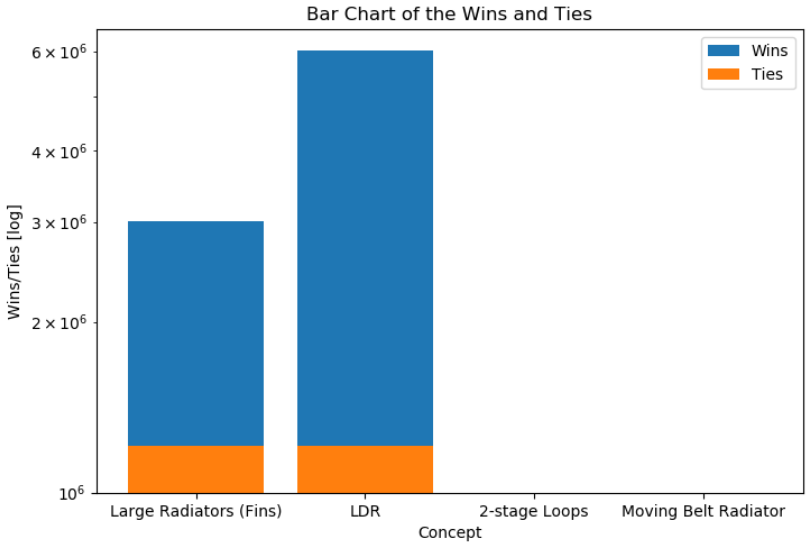

Figure 10.3: Bar chart displaying the results of the sensitivity analysis

10.3. Solution Implementation and Analysis

As discussed before, the main thermal control problem that the system would encounter is the overheating of the small parabolic dish and the relatively small reflector at the bottom of the large parabolic dish. A secondary issue would be the large temperature swings that the large parabolic dish goes through for each orbit. Based on the trade-off in Table 10.4, it is decided to use an LDR system to dissipate the large amount of waste heat. Furthermore, from the conventional methods, an aluminium coating will be applied to the outside of the large parabolic dish to improve its heat retention and absorption balances. The respective emissivity and absorbtivity of such a coating that will be used in the model are $\varepsilon = 0.3$ and $a = 0.2$ [i].

The LDR system will be modelled after reference literature, wherein the theoretical capabilities of a large-scale LDR system is described. The system will employ a triangular droplet sheet [44], with liquid lithium as its working fluid. Liquid lithium is chosen to optimise the specific heat rejection in the operating temperature range found in Section 10.1 [45, 46]. The general geometry of an LDR is modelled using the following system of equations [46, 47], where

Radiator area, in terms of radiator length L and aspect ratio A_r:

$$A = WL/2 = 0.5A_rL^2 \tag{10.8}$$

Radiator length, where the average in-flight temperature $T_e = T_0\left[3/\left(f^3+f^2+f\right)\right]^{1/4}$ with $f = T_0/T_1$, further expressed in terms of droplet velocity u, flight time t, optical depth $\tau = 3$, emissivity $\epsilon = 0.58$, density ρ, specific heat c, and droplet radius r:

$$L \equiv ut = 2u\tau cr\rho\Delta T/3\epsilon\sigma T_e^4 \tag{10.9}$$

[i]Emissivity: `https://www.engineeringtoolbox.com/emissivity-coefficients-d_447.html`; absorbtivity: `https://www.engineeringtoolbox.com/solar-radiation-absorbed-materials-d_1568.html`

Mass flow rate:

$$\dot{m}_f = (4/3) r u \rho \tau_0 A_r L \tag{10.10}$$

Using this system, and the necessary amount of heat to be rejected to make the hottest components adhere to requirement SSR.THC.PAY.2, a reference size of $L = 83$ m and $W = 33$ m, with $r = 50$ μ and $u = 22$ m/s has been chosen as a design point. Such a system would have a mass of around 820 kg, and a heat rejection capacity close to 6 MW_{th}. This design point is modular, such that it can be applied in tandem to increase the necessary heat rejection capacity locally.

Adding 21 of the described LDR systems in tandem for the back of the worker, and 18 for the back of the reflector, and using the aluminium coating on the back of the large dish, the heat balance is recalculated using the model. As illustrated by Figure 10.4, all the requirements from Section 10.1 for the main system are satisfied.

The total mass of the thermal control system would add up to 47.97 tons, including a 50% margin for heat pipes and fluids to distribute the heat as necessary.

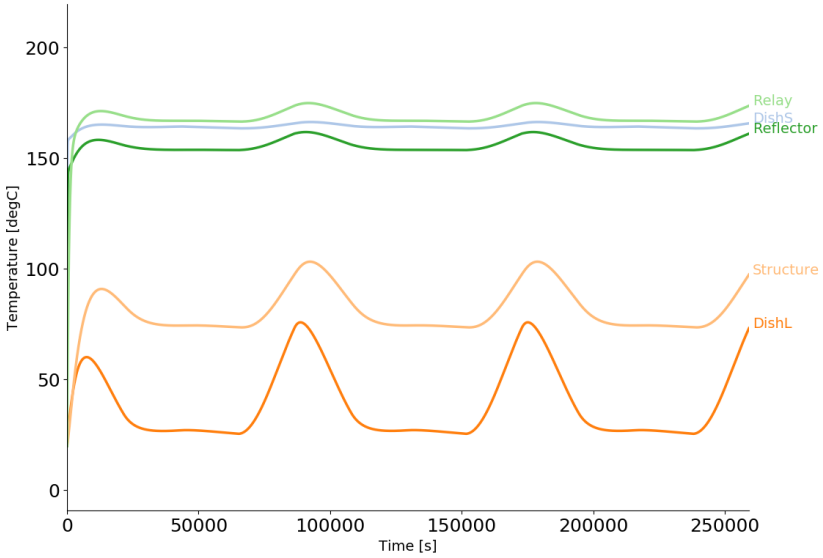

Figure 10.4: Temperature over time per component using a 10 second time-step for a 72 hour simulation in orbit, with added thermal control

11
Electric Power System

The following chapter covers the analysis, sizing and design of the electric power subsystem. Based on requirements under **TECH.PAY.Eps** id, subsystem functions are determined and possible solutions analysed. After selection of the most favourable solution, the design is integrated with the rest of the system and sized.

11.1. Problem Definition and Requirements

The conventional electric power system consists of power management and distribution unit, power source and energy storage.

11.1.1. Requirements

- **SSR.EPS.REQ.1**: The electrical power system shall provide for the generation, storage and distribution of electrical power to the spacecraft payloads and housekeeping loads during the entire mission life of 25 years.
- **SSR.EPS.REQ.2**: Operational orbit load: during sunlight 132,5 kilo watts, during eclipse 125 kilo watts.
- **SSR.EPS.REQ.3**: Peak load of additional 100 kilowatts for 20 seconds in every 350 minute period.
- **SSR.EPS.REQ.4**: Power management software to control the battery state of charge/discharge, temperature, charge/ discharge balance between batteries.
- **SSR.EPS.REQ.5**: Maximum worst-case battery DOD 70 percent during operational orbit.
- **SSR.EPS.REQ.6**: Testability shall be provided at the EPS level and the spacecraft level.
- **SSR.EPS.REQ.7**: Autonomous operation in all normal functions, unless overridden by ground command.
- **SSR.EPS.REQ.8**: EPS Reliability of 0.95 over the entire mission life, including the ground and space storage, if required.
- **SSR.EPS.REQ.9**: Single fault tolerant system where faults shall not propagate to other components, subsystems or systems.

11.2. Design options and selection

This section consists off design options study regarding different aspects of electric power system, like power generation, energy storage or distribution and management.

11.2.1. Power Generation

Power generation in space is currently limited to three options: fuel based, solar based and thermal. In practice most of the spacecraft today are powered using solar arrays, and only a couple of deep space or lunar missions are powered using fuel based nuclear reactors.

For this system which offers a large sun exposed area that is constantly oriented towards the star and considering the high power needs to support the thermal control system, combined with the long life cycle design, the choice of solar arrays is inevitable. A fuel based system would require enormous amounts of fuel to support a 25 year long life cycle, and the additional heat produced during energy conversion would amplify the thermal problems. Also the flat shape of solar arrays composes well with the rest of the systems design, contrary to the fuel based power generators, which are rarely flat.

Solar array technology is quickly developing and currently offers a number of space tested and highly efficient solutions. A small table summarising these technologies is given below:

Name	Efficiency EOL	Cost	Life span [yrs]	Additional
Single-crystal silicone	~20%	Medium	25+	Mature, temp prone, flexible
Multijunction GaAs	-36%	Expensive	20+	Radiation resistant, temp insensitive
Semicrystalline/Polycrystaline	~14%	Cheap	15+	Mature, reliable
Thin-film CdTe	~18%	Cheap	20+	Cheap and reliable

The solar array is directly integrated within the main parabolic dish (Queen) and will be in a shape of a ring. This means that with increased size, it takes away effective space from the payload. Over the designed life period of 25 years, the loss would accumulate to a significant number, so the solar array should be optimised in terms of the area. That leads to a design choice to use the technology with the highest efficiency, even at higher cost and lower sustainability.

11.2.2. Power Storage

Since the system is orbiting around Earth there are periods when our planet is obstructing the satellite-sun line. During the eclipse the system has to relay on a secondary power source or a power coming from power storage. Batteries, beside the ability to store, can also provide peak power to systems when needed.

Power storage methods for space applications range from chemical methods like batteries to mechanical methods like flywheel's. Chemical methods have a mass and size advantage over the mechanical methods, although they degrade faster. Due to advancements in battery technology and its specific capacity, it is a favourable technology that is widely used in satellites.

Currently there are four types of battery technologies considered for space applications. They vary with specific capacity, degradation factor, charge efficiency, environmental requirements and other characteristics. An overview of possibilities is presented below:

Name	Specific capacity [Wh/kg]	n_charge [%]	T_optimal [C]	Life span (80% DoD) [cycles]
NiCd	30-45	72	-5 - 10	~2000
NiH_2	50-65	75	-5 - 15	~4000
Li-ion	90-150	~98	-20 - 40	~2500+
Li-Po	150+	~98	0 - 40	~3000+

Nickel based cells were used in almost every spacecraft in 20th century because of their high specific capacity (at that time) and great lifetime. Currently, the technology evolved and the lithium based cells offer couple times higher energy density and a broader range of allowable temperatures. This simplifies the thermal management of the EPS. Lithium batteries also offer a significantly lower self-discharge rate.

Based on the table above the Lithium-ion technology is chosen for the power storage system. This choice is driven by the maturity and reliability of this technology in space application, contrary to the Li-po technology which is still relatively new and thus is thought to have a lower reliability.

11.3. Design Analysis

11.3.1. Power budget

Required power per subsystem was determined based on the components used, with a safety margin added. The loss in wires is based on voltage drop across wire of certain diameter and length. The power budget is presented in a table below.

Subsystem	Power	Duration (min)
ADCS	100W	-
EPS	300W	-
Payload	100 kW	1
C&DH	250W	-
Thermal control	120 kW	-
Recharge power		-
Wire Loss High-voltage	5060W	-
Wire Loss low-voltage	130W	-
total	126kW	

11.3.2. Power distribution and management

The role of this subsystem is to manage and distribute the power across the system. Special harness equipped with connectors, fuses and shielding connects all the subsystems to the electric power.

Depending on the current run through a wire, its diameter must be chosen accordingly to prevent failure. The maximum ampacity of wires is lower in space than on Earth due to lack of convective cooling.

There are 2 material options for the wires, namely aluminium and copper. Aluminium wires are lightweight but more expensive and have to be made thicker because of creeping in terminal connectors. Copper is very cheap and conductive, which makes it a perfect candidate for wiring. For integrity of copper wires it is advised to use wires wider than 20 AWG.

Due to presence of high power subsystems on board, it is decided to use 2 separate circuits - high and low voltage circuit. This will allow for a better harness design and more controlled current. High voltage circuit will be running 400V and low voltage circuit 28V. High voltage circuit will be used for powering the thermal control subsystem and the actuators from payload subsystem, while the low voltage is used for C&DH and ADCS.

For high voltage circuit the "250kcmil" AWG copper cables will be used, that allow for 300 Amperes in space environment, while for the low voltage circuit a AWG 12 copper cables will be used, with max allowed current of 25 amperes.

11.3.3. Battery sizing

For the majority of space missions the main function of the battery is to provide power for the spacecraft when the primary source, usually a solar array, is not generating power. During in orbit operation this happens during eclipse.

For GEO orbit which is a circular orbit a simplified 2D derivation can be used for determination of maximal eclipse duration. This is because their eccentricity is 0 and according to Kepler's second law about conservation of angular momentum, the velocity of the system in orbit is constant. That means that we can determine the eclipse using geometrical properties of circle like presented in a figure below:

$$\frac{1}{2}\Theta_{eclipse} = \arcsin\left(\frac{r_e}{r_{geo}}\right) \tag{11.1}$$

$$T_{ec} = T_{orb} \cdot \frac{\Theta_{eclipse}}{360} \tag{11.2}$$

Plugging in the numbers for geostationary orbit and 1436 minute period (1 sidereal day) yields a maximal eclipse duration of 69 minutes. To account for umbra and penumbra, which happen in reality with any light source impinging on a opaque object, 2 minutes should be added because of the partial eclipse. Satellite can experience a total of 71 minutes of eclipse.

This system has very different power needs than the majority of satellites. Usually the payload is the most

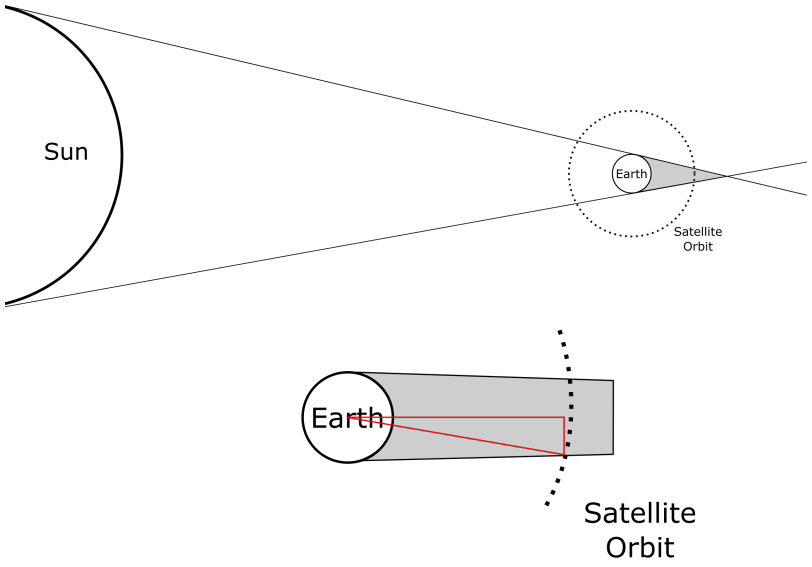

Figure 11.1: 2D eclipse problem

power demanding subsystem, but for this system the payload performs most of its mission passively so it doesn't require constant power. Electric power is only needed for this subsystem when the Sting and Relay are repositioned. Although the energy needed to perform this move is not high, because it takes very short amount of time and happens only 4 times per orbit, the peak power demands of the actuators are very high.

In theory this would mean that the solar array would have to be sized accordingly to the maximal power demand, but in our case it makes more sense to rely on a combined power of solar array and batteries to provide for the peak demands. This means that the battery unit has to be managed and allow for peak power demand support during charging.

Based on the provided power requirement for the payload actuator systems and the duration of the movements, which are 100 kW and 4 movements each around 12 seconds, it can be approximated that the 100 kW will be needed for 1 minute, so the energy needed is 1.67 kWh.

For continuous operation, the subsystems including wire losses require 126 kW of power. With a maximal eclipse duration of 71 minutes as calculated above, this totals to 149 kWh + 1.67 kWh Ĩ51 kWh. Since the durability of the battery is important the battery cannot operate at full Depth of Discharge, as this leads to a decrease in number of cycles. A safe assumption of DoD = 60 is made, which doesn't influence the durability negatively. This results in a battery with total capacity of 250 kWh.

Based on the sunlight and eclipse duration, the power required to charge the battery before next eclipse is 6.7 kW. This amount should be increased to 7.5 kW to account for the 98 % charging efficiency of Li-Po cells and the losses in battery management unit.

11.3.4. Solar array sizing

To determine the required area of the solar array, an energy balance and power budget has to be constructed. This budget should consist of power requirements of all the subsystems and losses, and the energy balance of the battery over one orbit should be positive. This can be presented in an equation:

$$\begin{aligned} &\int_{\text{sunlight}} (\,\text{solar flux} \times \text{PV conversion efficiency}\,) \cdot \mathrm{d}t = \\ &\int_{\text{sunlight}} (\,\text{loads} + \text{charge power} + \text{losses}\,) \cdot \mathrm{d}t \\ &+ \int_{\text{eclipse}} (\,\text{loads} + \text{losses}\,) \cdot \mathrm{d}t \end{aligned} \tag{11.3}$$

Below an updated power budget for the solar array is presented. It contains only the subsystems that

continuously require power from the solar array, while the payload actuator power needed is accounted in battery recharge power.

Subsystem	**Power**
ADCS	100W
EPS	300W
C&DH	250W
Thermal control	120 kW
Recharge power	7500W
Wire Loss High-voltage	5060W
Wire Loss low-voltage	130W
total	132.5 kW

Table 11.1: Power budget overview of IKAROS Honey

The array can be sized for this power required with a simple formula:

$$A_{solararray} = P_{req}/(SolarFlux * EOLefficiency) \tag{11.4}$$

The total required area for an array with GaAs cells with EOL efficiency of 24 % is 430 m^2. To account for variable solar flux and apply a safety margin a total area of 500 m^2 is needed. The solar array is located at the centre of the Queen, and is a ring of 3.25m width, with internal radius of 25m.

11.4. Results and verification

In the previous subsection different aspects of the EPS system were analysed and design choices were made. This section gathers the results, present the actual hardware used for EPS subsystem and performs a verification of the design process.

11.4.1. Hardware

For a complex space mission like this one there is no point in developing all the hardware by yourself. It is cheaper and better to rely on a space tested and certified hardware provided by companies that focus only on developing these components.

For the solar array an AzureSpace Quadruple Junction Solar Cell 4G32C-Advanced is chosen, mostly for its incredible BOL and EOL performance. It offers more than 33 % efficiency at BOL and around 24 % at EOL, after 10+ years. The choice for this product was also based on the experience of AzureSpace, which advertises that from 1.5 million cells that they put in space, none failed.

For the battery choice, a Li-ion technology was chosen which offers great specific capacity and promising number of life cycles. This technology is already used in many space mission, which ensures higher reliability. Tesla company is chosen as a provider of the battery pack, and their 100kWh battery pack will be used to construct a 250 kWh pack. Tesla and their provider, Panasonic, are one of the leaders in the battery industry. Their product is also offered at a very reasonable price, because as an EV manufacturer they have to decrease the cost per kWh as much as possible.

For the power distribution unit a solution from RUAG Space is chosen, namely their PCDU . They are the leaders in the market, and their units are used in many space projects. This product is highly customizable and modular so it can be adjusted for the specific needs of this system, for example accommodate redundant high and low voltage circuits.

11.4.2. Mass estimation

Since launching every kilogram to space is very expensive, mass budget of a subsystem is an important measure of performance. With the exact hardware chosen one can proceed with calculating the masses of the components.

For the solar array, only the cell weight is given. This is not very accurate because the mass of the cell is very low comparing to the protective coating and main structure. Instead, the calculation of solar array mass is based on an approximated specific energy output of the solar arrays. This value, provided by NASA Jet Propulsion Laboratory [48], is based on numerous currently operating solar arrays. According to S.Surampudi [48], for triple junction cells and a rigid array, the specific energy is 40W per kilogram. For an array producing 133 kW the weight is around 3.3 tonnes.

For the battery pack the mass estimation is significantly easier, because there is data available for the complete, ready-to install product. The 100 kWh version weighs around 640kg, so a 0.25 MWh version will weight around 1.6 tonnes.

Power distribution unit is customizable and will need adjustment for this use case, but the weight of a typical unit ranges from 40 to 60 kg.

Since the wires used for high-voltage circuit are of significant diameter, their weight is also included in the calculations. For a 250 kcmil cable made from copper, each meter weighs around 1.13 kg. For a redundant circuit which needs 2 wires in each direction and total wire length of around 2.5 km the total weight is 5.6 tonnes.

Mass budget for electric power subsystem is presented in Table 11.2 and the electrical flow diagram can be seen in Figure 11.2.

Component	Mass [kg]
Solar array	3300
Battery	1600
PDU	60
Wires	5600
total	10560

Table 11.2: Mass budget of EPS subsystem

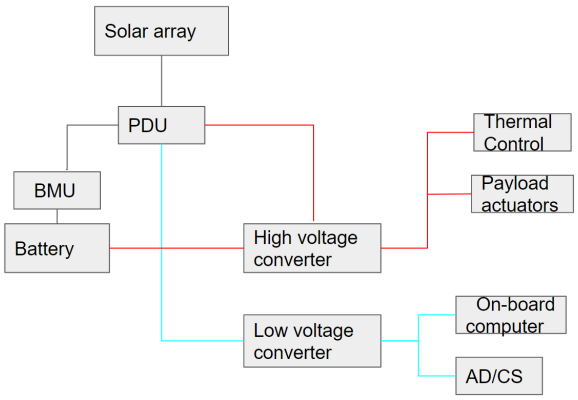

Figure 11.2: Electrical flow diagram

The electrical flow diagram above visualises the flow of electricity in the system. Starting from the solar array, the electricity is regulated by MPPT and passed to a PCDU. This unit distributes the power according to the needs, charges the battery and passes it to 2 circuits: high and low voltage. High voltage is used for thermal control and payload actuators, because they are very power needy. This is why we also see direct connection with battery that support the peak load periods. The low voltage circuit is used for on-board processing and AD/CS. Because of the frequent discharge/charge cycles, the battery is equipped with battery management system.

12
Command and Data Handling

In order for the spacecraft to function properly, it must have some way to deal with data from different subsystems, make calculations based on this data and have some sort of data connection with the ground station. This is what the subsystem described in this chapter is responsible for. The spacecraft will be equipped with an on-board computer that is connected to various subsystems, in addition to crosslink antennas that transmit to and receive data from the ground station.

12.1. Subsystem Requirements

- **SSR.CDH.TECH.1** The CDH system shall be able to receive and send commands to other subsystems.
- **SSR.CDH.TECH.2** The CDH system shall assess the state of functioning of the subsystems of the spacecraft.
- **SSR.CDH.COMM.1** The subsystem shall send and receive commands from the ground station.
- **SSR.CDH.COMM.1.1** The subsystem shall be able to transmit at least 1 Mb/s bits and receive at least 2 kb/s bits.
- **SSR.CDH.COMM.1.2** The data downlink shall have a link margin of at least 10 dB.
- **SSR.CDH.COMM.1.3** The data uplink shall have a link margin of at least 10 dB.
- **SSR.CDH.RISK.1** The subsystem shall have no single point of failure.

12.2. Hardware

12.2.1. On-Board Computer

Throughout the mission, a large amount of data must be decoded, collected, processed, encoded and transmitted. All this computational effort requires a processing unit with memory, storage and data connections. Fortunately, such on-board computers are readily available such as the Space Inventor OBC-P3[i]. This product has dual redundancy, which means that every component is present twice, which prevents a single point of failure. In addition, it has enough processing power and storage for the mission needs, so it has been chosen to be used on the spacecraft.

[i] OBC-P3. *Space Inventor*. `https://space-inventor.com/obc-p3/`

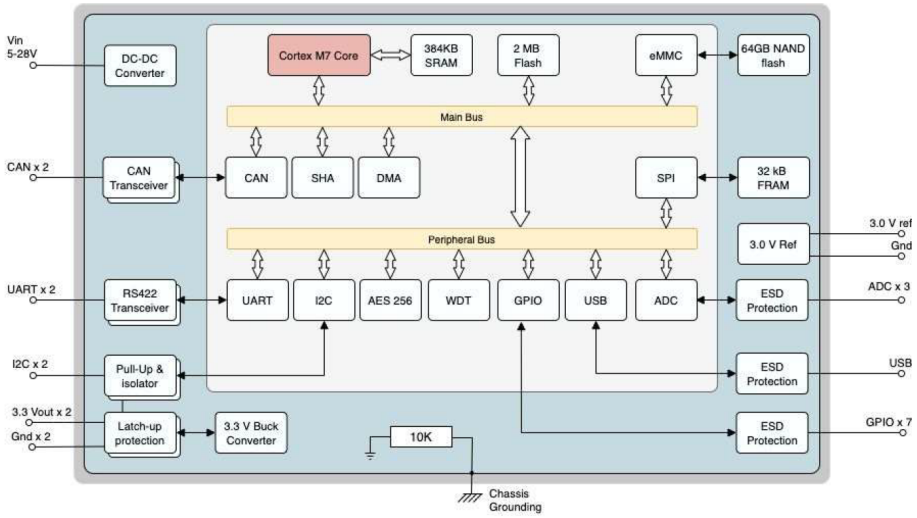

Figure 12.1: OBC-P3 System Architecture

12.2.2. Subsystem Architecture

The on-board computer is connected to each of the subsystems that can send and receive data, as well as the crosslink antenna; the layout of these connections is shown in Figure 12.2. The information from the antenna must first be decoded before it can be used, which is done by software on the OBC, the same goes for encoding outgoing data to the antenna. Through the I/O bus, the OBC sends and receives data from each of the subsystems shown. The data being sent are commands, inputs and relevant system information such as power requirements for the EPS. As for the received data, this consists of subsystem diagnostics and status, as well as any information required from a specific subsystem. All this data is handled through the bus and then by the CPU, which reads and writes memory and regularly backs up information into external storage. Commands are received by the antenna, decoded and then all relevant system information is transmitted back to the ground station. Note that the OBC has built-in redundancy and that this is extended to cover the entire subsystem, so that every connection is duplicated, which means that in case of any single failure, the system will continue to function without issues.

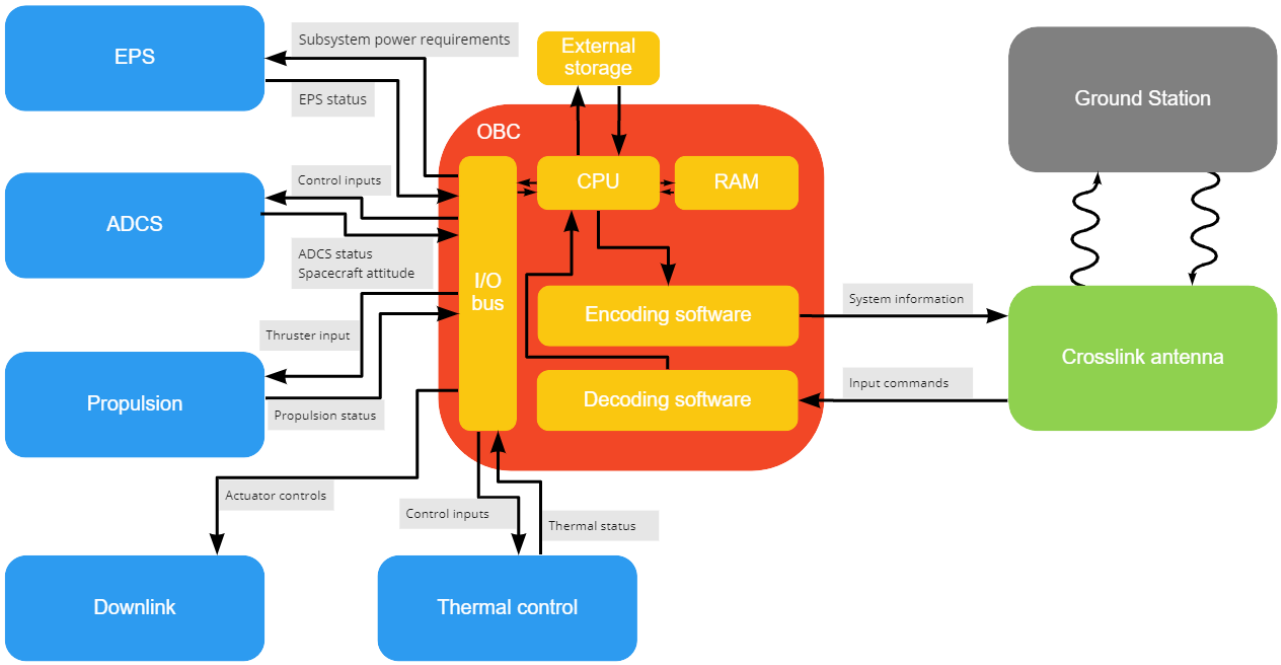

Figure 12.2: Data Handling Block Diagram

12.2.3. Antennas

The spacecraft is to be equipped with two parabolic antennas that function as crosslink antennas and have a diameter of 0.5 meters. The transmitter will have 1 Watt worth of power to be used for transmission. The reason why two antennas are used instead of one, is in order to provide redundancy, in case of an individual failure, the other component can be used which prevents a catastrophic failure.

On the ground station, two parabolic antennas with a diameter of 1 meter are used, also as crosslink antenna, in addition to a transmitter with 1 Watt of power for transmission. Using two antennas here is once again to provide redundancy.

12.3. Tracking, Telemetry and Command

Typical telemetry and telecommand data rates are around 1 Mb/s and 2 kb/s respectively, according to ESA data[ii]. Since this mission does not require additional large data transfers, these values have been chosen for the required data rates.

For the communications radio band, the Ku-band has been chosen, since this is suitable for large, commercial spacecraft and provides a relatively high frequency of between 14 and 14.5 GHz for uplink and between 12.5 and 12.75 GHz for downlink, and thus enables a high data transfer rate.

12.3.1. Signal Modulation

In order to transmit a signal, some medium of transmission must be chosen, which is then modulated to encode the data into the medium. The most obvious contender for this medium is electromagnetic radiation, specifically at frequencies around radio frequencies, these low frequencies are chosen in order to minimise energy consumption. Electromagnetic radiation consists of photons that act as a wave with an amplitude, frequency and a phase, these properties are visualised in Figure 12.3.

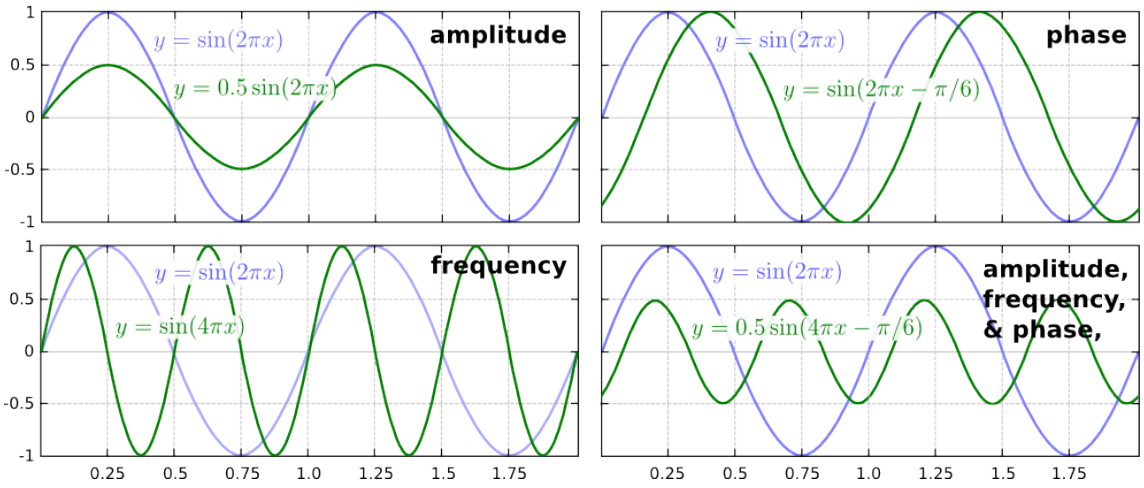

Figure 12.3: Visual Representation of Wave Properties

Each of these three properties in the carrier wave of the signal can be modulated to encode data, using the following methods: Amplitude-Shift Keyring (ASK), Frequency-Shift Keyring (FSK), Phase-Shift Keyring (PSK).

ASK works by altering the amplitude of the carrier wave to encode bits of data. In its simplest form, it uses a switch that opens and closes to complete a circuit, generating a wave whenever the circuit is complete. Then, this wave is decoded at the receiver by outputting a binary 1 whenever the wave is received and a 0 whenever it's not. This method of modulation is simple and requires little calculation, but is prone to be altered by constructive and destructive interference by other sources of radiation and for this reason it is not used in this mission.

[ii] BR-110 Layout. *ESA*. `http://www.esa.int/esapub/br/br110/br110.pdf`

A more advanced method would be FSK, where the carrier wave is continuous but its frequency is altered in order to encode bits. With Binary FSK, two frequencies are used, one to represent the binary 0 and the other to represent 1. While FSK has a higher signal-to-noise ratio and a lower error rate than ASK, it is also more complicated to encode and decode.

Finally PSK is considered, this method shifts the wave of the carrier signal in discrete increments in order to encode bits of information into the signal. This method, while complicated to encode, is very resilient to outside disturbances and thus can provides a reliable data stream to and from the spacecraft. This method can be applied to encoding singular bits at a time with Binary PSK, two bits at a time with Quadrature PSK or even more such as three bits at a time with 8PSK. The latter encoding has been chosen in order to maximise the data rate of the transmission, since it will provide for a high throughput while requiring a higher signal to noise ratio. This method modulates the signal to encode three bits of information by shifting it with the discrete phase increments, these angles and their associated bits are presented in Figure 12.4.

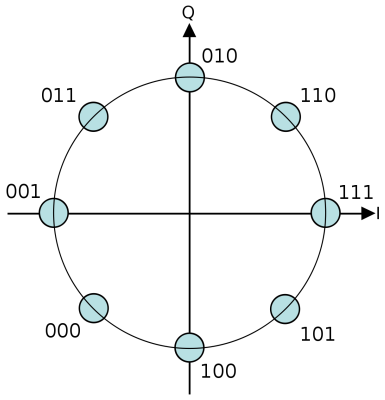

Figure 12.4: Discrete Phase Shifts of 8PSK Encoding

12.3.2. Link Budget

In order to maintain data integrity, a signal transmitted between a ground station and a spacecraft must have a sufficient energy to provide enough clarity that it can be distinguished from background noise. This data signal is modulated into a carrier wave with a certain bandwidth, which is the available range of frequencies for transmission.

This signal-to-noise ratio, or SNR, can be computed from a series of equations that consider the gains and losses along the path of transmission and the amount of noise present. A gain means an increase in signal strength and a loss signifies a decrease, so the former must be maximised while minimising the latter and while also avoiding significant increases in noise, which is expressed as system noise temperature. To simplify these calculations, a logarithmic scale is used for gains and losses so that these can be summed up instead of multiplied, this scale is referred to as decibel and is defined by the equation presented below.

$$X\,[dB] = 10 \cdot \log_{10} \frac{X}{X_{ref}}$$

The units of X can vary, leading to a decibel version of existing units. The ratio $\frac{X}{X_{ref}}$ refers to the gain or loss.

The noise of a system can be expressed in terms of spectral noise density, which is dependent on the system noise temperature, a characteristic that represents the amount of noise in a certain system. This spectral noise density can then be calculated as follows.

$$N_0 = k \cdot T_s$$

Where N_0 is the spectral noise density in W/Hz, k is the Boltzmann constant in J/K and T_s is the system noise temperature in Kelvin. Note that this temperature does not refer to thermal energy, but to the noise of the system.

The first component in the connection is the transmitting antenna. An isotropic antenna would spread out its produced signal power in all directions equally, but since this is inefficient, antennas can be focused towards a certain direction, which multiplies its produced power with a gain. The function for calculating its power is presented below.

$$W_f = \frac{P \cdot L_l \cdot G_t}{4\pi S^2} = \frac{EIRP}{4\pi S^2}$$

Where W_f is the power flux density [W/m^2], P is the power [W] of the transmitter signal and L_l is the antenna loss factor due to the connection between the antenna and the transmitter, this will be a value below 1. S [m] is the sphere radius assuming an isotropic antenna and $EIRP$ then refers to the Effective Isotropic Radiated Power [W], this value represents the power of a real antenna as if it were isotropic. There is also a loss incurred on this signal if it travels through the atmosphere, due to the influences of atmospheric particles and rain. This is referred to as the atmospheric and rain attenuation loss and it represented as L_a. It cannot be straightforwardly computed, but reference values exist for particular signal frequencies. When a signal is transmitted through space, it gets dispersed along the way, leading to a space loss L_s. This can be calculated using the formula below.

$$L_s = (\frac{\lambda}{4\pi S})^2$$

Where L_s is the space loss, λ is the wavelength of the signal in meters and S is the isotropic antenna sphere radius in meters. Another loss in the transmission is incurred due to pointing inaccuracies, this pointing loss can be computed in decibels using the following equation.

$$L_{pr}\,[dB] = -12 \cdot (\frac{e_t}{\alpha_{1/2}})^2$$

Where L_{pr} is the pointing loss [dB], e_t is the pointing offset angle in degrees and $\alpha_{1/2}$ is the antenna half-power beam width in degrees, which is essentially the angle at which the antenna power is halved. At the receiving end, other losses in the reception chain are further incurred on the signal, which can be represented together as the reception feeder loss, L_r.

Now, using the channel capacity C and the data rate R, both in bits per second, the energy per bit can be computed as follows. This variable represents the total received power times the duration of a single bit of data.

$$E_b = C \cdot \frac{1}{R} = \frac{P \cdot L_l \cdot G_t \cdot L_a \cdot G_r \cdot L_s \cdot L_{pr} \cdot L_r}{R}$$

Where E_b is the energy [J] per bit and G_t and G_r represent the gains of the transmitting and receiving antenna respectively. This leads to the formula of the signal-to-noise ratio, which is known as the link equation.

$$SNR = \frac{E_b}{N_0} = \frac{E_b}{k \cdot T_s} = \frac{P \cdot L_l \cdot G_t \cdot L_a \cdot G_r \cdot L_s \cdot L_{pr} \cdot L_r}{R \cdot k \cdot T_s}$$

Where SNR is the signal-to-noise ratio.

Below the results of the link budget calculations are presented. First in Table 12.1, the universal constants and the values related to Earth and the spacecraft orbit are presented. For the atmospheric and rain attenuation loss, a reference value is chosen that approximates the loss perceived in a mission such as this one.

Then in Table 12.2, the values of both the ground station and the spacecraft are presented. The losses, efficiencies and pointing angles in this table have been estimated based on previous literature and are reasonable estimates to the real values.

Finally, Table 12.3 presents the values and results of both the uplink and the downlink. Reference frequencies have been chosen within the Ku-band and from there the results have been computed.

The final signal-to-noise ratios for both links are above 10 dB, which satisfies the criterion for the link budget, thus closing the link. This means that the signal is sufficiently clear to be well understood in the presence of all the noise in the system.

Table 12.1: Link Budget Constants

Constant	**Symbol**	**Value**	**Unit**
Universal gravitational constant	G	6.67E-11	$m^3kg^{-1}s^{-2}$
Mass of Earth	M_E	5.97E+24	kg
Radius of Earth	R_E	6.37E+06	m
Orbit altitude	a	3.58E+07	m
Orbital velocity	V	3.07E+03	m/s
Atmospheric and rain attenuation	L_a	-0.5	dB
Boltzmann constant	k	1.38E-23	J/K

Table 12.2: Link Budget Ground Station and Spacecraft Variables

Variable	**Symbol**	**Ground station**	**Spacecraft**	**Unit**
Transmitter power	P_t	1	1	W
Transmitter loss	L_t	0.8	0.8	-
Receiver loss	L_r	0.7	0.7	-
Antenna efficiency	η	0.55	0.55	-
Parabolic antenna diameter	D	1	0.5	m
Transmitting antenna gain	G_t	40.79	33.79	dB
Receiving antenna gain	G_r	39.81	34.77	dB
Half power angle transmitter	$\alpha_{1/2t}$	1.49	3.33	deg
Half power angle receiver	$\alpha_{1/2r}$	1.67	2.98	deg
Pointing offset angle transmitter	e_{p_t}	0.15	0.33	deg
Pointing offset angle receiver	e_{p_r}	0.17	0.30	deg
System noise temperature	T_s	600	120	K

Table 12.3: Link Budget Uplink and Downlink Variables

Variable	**Symbol**	**Uplink**	**Downlink**	**Unit**
Frequency	f	14.1	12.6	GHz
Wavelength	λ	2.13E-02	2.38E-02	m
Data rate	R	2.00E+03	1.00E+06	bit/s
Space loss	L_s	-2.08E+02	-2.07E+02	dB
Antenna pointing loss	$L_p r$	-0.24	-0.24	dB
Effective isotropic radiated power	$EIRP$	9.59E+03	1.92E+03	W
Energy per bit	E_b	1.40E-17	2.24E-20	J
Spectral noise density	N_0	8.28E-21	1.66E-21	J
Signal-to-noise ratio	SNR	32.2826	11.3056	dB

13
System Integration

13.1. Hardware Diagram

Figure 13.1 shows the hardware diagram of the IKAROS system. The hardware components of each subsystem is shown and interconnected with the rest of the subsystems. There are fuel, power, data and command flows in the diagram. The legend illustrates which line represents which type of flow.

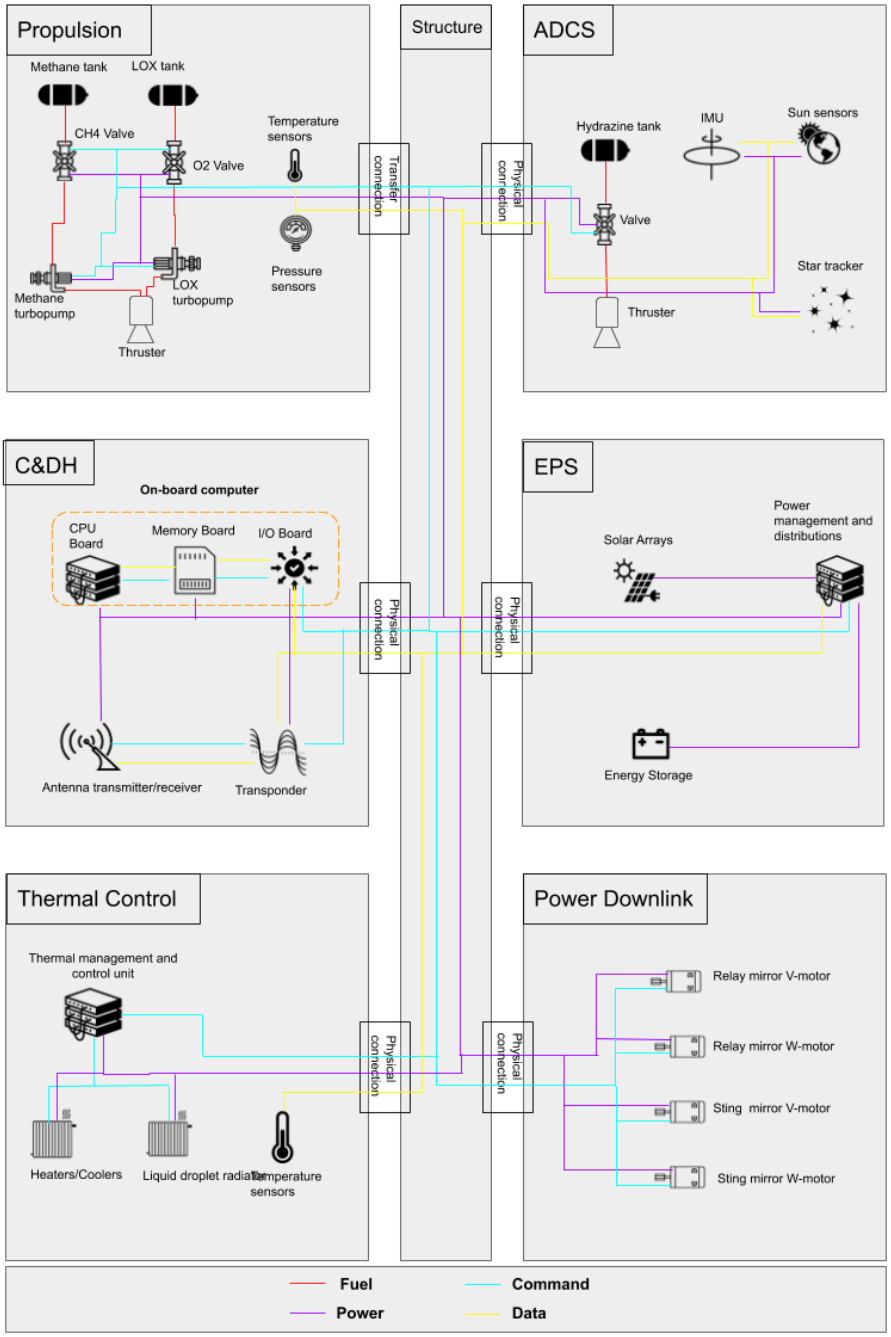

Figure 13.1: Hardware Diagram IKAROS system

13.2. Software Diagram

In this section the software diagram will be presented. As the project is not aimed to provide a very detailed design, the software diagram will be quite generic and will only aim to convey where software and firmware is needed for the operation of the spacecraft As can be seen in Figure 13.2 there are quite a few hardware component recognisable from the hardware diagram. This is because it is needed to convey an overview to where the software is connected and to what purpose the software is being used. The main hub for all the software operations is the On-board computer, which is the main controller of the spacecraft system. The software currently are given very generic names, this is because the software development that is needed for this spacecraft was outside of the scope of this project and needs to be worked out further in a later design phase.

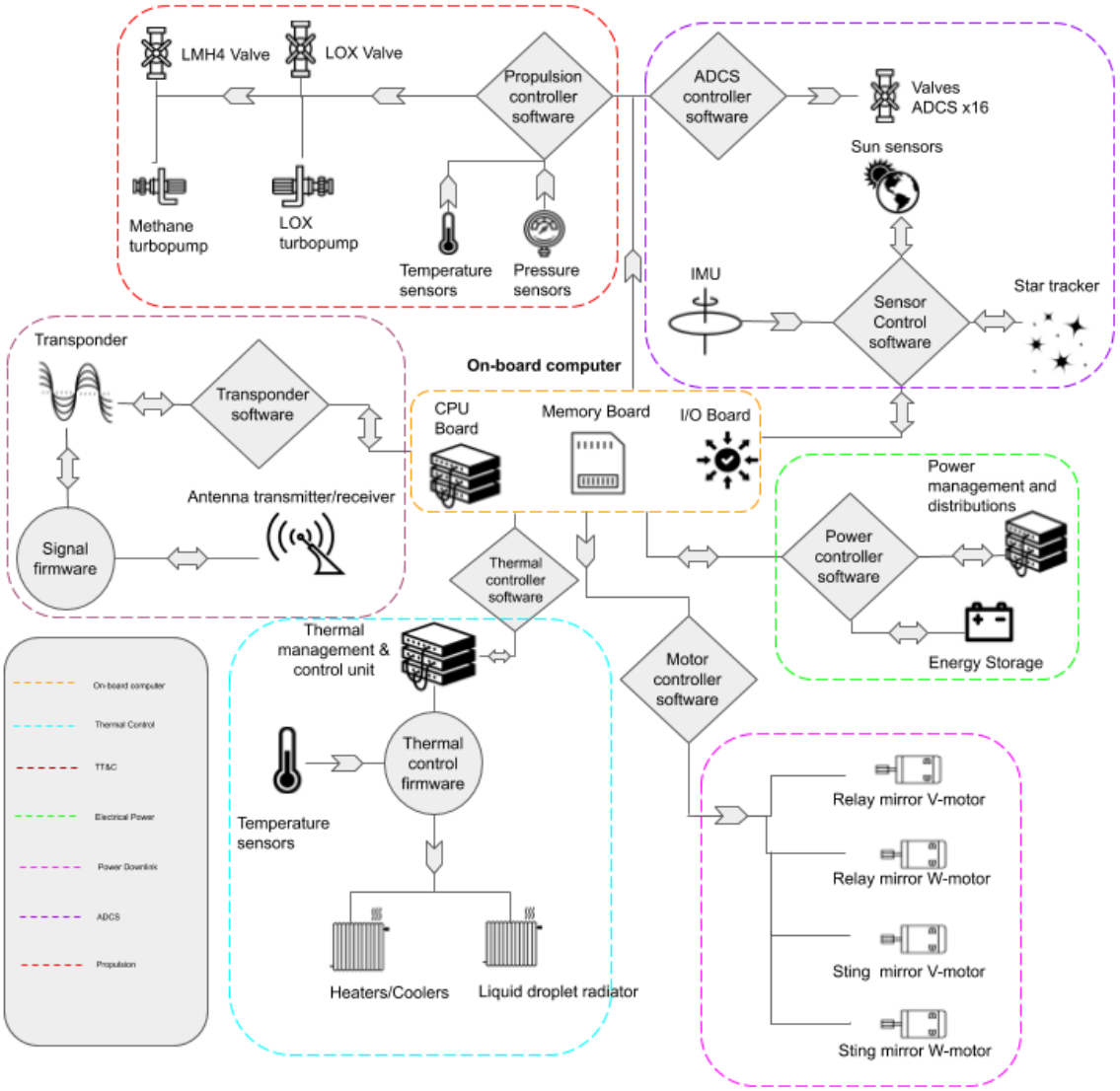

Figure 13.2: Software Diagram IKAROS system

14
Resource Allocation & Budget Breakdown

In this chapter the resource allocation and budgets will be discussed. For a better understanding of the resource distribution within the system, a breakdown on a sub-system level is presented.

Subsystem	AD/CS	C&DH	EPS	Thermal Control	Propulsion	Power Downlink	Structures	AIV
Mass [kg]	25	3.5	10 560	47 970	5 847 953	575 896	11 452 600	15 000
Power [W]	100	250	300	120 000	50	100 000	-	-

Table 14.1: Breakdown of subsystem mass and power usage.

14.1. Mass Budget

This section will go over the mass budget of the project. As can be seen in the Table 14.1 above, the majority of the system weight is located within the structure. This is not surprising, considering the area that the system needs to span to perform its mission. The second heaviest subsystem is the propulsion, which includes the mass of the propellant needed for the transfer manoeuvres.

14.2. Power Budget

In this section the power budget will be discussed. As can be seen in the Table 14.1 above, the most power consuming subsystem is the thermal control. This was expected because the system concentrates a significant amount of light into smaller surfaces, which results in high temperatures. To keep the thermal balance a high performance thermal control is needed. The second most demanding subsystem seems to be the payload, precisely the actuators used for pointing the concentrated beam. They use around 100 kW during operation, but they are only powered for a short amount of time per orbit.

14.3. Comparison with preliminary budget

In the baseline report for this project an initial estimate of technical budgets was made. Because this was done in the initial phase of the project, where not much technical detail was known about the system configuration or the subsystems, this estimation was based on other space satellites orbiting in GEO orbit. These results are presented below, and are an average of subsystems proportion to the total mass and power use.

Subsystem	AD/CS	C&DH	EPS	Thermal Control	Propulsion	Power Downlink	Structures	AIV
Mass [%]	6.9	3.1	29.5	5	8.7	28.4	17.1	-
Power [%]	1.6	3.4	1.5	6.3	0.2	77.4	-	-

Table 14.2: Initial estimation in percent based on large GEO satellites

Below a mass and power budget, also presented as a percentage of total of either power use or mass. As can be seen in the table, the most significant difference is in the structures subsystem, which in the final design accounts for around 63 % of total system mass, while in a conventional GEO telecommunication mission this is only around 17 %. This difference is caused by the enormous supported area required by the payload, which is normally not the case. Due to the weight of the whole system the required

propellant amount is also notable, which is why the propulsion subsystem estimate differs by so much. The weight of other subsystems doesn't increase so much with the size increase, which is why their weight mass contribution seems marginal.

Subsystem	**AD/CS**	**C&DH**	**EPS**	**Thermal Control**	**Propulsion**	**Power Downlink**	**Structures**	**AIV**
Mass [%]	<0.01	<0.01	<1	<1	32	3.2	63	<0.1
Power [%]	<1	<1	<1	90	<1	75	-	-

Table 14.3: Current resource distribution in percent for Honey system

15
Mission Analysis

In order to start the project effectively, a thorough planning for operations and logistics needs to be made. This plan should be considered in conjunction with the project Gantt chart and the production plan. The production plan will need to adhere to the time frame set in the project Gantt chart.

15.1. Operations and Logistics

In order to understand the logistics that go into a project such as IKAROS, the process is best broken down into smaller chunks for a better overview. As IKAROS is a project that will span over many years, it was decided to represent the operation and logistics in a chronological order. This section's chunks coincide with the splitting of costs in Section 18.4.

15.1.1. Infrastructure and planning

Prior to the first launch of the system, certain pre-launch arrangements must be made. The first and most important pre-launch arrangement is to find and build, buy, or rent infrastructure for production, moving assemblies, storing parts, monitoring, ground station and launching. These are physical locations that need to be reserved for when they are needed, although if these physical locations are built/bought they may be commissioned for other mass production activities. Some of the locations and infrastructure can be combined such as the production plant and monitoring station. However, this merging comes with physical restrictions. By combining locations, talent and resources, these will all need to be transported to the ground station location (India) in one way or another. As the ground station location is fixed, this molten salt generator reservoir, in combination with a RO desalination plant, will also be needed.

15.1.2. Development and Testing

After a location and design have been established, parts which cannot be sourced off-the-shelf must be designed, produced and tested. An example of such parts are the structural supports. Assuming that the design is finalised all the way down to part design, this can be carried out by a team of highly skilled, multi-disciplined engineers. The team will need sufficient testing tools to simulate the launch and environment in space. This means that testing jigs and a clean-room may also be required. Once the prototypes have passed all the tests, a demonstration prototype can be made to show investors that IKAROS may or may not perform according to the calculations. Once the prototypes pass all required tests, the actual production of IKAROS can begin. All the parts that need to be developed can be found in Table 18.3, labelled 'In-House' in the second column.

15.1.3. Order parts and integration testing

In conjunction with the development of in-house part designs, a team will need to source the parts that can be bought off-the-shelf. Apart from the transportation time and cost, these parts also need to be integrated for the IKAROS design. These parts are often designed such that they can compliment many designs. This means that parts will likely require brackets in order to fasten them securely to the Queen's structure. These brackets and fasteners will also need to be tested for the loads that they will carry/experience.

15.1.4. Manufacturing and testing parts

Once parts and brackets are designed, they also need to be made. All the parts will have varying requirements in terms of tolerance and size. To prevent the loss or double production of a part which creates waste, blockchain manufacturing and testing will be implemented. Through the use of smart contracts

and agreements on processes, the whereabouts and status of all parts will always be known [49].

15.1.5. Module assembly and launch preparations

Once parts have been made, tested and verified, the part can be assembled into a module. The assembly of the modules is difficult because of the size of the individual modules. These module assemblies will need to have jigs which can be used to hold and place parts. This process will cost a lot of time and will likely need to be done with multiple modules at the same time in order to keep up with launch dates.

15.1.6. Transportation of Modules

One of the sustainability goals is to source locally within Europe (manufacturing and production) as stated in Chapter 19. This means a lot of moving of parts, modules and people. As SpaceX launches from Boca Chica, Texas and Cape Canaveral in Florida, the modules will need to be sent to these places. This means moving modules or parts there either by land and air or water. These mediums differ in price and travel time. People will likely need to be moved by air, otherwise it will take too long and only add unnecessary costs. The modules will likely require specialised ships that can take extra large constructions. This will likely at a slightly higher price than for a container.

15.1.7. Launch vehicle integration

As soon as the modules and parts arrive at the launch site, these need to be mounted onto the launch platform and verified. This will be in conjunction with the staff of SpaceX. This will take time and needs to be taken into account to make the launch window. Something that affects this launch window is the weather and local meteorological conditions. If a launch were to be cancelled, a new window needs to be established. If this new window coincides with another launch, this may push and delay other launches. In order to prevent time lost, having the system integrated and queued early should allow for time lost to be made up; margins are included in the launch window estimates to account for possible delays.

15.1.8. Launching Modules

As soon as the launch preparations are done, the system needs to be monitored. Partly by SpaceX who need to ensure a safe and reliable launch. The IKAROS team will need to monitor the launcher from a separate mission control station. Once the launcher ignites its engines, the g-forces will vary and the system will need to carry these loads. The team will need to monitor these structures and in case of failure, improve this structure and launch again. Every launch six Starships will take off simultaneously, where three are carrying the cargo and the other three will carry fuel for the refuel mission in parking orbit. The launch to the parking orbit with a height of 500 km is estimated to take 1 hour as discussed in Section 5.4.

15.1.9. Refuel Starships

Having the three pairs of Starships in parking orbit, the refuelling of the cargo Starship can begin. Every pair needs to align as shown in Figure 15.1 by using their ADCS. Once in position, the transfer systems can be connected and the fuel is ready to be pumped from the refuel Starship (Right) to the Cargo Starship (Left). The refuel Starship has connections between its tanks and the payload being the fuel. The LOX and NH4 is pumped separately to the different tanks. This procedure of aligning, connecting, pumping, disconnecting, and separating is estimated to take 24 hours.

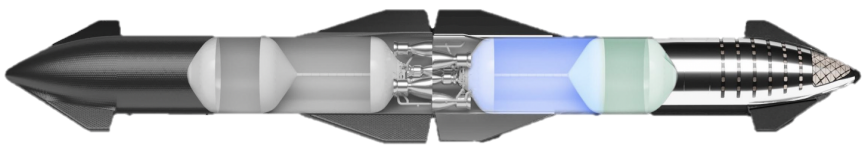

Figure 15.1: Refuelling in parking orbit of one Starship pair [50].

15.1.10. On-Orbit Docking in GTO

The first modules to reach the assembly orbit in GTO will be assembly modules which will align to add themselves to the configuration with their ADCS systems. Connections will be made that will transfer the loads delivered by the 7 engines. Every time this modules passes the perigee, modules can be added. This is, however, not the case as the turnover time takes longer than the period of the GTO.

15.1.11. Transfer from GTO to GEO

This transfer will also need a team of engineers that can oversee the transfer. Because of the sheer size of the modules, the transferring of the modules is going to take around two years as presented in the project guide [51]. This will need constant monitoring of the propulsion system and the path for every module. The transfer will only propagate when all modules in the Assembly Module are connected properly and ready to take the loads of the 7 Raptor engines.

15.1.12. On-Orbit Assembly in GEO

The undocking of the Starship modules from the Assembly Module can now be performed for relevant Starship modules which can then be unpacked after which assembly can commence. This will require robust planning in the allocation of Starship modules to particular subsystems, i.e. the first Assembly Module will contain all the necessary components to assemble the skeleton of the Queen with ADCS. Thermal control and EPS will also likely be in the first sequence of assembly. Next, the reflector systems can be attached to the system with the correct attitude and rotation such that thermal control is within the limits of these components during assembly, before these subsystems can be deployed for operation.

The time it takes for this assembly process is difficult to estimate, but based on existing systems and with task times estimated in Chapter 8 it is likely that this assembly time will be less than the transfer time for one assembly module and thus assembly can take place concurrently with the transfer of consecutive modules. Therefore, a maximum assembly time for one assembly module will be 110 days, leading to an overall assembly time of 1.2 years assuming zero downtime of the robotic assembly system. To account for this, an average eclipse time of 22 days per year will be taken for when the assembly systems are not able to operate, leading to 1.3 years for full system assembly. This time also assumes that there are no errors encountered during the assembly process, and therefore a 30% safety margin will be added to this time due to the relatively low TRL of the assembly system, leading to a final assembly time of ≈ 1.7 years.

In a scenario where the system would be assembled at an orbit closer to or in LEO, it would be greatly beneficial for time and precision to have a human-assisted assembly and have possible savings in robotic investment, however due to the requirements and constraints of the project this is not desirable in GEO.

15.1.13. Deployment

Once all the modules are assembled and in GEO, the Queen will need to be folded out as described in subsection 8.3.3. The process of unfolding will be reliant on the performance of the electric motors and cable attachments used, but can be done relatively fast compared to the time needed to assemble all subsystems and verify their integration. The estimated time for assembly will therefore not include the deployment time, as assembly will be the limiting case.

Once the orientation of Honey is validated to be safe, the program can begin sending down concentrated light to the ground station through the deployment of the Queen as the Worker should already be deployed at this time.

15.1.14. Perform mission and maintenance

As time goes on, parts such as the mirrors and solar panels will degrade. In order to be able to perform the mission effectively, these parts will need to be replaced. If this does not happen, the mirrors may overheat and/or the system will not generate enough power. In order to maintain the mirrors, a total of 10 extra launches will be needed to replace the mirrors. This number is calculated using the logarithmic degradation and setting a minimum efficiency requirement. The calculations show that roughly every five years, two sections of mirrors will need to be replaced equating to two Starships (each section is sized

	Task Name	Duration	Start	ETA
1	Post-DSE Project	35 days	16.04.12	1.06.12
2	Pre-launch arrangements	7 years	2021	2028
3	Hire relevant talent	1 year	early 2021	early 2022
4	Find and rent infrastructure	1,5 years	half 2021	late 2022
5	Manage new tech development	4,5 years	late 2021	early 2026
6	Set up simulated testing environment	1,25 years	early 2022	early 2023
7	Acquire commercial parts	0,5 years	early 2023	half 2023
8	Assess necessary integration methods	1 year	early 2023	early 2024
9	Integrate parts	1 year	half 2023	half 2024
10	Test integration	1,25 years	late 2023	early 2025
11	Create demonstrator prototype	2 years	late 2023	late 2025
12	Set up jigs	1 year	late 2024	late 2025
13	Assemble into pre-launch modules	2 years	late 2024	late 2026
14	Set up specialised shipping	1 year	early 2026	late 2026
15	Send to Boca Chica / Cape Canaveral	1 year	late 2026	late 2027
16	Launch phase	4 years	2028	2032
17	Mount Starship modules and verify	series	early 2028	early 2032
18	Wait for launch window	series	early 2028	early 2032
19	Set up system monitoring	series	early 2028	early 2032
20	Ignition	series	half 2028	half 2032
21	Launch to LEO in pairs of six	series	half 2028	half 2032
22	Refuelling	series	late 2028	late 2032
23	Launch to GTO	series	late 2028	late 2032
24	Post-launch assembly	6 years	2032	2038
25	On-orbit docking in GTO	4,5 years	early 2032	half 2036
26	Transfer from GTO to GEO	4 years	half 2033	half 2037
27	On-orbit assembly in GEO	4 years	early 2034	early 2038
28	Deploy fold-out mechanisms	2 years	early 2037	early 2039
29	Mission duration	26 years	2039	2065
30	Monitor function, location and attitude	26 years	early 2039	early 2065
31	Perform maintenance missions	15,5 years	early 2044	half 2059
32	Initiate EOL procedure	1 year	early 2064	early 2065
33	Transfer to disposal orbit	1 year	late 2064	late 2065

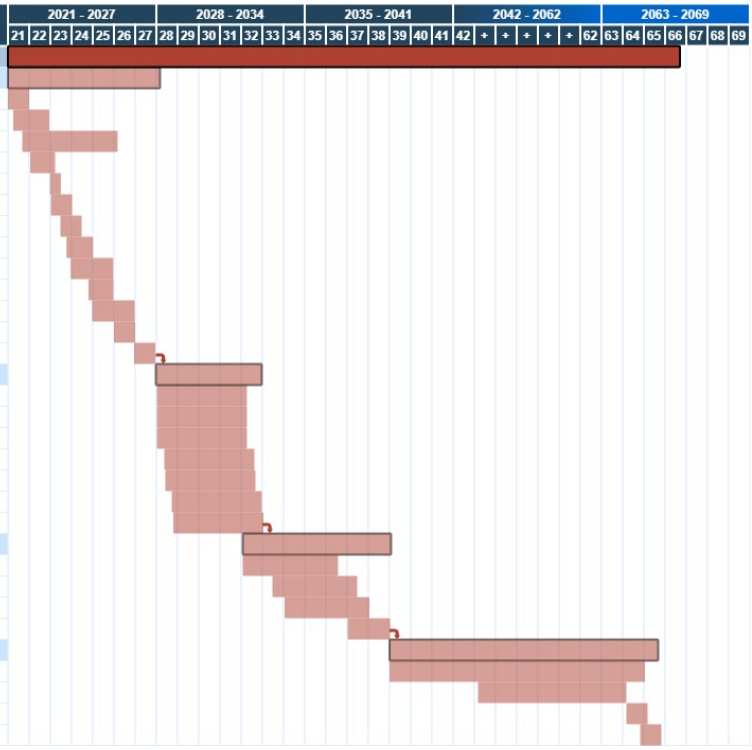

Figure 15.2: Gantt Chart showing the necessary activities and preliminary timeline after the DSE

equal to 1 Starship). The solar array will also need to be replaced, in the 12th year and the beginning of the 25th however since the system will only need to operate another year, the last maintenance mission will not be carried out. In order to replace the solar array, only a single Starship will be required. The solar array only weighs 3.3 tons and therefore it would be ideal if the launch can be shared with another mission to reduce the launch cost.

15.1.15. End-Of-Life

As Honey reaches the end of its life, it becomes time to place the system into a disposal orbit as at this altitude retrieval would be very costly. Using the initial orbital height of 35,786km of the geostationary orbit and aiming for a 36,138km disposal orbit (super GEO storage orbit [52] with 50km margin) the δv needed to dispose of the missions can be calculated as seen in Equation 15.1 yielding a Δv of 0.0122km/s.

$$\Delta v = \sqrt{\frac{\mu}{r_{geo}}} - \sqrt{\frac{\mu}{r_{disposal}}} \tag{15.1}$$

15.2. Project design & development logic

An initial estimate for the planning of post-DSE activities is given in Figure 15.2. Because of the large timescale, the Gantt chart is given in years. A preliminary start and end season is given for each foreseen activity. This planning, however, may changed based on the availability of technology, resources, and stakeholder support.

15.3. Communication Flow Diagram

In Figure 15.3 the Communication Flow Diagram of the IKAROS system is laid out. It illustrates the flow of data and commands between all primary subsystems of the system and the ground segment by the arrows. The colour of the arrow indicates from which block the communication flows.

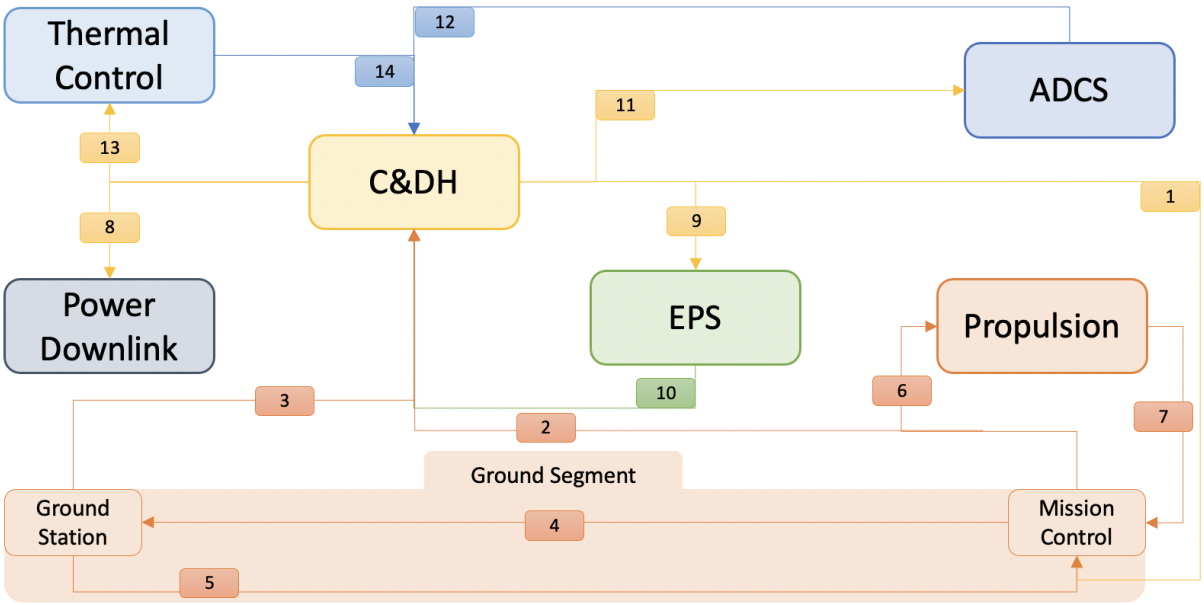

Figure 15.3: Communication Flow Diagram

Underneath a description of each flow is given. The numbers can be traced back in Figure 15.3.

1. Data of Navigation/Subsystem performance
2. Commands for Navigation/updating softwares
3. Commands for correcting pointing of the downlink
4. Satellite system performance
5. Reporting Ground station performance data
6. Commands for ADCS during transfer assembly/engines during transfer
7. Data for ADCS during transfer assembly/engine performance during transfer
8. Commands for the motors in the pointing mirrors
9. Commands on power distribution
10. Power usage/battery performance data
11. Commands for ADCS thrusters/sensor pointing
12. Attitude determination outputs, thruster performance
13. Commands on the flow rate of the liquide droplet radiator/Opening louvres/settle target temperature
14. Temperature sensor data

15.4. Production Plan

15.4.1. Original Equipment Manufacturing

Because some parts simply cannot be ordered, they must be made using conventional manufacturing methods. These methods are constrained by the necessary tolerances on the parts and the material choices. The following parts must be made in-house because they are not available off-the-shelf.

- Propellant tank
- ADCS tank
- Liquid Droplet Radiator
- Multi-layer Insulation
- Louvres
- Truss-structures
- Queen's Mirrors
- Worker's Mirrors
- Stinger's Mirrors
- Relay's Mirrors
- Mechanisms

Propellant Tank
In order to make lightweight and reliable propellant tanks, using composites is the easiest way to make a complex shape. The shape will likely be a cylindrical tank with circular ends as this shape is best at managing the internal stresses. By choosing this shape, a continuous fibre can be woven, impregnated with resin and cured in an autoclave. Once the propellant tank prototype is manufactured, it can be pressure tested to 150%, if the tank successfully passes the test, it indicates the walls can handle the internal loads and the tank may be produced to be put on IKAROS. As there is no real production line method for this, the final tanks will need to follow the same manufacturing process as the prototype.

ADCS Tanks
The process that will be used for the propellant tank can also be applied for the ADCS tanks. ADCS tanks can also be made using aluminium tanks however this will add another layer of processes to the manufacturing hence it is decided that these tanks will also be made and tested the same way as the propellant tanks only smaller. This way these processes can share the materials, the autoclave and testing procedure.

Liquid Droplet Radiator
The liquid droplet radiator is to be manufactured and assembled. The main parts of this system are the pumps, the nozzles and the liquid lithium. The pumps will need to be made such that they can handle the lithium and that they are able to work in the space environment. The nozzles are a simple design but require a lot of time to manufacture. The nozzles are similar to drilling a hole, however the system will require in the order of a million of these holes. These holes need to be drilled and cleaned thoroughly, otherwise the lithium will not be released consistently. Finally, in order to aid the moving of lithium, piping will need to be made which can hold the lithium. This could be the biggest problem because the system will require low-mass fluid handling components[53]. The testing of the LDR fully may only be possible in space due to the fact that the lack of gravity is a key factor. however on earth testing of components such as the pumps and nozzles can be done. The nozzles will need to suffice a flow rate and the pumps will need to be able to provide that flow rate.

Multi-Layer Insulation
The Multi-Layer Insulation is a simple stack of aluminized mylar sheets. These sheets are available for purchase but need to be stacked to a required thickness. The stacking of sheets is a simple process however the sheets also need to be perforated and applied to the parts correctly, otherwise it would defeat the purpose of using the sheets. As the sheets will need to wrap around complex shapes, they may need to be cut according to size by using a laser cutter. Depending on the part, there may need to be more or less layers. The Testing of the MLI will be done by placing a heat source on one side and measuring the gradient/temperature on the other side. If possible, this should be done in a vacuum chamber in order to simulate the environment of space.

Louvres
The louvres are a simple shape but require parts to be made and assembled. By using sheets of 6061-T6 aluminium, the louvres' parts can be sized, cut and assembled. The louvres do not require thick sheets and can be cut by a laser-cutter. The panels can then be assembled using rivets. The louvres can easily be tested in a similar fashion to the MLI.

Truss Structures
Truss structures or frames are common structures in many fields of engineering as they provide a lightweight alternative to solid beams. These trusses are most often manufactured through the joining of individual beams with relatively small cross-sections, either through welding or adhesives, depending on the particular use case. For IKAROS' frames, arc welding is the best option for space-grade parts such as the Aluminium 6061-T6 that will be used for the trusses in the satellite.

The large truss structures themselves cannot be produced as single parts due to the size, and therefore will be manufactured as folded sets (hinged) of larger beams that are then unfolded and joined with one

another to form, for example, the ≈ 500 m trusses. For this mechanism to work, these individual sets of trusses must be produced with connection interfaces such as tapered ends that can lock in place when unfolded.

Main production methods used:

- Extrusion
- Welding

Queen's Mirrors
The composite materials used for the reflective foil on the Queen structure will be the same as that used for the Worker, Relay, and Sting but to avoid issues with thermal flux the thicknesses will differ. The Queen structure will be able to use a coated aluminium foil with a maximum 0.125mm thickness, this allows for a rolled storage method in the launch vehicle.

In order to roll these foils, standard aluminium roller production can be used to roll the sheets out to the required thickness. The key in the production of this subsystem will be employing lean manufacturing techniques to reduce the cost of producing such a high number of similar elements.

Main production methods used:

- Aluminium rollers
- Silver electroplating

Worker's Mirrors
The panels for the Worker are thicker than those of the Queen, and thus are more rigid. This requires alternative production techniques to build the overall structure, which must be folded for storage requirements. The overall manufacturing process will, however, be the same as for the Queen as these Aluminium sheets can still employ aluminium rollers. The shape of each panel must then be cut according to the folds of the Worker, which must be chosen for its desired shape and depth (see Chapter 8 for more information). It is optimal to launch this subsystem in one piece to optimise mass and launch costs, this will require optimisation in fold locations for storage and in structural design of the individual panels.

Main production methods used:

- Aluminium rollers
- Silver electroplating
- Shearing or Laser Cutting

Relay and Sting Mirrors
The Relay is too large of a system to be launched as one piece, and so it must instead be assembled on-orbit. The Sting is smaller in size, and could likely use a folding technique similar to that of the Worker but ultimately to achieve lean manufacturing processes and assembling efficiency the Relay and Sting systems will use the same flat rigid panels as each other. This allows for simplicity both in the production process on the ground, and in the on-orbit assembly process.

Hexagonal panels will need to be cut to shape towards the edge of both systems' ideal elliptical shape, but again standardisation in the types of panels that will be used is ideal for large-scale manufacturing and so some losses will be incurred here. Similar to the Queen and Worker, aluminium rollers may be used to manufacture the panels and silver coating can be automatically applied through electroplating.

Main production methods used:

- Aluminium rollers
- Silver electroplating

- Shearing

Mechanisms
The mechanisms found in the IKAROS are used primarily to rotate and/or translate parts of the system. Those used for rotation and for the deployment of the Queen's reflectors use electric motors bought off-the-shelf to allow for variable rotation to a high degree of accuracy. Actuators will be required for the deployment of the Worker from its folded state to operational state, these can likely be bought off-the-shelf and configured for this purpose.

Hinge and locking mechanisms will also need to be designed for the deployment of a number of these systems, such as those mentioned for the stowing of the truss structure and for the deployment of the Worker and Queen. These mechanisms can be easily manufactured in-house but the time needed to design and test these mechanisms will be higher as they must be reliable – common methods can also be found to achieve these purposes.

Main production methods used:

- Drilling
- Lathing
- Computer Numeric Control (CNC)

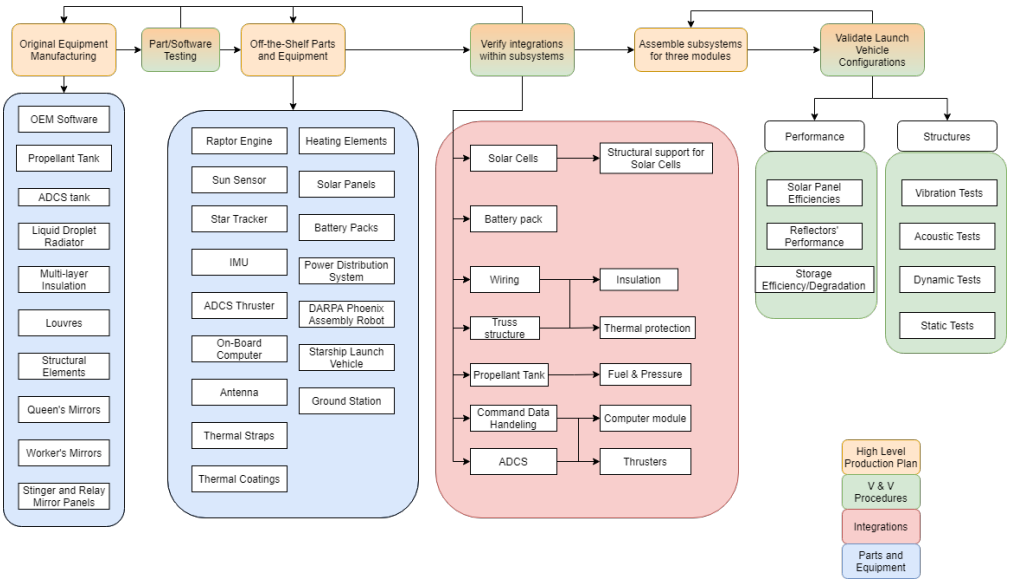

Figure 15.4: On-Ground Production Plan

16
Risk Management

In this chapter the Risk management of this project will be discussed. An adequate risk management is of vital importance for the success of the project. This chapter will consist of a risk identification section in Section 16.1, which will go over the several risk that may arise from the different subsystems of the SBSP system. After the risks have been identified the risk will be assessed and fitting mitigation strategies will be documented in Section 16.2 such that risks, wherever possible, are reduced to increase the chance of a successful project. The results of the risk assessment are finally finalised in two risk maps, one for pre-mitigation risk scores and one for post-mitigation risk scores, which can be found in Section 16.3. Finally, there will be a Reliability, Availability, Maintainability and Safety analysis conducted in Section 16.4.

16.1. IKAROS system Risk Identification

This section will go over the identification of the different risks that may occur in the different subsystems of the IKAROS system. Every risk will get a unique identifier that can be used in further reference. The risks are displayed in a list, with each risk having a description that explains what each risk entails.

- **R.PRJ.1:** The time the project takes until the system functions exceeds the time requirement.
- **R.PRJ.2:** The R&D and manufacturing costs exceed the budget.
- **R.PRJ.3:** The operating costs exceed the budget.
- **R.PRJ.4:** The mission will interfere with other missions in space.
- **R.PRJ.5:** TRL's will not be high enough when the mission starts.
- **R.PRJ.6:** The government does not allow the continuation of the project, due to a number of reasons.
- **R.PROP.1:** Catastrophic error in combustion, which causes an explosion.
- **R.PROP.2:** Blow out, causing the thruster to stop working.
- **R.PROP.3:** Valves are stuck and will not close.
- **R.PROP.4:** Pressure drop due to a fault in the system.
- **R.PROP.5:** Boil off of the propellant due to fault in thermal control system, which makes the fuel and oxidiser gaseous.
- **R.ADCS.1:** Thruster failure, which makes the ADCS system unusable.
- **R.ADCS.2:** Inaccurate sensors which causes problems in the control of the s/c.
- **R.ADCS.3:** Lack of hydrazine to propel the thrusters
- **R.ADCS.4:** Fault in the calibration of the IMU unit.
- **R.ADCS.5:** Disturbance due to unforeseen event.
- **R.C&DH.1:** Malfunction of the CPU/Memory of the on-board computer, which does not allow communication and command of the system.
- **R.C&DH.2:** Faulty software which results in a subsystem that can not be controlled properly.
- **R.C&DH.3:** Disturbance of the signal that causes loss of communication with ground control.
- **R.C&DH.4:** Faulty antenna which causes a loss of communication with ground control.
- **R.STRUC.1:** Bending stresses exceed the maximum stress of the structure, which results in structural failure.

- **R.STRUC.2:** Fatigue loading causes the structural components to wear out.
- **R.STRUC.3:** Thermal conditions causes the material to become to brittle and eventually to fail.
- **R.STRUC.4:** Thermal loads exceed the maximum loads the structure can bear and thus results in structural failure.
- **R.POW.1:** There is a faulty power cable which causes a loss of power to a subsystem.
- **R.POW.2:** Short circuiting resulting in a fire.
- **R.POW.3:** Batteries get overcharged, which damages the batteries.
- **R.PAY.1:** The actuators of the Relay and Sting mirror are faulty, which results in the inability to point the light at a ground harvesting station.
- **R.PAY.2:** Meteorite impact on the mirrors.
- **R.PAY.3:** Thermal control fails to keep the temperatures to a reasonable value, which results in the melting of the mirror.
- **R.PAY.4:** Mirrors get covered by cosmic dust.
- **R.PAY.5:** Mounting of the mirrors deviate from design, resulting in misaligned reflection.
- **R.ASSEM.1:** Fault in connecting the assembly stages in the transfer module, which causes a catastrophic failure of the mission.
- **R.ASSEM.2:** Fault in refuelling of Starship in the parking-orbit
- **R.ASSEM.3:** Faulty deployment, which causes subsystems to not function properly.
- **R.ASSEM.4:** Inaccuracy or failure of assembly in GEO.
- **R.ASSEM.5:** Disassembly at EOL is not done successfully, which results in the system not being able to be positioned in the graveyard orbit.
- **R.THERM.1:** Subsystems getting overheated, because thermal control system not working properly.
- **R.THERM.2:** Radiator faults, which causes the thermal control system to not work effectively.
- **R.THERM.3:** Temperature sensor that is defect, which causes a fault in the control of the thermal system.
- **R.GROUND.1:** Ground station lost communications with the s/c.
- **R.GROUND.2:** Light beam misses ground station
- **R.GROUND.3:** Defect solar panels ground station
- **R.GROUND.4:** Failure in Power distribution net on the ground.

16.2. Technical Risk Assessment of the IKAROS system

This section will go over the assessment of the risks that are previously identified in Section 16.1. This will be done in the form of a large table (Table 16.1) that will provide the pre-mitigation and the post-mitigation scoring respectively. The table will also include the mitigation strategy that is specified for the risk involved and will give a short description of what the risk entails. The scoring of the different risks and the mitigation strategies were found by discussions with the different departments working on the various subsystems.

Risk ID	**Description**	**Mitigation Strategies**	**Pre Score (prob, imp)**	**Post Score (prob, imp)**
R.PRJ.1	The time the project takes until the system functions exceeds the time requirement.	Keeping up a Gantt chart and have regular meetings regarding the schedule	(3, 2)	(1, 2)
R.PRJ.2	The R&D and manufacturing costs exceed the budget.	Include a margin in the budget, make sure that the budget considered for every R&D step and have meetings about the cost efficiency	(3, 2)	(1, 1)
R.PRJ.3	The operating costs exceed the budget.	When designing the s/c the operational cost should always be kept in mind, clear and consistent communication limits over-budgeting	(2, 3)	(1, 3)
R.PRJ.4	The mission will interfere with other missions in space.	Constant communication with other nearby ongoing missions, no unplanned manoeuvres without consulting	(2, 3)	(1, 3)
R.PRJ.5	TRL's will not be high enough when the mission starts.	When selecting technology always keep the TRL in mind and have regular scheduled meetings about the TRL of the whole system, update planning where necessary	(2, 4)	(1, 3)
R.PRJ.6	The government does not allow the continuation of the project, due to a number of reasons.	Dedicated legal team to enhance communication with the government and adherence to local laws and regulations, generate a back-up plan	(3, 4)	(1, 2)
R.PROP.1	Catastrophic error in combustion, which causes an explosion.	Extensive ground testing of the propulsion system to prevent such a large unexpected error	(2,4)	(1,4)
R.PROP.2	Blow out, causing the thruster to stop working.	Making a study about the stability of the combustion process and re-ignition	(2,3)	(1,2)
R.PROP.3	Valves are stuck and will not close.	Testing the valves extensively and well lubrication of the valves	(2,4)	(1,4)
R.PROP.4	Pressure drop due to a fault in the system.	Have a separate pressure tank that can provide pressure to the system if necessary	(2,3)	(2,2)
R.PROP.5	Boil off of the propellant due to fault in thermal control system, which makes the fuel and oxidiser gaseous.	Testing the effectiveness of anti-boiloff measures to ensure that boiloff will not happen	(4,2)	(2,2)
R.ADCS.1	Thruster failure, which makes the ADCS system unusable.	Have additional thrusters that act as redundancy of the system	(3,3)	(3,1)
R.ADCS.2	Inaccurate sensors which causes problems in the control of the s/c.	Have redundant sensors to be able to check the accuracy of the sensor and to have spare sensors if one breaks	(2,3)	(1,3)
R.ADCS.3	Lack of hydrazine to propel the thrusters	Spare hydrozine that can provide the system with fuel when necessary	(2,3)	(1,3)
R.ADCS.4	Fault in the calibration of the IMU unit.	Test the calibration beforehand and have redundant IMU units	(2,3)	(1,3)
R.ADCS.5	Disturbance due to collision events of space debris or meteorites.	Precise tracking of the bodies passing by and proper communication with other satellites.	(2,4)	(1,4)
R.CDH.1	Malfunction of the CPU/Memory of the on-board computer, which does not allow communication and command of the system.	Have backup computer systems that can take over in case of the malfunctioning of the main computer	(1,5)	(1,2)
R.CDH.2	Faulty software which results in a subsystem that can not be controlled properly.	Built-in fail safes in the software	(3,5)	(1,2)
R.CDH.3	Disturbance of the signal that causes loss of communication with ground control.	Verifying that the gain on the antennas is strong enough to account for the most common disturbances	(2,4)	(2,2)
R.CDH.4	Faulty antenna which causes a loss of communication with ground control.	Have a redundant antenna that can be used in case the main one breaks	(1,4)	(1,1)
R.STRUC.1	Bending stresses exceed the maximum stress of the structure, which results in structural failure.	Introduce a safety factor in the design that accounts for this	(2,4)	(1,4)
R.STRUC.2	Fatigue loading causes the structural components to wear out.	Make a proper design that is accounting these fatigue loads	(2,3)	(1,3)
R.STRUC.3	Thermal conditions causes the material to become to brittle and eventually to fail.	Do testing of the thermal control system to ensure that it will be able to minimise the thermal loads on the structure	(2,3)	(1,3)

Risk ID	**Description**	**Mitigation Strategies**	**Pre Score (prob, imp)**	**Post Score (prob, imp)**
R.STRUC.4	Thermal loads exceed the maximum loads the structure can bear and thus results in structural failure.	Introduce a safety factor in the design that accounts for this	(2,4)	(1,4)
R.STRUC.5	Torsion load from thrusters causing the big parabolic dish to twist to unacceptable levels	Consider this further in designing phase	(2,2)	(1,1)
R.STRUC.6	Vibrations of the mirrors + mirror sheets due to manoeuvres causing misalignment of sunbeam to a large degree	Consider this in detail in a further design phase	(3,4)	(1,4)
R.STRUC.7	Inaccurate centre of mass & moment of inertia due to assumptions made	Make sure assumptions are conservative	(4,3)	(4,1)
R.POW.1	There is a faulty power cable which causes a loss of power to a subsystem.	Have redundant power cables and use parallel wiring whenever possible	(2,4)	(1,1)
R.POW.2	Short circuiting resulting in a fire.	The circuit must be tested extensively on the ground before launch and fused properly	(2,4)	(1,2)
R.POW.3	Batteries get overcharged, which damages the batteries.	Reliable and proven battery management technology	(2,4)	(1,4)
R.PAY.1	The actuators of the Sting mirror are faulty, which results in the inability to point the light at a ground harvesting station.	Have redundant actuators to account for this	(1,4)	(1,1)
R.PAY.2	The actuators of the relay mirror are faulty, which results in the inability to point the light at a ground harvesting station.	Have redundant actuators to account for this	(1,2)	(1,1)
R.PAY.3	Meteorite impact on the mirrors.	Temporarily rotate reflectors to present a smaller area of impact	(2,3)	(1,3)
R.PAY.4	Thermal control fails to keep the temperatures to a reasonable value, which results in the melting of the mirror.	Have isolation on the mirror to keep the heating to a minimum	(1,4)	(1,2)
R.PAY.5	Mirrors get covered by cosmic dust.	Have a cleaning robot or mechanism	(3,2)	(1,2)
R.PAY.6	Mounting of the mirrors deviate from design, resulting in misaligned reflection.	Reconfigure the on-board computer's model of the reflector to mitigate the misalignment	(4,4)	(4,1)
R.ASSEM.1	Fault in connecting the assembly stages in the transfer module, which causes a catastrophic failure of the mission.	Increase strength of interface connection while reducing points of attachment, increase angle of conical attachment point and/or size of attachment point	(3,4)	(2,4)
R.ASSEM.2	Fault in refuelling of Starship in the parking-orbit	Attempt to retry refuelling operation, add another refuelling mission if necessary, increase amount of fuel taken to orbit (reserve)	(2,3)	(1,2)
R.ASSEM.3	Faulty deployment, which causes subsystems to not function properly.	Add spare parts to launch in case certain parts need to be replaced (this can be achieved by assembly system)	(1,2)	(1,1)
R.ASSEM.4	Inaccuracy or failure of assembly in GEO.	Add spare parts to launch in case certain parts need to be replaced (this can be achieved by assembly system)	(1,3)	(1,2)
R.ASSEM.5	Disassembly at EOL is not done successfully, which results in the system not being able to be positioned in the graveyard orbit.*	-	(2,1)	(2,1)
R.THERM.1	Subsystems getting overheated, because thermal control system not working properly.	Sensors measure the temperature of the subsystem and active thermal control is activated when approaching upper or lower limit of the parts as specified in the specifications sheet	(2,4)	(2,2)
R.THERM.2	Radiator faults, which causes the thermal control system to not work effectively.	Have parallel connections and redundancy by making multiple smaller radiators rather than fewer big ones	(2,3)	(3,1)
R.THERM.3	Temperature sensor that is defect, which causes a fault in the control of the thermal system.	Have at least 3 sensors, having 2 of the same and one different will prove that this sensor has defected, use historical data and logic to determine if a value is realistic.	(1,4)	(1,2)

Risk ID	Description	Mitigation Strategies	Pre Score (prob, imp)	Post Score (prob, imp)
R.GROUND.1	Ground station lost communications with the s/c.	PRE: ensure redundancy in ground station communications, DURING: satellite points based upon last known point	(1,1)	(1,1)
R.GROUND.2	Light beam misses ground station	PRE: ground station size is scaled to have margin for error in pointing equal to pointing accuracy DURING: temperature sensors determine location of beam and adjust accordingly	(3,1)	(1,1)
R.GROUND.4	Failure in Power distribution net on the ground.	PRE: Redundancy is implemented in the power distribution net DURING: the power distribution system is repaired	(1,1)	(1,1)

Table 16.1: Risk assessment prior and after mitigation strategy

16.3. Risk Maps

The section will function as a summary of the risk assessment, giving an overview of the technical risks that are involved in the project, the risk's identifiers will be portrayed in two risk maps, which will have an easy-to-understand colour code to see which risk is greater. There will be a pre-mitigation risk map (Table 16.2) and a post-mitigation risk map (Table 16.3).

Impact/Probability	Very Low	Low	Medium	High
Large	CDH.1 CDH.4 PAY.1 PAY.4 THERM.3	PRJ.5 PROP.1 PROP.3 ADCS.5 CDH.3 POW.1 POW.2 POW.3 THERM.1 STRUC.1 STRUC.4	PRJ.6 STRUC.6 CDH.2 ASSEM.1	PAY.6
Moderate	ASSEM.4	PRJ.3 PRJ.4 PROP.2 PROP.4 ADCS.2 ADCS.3 ADCS.4 ASSEM.2 THERM.2 PAY.3 STRUC.2 STRUC.3	ADCS.1	STRUC.7
Mild	PAY.2 ASSEM.3	STRUC.5	PRJ.1 PRJ.2 PAY.5	PROP.5
Small	GROUND.1 GROUND.3	ASSEM.5	GROUND.2	

Table 16.2: Risk Map before risk mitigation

Impact/Probability	Very Low	Low	Medium	High
Large	PROP.1 PROP.3 ADCS.5 STRUC.1 STRUC.4 STRUC.6 POW.3	ASSEM.1		
Moderate	PRJ.3 PRJ.4 PRJ.5 ADCS.2 ADCS.3 ADCS.4 STRUC.2 STRUC.3 PAY.3			
Mild	PRJ.1 PRJ.6 PROP.2 CDH.1 CDH.2 POW.2 PAY.4 PAY.5 ASSEM.2 ASSEM.4 THERM.3	PROP.4 PROP.5 CDH.3 THERM.1		
Small	PRJ.2 CDH.4 STRUC.5 POW.1 PAY.1 PAY.2 ASSEM.3 GROUND.1 GROUND.2 GROUND.3	ASSEM.5	ADCS.1 THERM.2	STRUC.7 PAY.6

Table 16.3: Risk Map after risk mitigation

16.4. Reliability, Availability, Maintainability and Safety (RAMS)

This section will go over the RAMS analysis of the IKAROS system.

Reliability

The reliability of the system as a whole is of vital importance to the success of the system. The reliability of the system depicts the probability that the system is behaving in a satisfactory manner and thus the IKAROS system shall need a high reliability if it aims to become a success. To achieve a high reliability several measures can be taken. One such a measure is the introduce redundancy to the system. If there are backups to vital systems than the chance of the mission failing due to an error are diminished. When one introduces to many redundant systems the performance of the system may go down, thus a trade of should be made between reliability and performance. In the previous section in Table 16.1 it could be seen that for a lot of mitigation strategies redundancy in systems are pointed as the solution the make the risks acceptable.

Availability

To make the most use of the system the system should be operational most of the time. This is already taken into account when designing the different orbits that the final system should take. For the reason of availability (and other reasons) a GEO orbit was chosen, such that the satellite could always point towards the same solar array station on earth and have a minimal amount of eclipse time of around 20 days, with a maximum eclipse time of 72 minutes. The amount of downtime that system will experience is therefore quite limited.

Maintainability

The maintainability of the system is also something that is important in determining the success of the project. The operation is mostly in space, which will make the maintenance quite a challenge and sometimes not financially or technically feasible. In this system there is a big assembly module needed to put all the different parts together. The assembly module could also function as a simple maintenance module after it has assembled the system in GEO. Unfortunately due to the time constraints of this project, the design of such a module could not be provided. However, it can be said that the robotic arms that are used in the assembly can also be used for maintaining the system and with some small difference in tools that can be put on the arm the assembly module could be a really effective maintenance module.

Safety

The safety of the project is also of paramount importance to the success of the project. What is meant by safety in this project is, the safety of the people working in the factories, safety for the environment and safety for other space projects. There should be in later design phases of the project a clear structured way of addressing the safety concerns that the system may give rise to. There could be a team of safety engineers for instance, whose main task would be that the mirror and the concentrated sunlight would not be able to cause any harm to other projects and for the people on earth.

17
Verification and Validation

17.1. Sensitivity Analysis

During the detailed design phase, trade-off models are used to determine the optimal design choices, namely in Chapter 5, Chapter 6, Chapter 7, and Chapter 10. To determine how changes in the used variables and weights affect the outcome of the trade-off, a sensitivity analysis is used. The sensitivity analysis is a way to measure the uncertainty of the trade-off outcome, so that the outcome can be validated. In order to model the different possibilities of changed weights and values, an algorithm was developed according to the Monte-Carlo methods, and applied to the weights and values of each criterion. By changing the weights the outcomes of the trade-off change reducing the effects of subjectivity. When two concepts are very close, the sensitivity analysis can reveal which concept would win if the weights are tweaked because often a concept will win because the weights are in favour of that concepts and vice versa. By taking a 30% range of values both ways for every weight and every combination, a large enough range of trade-offs is performed to reduce these effects of subjectivity and reveal the robustness of the trade-off.

17.2. Verification and Validation Procedures

Before a spacecraft is launched into orbit, elaborate testing is done on components, subsystems and the entire system, as well as on calculations and models used for the design. This is done in two parts, verification and validation.

Verification is a test that checks whether calculations, programs or components fulfil their function without errors or inaccuracies. It can be more generally described as testing whether the solution to a certain problem is correctly computed, regardless whether or not it is the correct solution. For calculations this means that the results are correct and no calculation errors were made, for programs it means that the code doesn't contain errors. Verification is not sufficient if it would be the only testing methodology used, because it does not check whether the intended function of each component or program is the correct function.

Validation, on the other hand, is used specifically for this purpose. It is used to check whether the calculation is the correct calculation to be used in that particular situation. In more general terms, this means that it tests whether the solution applied to the problem is appropriate, disregarding whether that solution is correctly applied, which would have been confirmed during verification. Validation uses real-world examples to compare to predicted values, in order to ensure that the models used for calculation are indeed representative of real world situations.

17.2.1. Software Verification

All the required programs and scripts for this project are written in Python. Before a single line of code was written, a document had been set up to provide guidelines for writing, documenting and testing code. This document covered mainly the following topics:

- Variable naming conventions
- Commenting and documentation
- Collaboration
- Testing

Naming conventions have been specified mainly for easing internal communications, but also to simplify collaboration and thus reduce errors. The same goes for commenting and documentations, but in addition, they also make it easier for the programmers themselves to understand their own code. Collaboration has been done through GitHub, which greatly simplifies the process and also provides a means of version control. The last point, testing, is described in more detail below.

An example of verification and validation in a software project is shown in Figure 17.1. This project extends much further than only software development, but this figure is still a good reference for software testing methodology and is thus relevant.

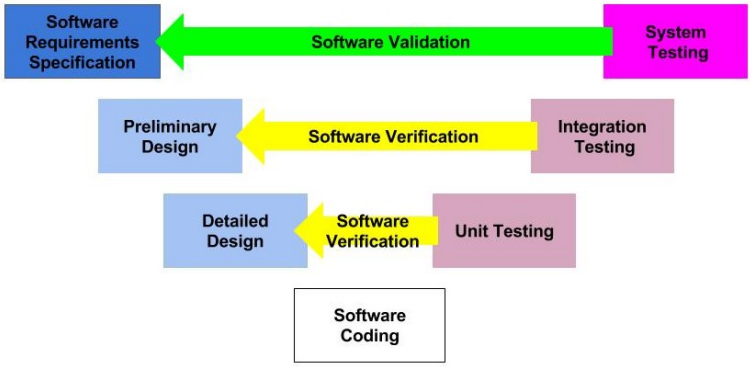

Figure 17.1: Software Verification and Validation

17.2.1.1. Testing Methodology

After some research, it has been found that there is a safe method to write programs in a way that minimises errors. This method can be thought of as *fail first, pass later*. What this entails is that for every program or script that is made, the creator first makes a test class for it. Then, whenever a new function is added, it is first left empty while the programmer considers the input and output parameters, which are also immediately documented in the code comments.

After these have been determined but before the function body is written, the creator of the code makes test cases for all possible outputs of the aforementioned function, that verify whether all the calculations in the function are correct. Then this test method is run and, naturally, it fails completely. This failure is a crucial part of the progress, because it verifies that the tests can indeed fail and that they will fail if there is no function body. After this failure, the actual function body gets written and subsequently the tests are run again, iterating this process until all tests pass. In this way one can be sure that the reason these tests pass is because of the content in the function.

The software used for testing in this project is the open-source unittest.py[i] module, due to its versatility, simplicity and elaborate online documentation. A file has been made for this module containing all important functions and elaborate comments explaining each of them in great detail. These are then be used as a template to design test classes for every class that is used throughout the project.

17.2.1.2. Test Cases

Each of the test methods should verify several characteristics of the output variable or variables, these are summarised below. The most general checks are mentioned first, then they become more specific further down the list.

- Number of output variables: This should be the same number as expected.
- Variable types: Each of the output variables should be of the correct type, this can be float, bool or int, for example. Since the variable type is not statically determined at initialisation in Python, one must check that the output type is as expected, as implicit type casts could have occurred within the function.

[i] https://docs.python.org/3/library/unittest.html

- Length of lists and strings: If the variable is a list, tuple, string or any other container for a series of values, the length of it should be verified, in order to prevent situations where one tries to access an element beyond its size.
- Numerical variable range: If the variable is of some numeric type (such as int or float), verification is required that the variable does not exceed this range, this goes for both the lower and the upper bound.
- Expected values: If all the above has been confirmed, one must verify that the outcomes of a function are as expected, for numerical values this means that it should be reasonable result of the calculation performed in the function. This is done by comparing the values with an approximation of the same calculations and making sure these do not diverge too greatly.

17.2.1.3. Unit Tests

A unit test is the simplest building block of a test class, it verifies the calculations of a single function. This was used amply for the numerical models in this project, for example in the Astrodynamics part several unit

17.2.1.4. Integration Tests

Going further, integration tests are used to verify the interaction between several functions. These are made after passing the unit tests, but before writing the code that provides this interaction, thus testing the interaction itself. This sort of testing was done with the downlink and structures department as the structure changed the layout of the satellite and vice versa. Testing had to be performed where the two scripts communicated to ensure that it was working as expected.

17.2.1.5. System Tests

As a final verification, system tests are made that run on the entire program, thus providing a final confirmation that everything works properly on the largest scale. For this project the departments worked in encapsulated scripts and only a few of these scripts required inter department communication between them (those who did were tested at integration). So in this context, the system level tests were the ones in each department capsule to ensure the model for that department was working as intended based solely on inputs and outputs. When all of the system tests run without errors, the program can be considered completely verified.

17.2.2. Calculation verification

The calculations performed in the project are based on well established laws of physics and formulas that have been in use for long periods of time. Using these scientific tools, analytical models describing physical phenomena through mathematics can be made. Unfortunately, analytical models often lack in efficiency and they fail to take into account the full complexity of world, instead simplifying it into ideal situations. For these reasons, numerical models were developed. E

17.2.2.1. Analytical Model

Throughout this project, several analytical models were developed. These models relied on theory and came with certain assumptions and limitations that had to be considered. For example. the structures department sized the trusses analytically but it did so with the assumption that the trusses were massless relative to the mirror masses. In reality, of course, the trusses are not massless and therefore also contribute to the deflection of the beam but for the current conceptual design this was not accounted for.

To verify the analytical models, reference data was used where appropriate to fill in values. For example, in Chapter 7 and Chapter 12, reference data from geostationary satellite missions and from the manufacturers of components is used for inputs. Then, using well-known and verified equations, an analytical model is formed that is used for the computations, since these models exist purely out of existing formulas that have seen extensive usage, they can be considered verified as well.

17.2.2.2. Numerical Model

Numerical models were also constructed for certain departments. These can be described as cruder methods that can predict outcomes on large data sets with high accuracy. While it is possible to calculate a numerical model by hand, computers are exceptionally suitable for running numerical models with repetitive but simple calculations. The two main numerical models developed were the thermal and the astrodynamics department models.

To verify these models analytical solutions based on simplified models could be used to ensure the results were correct. For example, in the thermal control subsystem there were certain points in the spacecraft where the expected temperature could be calculated analytically such as the Worker since the heatflux here is largely dominated by the inefficiency of the reflectivity of the mirror. Then the results of the numerical and analytical model could be compared to verify the correctness of the numerical model constructed. Here a 5% tolerance margin was used, meaning if the results would show a discrepancy larger than that they would have to be adjusted. The 5% thresh-hold was decided to be acceptable at this level given it is still at the conceptual design level. Similarly, conditions for the astrodynamic model could be solved analytically at specific points of interest to ensure that the analytical model did not diverge from the analytical answers too much.

17.2.3. Assembly Verification

When a spacecraft mission is conducted, great care must be taken that all parts fulfil the minimum requirements of performance and do not have any faults or cracks in the structure. Doing maintenance during a space mission is a non-trivial task, so the standards of quality of such missions are significantly higher than in other industries. Because of this, space missions are designed with redundancy in mind, in order to avoid that the unlikely but not implausible scenario of a single component failure cripples the entire spacecraft and dooms the mission.

For every part used in this project, the highest TRL possible is desirable, since those components that have a good track-record have been proven to be reliable. But this is not always possible, some of the technology used is relatively new and in order to fulfil the ambitious goals of this project, the boundaries of human technological innovation must be pushed and one must occasionally tread into the unknown waters of unproven technology.

17.2.3.1. Qualification and Acceptance

Any design process for a space mission should make use of two important verification procedures, namely qualification and acceptance.

These are standard procedures for the space industry and were developed collaboratively by the DoD, NASA and the ECSS. They specify the fundamental concepts of verification of space systems and name the criteria for verification. An indication of the ECSS[ii] specifications is depicted in Figure 17.2.

[ii] https://ecss.nl/

Figure 17.2: ECSS Qualification and Acceptance

Qualification is the process of verifying that the design meets the requirements and specification of the system. This procedure will be performed by means of **Analysis**, **Testing**, **Inspection** and **Demonstration**. Acceptance is then used to prove that the physical structure is free of defects and that the system meets the performance criteria. This procedure is checked using **Testing**, **Inspection** and **Demonstration**.

17.2.3.2. Physical Connectivity Verification

Before the spacecraft is launched to orbit, it is desirable to conduct elaborate tests in order to verify the connections between the various components of the spacecraft. These can be separated into several categories:

- Mounted connections: When Components are to be mounted or connected together for structural purposes, this should be attempted at a ground-based testing facility before launch, in order to verify the fit of this connection.
- Electrical connections: If there is a cable connecting components, it should be tested beforehand to verify that this cable fits and that it can handle the required voltage and amperage.
- Data connections: Whenever there is a connection between components that requires the transmission of data, this should also undergo verification before launch, to make sure that this cable can be attached to both components and that it can handle the necessary bandwidth.

17.2.3.3. Assembly Simulation

After all the system components are independently verified and are connected at the ground-based testing facility, a simulation should be run that mimics a real operating environment, which then verifies the entire system as a whole. Using this software, the inter connectivity of components, sub assemblies and subsystems can be tested, verifying the actuation of movable components, electrical connections and data transfers. In addition the on-board computer can be fully verified with its connections to all the other system components, in addition to the uplink and downlink data transmission signals to the ground station. This testing program thus servers as a final verification for the spacecraft as a whole.

17.2.4. Validation

While verification is a testing method that checks for errors in calculation, validation is used to make sure that the correct calculation is done. This can be done in various ways, but it requires some comparison to

something that either has been tested in a real-life scenario previously or a numerical method so robust and so extensively tested that its outputs can be used as validation data. Although there have not been any space missions quite at the scale of this one, there still exists a large amount of reference data out there concerning space missions and the design of a spacecraft.

17.2.4.1. Calculations

When calculations are done, whether in a programming language or by hand, they must be validated using some form of validation data. This can be done by making use of existing literature describing previous satellite missions, so for each value to be calculated, a reference in literature is located that has comparable inputs, so that its outputs can be compared to the outputs of the calculation. Of course there rarely is a mission with the exact same values, but this method is still robust enough to provide a good order of magnitude approximation that can serve as a validation tool for calculations.

For example, in Chapter 7 and Chapter 12, the obtained results were compared directly with reference data from existing geostationary satellite missions. For some other subsystems, this got more complicated considering the novelty of this mission, so more assumptions had to be made and the results were then scaled to the order of magnitude of the spacecraft described in this report.

17.2.4.2. Components

For every component of the spacecraft, its previous use in space missions should be investigated, if present. One would look at all the missions that the component has been used in and then use that data as a validation for the performance. If there has not been any previous use, then reference literature must be used that makes use of comparable components so that the performance of these components can be put side-by-side to the predicted performance of the components used in this mission. Using this method, it can then be validated whether the component performs as expected in a real situation and if not, the calculations must be adjusted and the component must be reanalysed to determine whether it still fulfils the requirements specified by the system.

17.2.4.3. Assembly

A more difficult situation is validation of the entire assembly. For this a more extensive literature research is needed and more assumptions have to be made, since the assembly itself diverges significantly from existing space missions. Still, using approximations, some estimations can be made on the functioning of the system as a whole and the integration of the various subsystems within the spacecraft. This combined with the previously described full system testing at a ground-based testing facility provides sufficient evidence for nominal functioning of the system throughout the mission. Risks always remain, but that is an inevitable consequence of conducting operations in space, let alone such an ambitious project as this one.

17.2.5. Implementation

The methods described in the previous sections somehow have to be applied to the design process, so a framework must be created to take care of this. The most essential part to having any sort of organisational structure in a team is of course communication. Thus the various components and subsystems are carefully documented and their status in regards to verification and validation is continuously monitored. A task can only be considered done when it has undergone and passed all verification and validation procedures, only then can it be marked completed. In addition to this, team members regularly check each other's work to ensure nothing is left out and no mistakes are made. In this way, quality can be assured for all parts of the process.

17.3. Performance Analysis

In this section, the general performances of the system are laid out. Table 17.1 shows these performances, the subsystem responsible for them, their values, and the reference chapter to check where the numbers come from.

Performance	Subsystem	Value	Unit	Reference Chapter
Transfer time	Propulsion	442	days	Chapter 5
Assembly time	AIV	1.7	years	Chapter 8
Power delivery	Downlink	413	MW	Chapter 11
System efficiency	Downlink	41.6	%	Chapter 4
System life time	System	25	years	Chapter 15
Pointing accuracy	ADCS	10e-10	deg	Chapter 7
Attitude determination accuracy	ADCS	2.78e-3	deg	Chapter 7
Slew rate around x,y,z-axis	ADCS	0.5, 4.1, 1	deg/hr	Chapter 7
Battery storage	EPS	250	kWh	Chapter 11
System power usage	EPS	133	kW	Chapter 11
Solar array power	EPS	210-150	kW	Chapter 11
SNR for uplink, downlink	C&DH	32.3, 1.3	dB	Chapter 12

Table 17.1: Performance analysis overview

17.4. Compliance Matrix

In the midterm report, a list of requirements was made that covered general mission and system requirements, as well as subsystem specific requirements. In this report, each section describing a subsystem also lists the requirements specific to that subsystem. In order to verify the fulfilment of all of the requirements made for this mission, a compliance matrix has been set up that contains all the requirements from each subsystem and the system and general requirements taken from the midterm report, this compliance matrix is shown in Table 17.2. Then it shows whether this requirement has been fulfilled and if not, a comment is added to elaborate on the reasons behind it. For each requirement, it also lists the section in which the fulfilment of the requirement takes place.

Requirement	Description	Compliance	Reference Chapter	Comment
GEN.PRJ.1	The system shall employ modular components.	✓	Baseline Report	
GEN.PRJ.2	The system shall be brought to orbit in a maximum of 350 launches.	X	Chapter 5	System takes 220 launches, refuelling missions at least 440 launches
GEN.PRJ.3	The target orbit shall give one ground station the chance to harvest the energy provided by the system.	✓	Baseline Report	
GEN.PRJ.4	The system shall be disposed of in a graveyard orbit of a height 36138 km from surface.	✓	Chapter 5	
GEN.PRJ.5	The system shall not interfere with other geostationary satellites.	✓	Baseline Report	
GEN.PRJ.6	The system shall not release toxic materials into the Earth atmosphere.	✓	Chapter 19	
GEN.PRJ.7	The system shall be launched using a reusable launch platform.	✓	Baseline Report	
GEN.PRJ.8	The system shall obtain a minimum Economic Sustainability Indicator equal to <0.42>.	✓	Chapter 19	
GEN.PRJ.9	The system shall obtain a minimum Social Sustainability Indicator equal to <0.48>.	X	Chapter 19	S.I. is 0.443
GEN.PRJ.10	The system shall obtain a minimum Environmental Sustainability Indicator equal to <0.33>.	✓	Chapter 19	
GEN.PRJ.11	The system shall not break any laws	✓	Baseline Report	
GEN.PRJ.12	The system shall not violate stakeholder regulations during its entire life cycle.	✓	Baseline Report	
GEN.PRJ.13	The project shall meet all general requirements outlined by the European Cooperation for Space Standardization (ECSS) in ECSS-E-ST-10C prior to the launch schedule.	✓	Baseline Report	
GEN.PRJ.14	The system shall have a maximum operational cost of 16 billion euros.	✓	Chapter 18	
GEN.PRJ.15	The system shall have launch costs of no more than 300 $/kg to LEO.	✓	Chapter 18	
GEN.PRJ.16	The system shall operate in orbit of height from 800 km to 35500 km.	✓	Chapter 5	
GEN.PRJ.17	Launch shall take place if and only if all safety standards outlined by the ECSS are met prior to Launch.	✓	Baseline Report	
GEN.PRJ.18	The system shall be launched between 2028 and 2032.	✓	Chapter 15	
GEN.PRJ.19	The system shall be assembled in space between 2032 and 2038.	✓	Chapter 15	
GEN.PRJ.20	The system shall be fully operational before the end of 2039.	✓	Chapter 15	
GEN.SYS.1	The system shall rely on solar power for power generation.	✓	Chapter 4	
GEN.SYS.2	The system shall have a life expectancy of at least 25 years following assembly of the system.	✓	Chapter 15	
GEN.SYS.3	The system shall deliver a usable power of 100 MW.	✓	Chapter 4	
GEN.SYS.4	The system shall consist of modules of maximum 100 tonnes.	✓	Chapter 4	
GEN.SYS.5	The structure shall avoid single point failure.	X	Chapter 9	More redundancy adds to much mass
GEN.SYS.6	The system shall use only components marked as at least TRL 4 as of December 2026, according to ISO 16290:2013.	✓		Not a specific
GEN.SYS.7	The system shall have no risk events with medium to high probability and large impact.	✓	Chapter 16	
GEN.SYS.8	The system shall have a total mass of less than 35000 tonnes.	✓	Chapter 14	

Requirement	Description	Compliance	Reference Chapter	Comment
GEN.SYS.9	The system shall operate within a pressure range of 10^{-6} and 10^{-9} torr.	✓		Not discussed
GEN.SYS.10	The system shall operate in the presence of Atomic Oxygen with energy of 5.2 eV.	✓		Not discussed
GEN.SYS.11	The system shall operate nominally under ultraviolet radiation of at least 1399 W/m^2.	✓		Not discussed
GEN.SYS.12	The system shall operate in the presence of particles with an energy between 40 keV to 700 keV .	✓		Not discussed
GEN.SYS.13	The system shall operate in the presence of plasma.	✓		Not discussed
GEN.SYS.14	The system shall communicate within the bandwidth allocated by the International Telecommunications Union (ITU)	✓	Chapter 12	
SSR.DOWN.BLIND.1	The downlink layout will allow for a 360° range in which the power can be transmitted.	✓	Chapter 4	
SSR.DOWN.BLIND.2	The angle γ shall be $\geq \beta$ related to blindspot mitigation.	✓	Chapter 4	
SSR.DOWN.BLIND.3	The Sting reflector shall be sized to allow for redirecting the power under an angle of ρ.	✓	Chapter 4	
SSR.DOWN.BLIND.4	The Relay reflector shall be sized to allow for redirecting the power under an angle of $\frac{\pi-\delta}{2}$ and $\frac{\pi-\rho+\alpha}{2}$.	✓	Chapter 4	
SSR.DOWN.FOV.1	The reflectors shall be able to direct the beam over the Equatorial plane, during any time of the year.	✓	Chapter 4	
SSR.DOWN.FOV.2	No more than 0.15 days/year downtime shall be used for aligning the FOV of the reflectors	✓	Chapter 4	
SSR.DOWN.FOV.3	The reflectors shall have a pointing accuracy equal to at least 2 arcseconds	✓	Chapter 4	
SSR.DOWN.FOV.4	The reflector actuators shall not induce a torque larger than 23.7 kNm.	✓	Chapter 4	
SSR.DOWN.GROUND.1	The ground station shall have no operational downtime.	✓	Chapter 18	
SSR.DOWN.GROUND.2	The ground station shall accommodate a pointing accuracy of 2 arcseconds.	✓	7	
SSR.DOWN.GROUND.3	The ground station shall accommodate a spot size with a radius equal to the Aperture radius	✓	Chapter 4	
SSR.LAU.ORB.1	The peragee of the parking orbit shall have an orbit height of 500 km.	✓	Chapter 5	
SSR.LAU.ORB.2	The transfer time of the whole system shall not exceed two years.	✓	Chapter 5	
SSR.LAU.ORB.3	The total propellant mass of the transfer mission shall not exceed 6M kg.	✓	Chapter 5	
SSR.LAU.ORB.4	The Starship modules should be connected in assembly modules before arriving in GEO.	✓	Chapter 5	
SSR.PROP.THRUST.1	The system shall be able to provide a Delta-V of 1450 $[m/s]$.	✓	Chapter 6	
SSR.PROP.THRUST.2	The system shall have a minimum burn time of 500 $[sec]$.	✓	Chapter 6	
SSR.PROP.THRUST.3	The system shall have a maximum acceleration of 4.0 $[m/s^2]$.	✓	Chapter 6	
SSR.PROP.FUEL.1	The fuel shall have a flammability range of 2-80%.	✓	Chapter 6	

Requirement	Description	Compliance	Reference Chapter	Comment
SSR.PROP.FUEL.2	The minimum fuel flow of the system shall be 500 [kg/s||m^3/s].	✓	Chapter 6	
SSR.PROP.BUD.1	The engine shall have a maximum mass of 2000 [kg].	✓	Chapter 6	
SSR.PROP.BUD.2	The system shall have a maximum volume of <tbd>[m^3].	-	Chapter 6	Unable to know, so removed it.
SSR.PROP.BUD.3	The system shall be able to provide a minimum delta-v of 1450 [m/s].	✓	Chapter 6	
SSR.PROP.AIV.1	The system shall be able to be integrated into to the transfer module.	✓		
SSR.PROP.AIV.2	The system shall be validated.	✓	Chapter 6	
SSR.PROP.EOL.1	The system shall be able to perform the transfer to the graveyard obit after the end of its operational life, which requires a delta V of 7.5 [m/s].	✓	Chapter 6	
SSR.PROP.EOL.2	The system shall be able to safely deactivate the PSS at EOL.	✓	Chapter 6	
SSR.PROP.THERM.1	The system shall be able to keep the fuel at a temperature below 100 [K].	✓	Chapter 6	
SSR.PROP.ENV.1	The fuel of the PSS shall be produced in a way that is not toxic for its environment according the local laws and environmental laws.	✓	Chapter 6	
SSR.PROP.ENV.2	The production of the system shall not expose the workers to any safety hazards.	✓	Chapter 6	
SSR.ADCS.CON.1	The ADCS system shall provide attitude control around 3 axes.	✓	Chapter 7	
SSR.ADCS.CON.1.1	The ADCS system shall provide 0.99 degrees rotation around the y-axis per day to correct for the earth rotating around the sun.	✓	Chapter 7	
SSR.ADCS.CON.1.2	The ADCS system shall correct for the orbital perturbations	✓	Chapter 7	
SSR.ADCS.CON.1.2.1	The ADCS system shall correct for Solar radiation torque	✓	Chapter 7	
SSR.ADCS.CON.1.2.2	The ADCS system shall correct for Magnetic field torque	✓	Chapter 7	
SSR.ADCS.CON.1.2.3	The ADCS system shall correct for Gravity Gradient Torque	✓	Chapter 7	
SSR.ADCS.CON.2	The ADCS system shall have a pointing accuracy of 1.0 degrees.	✓	Chapter 7	
SSR.ADCS.CON.3	The ADCS system shall be able to slew at a rate of at least 1 degrees per 180 minutes around each axis.	✓	Chapter 7	
SSR.ADCS.DET.1	The most accurate sensor shall determine the attitude with an accuracy of at most 15 arc seconds.	✓	Chapter 7	
SSR.ADCS.DET.1	The direction of the sun shall be determined with an accuracy of at least 0.5 degrees.	✓	Chapter 7	
SSR.ADCS.RISK.1Ã£	The ADCS of the satellite shall have no single point of failure.	✓	Chapter 7	
SSR.AIV.ROB.1	The The robotic assembly system shall use an off-the-shelf robotic assembly system, and associated requirements.	✓	Chapter 8	

Requirement	Description	Compliance	Reference Chapter	Comment
SSR.AIV.ROB.2	The system assembly shall be automated where the tip precision necessary does not exceed that of the robotic arm's accuracy.	✓	Chapter 8	
SSR.AIV.ROB.3	The assembly will be telecontrolled where the tip precision necessary is less than 5 mm.	✓	Chapter 8	DARPA approx 1mm
SSR.AIV.ROB.4	The robotic arm(s) shall have a tip position accuracy of at least 5 mm.	✓	Chapter 8	
SSR.AIV.ROB.5	The robotic assembly system shall have 6 degrees of freedom.	✓	Chapter 8	
SSR.AIV.ROB.6	The robotic assembly system shall employ optical torque sensors for collision detection and reaction.	✓	Chapter 8	
SSR.AIV.ROB.7	The robotic assembly system shall not exceed 100 tonnes in mass.	✓	Chapter 8	
SSR.AIV.ROB.8	The robotic arm(s) shall have a maximum tip speed of 100 mm/s.	✓	Chapter 8	DARPA <European Robotic Arm
SSR.AIV.ROB.9	The robotic assembly system shall cost no more than FY20 64.6 million.	-	Chapter 8	Modelled on the European Robotic Arm
SSR.AIV.POW.1	The robotic assembly system shall have a maximum total idle time of 100 days.	✓	Chapter 8	Eclipse time less than this over assembly time
SSR.AIV.INT.1	The system shall employ a Physical (Fit) Verification through optical confirmation.	✓	Chapter 8	DARPA
SSR.AIV.INT.2	The robotic assembly system shall employ optical sensors with a resolution of at least 2mm.	✓	Chapter 8	
SSR.AIV.INT.3	The robotic assembly system shall relay and retry failed connections.	✓	Chapter 8	
SSR.AIV.INT.4	The system shall employ an in-space Multi-element Integrated Test to verify simulated system functionality (connections).	-	Chapter 8	To be done during testing of subsystem
SSR.AIV.INT.5	The subassemblies needed for on-orbit assembly in GTO shall employ standard interface points for robotic assembly.	✓	Chapter 8	
SSR.AIV.INT.6	The system shall be assembled in a maximum of 2200 days.	✓	Chapter 8	<1000 days
SSR.AIV.DEP.1	The system shall employ an in-space Multi-element Integrated Test to verify simulated system functionality (deployment).	-	Chapter 8	To be verified during testing
SSR.AIV.DEP.2	The power system shall be deployed within 24 hours of assembly.	✓	Chapter 8	
SSR.AIV.DEP.3	The payload and power systems shall be deployed in the target orbit.	✓	Chapter 8	
SSR.STRUC.LAU.1	The launch module shall be able to withstand a steady state axial acceleration of 6g's.	✓	Chapter 9	
SSR.STRUC.LAU.2	The launch module shall be able to withstand a steady state lateral acceleration of 3.5g's.	✓	Chapter 9	

Requirement	Description	Compliance	Reference Chapter	Comment
SSR.STRUC.LAU.3	The launch module shall be able to withstand a lateral vibration of 25Hz.	✓	Chapter 9	
SSR.STRUC.LAU.4	The launch module shall be able to withstand acoustic loads of up to 137.7dB.	-	Chapter 9	Can't be sized at this stage
SSR.STRUC.LAU.5	The launch module shall be able to withstand a shock load of <TBD>.	-	Chapter 9	Starship doesn't provde a load
SSR.STRUC.ORB.1	The structure shall be able to withstand transfer loads of <TBD>.	-	Chapter 9	This hasn't been determined
SSR.STRUC.ORB.2	The structure shall be able to withstand manoeuvre loads due to a 1 degree change in attitude in 30 minutes about every axis.	✓	Chapter 9	
SSR.STRUC.ORB.3	The structure shall be able to withstand thermal loads due to temperature differences in the structure.	-	Chapter 9	This wasn't sized at this stage
SSR.STRUC.ORB.4	The structure shall be able to withstand impact of micro debris with a diameter of up to 2cm.	-	Chapter 9	An estimate of how many will collide was done, but no idea how to size for impact toughness
SSR.STRUC.ORB.5	The structure shall be able to withstand impact of micro meteorites with a mass of up to 1gram.	-	Chapter 9	An estimate of how many will collide was done, but no idea how to size for impact toughness
SSR.STRUC.ASS.1	The structure shall allow for allow for the integration of the subsystems.	✓	Chapter 9	
SSR.STRUC.MAI.1	The structure shall allow for maintenance of the spacecraft.	-	Chapter 9	This was not thought about at this stage
SSR.STRUC.PAY.1	The truss connecting the Queen with the Worker shall have a maximum deflection of 1mm.	✓	Chapter 9	
SSR.STRUC.PAY.2	The truss connecting the Queen with the Sting shall have a maximum deflection of 5mm.	✓	Chapter 9	
SSR.STRUC.PAY.3	The truss connecting the Queen with the Relay shall have a maximum deflection of 5mm.	✓	Chapter 9	
SSR.THC.TOP.1	The thermal control subsystem shall prevent overheating and under-cooling of components	✓	Chapter 10	
SSR.THC.PAY.2.1	The thermal control subsystem shall maintain large parabolic mirror temperatures between -10°C and 100°C	✓	Chapter 10	
SSR.THC.PAY.2.2	The thermal control subsystem shall maintain temperatures of the small dish, relay, and reflector mirrors between 0°C and 175°C	✓	Chapter 10	
SSR.THC.PAY.3	Active thermal control subsystems shall use loops in parallel.	✓	Chapter 10	
SSR.THC.POW.1	The thermal control subsystem shall maintain battery temperatures between 0 °C and +20 °C.	✓	Chapter 10	
SSR.THC.POW.2	The thermal control subsystem shall maintain solar array temperatures between -60 °C and +60 °C.	✓	Chapter 10	
SSR.THC.AIV.1	The thermal control of assembly robotics shall maintain temperatures between -15°C and +50°C.	-	Chapter 10	Solution is given but not worked out

Requirement	Description	Compliance	Reference Chapter	Comment
SSR.THC.PROP.1	The thermal control subsystem shall keep the propulsion components' temperatures between -5°C and +40°C.	-	Chapter 10	Solution is given but not worked out
SSR.THC.PROP.2	The thermal control subsystem shall keep temperature of propellant between 2 °C and 100 °C.	-	Chapter 10	Solution is given but not worked out
SSR.THC.STRUC.1	The thermal control subsystem shall maintain the temperatures of mechanisms between +5°C and +50°C during operation.	-	Chapter 10	Solution is given but not worked out
SSR.THC.MEAS.1	The thermal control subsystem shall measure the temperature of other subsystems.	✓	Chapter 10	
SSR.THC.TOP.2	The thermal control subsystem shall prevent complications due to large temperature gradients.	✓	Chapter 10	
SSR.THC.PROP.3	The thermal control subsystem shall ensure a temperature difference of <5°C between propellant tanks.	-	Chapter 10	Solution is given but not worked out
SSR.THC.STRUC.2	The thermal control subsystem shall ensure a spatial temperature gradient of structural elements of <3°C/m.	✓	Chapter 10	
SSR.THC.TOP.3	The thermal control subsystem shall prevent complications due to rapid temperature changes.	✓	Chapter 10	
SSR.THC.ELEC.1	The thermal control subsystem shall ensure a temperature gradient over time for electrical components of <5°C/hour.	-	Chapter 10	Solution is given but not worked out
SSR.EPS.REQ.1	The electrical power system shall provide for the generation, storage and distribution of electrical power to the spacecraft payloads and housekeeping loads during the entire mission life of 25 years.	✓	Chapter 11	
SSR.EPS.REQ.2	Operational orbit load: during sunlight 132 500 watts, during eclipse 125 000 watts.	✓	Chapter 11	
SSR.EPS.REQ.3	Peak load of additional 100 kilowatts for 20 seconds in every 350 minute period.	✓	Chapter 11	
SSR.EPS.REQ.4	Power management software to control the battery state of charge/discharge, temperature, charge/ discharge balance between batteries.	✓	Chapter 11	
SSR.EPS.REQ.5	Maximum worst-case battery DOD 70 percent during operational orbit.	✓	Chapter 11	
SSR.EPS.REQ.6	Testability shall be provided at the EPS level and the spacecraft level.	-	Chapter 11	Full analysis hasn't been performed yet
SSR.EPS.REQ.7	Autonomous operation in all normal functions, unless overridden by ground command.	✓	Chapter 11	
SSR.EPS.REQ.8	EPS Reliability of 0.95 over the entire mission life, including the ground and space storage, if required.	-	Chapter 11	Full analysis hasn't been performed yet

Requirement	Description	Compliance	Reference Chapter	Comment
SSR.EPS.REQ.9	Single fault tolerant system where faults shall not propagate to other components, subsystems or systems.	✓	Chapter 11	
SSR.CDH.TECH.1	The CDH system shall be able to receive and send commands to other subsystems.	✓	Chapter 12	
SSR.CDH.TECH.2	The CDH system shall assess the state of functioning of the subsystems of the spacecraft.	✓	Chapter 12	
SSR.CDH.COMM.1	The subsystem shall send and receive commands from the ground station.	✓	Chapter 125	
SSR.CDH.COMM.1.1	The subsystem shall be able to transmit at least 1 Mb/s bits and receive at least 2 kb/s bits.	✓	Chapter 12	
SSR.CDH.COMM.1.2	The data downlink shall have a link margin of at least 10 dB.	✓	Chapter 12	
SSR.CDH.COMM.1.3	The data uplink shall have a link margin of at least 10 dB.	✓	Chapter 12	
SSR.CDH.RISK.1	The subsystem shall have no single point of failure.	✓	Chapter 12	

Table 17.2: Compliance Matrix

17.4.1. Unmet Requirements

GEN.PRJ.2, ***GEN.PRJ.9***, ***GEN.SYS.5***, ***GEN.SYS.7*** are the requirements that the system does not comply with. The first one states that the number of launches can not exceed 350. IKAROS has at least 440, causes the system to violate this requirement. This is not a killer requirement as the system can still work; only launch costs and time will increase. For the second one, the project does not reach a Social Sustainability Indicator of 0.48. It misses out on just 0.04, what does not bring the project into extreme danger. Also, the SI was just made to trade off concepts. It was not made for this requirement which makes it a less hard one. Then for ***GEN.SYS.5***, where the structure was not allowed to have a single point of failure. If there had been designed for this, a substantial mass increase would have followed. This is because, for every strut, there has to be a spare one. The requirement is considered to be somehow unimportant as the system could still operate if not everything is fail-safe. To conclude, the unmet requirements do not lead to a mission failure, making it worthwhile to continue with the project.

17.4.2. Requirements that are still unknown

Next to the four unmet requirements, the results of nineteen requirements were not determined yet. Some requirements like ***SSR.STRUC.LAU.4*** can not be determined because the level of detail achieved in this report is not sufficient to calculate the values of these parameters. To meet these requirements, further detailed design will need to be performed. Other requirements, such as ***SSR.STRUC.LAU.5*** require data from partners which was unable to be acquired in the time frame/ context of the Design Synthesis exercise. The third kind of unknown requirement are like ***SSR.THC.AIV.1***, where the solution to these requirement was determined but no calculations were made to back up the decision, thus not answering the requirement. And finally, there are requirements like ***SSR.EPS.REQ.8***, which were not determined due to the time requirement to fulfil them, which was not available, or where the available resources where shifted to higher priority tasks. An additional sort of requirement was ***SSR.AIV.INT.4***, requiring the actual testing of the system before the requirement could be met. Once again, all these requirements are not driving requirements, and will thus not prevent the system from being further designed.

18
Business and Market Analysis

The business and market analysis chapter will cover an extensive market analysis which dives into market trends and predictions of the target market. The market analysis section will use a SWOT table to indicate the properties with respect to the market. The market section goes on to look at possible applications and choose the most profitable utility. The chapter goes on to break down the costs based on the parts needed for subsystems, launches and operations related to infrastructure. A table and visual interpretations of the results are presented. Finally the two sections are combined to present a profitability and return on investment estimation.

18.1. Market Analysis

In the market analysis, the market trends and predictions for India are discussed. The goal of the market analysis is to assess the options and the system from a business perspective to come to a 'most profitable' business model. The market analysis will use a SWOT analysis to determine the optimal market for IKAROS.

18.1.1. Market Volume and Trends

The market that has been selected for the IKAROS project is the quasi-developing country of India. India has been developing rapidly over the last few decades and has one of the largest populations on the planet. With this growth comes an increasing energy demand; India's energy consumption in 2018 was as high as 1309.44 TWh over the entire year[i], meaning that the average daily demand was around 150 GW and an average annual growth of 5.4% was measured. Current predictions see the demand doubling (and possibly even tripling) by 2040 [54].

The COVID-19 pandemic has had a distinct impact on this growth however, with the International Monetary Fund (IMF) already predicting back in April 2020 a global recession in the next couple of years. Losses in Indian GDP are predicted to be in the double digits and associated contractions in the energy sector following suit [55]. This should not be an impediment to the IKAROS project, which is expected to commence operations in 2032 as per the launch goal. By this time, the economic downturn due to the global recession should have mostly subsided and the market will have grown beyond current levels [56].

18.1.2. Target Market and Need

As discussed in previous reports, the energy market in India is controlled by large Distribution Companies, which supply power directly to residential and commercial customers[57]. These DISCOMs have significant liquidity and cash-flow problems however, and are thus not a reliable partner for a project that already includes many possible sources of risk as discussed in the Midterm's Risk Management chapter. The alternative to this is selling directly to bulk customers[58]. This can be extended even further by using the power in-house to sell a more profitable product. This is the target market which was deemed most profitable for the IKAROS project and the advantages that it possesses as is seen in Table 18.2.5.

The approach chosen for the IKAROS project is one of the market adaptations discussed in the Midterm report, namely the desalination and purification of water to provide water to municipal utilities.

As discussed in that report, India mainly relies on wells which tap into groundwater and rivers like the Indus river which carries glacial snowmelt from the Himalayas. Both of these sources are impacted significantly by global climate change and will only continue to do so in the future as global warming

[i] IEA, India, interactive statistics, `https://www.iea.org/countries/india` (accessed 14 January 2020)

accelerates[59].

The ground station will be integrated with a Reverse Osmosis desalination plant which will be situated near the western coast of the Indian subcontinent, in the province of Maharashtra. A desired location would be near the provincial capital of Mumbai, a colossal metropolis with a staggering population of over twenty million people.

As discussed in a 2016 USAID report, the city of Mumbai has a large disparity between current supply and demand, which will only be amplified in the future with an expected growth in demand of 71%[60][61]. The city of Mumbai was also considering the viability of establishing desalination plants as of the end of 2020, thus indicating a willingness to support projects as envisioned for the IKAROS system[62].

A RO plant makes use of the gradient in concentrations between two solutions, with the gradient a result of an external pressure. As of the writing of this report, this technique is the most efficient, with a per cubic meter power usage of 4.4 kilowatt hours. An alternative to this process is Multi Effect Distillation desalination, where the water is turned into steam to separate it from the particulates. This technique has a lower efficiency, thus RO is selected.

Expected generation capacity for a RO plant with a power input of 100 Megawatts would be around 23000 cubic meters of water per hour[63]. Water supplied to commercial zones and offices in Mumbai has a cost of circa Rs.90 per 1000 litres, which translates to an hourly revenue of circa 22 thousand Euros, significantly higher than the approximately potential 5 thousand Euros that could be obtained from selling the power directly at the local rates which are around Rs.4.63 per kilowatt̩hour[64][65][66]. This increase in revenue will of course be slightly offset by the increased operating cost of the ground station and the increased construction cost. These costs are estimated in Section 18.4.

18.1.3. Competitors and Barriers

Of course, this does not mean there are no competitors in this area. Water desalination, though an industry still very much in the early stages of widespread exploitation, has already surpassed the goals set by the desalination plants envisioned by the IKAROS project. The Saudi Ras Al-Khair Power and Desalination plant started construction in 2011 and was commissioned just a few years later with a capacity of 43 thousand cubic meters per hour, twice that of the plant intended for the IKAROS project[67]. Thus the technology has already proven its viability and effectiveness. There are reasons to believe that the advantages of the IKAROS project would not diminish significantly though, which are as follows:

- Any disconnected desalination plant which purchases either electricity or steam has higher overhead expenses when compared to the vertically integrated IKAROS plant.
- India's intention to primarily support its growth in power demand through the use of renewables would make it counter intuitive to construct a fossil-fuelled power station solely to desalinate water[68].
- Hydroelectric power is strongly dependent on flow rate from the upstream watershed and thus directly proportional to precipitation. Drought, and thus high demand for water would thus lead to a lower power output and thus desalination capacity [69].
- Solar and wind are unable to guarantee 24/7 operation without significant storage capacity and thus will be unable to meet the increased demand during peak hours. This situation might change by 2032 however, with battery technology being able to be scaled up to sufficient levels.

The combination of the expected increase in demand (and associated increase in cost) combined with the high seed cost ensure that the IKAROS project, once in operation, shall hold a competitive position in the utility market and produce a highly reliable source of revenues.

18.2. Strength, Weakness, Opportunity and Threat

A good way of determining the competitiveness of the project is by performing a SWOT analysis on the system. Such an analysis has already been performed in the Baseline report, and as will be shown, many of the same aspects carry over.

18.2.1. Strengths

The first strength is its renewable nature, as discussed in the previous reports. This advantage is manifold insofar as it reduces overhead expenses due to a lack of need for fuel for operations (outside of the fuel needed to perform maintenance missions of course) whilst also reducing the system's impact on the environment, as discussed in Chapter 19. This renewable nature also makes it eligible for many of the subsidies that are awarded to new renewable power generation plants as discussed in Section 18.3, including tax reductions through accelerated deprecation[70].

The second strength the IKAROS system brings forth is its ability to operate 24/7, giving it a significant leg up over traditional renewables which, unless fashioned in a composite arrangement with a storage method, are unable to provide full-time operation and are vulnerable to the day-night cycle. The IKAROS system shall have a downtime no larger than 3,5 days as defined in the Midterm report by requirement **TECH.PAY.Pow.1**.

The third strength of the IKAROS system is the vertically integrated nature of the ground station as discussed in subsection 4.3.4. This allows the IKAROS system to produce a highly sought after product without being reliant on intermediaries.

The final strength of the IKAROS system is the output product. Water, as discussed in Section 18.1, is a highly sought after good, which will only become more scarce in the future, setting up the system for future success.

18.2.2. Weaknesses

The following weaknesses were identified in the Baseline report. The biggest economic weaknesses of the IKAROS project lie in three main areas: the first one is the prohibitively high seed cost, with estimates going as high as around ten thousand dollars per kilowatt [71], which is astronomical when compared to wind (1200$/kW) [72], solar (1210$/kw) [72] and fossil fuels (700-1300$/kW). This thrusts space-based solar power into the region of nuclear power plant construction (4000$/kW) [73].

This high startup cost acts as a barrier to widespread implementation and increases reliance on subsidies and other incentive programs. Another issue entails the relatively high maintenance cost due to the exposure of the satellite to the harsh space environment [71]. Finally, a large constraint on the wider implementation of SBSP satellites is the saturation of the Geo-synchronous Equatorial Orbit [74]. Of these weaknesses, the first two still apply, even with the conversion to selling water.

A third weakness is the satellite's downlink system. A beam with a radius of tens of meters will constantly be shining down with an intensity higher higher than 35 suns. This might lead to interference with systems operating at lower altitudes that have sensitive instrumentation. This is a liability that is further discussed in the Midterm's Risk Management chapter.

Finally a fourth weakness is the system's long throughput time, in the order of magnitude of years. A lot can change in a few years, both with regards to a company's financial health but also to the market at large. The long throughput time makes the system inflexible and unable to quickly adapt to changes in its fiscal environment.

18.2.3. Opportunities

Three big opportunities present themselves that the system can take advantage of. The first one entails the current absence of desalination plants on India's western coast. Water supply near the city of Mumbai, the preferred ground station location, is primarily dependent on upstream lakes and rivers, sources that do not scale easily and will be negatively impacted by global climate change[ii]. This absence means that a scalable supply of water would easily find its niche there with a current lack of competitors. The second is the already significant disparity between supply and demand in the metropolis, with clean water supply being a luxury rather than a right[75]. A potential new supplier would thus be supported in a significant manner by the local government, allowing for potential decreases in ground station construc-

[ii]The Mumbai Pages,"Water Supply",`https://theory.tifr.res.in/bombay/amenities/water/`

tion cost[76]. Finally, India's economy is in a long term trend of growth that is not expected to cease until the half century point, leading to investment being stimulated by low interest rates[71].

18.2.4. Threats

Once again, the threats identified in the Baseline report carry over to the final design. These are as follows: The first threat to the IKAROS project is a problem for every object in orbit, but acquires significantly more salience due to having a surface area in the magnitude of square kilometers; space debris. Even a particle as small as 1 millimeter can pose a threat to the thin satellite array skin and body [77].
Although collisions in the Queen may only lead to slight reductions in performance, the accumulation of these small reductions over time may create significant obstacles to achieving optimal performance. This is compounded by the sizeable amount of debris that is present in Geo-synchronous Equatorial Orbit, the chosen orbit for the IKAROS satellite [78].

Another threat is presented by the reliance on external contractors to access the satellite for e.g. maintenance or replacement of faulty arrays. Commercial launch companies like SpaceX have a limited number of launches they can perform every year and the required capacity might not be available. If a large part of the satellite requires repairs that cannot be performed by robots with the resources present on the system, every hour that the system is not operating at maximum capacity is an hour of missed income; having to wait a month for the next launch might cause losses in the order of tens of millions, which is a significant opportunity cost to consider.
This limitation reduces the system's competitiveness with Earth-based sources which can quickly access their facilities and where even the most critical failures can be replaced in a matter of weeks if not days.

To round off this section, one more threat to the commercial viability must be discussed: competition with other SBSP systems. Once the IKAROS project has hypothetically proven its viability, it leaves open the opportunity for many other companies to create their own similar systems and start competing in what is now a practically empty environment.

18.2.5. SWOT Table

These Strengths, Weaknesses, Opportunities and Threats are summarised in Table 18.1 below, which gives a quick overview.

Strengths	**Weaknesses**	**Opportunities**	**Threats**
Renewable	High seed cost	Absence of desalination plants	Space debris
24/7 operation	High maintenance cost	High growth in market	Reliance on external contractors for access
Vertically integrated ground station design producing rare commodity	Downlink may be liability	Regulatory environment conductive	Many competitors if feasibility proven
Higher solar radiation w.r.t. ground-based	Inflexible	High disparity demand/supply	

Table 18.1: SWOT Table

18.3. Sources of Income

The sources of income can be divided into three substantial groups: revenues, subsidy and investment. The combination of these three over the useful lifetime of the satellite leads to the total assets that are available to finance the IKAROS project's different expenses, which are discussed in Section 18.4.

18.3.1. Revenues

: In Section 18.1 it was described that the source of revenue would be desalinated sea water. This water would be sold to the municipal water system for use in commercial and industrial applications. The total revenue over the lifetime of the system can be calculated by Equation 18.1

$$Revenue_{Lifetime} = Lifetime \cdot 365.25 \cdot 24 \cdot Water_{Hourly} \cdot e_{m^3} \tag{18.1}$$

Plugging the established values for the IKAROS project,namely a lifetime of 25 years, an hourly water production of 22727.27 cubic meters and a water price of Rs.90, a value of **4.93 Billion €** is obtained.

18.3.2. Subsidy

The Indian government is very involved in subsidising renewable energy capacity. The IKAROS project would be attempting to receive part of the Rs.5050 crore viability gap funding to develop 5000 Megawatts of solar power capacity. This would equate to about **1.1Billion €**.

18.3.3. Investment

Investment here does not mean investment in its traditional fashion. As will become apparent in Section 18.4, the costs of the project will far outweigh the expected income. This difference will have to be made up by private capital, supplied either by Airbus or another sponsor of the IKAROS project. The exact investment required will be presented in Section 18.5.Additionally, an initial loan of **0.25 Billion €** to finance the project by the Japan International Cooperation Agency in its nascent stage will be sought. This agency has previously awarded a loan of **0.237 Billion €** for the construction of the Chennai Seawater Desalination Plant in India[iii]

18.4. Cost Analysis and Breakdown

After designing the subsystems, the level of detail is sufficient to make an estimate of the cost of the system across the entire lifetime of the system. The costs of all the known parts are divided into two categories: Off-the-Shelf and to be made in-house. Each category has three sets of costs; the value or cost of a purchase, the transportation costs and the development costs. These costs are then added to costs related to launches, operations, maintenance and EoL.

18.4.1. Cost of parts

The value of a part is determined by the price set by a manufacturer or the cost of design, materials, machining and labour. When having to design a part, a budget is set because it is extremely difficult to estimate these costs accurately. Transportation costs are added because the system will need to moved from one facility to another. The transport cost also includes any import taxes that apply, in the case for satellite parts this import tax is 6.4% [79]. Development costs are broken down into the cost of designing, researching and testing a part based on TRL and the value of materials and machining costs. The transport costs are based on what couriers charge per kg per kilometer. This does not take time into consideration but does make it easier to estimate the transportation costs based on some constants, popular shipping routes and transportation logic [**?**]. The values of the costs per transport method can be found in Table 18.2.

Method	€/$(ton \cdot km)$
Aircraft	0.18
Small Ship	0.013
Medium Ship	0.033
Large Ship	0.023
Train	0.017
Truck High	0.189
Truck Low	0.092

Table 18.2: Table of prices per shipping method

[iii] author = JICA,title = JICA Assists to Transform Seawater into Drinking Water by Extending an ODA Loan of INR 1,800 Crore to Project for Construction of Chennai Seawater Desalination Plant , `https://www.jica.go.jp/india/english/office/topics/press180402$_$02.html(accessed14January2020)`

In order to estimate the development costs, two factors are included. The testing is taken to be between 20% and 30% [80]. To assure sufficient testing is done, 30% is taken as a base value. In the case that a part is bought off-the-shelf, an integration development cost is added, this is taken at 3% of the price because parts will often have guidelines to their installation procedure and the complexity of a part scales with it's price and vice versa.

18.4.2. Launch Costs

Once the parts of a module are assembled on Earth they need to be shipped to the launch site, these costs of transportation are also included in the cost of launching as they are only relevant when a module is launched into space.

The launch costs are relatively easy to calculate as the launch vehicle contractor will cover most of these costs and charge a single amount. Based on the mass of the entire system, the amount of launch vehicles can be calculated. Also the launch vehicles needed for maintenance are included. In the project guide, a cost of 300 e/kg [51] and the launch vehicle of choice is SpaceX's Starship.

18.4.3. Maintenance Costs

For maintenance costs, only the parts that degrade heavily are considered. These are the mirrors and solar panels, however the photo-voltaic cells can be designed such that they do not need to be replaced as often as the mirrors which degrade on an atomic level. Other parts are designed in a safe-life way such that they are expected not be replaced.

The cost model of the maintenance is based on the amount of parts that need to be replaced and the launches it will require. A simple time based model is programmed which models the degradation per month and only replaces a section of 100 tonnes at a time and then resetting the efficiency to model a new part. By selecting highly efficient panels and mirrors, less extra maintenance launches are needed and therefore reducing the cost of maintenance.

18.4.4. Operational Costs

The operational costs contain mostly salaries of the engineers and the facilities. In order to estimate the salaries, an average European salary is taken to be sufficient for the engineers monitoring the system. Instead of trying to figure out the costs of part time engineers and builders, it is decided to group these together under contractors for which a budget is assigned. For all the permanent positions a salary of 52000 Euros is assigned per person all inclusive. Based on the findings in a study about the commercial reality of desalination plants, simple process plants only require around 200-250 people. These facilities do not use any fancy technology but rely on the evaporation of the water by sunlight [81]. Adding another 110 people to this for the operations of IKAROS, a high estimate of 350 people is taken.

The operational costs include the building of a ground station. The building and logistics to make the ground station are outsourced to contractors and thanks to the location (India), the low cost of labour will reduce the cost of a ground station significantly. 500 million Euros are assigned to the building including a 10% reserve of 50 Million Euros.

18.4.5. End-Of-Life Costs

The end of life costs is the cost of transferring the system into the graveyard orbit. These costs will be mainly fuel to transfer IKAROS into the desired orbit.

18.4.6. Cost summary

In order to obtain a return on investment, a cost estimation based on the main and larger parts can be used, These parts will make up majority of the system cost. To summarise the costs and their relative size to each other pie-charts are presented and Table 18.3 presents the values as a quantity.

Part/Method	Manufacturing	Import Tax	Cost per unit (€)	Units
raptor engine	Off-The-Shelf	6.4%	1797400.0	40
propellant tank	In-House	None	554900.0	40
sun sensor	Off-The-Shelf	None	12800.0	2
star tracker	Off-The-Shelf	None	48100.0	2
IMU	Off-The-Shelf	None	1800.0	2
ADCS thruster	Off-The-Shelf	None	10700.0	16
ADCS tank	In-House	None	52300.0	16
On-Board computer	Off-The-Shelf	None	8000.0	1
Antenna	Off-The-Shelf	None	2200.0	3
Liquid Droplet Radiator	In-House	None	10849900.0	2
Thermal straps	Off-The-Shelf	None	2200.0	25
Thermal coatings	Off-The-Shelf	None	8600.0	2
Multi-layer Insulation	In-House	None	3858100.0	1
Louvres	In-House	None	534300.0	1
Heating elements	Off-The-Shelf	None	1100.0	56
Solar Panels	Off-The-Shelf	None	67600.0	2
Battery packs	Off-The-Shelf	6.4%	39700.0	2
Power Distribution System	Off-The-Shelf	6.4%	11300.0	2
Transfer fuel	In-House	None	10750900.0	1
Truss-structures	In-House	None	24573400.0	1
Queen's 'Mirrors	In-House	None	60474900.0	1
Worker's 'Mirrors	In-House	None	645900.0	1
Stinger's 'Mirrors	In-House	None	828000.0	1
Relay's 'Mirrors	In-House	None	1823000.0	1
Assembly robot	Off-The-Shelf	6.4%	168719500.0	3
Mechanisms	In-House	None	120000.0	300
Module transport	Off-The-Shelf	None	6376900.0	1
Ground station	In-House	None	500000000.0	1

Table 18.3: Table of costs for IKAROS

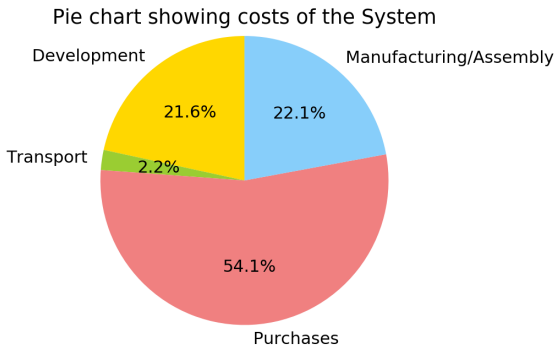

Figure 18.1: relative costs of the system

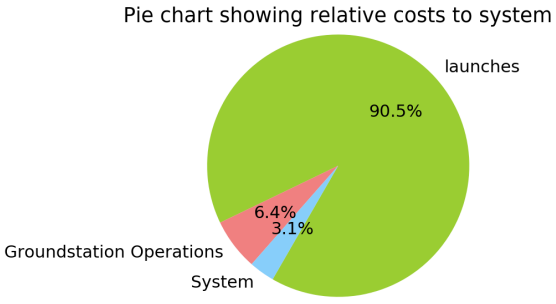

Figure 18.2: Relative cost of the entire project

Items	Cost Million Euros
Development	101.9
Manufacturing/Assembly	104.3
Purchases	255.2
Ground Station	500.0
Salaries/Contractors	455.0
Transportation	10.6
Launches	13560.0
Total	14986.95

Table 18.4: Overview of costs in table format

18.5. Projected Return on Investment

By combining the market analysis and the cost prediction, a profit forecast can be made. The profit forecast indicates the return on investment for all investing parties. In order to make an insightful profit forecast the following are considered to show to investors. The potential return on investment, a break even point in time, the point of no return for investors and possible scaling opportunities.

18.5.1. Break even point & ROI

The break even point of a project is defined as the point in time where the total revenue surpasses the total cost. As mentioned in Section 18.1, the costs are so big that the project requires extra funding in order to break even. To portray the costs over time, the costs are modelled into a cost curve to show potential investors at what time the project requires more funding. In the sixth year of the project, the year during deployment, the costs of the project already exceed 95% of the total costs. As the orange line does not cross the blue line, there is no break even point and as it stands, IKAROS has a negative ROI. The point of no return is a conceptual point based on the 80-20 rule. For IKAROS, the 80% of costs is achieved during launching because it makes up almost 90% of the total costs.

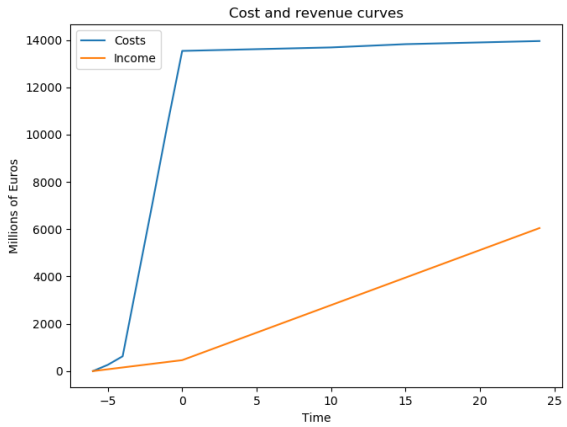

Figure 18.3: Graph displaying cost and income over the lifetime of the project.

18.5.2. Requirements For Profit and scalability

In order for IKAROS to become profitable, either the cost must decrease or the income must go up. The cost of launching is too big of a part of the total cost as can be seen in Figure 18.2. Looking to decrease the cost elsewhere may affect the quality of the design. IKAROS is a one of a kind and would acquire 100% of the market share for SBSP systems however it would only acquire 0.029% of the total water production market of India. A small share but still enough to provide a medium sized city with water.

The concept has two options for profitability, either the income must go up through extra funding/subsidy or the launch costs must reduce. Currently there are predictions for a lowered launch cost of just 2 Million dollars per launch [82]. This would reduce the launch costs by a factor 15 which has significant impact on the overall cost of the project. This would bring the cost per kilogram down to 20 dollars, this is an extremely low number and there is a lot scepticism if this is even possible. If the income were to increase through large funding and private investors, the project would require another 7909 Million Euros to break even by the end of life. The problem with this is that private investors will also want something in return, this could be a percentage of ownership or monetary returns. When comparing the graphs in Figure 18.4 and Figure 18.5, one can see that funding can allow for a break-even at the end of lifetime, whereas the cheaper launch costs can allow for a break even point in the fifth year and a final projected return-on-investment of 154%.

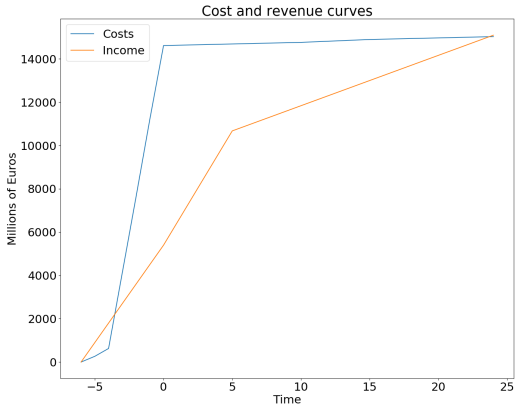

Figure 18.4: Graph displaying cost and income over the lifetime of the project with extra funding over time.

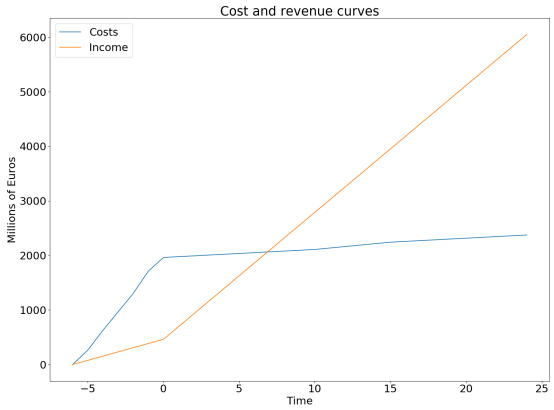

Figure 18.5: Hypothetical cost-income curve if a 2 million dollar launch were to exist.

From a business perspective, there are also some new technologies that will need to be developed and have high value to other parties. Technologies such as the liquid droplet radiator can be sold separately for a lot of money. The foil developed for the Queen is lightweight and rolls out, this is something that can be useful for solar sailing and the technology will be readily available. Anything that needs to be made in-house can be offered at a fair price because the intellectual property belongs to the IKAROS project.

19
Sustainable Development Strategy

In this chapter, the Indicator of Sustainability that was established in the previous reports will be used to measure and compare the final design to the initial Honey concept.This will be followed by a discussion on the source of these differences. Next the strategy approached for the incorporation of sustainability in the final design is presented. Finally an argument will be made about the improvements in sustainable design that are not measured by this indicator due to the lack of available detail when it was established. The section will be rounded off with possible avenues that might be approached to improve the sustainability of the design.

19.1. Indicator of Sustainability

The top-level formulae, as established in the previous reports, are presented below:

$$IS = \frac{4 \cdot ENSI + 2 \cdot SOSI + 4 \cdot ECSI}{10} \tag{19.1}$$

Where ENSI is the environmental sustainability, SOSI social sustainability and ECSI economic sustainability. The formula for each of these is given below in Equation 19.2, 19.3 and 19.4, where the weights are multiplied by the score for each criteria.

$$ECSI = \frac{w_{11} \cdot S_{Prof} + w_{12} \cdot S_{Mark} + w_{13} \cdot S_{Miss} + w_{14} \cdot S_{Comp} + w_{15} \cdot S_{Regl} + w_{16} \cdot S_{Scal}}{22} \tag{19.2}$$

$$SOSI = \frac{w_{21} \cdot S_{HuDI} + w_{22} \cdot S_{Gend} + w_{23} \cdot S_{IncI} + w_{24} \cdot S_{LocS}}{20} \tag{19.3}$$

$$ENSI = \frac{w_{31} \cdot S_{LaIM} + w_{32} \cdot S_{SpDR} + w_{33} \cdot S_{ToMM} + w_{34} \cdot S_{REMM} + w_{35} \cdot S_{TrRE}}{19} \tag{19.4}$$

For a more in-depth explanation of the scores and their weights, please refer to the Midterm Report for the IKAROS project. In Table 19.1 the difference in scores between the IKAROS system and the Honey Concept are outlined.

Criteria #	**1**	**2**	**3**	**4**	**5**	**6**
Economic	0.8->0.4	0.4	0.8	0	0.58	0.5
Social	0.98->0.96	0.9->0.23	0.52->0.24	1->0		
Environmental	0.84->0.74	0.25->0.5	1->0.75	1->0.75	1->0.13	
ENSI	0.53->0.407					
SOSI	0.88->0.443					
ECSI	0.86->0.592					
IS	0.8->0.4882					

Table 19.1: Difference in Sustainability Scores between the Honey Concept and the IKAROS system

The criteria of economic sustainability that changed was the profitability. As was already discussed in Section 18.4 the cost of the project will be around 14.986 million €. This is significantly higher than the

estimated cost of the Honey concept, which was $3,169 million. This more than doubling in cost can be attributed to the higher level of detail reached in the design phase, when compared to the the detail in the Midterm trade-off.

The social sustainability scores for the design went down across the board, due to the sourcing of the transfer engines and due to the assembly robot being sourced from the United States of America. Once again, the rationale behind these choices can be found in Chapter 6 and Chapter 8. These choices were thus made to achieve a certain technical performance, making the associated decrease in score an unfortunate consequence.

Finally, almost all the environmental scores went down across the board as well. The launcher impact mitigation went town to 0.74 with the increased number of launches equal to 440 as discussed in Chapter 5. This increase is once again the consequence of a higher level in detail driving up the mass estimates. This is followed by the only increase in score between the two designs: space debris reduction. Due to the removal of the fragile lens, the likeliness of a large amount of particulate space debris being produced during an accident has decreased. The toxic and rare earth material score have both gone down, however, due to their use in the Gallium-Arsenide solar cells for the system power as presented in Chapter 11. Finally, the sourcing distance score has also decreased because of the sourcing of certain components from the U.S., granting a lower score.

19.2. Sustainability in the Design Process

Incorporating the sustainability into the design process was approached in two ways. The first involved the incorporation of a trade-off factor called "sustainability". This factor would mostly concern environmental sustainability. As can be seen in Chapter 7, wherever possible, social sustainability was taken into account as well. These trade-offs were performed in Chapter 7, Chapter 5, Chapter 6 and Chapter 10. The second approach was mainly concerned with economic sustainability. Improving economic sustainability is possible by reducing costs. Thus, a cost optimised design was pursued, both in aforementioned trade-offs but also in the overall design process. An incentive was added to environmental sustainability as well as to the cost through the use of high transport costs, thus penalising those components that would be sourced from further away, which would also increase transport-related emissions.

19.3. Improvements to Sustainability

As mentioned in the introduction, this Indicator of Sustainability was tailored to perform the trade-off the Midterm report, thus has its shortcomings when using to appraise the final design. The IKAROS project has certain aspects that influence its sustainability that were not included in the Indicator of Sustainability. These will be discussed here.

First off, the system will be fully assembled in the Airbus Defense and Space Facility in Oegstgeest, minimising the amount of outsourcing to countries which have lower labour standards than the Netherlands, which has decent standards when compared countries like China and the U.S.[i]. As discussed in Section 18.4, allocations are made for 350 employees at all skill levels throughout the lifetime of the IKAROS project, excluding the dozens of employees working at the ground station that will be paid fair wages, which is one of the big contributors to social sustainability.

Next, the system will be directly providing water to a quasi-developing country that already has water shortage issues that are predicted to only be exacerbated in the next decade[83]. Having access to clean water is one of the main requirements for social development and is goal 6 of the United Nation Sustainable Development Goals[ii]. The IKAROS project will be aiding in reaching this goal, and will pave the way for wider implementation of desalination plants. This both contributes to social and environmental sustainability, as a relief from the burden of water shortages will both help communities develop and combat drought and desertification.

[i] ITUC,"https://survey.ituc-csi.org/", (Accessed 15th of January 2020

[ii] UN,'Goal 6: Ensure access to water and sanitation for all',https://www.un.org/sustainabledevelopment/water-and-sanitation/, (accessed 15th of January 2021

Rounding off, this switch from a commodity to a public good also boosts the revenues that can be achieved, reducing the burden of the cost on the sponsor of the IKAROS project, increasing economic sustainability.

19.4. Reductions in Sustainability

Of course as mentioned before, sustainability was reduced in some aspects as well. Two areas are readily apparent: the economic sustainability through the cost and the environmental sustainability due to the environmental impact reverse osmosis desalination is associated with.

The deterioration to the economic sustainability is a direct resultant of the negative Return On Investment, as mentioned in Section 18.5, which will significantly harm the long term viability of the project. This is coupled with the inherent weak sustainability of the project due to the long pre-operations duration which significantly hampers flexibility in the face of unexpected changes due to circumstances. Justifying the IKAROS project to any potential investors would involve convincing them that the value of obtaining experience in the construction and operation of large scale satellites combined with the social benefit of providing clean water to developing communities is worth the multiple billion dollar deficit.

Finally, the process of desalinating water has a twofold impact that damages the environment. The first involves the destruction of marine organisms that enter the intakes of the facility, which can be mitigated by reducing flow speed, allowing fish to escape out of the flow[84]. The second is the brine released as byproduct of the reverse osmosis process. This is water with a very high salt content, which has also been deoxidised, making it settle on the bottom of the ocean and killing off marine life[85]. These impact are very much unsustainable, and thus require extra measures to make sure that their impact is mitigated to a reasonable extent.

19.5. Improving the Sustainability

As of the time of writing this report, the IKAROS design's sustainability is less than optimal, and certain strategies can be pursued to improve it in the future.

To improve the economic sustainability of the design, certain avenues are available, as presented below:

- Reduce total cost by reducing both the share and the total magnitude of the launch costs.
- Further integrate design vertically by selling higher priced goods.
- Reduce seed cost and inflexibility by switching to more modular design with a constellation of smaller satellites.
- Increase ground station efficiency by directly using steam to desalinate water.
- Switch to Multi Effect distillation once specific power requirements go down for that process.

20
Conclusions and Recommendations

The goal of this project was to design a Space Based Solar Power system that is launched to GEO and then assembled by robotics into a SBSP satellite, that will deliver a continuous 100 MW of solar energy to Earth, in order to provide mankind with a continuous and boundless flow of clean energy without the environmental, social and economic limitations of conventional renewable energy. Throughout the design, several conclusions were made on the feasibility, technology readiness, and assumptions that were considered. Based on these conclusions, several recommendations can be given for future endeavours.

20.1. Conclusions

One of the main challenges was assembly in space. This is ultimately limited by size, time, and computational capabilities. Most of the necessary technology has been demonstrated on a small scale, making it technically feasible, but something of this size has never been attempted before. A structural limitation that was found using current methods, was the available sheet size. The current number of spokes in the design is limited by that, instead of the structural rigidity. Additionally, in order to fit into the launcher, the sheet length is further limited. To compensate, a foldable design is chosen that might split up the mirror components in smaller sections.

Thermal control was initially seen as one of the larger challenges of project IKAROS. A promising solution to this challenge was found in Liquid Droplet Radiator (LDR) technology. Although it has a low Technology Readiness Level (TRL), it stands to be up to ten times more effective than traditional thermal management methods. It was also found that these traditional methods would not be able to provide satisfactory thermal control for a high waste-heat system like 'Honey'. Furthermore, even with LDR technology, thermal control is the subsystem with the highest power demand.

From the perspective of a business case, it was found that the concept is not ready for an economically sustainable implementation in India. At this point in time, it would be cheaper to set up traditional renewable energy with downtime-storage capabilities than to launch an SBSP system into orbit. This is mainly due to the launch costs, which make up 90+% of the total cost. Furthermore, the low price level of electricity globally set a limit on the achievable revenue. Unless the price of electricity goes up an order of magnitude or the price of launching goes down an order of magnitude, neither of which is likely to happen based upon past patterns and future predictions, electricity will not be a profitable use case. A possible solution was found for the desalination of water for local use or private water bottling and shipping, although the latter would also increase initial cost, overhead, and pollution. Additionally, to carry the economic sustainability to an acceptable level, environmental sustainability had to be partly sacrificed.

20.2. Future Outlook

At the request of the client, a small investigation as to the requirements to break even are performed. Three scenarios are envisioned.

Break Even with current launch costs

In this scenario, the price of the product that the IKAROS project would sell would be increased until the projected cost would equal the projected revenues. These values could then be scaled for different levels of power generated (in a range of 1 to 100 Megawatts). Figure 20.1 illustrates the trend-line for decreased launch costs. If all other factors remain the same, the launch costs would still have to decrease by a factor 3,97 to break even for this project.

Break Even with reduced launch costs

This scenario envisions the reduction of launch costs in the future. The product would remain at the same price as established in Section 18.1. Figure 20.1 illustrates the trend-line for increased revenue per Watt. If all other factors remain the same, the revenue per Watt would still have to increase by a factor 3,04 to break even for this project.

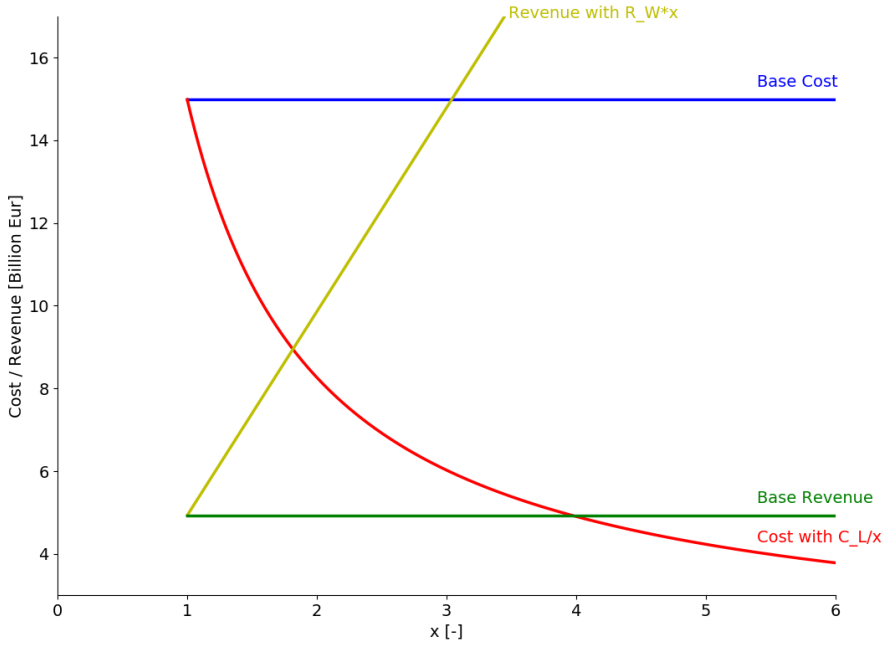

Figure 20.1: Cost and revenue trend for varying launch costs C_L or revenue per Watt R_W

Satellites in Low Earth Orbit

In the final scenario, the satellite would be moved to a LEO, with multiple satellites in the same orbit, to be assembled at the International Space Station, which would be converted to a manufacturing and assembly facility. The logic behind this is sound: as discussed in Chapter 5, the SpaceX Starships that would currently be used would require refuelling to get the system into GEO. For every Starship filled with payload, two more would have to follow with fuel. However, these Starships can put a 100 tonne payload into a 500 kilometer LEO without refuelling, thus cutting the launch costs by over 65%. As mentioned in Section 18.4, the launch cost are almost 90 percent of the total costs, leading to a significant decrease.

The situation for a LEO IKAROS satellite would not all be positive however. Because of the lower altitude, the system would rapidly be moving over the surface of the earth. The International Space Station, which is in the same orbit, has an orbital period of 1,5 hours. The ground speed for the system would thus be over 25 thousand kilometers per hour, as opposed to the near zero ground speed for a GEO IKAROS satellite. Ignoring the horrific implications this would have for ADCS, this means that the satellite would constantly have to switch ground stations to beam down its power. Another significant issue this entails is the limited FOV the system would have due to the low altitude. This would lead to the system only being able to beam power to a ground station for about 10 minutes. This would lead to a requirement for at least 9 satellites in orbit to get 24/7 coverage. Of course, this would not lead to 24/7 coverage, because the satellites would have an eclipse time of about half an hour per period. This would thus prevent them from providing power during most of the night time, except in the early morning before the sun rises and in the evening when the sun has just set. Finally, the satellites would also never be at an optimal angle above the ground station, namely perpendicularly above the surface. They would come in and go out at an oblique angle, which would lead to an average angle of 45 degrees, significantly reducing the absorbed power and increasing the reflected power, but this will be neglected in our calculation. Finally, to make

sure the satellites aren't idle whilst they are at a different part of the orbit, more ground stations would be required. Based on this, the costs and revenues were estimated (calculated based upon costs as per Section 18.4).

- Launch Costs: 40680 million Euros
- Ground Station: 4500 million Euros
- System Costs: 3887.8 Million Euros
- Total Costs: 49067.8 Million Euros
- Predicted Revenues: 29580 million Euro

20.3. Recommendations

The effectiveness of the assembly and integration system is directly proportional to the assembly speed. The assembly speed in space can be greatly improved through future developments in AI powered swarm technologies, as well as the development of on-ground simulations or computational models that optimise the assembly procedure before the mission. Such free-flying swarm robotics could be used after assembly for maintenance, or even to collect and recycle parts from other satellites in GEO or satellites in the graveyard orbit. Concerning the mirror sheets in the large parabola, through the development and application of larger sheets, the necessary number of spokes could be minimised purely based on structural rigidity. Furthermore, if the sheets with shape memory could be employed, overall performance would benefit. Lastly, to improve overall system precision, the possibility of a large-scale focusing lens could be further investigated.

In terms of structures, the main recommendations revolve around designing for loads further along the design phase. Ultimately, all the loads in the load cycle need to be considered but at this stage the most important aspects to be looked into would be the impact toughness of the foils and their resistance to on orbit vibrations. Another recommendation would be to change the configurations of the trusses for the Relay/Sting to increase their geometrical stiffness to reduce their mass. Additionally, the concentric rings in the Queen's skeleton should be sized for the torque loads it will experience during thruster manoeuvres. Furthermore, a more detailed configuration for the launch modules should be established that would allow for the sizing of e.g acoustic loads. A mass saving in the launching supporting structure is also possible by using composites (were not considered as the approach assumed an isotropic material) or a thinner metal cylinder with supporting stringers instead of a solid "monocoque" structure. Lastly, contacting SpaceX regarding other Starship specific loads not detailed in their users manual (such as shock loads) would be useful for further launch structure designing.

From a business and operations perspective, the first recommendation would be to reduce the costs of launch to drastically improve the economic sustainability of the project. To improve the environmental sustainability, the development of more reliable low-energy desalination techniques, like Multi Effect Distillation (MED), could reduce pollution, and atmospheric losses could be partly mitigated by use of windmills near the ground-station. A second recommendation would be to reconsider the underlying business case of the project. The added value of a multi-billion euro space system to produce renewable energy is found to be minimal. Towards the end of the design, a purpose shift was made to the large-scale desalination of water; it can be recommended to reiterate the project from scratch with this in mind. Furthermore, to lower the financial risk involved, a technology demonstrator could be developed first. Such a demonstrator would operate on a much smaller scale, to show the viability of the necessary new technologies. This small-scale system could then be up-scaled to a constellation, which would conjointly improve flexibility of response to changing conditions over the long lifetime.

Bibliography

[1] SpaceX. Starship. URL https://www.spacex.com/vehicles/starship/.

[2] SpaceX. First private passenger on lunar starship mission, September 2018. URL https://www.youtube.com/watch?v=zu7WJD8vpAQ&ab_channel=SpaceX.

[3] Elon R. Musk. Estimation of the mass of the raptor engine, October 2019. URL https://twitter.com/elonmusk/status/1183866120240955392.

[4] Elon R. Musk. Estimation of chamber pressure of the raptor engine, June 2020. URL https://twitter.com/elonmusk/status/1273871381353033729?s=19.

[5] Milad Pasand, Ali Hassani, and Mehrdad Ghorbani. A study of spacecraft reaction thruster configurations for attitude control system. *IEEE Aerospace and Electronic Systems Magazine*, 32(7):22–39, July 2017. doi: 10.1109/maes.2017.160104. URL https://doi.org/10.1109/maes.2017.160104.

[6] Deanna Sessions, Joshua Ruff, Francisco Espinal, Gregory Huff, Sameer Jape, Edwin Peraza Hernandez, Dimitris Lagoudas, Darren Hartl, and Beatriz Borges. Folding, tessellation, and deployment of an origami-inspired active-material-enabled self-folding reflector antenna. pages 929–930, 07 2018. doi: 10.1109/APUSNCURSINRSM.2018.8609355.

[7] Edwin Peraza Hernandez, Darren Hartl, and Dimitris Lagoudas. Analysis and design of an active self-folding antenna. page V05BT08A049, 08 2017. doi: 10.1115/DETC2017-67855.

[8] RenÃl' Schwarz. *Keplerian Orbit Elements*. RenÃl' Schwarz, 2017.

[9] Space Exploration Technologies Corp. *STARSHIP USERS GUIDE*. Space Exploration Technologies Corp., 2020.

[10] Brad Jones. Nasa's new ion thruster. 2017. URL https://futurism.com/nasas-new-ion-thruster-breaks-records-could-take-hu

[11] NASA. Soyuz undocking/landing timeline, 2010. URL https://www.nasa.gov/mission_pages/station/structure/elements/soyuz/landing_timeline.html.

[12] M. Borst. Mass optimisation of cryogenic fluid systems for long-duration space missions. 2020.

[13] L.J. Hastings. An overview of nasa efforts on zero boiloff storage of cryogenic propellants. 2001.

[14] Ariane Group. Hm7b engine. URL https://www.ariane.group/wp-content/uploads/2020/06/HM7B_2017_11_PS_EN_Web.pdf.

[15] EADS. Vinci thrust chamber cryogenic upperstage. URL https://web.archive.org/web/20061028183532/http://cs.space.eads.net/sp/PDF/vinci.pdf.

[16] M. Ball. The hydrogen economy - vision or reality?, 2016. URL https://www.sciencedirect.com/topics/engineering/hydrogen-production-cost.

[17] Sam Dinkin. Increasing the profit ratio, 2016. URL https://www.thespacereview.com/article/2893/1.

[18] Micheal A. Green. Hydrogen safety issues compared to safety issues with methane and propane. 2005.

[19] HySafe.org. Initial guidance for using hydrogen in confined spaces. URL http://www.hysafe.org/download/1710/HYSAFE_D113_version_1.1.pdf.

[20] Public Health England. Methane general information, January 2019. URL https://assets.publishing.service.gov.uk/government/uploads/system/uploads/attachment_data/file/769766/Methane_PHE_general_information__070119.pdf.

[21] A. Maximo, et al. Robotic technologies for in-space assemblfy operations. 2017.

[22] Mark Wylie. A novel telescopic boom deployment system for use in upper atmosphere research. January 2010.

[23] Kelvin Roovers. geometric design of deployable scissor grids consisting of generalized polar units. Maart 2018. doi: 10.20898/j.iass.2017.193.865.

[24] Haibo Ma. Study on the criterion to determine the bottom deployment modes of a coilable mast. September 2017. doi: 10.1016/j.actaastro.2017.09.035.

[25] Bindi You, Dong Liang, Zhihui Gao, Yiming Sun, Peibo Hao, Jianmin Wen, and Yang Zhao. Chapter ten - dynamics modeling of flexible multibody structure for a spacecraft mechanism with nonlinear factors. In Jian Liang, Bindi You, Deqing Huang, Si-Lu Chen, and Lei Liu, editors, *Precision Motion Systems*, pages 217 – 259. Butterworth-Heinemann, 2019. ISBN 978-0-12-818601-5. doi: https://doi.org/10.1016/B978-0-12-818601-5.00018-4. URL http://www.sciencedirect.com/science/article/pii/B9780128186015000184.

[26] Wijker J.J. *Spacecraft Structures*. 2008. ISBN 978-3-540-75552-4. doi: 10.1007/978-3-540-75553-1.

[27] Larson and Wertz. *Space mission engineering : the new SMAD*. Space technology library ; v. 28. Microcosm Press, Hawthorne, CA. ISBN 9781881883159.

[28] Y. S. Touloukian, Purdue University, and Thermophysical Properties Research Center. *Thermophysical properties of high temperature solid materials Vol I*. MacMillan, New York, 1967.

[29] Norman E. Phillips. Heat Capacity of Aluminum between 0.1 K and 4.0 K. *Physical Review*, 114(3):676–685, may 1959. ISSN 0031-899X. doi: 10.1103/PhysRev.114.676. URL https://link.aps.org/doi/10.1103/PhysRev.114.676.

[30] Edgar H. Buyco and Fred E. Davis. Specific Heat of Aluminum from Zero to Its Melting Temperature and Beyond Equation for Representation of the Specific Heat of Solids. *Journal of Chemical and Engineering Data*, 15(4):518–523, 1970. ISSN 15205134. doi: 10.1021/je60047a035.

[31] Engineering ToolBox. The radiation heat transfer emissivity coefficient of some common materials as aluminum, brass, glass and many more, 2003. URL https://www.engineeringtoolbox.com/emissivity-coefficients-d_447.html.

[32] David G Gilmore. *Spacecraft thermal control handbook. Volume I, Volume I,*, volume I. 2002. ISBN 9781601192035 1601192037. URL http://app.knovel.com/hotlink/toc/id:kpSTCHVFT2/spacecraft-thermal-control.

[33] Lee Smith. The abcs of multi-layer insulation for spacecraft. 2019. URL https://www.designnews.com/materials-assembly/abcs-multi-layer-insulation-spacecraft.

[34] D. Hall and Alfred Fote. Thermal control coatings performance at near geosynchronous altitude. *Journal of Thermophysics and Heat Transfer*, 6:665, 10 1992. doi: 10.2514/3.11549.

[35] Mihai Andrei. Why satellites have those golden foils on them - and how it saves a lot of lives. 2017. URL https://www.zmescience.com/space/satellites-golden-foils-20092017/.

[36] Tyler Link. Tai delivers graphite fiber thermal straps for nasa's ixpe mission. 2019. URL https://www.techapps.com/blog/tai-delivers-graphite-fiber-thermal-straps-for-nasas-ixpe-mission.

[37] Abe Hertzberg. Thermal management in space. 1994. URL https://space.nss.org/settlement/nasa/spaceresvol2/thermalmanagement.html.

[38] Cho Han and Joon-Min Choi. Thermal analysis of spacecraft propulsion system and its validation. *KSME International Journal*, 18:847–856, 05 2004. doi: 10.1007/BF02990304.

[39] Robert L. Fusaro. *Lubrication of Space Systems Challenges and Potential Solutions*. Lewis Research Center, 2020.

[40] Gregory L Matloff and Les Johnson. *Applications of the Electrodynamic Tether to Interstellar Travel*. Dept. of Physical and Biological Sciences, New York City College of Technology, 2005.

[41] Gerald L. Buckner and Ronald F. Tuttle. The liquid droplet radiator in space: A parametric approach. In *Transactions of the Fifth Symposium on Space Nuclear Power Systems*, pages 313–316, 1988.

[42] K. Alan White. *Moving Belt Radiator Development Status*. Lewis Research Center, 1988.

[43] Albert J. Juhasz and George P. Peterson. *Review of Advanced Radiator Technologies for Spacecraft Power Systems and Space Thermal Control*. Lewis Research Center, 1994.

[44] Thomas E. Botts, James R Powell, and Roger Lenard. Magnetically Focused Liquid Drop Radiator.

[45] K. Alan White. Liquid droplet radiator development status. *AIAA 22nd Thermophysics Conference, 1987*, 1987. doi: 10.2514/6.1987-1537.

[46] Robert T. Taussig and A. T. Mattick. Droplet radiator systems for spacecraft thermal control. *Journal of Spacecraft and Rockets*, 23(1):10–17, 1986. ISSN 00224650. doi: 10.2514/3.25077.

[47] Gerald L. Buckner. *The Liquid Droplet Radiator in Space: A Parametric Approach*. PhD thesis, Air Force Air University, Ohio, 1987.

[48] Subbarao Surampud. Overview of the space power conversion and energy storage technologies, Jan 2011.

[49] LeewayHertz. Blockchain manufacturing âĂŞ enabling supply chain traceability, 2019. URL https://www.leewayhertz.com/blockchain-manufacturing/.

[50] SpaceX. Starship update. URL https://www.youtube.com/watch?v=sOpMrVnjYeY.

[51] Marc Naeije. *The power is out there: Space Based Solar Power*. TU Delft, 2020.

[52] NASA. Nss 1740.14: Guidelines and assessment procedures for limiting orbital debris. Technical report, National Aeronautics and Space Administration, 1995.

[53] A.T. Mattick and A. Hertzberg. The liquid droplet radiatorâĂŤan ultralightweight heat rejection system for efficient energy conversion in space. *Acta Astronautica*, 9(3):165 – 172, 1982. ISSN 0094-5765. doi: https://doi.org/10.1016/0094-5765(82)90084-4. URL http://www.sciencedirect.com/science/article/pii/0094576582900844.

[54] International Energy Agency. India 2020: Energy policy review. *IEA*, 2020.

[55] Tejal Kanitkar. The covid-19 lockdown in india: Impacts on the economy and the power sector. *Global Transitions*, 2: 150–156, 2020.

[56] Peter Goodman. Why the global recession could last a long time. *The New York Times*, 1, 2020.

[57] Soham Ghosh. Loss reduction and efficiency improvement: a critical appraisal of power distribution sector in india. *International Journal of Modern Engineering Research*, 2(5):3292–3297, 2012.

[58] Neeraj Kumar and MM Tripathi. Solar power trading models for restructured electricity market in india. *Asian Journal of Water, Environment and Pollution*, 17(2):49–54, 2020.

[59] Food and Agriculture Organisation of the United Nations. Water scarcity, 2020. URL http://www.fao.org/assets/infographics/FAO-Infographic-water-scarcity-en.pdf.

[60] M. S. Eeshanpriya. Mumbai to need 71% more water by 2041 say bmc study. August 2019. URL https://www.hindustantimes.com/mumbai-news/mumbai-to-need-71-more-water-by-2041-bmc-study/story-NS3k4KIB5CTZX3CwPUWDYL.html.

[61] USAID. Drinking water supply for urban poor: city of mumbai. October 2016. URL https://www.safewaternetwork.org/sites/default/files/Safe%20Water%20Network_Mumbai%20City%20Report.pdf.

[62] Mehul R. Thakkar. Mumbai civic body's desalination plant project: Why not focus on water conservation, ask experts. November 2020. URL https://www.hindustantimes.com/mumbai-news/mumbai-civic-body-s-desalination-plant-project-why-not-focus-on-water-conservation-ask-experts/story-2Rts4Z19QmBYpHPDIbQkqL.html.

[63] Raju Abraham and Ramasamy Venkatesan. Costing and evaluation of desalination technologies-a case study in india. 01 2015.

[64] HYDRAULIC ENGINEER'S DEPARTMENT and CHIEF ENGINEER (SEWERAGE OPERATION)'S DEPARTMENT. *Water Charges Rules and Sewerage & Waste Removal*. Feb 2015. URL https://portal.mcgm.gov.in/irj/go/km/docs/documents/MCGMDepartmentList/HydrallicEngineer/DOCS/WaterChargesRuleseffectivefrom01.04.2015_English.pdf.

[65] P. Aggarwal, et al. Unpacking india's electricity subsidies: Reporting, transparency, and efficacy. Technical report, The International Institute for Sustainable Development, December 2020. URL https://www.iisd.org/system/files/2020-12/india-electricity-subsidies.pdf.

[66] Prakash Rao, William R Morrow III, Arian Aghajanzadeh, Paul Sheaffer, Caroline Dollinger, Sabine Brueske, and Joe Cresko. Energy considerations associated with increased adoption of seawater desalination in the united states. *Desalination*, 445: 213–224, 2018.

[67] Anthony Bennett. 50th anniversary: Desalination: 50 years of progress. *Filtration+ Separation*, 50(3):32–39, 2013.

[68] Aparna Sawhney. Striving towards a circular economy: climate policy and renewable energy in india. *Clean Technologies and Environmental Policy*, pages 1–9, 2020.

[69] Francisco J Tapiador, Arthur Y Hou, Manuel de Castro, Ramiro Checa, Fernando Cuartero, and Ana P Barros. Precipitation estimates for hydroelectricity. *Energy & Environmental Science*, 4(11):4435–4448, 2011.

[70] Gireesh Shrimali, Sandhya Srinivasan, Shobhit Goel, and David Nelson. The effectiveness of federal renewable policies in india. *Renewable and Sustainable Energy Reviews*, 70:538–550, 2017.

[71] Andrew Wilson, Massimiliano Vasile, and George Dietrich. A process-based life cycle sustainability assessment of the space-based solar power concept. 10 2020.

[72] International Renewable Energy Agency. *Renewable Power Generation Costs in 2018*. 2018.

[73] Institute for Energy Economics and Financial Analysis. *Bad Choice: The Risks, Costs and Viability of Proposed U.S. Nuclear Reactors in India*. March 2016.

[74] K.G. Gibbons. *Orbital Saturation:The necessity for international regulation of geosynchronous orbits*. 1979. 9 Cal. W. Int'l L.J. 139 (1979).

[75] Stephen Graham, Renu Desai, and Colin McFarlane. Water wars in mumbai. *Public Culture*, 25(1 (69)):115–141, 2013.

[76] Nikhil Anand. Pressure: The politechnics of water supply in mumbai. *Cultural Anthropology*, 26(4):542–564, 2011.

[77] Heiner Klinkrad. Space debris. *Encyclopedia of Aerospace Engineering*, 2010.

[78] Thomas Schildknecht, Reto Musci, Carolin Früh, and Martin Ploner. Color photometry and light curve observations of space debris in geo. In *Proceedings of Advanced Maui Optical and Space Surveillance Technologies Conference*, pages 17–19, 2008.

[79] Council Regulation (EEC). On the tariff and statistical nomenclature and on the common customs tariff. 1987.

[80] Trevor Watkins. The practice of product testing in the new product development process: The role of model-based approaches. 1998. URL `https://www.emerald.com/insight/content/doi/10.1108/EUM0000000004789/full/html`.

[81] Peter G. Nicoll Neil A. Thompson. *FORWARD OSMOSIS DESALINATION: A COMMERCIAL REALITY*. IDA World Congress - Perth Convention and Exhibition Centre (PCEC), 2011.

[82] Darrell Etherington. Elon musk says spacexâĂŹs starship could fly for as little as $2 million per launch, 2019. URL `https://techcrunch.com/2019/11/06/elon-musk-says-spacexs-starship-could-fly-for-as-little-as-2-million-per-launch/`.

[83] Rajat K Chakraborti, Jagjit Kaur, and Harpreet Kaur. Water shortage challenges and a way forward in india. *Journal: American Water Works Association*, 111(5), 2019.

[84] Thomas M Missimer and Robert G Maliva. Environmental issues in seawater reverse osmosis desalination: Intakes and outfalls. *Desalination*, 434:198–215, 2018.

[85] JV Del Bene, Gerhard Jirka, and John Largier. Ocean brine disposal. *Desalination*, 97(1-3):365–372, 1994.